International Atomic Energy Agency

INDC(NDS)-238
Distr. L

INDC INTERNATIONAL NUCLEAR DATA COMMITTEE

MEASUREMENT, CALCULATION AND EVALUATION OF PHOTON PRODUCTION CROSS-SECTIONS

Proceedings of the
Specialists' Meeting organized by the
International Atomic Energy Agency

and

Co-sponsored by the Czechoslovak Atomic Energy Commission

Smolenice, the Czech and Slovak Federal Republic
5 - 7 February 1990

Edited by

N.P. Kocherov
IAEA Nuclear Data Section

November 1990

IAEA NUCLEAR DATA SECTION, WAGRAMERSTRASSE 5, A-1400 VIENNA

International Atomic Energy Agency

INDC(NDS)-238
Distr. L

INDC INTERNATIONAL NUCLEAR DATA COMMITTEE

MEASUREMENT, CALCULATION AND EVALUATION OF PHOTON PRODUCTION CROSS-SECTIONS

Proceedings of the
Specialists' Meeting organized by the
International Atomic Energy Agency

and

Co-sponsored by the Czechoslovak Atomic Energy Commission

Smolenice, the Czech and Slovak Federal Republic
5 - 7 February 1990

Edited by

N.P. Kocherov
IAEA Nuclear Data Section

November 1990

INDC(NDS)-238
Distr. L

MEASUREMENT, CALCULATION AND EVALUATION OF PHOTON PRODUCTION CROSS-SECTIONS

Proceedings of the
Specialists' Meeting organized by the
International Atomic Energy Agency

and

Co-sponsored by the Czechoslovak Atomic Energy Commission

Smolenice, the Czech and Slovak Federal Republic
5 - 7 February 1990

Edited by

N.P. Kocherov
IAEA Nuclear Data Section

November 1990

Reproduced by the IAEA in Austria
January 1991

91-00090

INTRODUCTION

The need for more accurate and more complete data on photon production in neutron and proton interactions with nuclei was explicitly expressed at several IAEA meetings. In particular the Advisory Group Meeting on Nuclear Theory for Fast Neutron Nuclear Data Evaluation organized by the Nuclear Data Section in Beijing, 12-16 October 1987 has recommended to convene a Specialists' Meeting on Measurement, Calculation and Evaluation of Photon Production Cross-Sections. This topic was considered to be of growing importance for a number of applications such as fusion technology, nuclear borehole logging, shielding, mineral analysis, etc.

It was proposed to discuss the following items:

1. Nuclear data needs, required accuracies and gaps in existing data.

2. Experimental techniques of measuring gamma-production in neutron interactions (coincidences, timing, correlations, special devices etc.).

3. Theoretical models and code comparison for the calculation of photon production cross-sections and spectra. Some related quantities like gamma-ray strength functions, semi-direct and precompound gamma-ray emission were also included.

The ideas of the participants on these topics were formulated in detail in their conclusions and recommendations which are contained in this report.

CONTENTS

SESSION I: EXPERIMENTAL MEASUREMENT AND TECHNIQUES
Chairman: P. Oblozinsky

1. S. Wender, R.O. Nelson and C.M. Laymon:
Gamma-ray production cross-section measurements using a white neutron source from 1 to 400 MeV 9

2. S. Hlavac and P. Oblozinsky:
Measurements of γ-ray production from $^{52}Cr(n,x\gamma)$ reactions at 14.6 MeV 21

3. A.A. Filatenkov and S.V. Chuvaev:
Measurements of gamma-rays from ^{232}Th. ^{235}U, and ^{238}U fission fragments 31

SESSION II: CALCULATION OF PHOTON CROSS-SECTIONS
Chairman: J. Kopecky

1. E. Betak and P. Oblozinsky:
Preequilibrium γ emission in nuclear reactions (Review) 39

2. H. Kalka:
γ-emission within a statistical multistep reaction model 49

3. P. Oblozinsky and M.B. Chadwick:
Gamma ray emission from multistep compound reactions 63

4. P. Oblozinsky:
Preequilibrium emission of hard photons in proton-nucleus reactions 75

5. E. Betak and F. Cvelbar:
Neutron-gamma competition in nucleon-induced reactions . . . 83

6. G. Maino, A. Mengoni and P. Oblozinsky:
Calculation of photon production cross sections and spectra from $^{52}Cr(n,x\gamma)$ reactions at 14.6 MeV 91

7. J. Kopecky and M. Uhl:
Present status of gamma-ray strength functions and their impact on statistical model calculations 103

8. M. Uhl and J. Kopecky:
Calculations of capture cross-sections and gamma-ray spectra as a tool for testing strength function models . . . 113

9. F. Becvar, R.E. Chrien and J. Kopecky:
Two-step cascade transitions following neutron capture: a new source of information on photon strength functions . . . 127

SESSION III: EVALUATION
Chairman: S. Wender

1. A.A. Nosov, A.A. Rimski-Korsakov, R.M. Yakovlev, M.N. Zubkov:
High energy gammas in nuclear collisions: Necessary data . . . 145

2. S. Hlavac and P. Oblozinsky:
Evaluation of discrete γ-ray production cross sections
in (n,xγ) reactions on Al for nuclear geophysics 149

CONCLUSIONS AND RECOMMENDATIONS 187

LIST OF PARTICIPANTS 193

SESSION I: EXPERIMENTAL MEASUREMENT AND TECHNIQUES

Chairman: P. Oblozinsky

Gamma-Ray Production Cross Section Measurements Using A White Neutron Source From 1 to 400 MeV

S. A. Wender, R. O. Nelson and C. M. Laymon

Los Alamos National Laboratory
Los Alamos, NM 87545

Abstract

The continuous energy (white) neutron source at the Los Alamos Meson Physics Facility (LAMPF) is used to measure photon-production cross sections over a wide range of neutron energies. Detector systems have been or are being developed to measure gamma rays in the energy range from hundreds of keV up to several hundreds of MeV. In particular a high resolution Ge detector system is used to detect gamma rays from several hundred keV to over 6 MeV. A 5 crystal BGO detector system is used for measuring gamma-rays from 1 MeV to approximately 20 MeV. A large volume BGO detector with an active shield is used to measure gamma rays in the range from 5 to 40 MeV. We are presently developing a multi-element gamma-ray telescope to measure gamma rays with energies from 50 MeV up to several hundred MeV.

Introduction

The high energy and high intensity of the continuous energy (white) neutron source at the Los Alamos Meson Physics Facility (LAMPF) makes possible the measurement of gamma-ray production cross sections for incident neutrons in the energy range from below 1 MeV to over 400 MeV. Several recent publications[1,2] have described the operating parameters of the neutron source in detail so we will include only a short description of it here. We will then describe the program of gamma-ray measurements that are associated with this source including past, present and planned experiments.

There are several advantages in using a white neutron source for gamma-ray measurements. First, a wide range of neutron energies is available. In the case of this source, neutrons with energies from below 1 MeV to over 400 MeV are produced. Second, the energy coverage is continuous. In most cases, the neutron energy resolution is not limited by the source but rather by the length of the flight path and the time resolution of the detector system. Third, data is acquired simultaneously at all neutron energies. This greatly reduces the systematic errors associated with taking sequential runs at different energies over a long period of time when studying the energy dependence of the cross sections. Fourth, at any one time, the neutron beam is shared amongst several experiments. This greatly reduces the competition for beam time compared to facilities that

require the dedicated use of the entire accelerator for experiments. In the past, typical experiments have run for several months.

There are some disadvantages to using a white neutron source. First, experiments tend to be more complicated because the energy of the incident neutron must be determined experimentally. Clearly, this complication can be an advantage if one is interested in measuring the energy dependence of a reaction. Second, backgrounds are more difficult to understand because neutrons are present at all times. Third, it is necessary to know the velocity of the scattered particle. Because this is not a problem for photons, white sources are ideal for gamma-ray measurements.

Neutron Source

Neutrons are produced following spallation reactions induced by the 800 MeV pulsed proton beam from the LAMPF accelerator incident on the neutron production target. The present production target consists of a cylinder of tungsten 7.5 cm long and 3 cm in diam. The target is situated in a vacuum chamber 2 m in diam and 1.2 m high which is surrounded by approximately 7 m of steel and magnetite concrete. There are penetrations in this shield at 15^{o} to the left and to the right, 30^{o} left and right, 90^{o} left and right and 60^{o} right with respect to the incident proton beam in the horizontal plane. The beam to each flight path is separately controlled by individual shutters. As the neutrons drift along the collimated flight path, they become dispersed in time and energy. It is then possible to tag the energy of the incident neutron by measuring its time-of-flight (TOF) relative to the time-of-arrival of the proton pulse. The non-relativistic expression for the TOF of the neutron is:

$$TOF = 72.3*l*E_n^{-.5}$$

where the TOF is in nsec, the flight path, l, is in meters and the neutron energy, E_n, is in MeV. The neutron energy resolution is given by : $\Delta E/E = - 2*\Delta T/TOF$. From this relationship it is clear that the resolution improves with increasing flight path; however, the intensity decreases with longer flight paths.

The proton beam has a time structure consisting of macropulses which are typically 625 μsec long with a repetition rate of 40 Hz. Within each macropulse are sharp (<300 psec wide) micropulses. The number of micropulses/sec depends on the macropulse rate and the pulse-to-pulse separation of the micropulses which is an adjustable parameter. In the past, typical separations have been 1.8 μsec; however, separations as small as 360 nsec are possible.

The energy dependence of the neutron flux depends on the angle of the flight path relative to the incident proton beam and the material of the neutron production target. A plot of the measured neutron intensity as a function of neutron energy for our tungsten target at 15^{o} is shown in

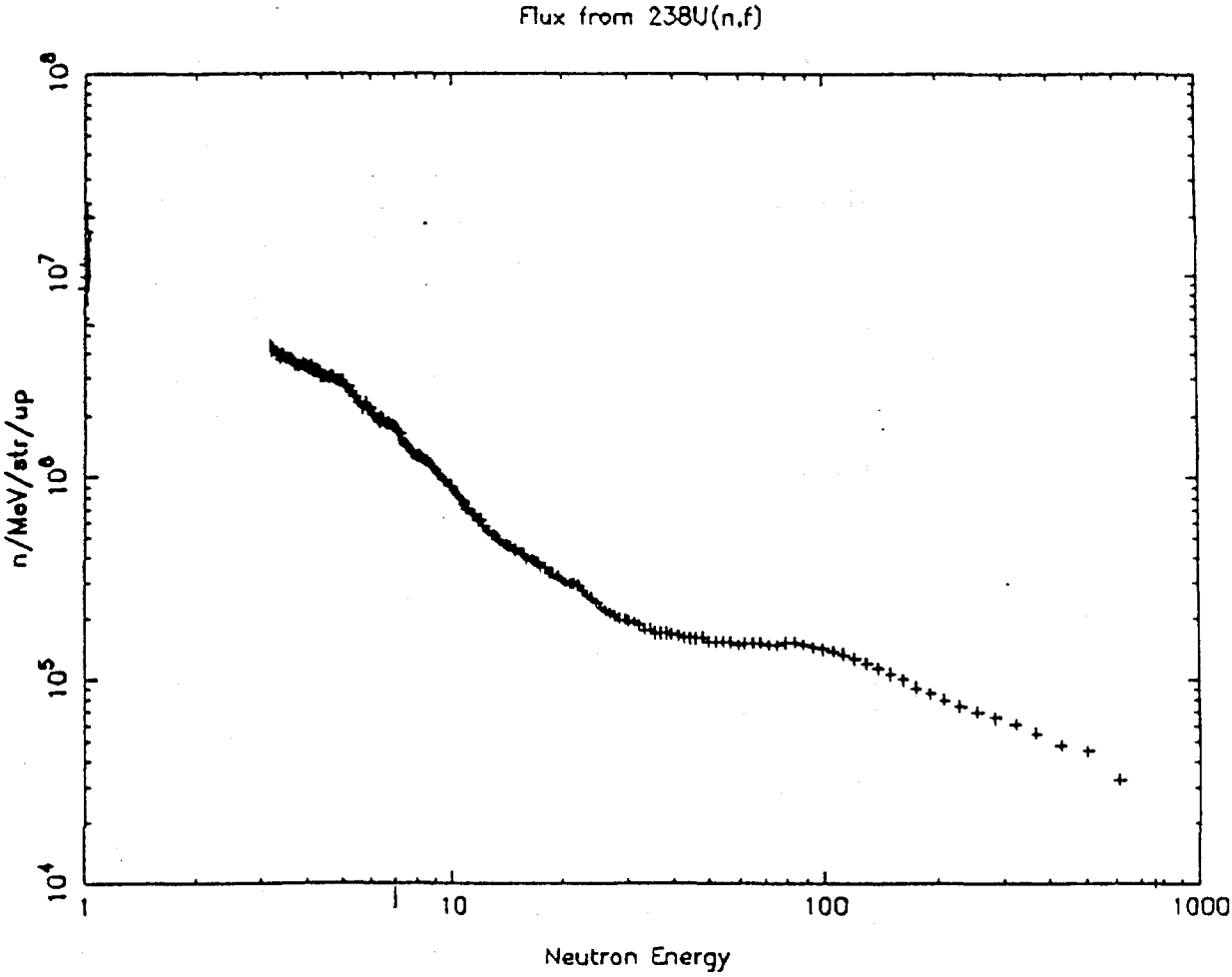

1. Measured neutron flux as a function of neutron energy from the white neutron source at 15° with respect to the incident proton beam. The units are neutrons/MeV/str/micropulse.

fig. 1. The vertical scale in fig. 1 is the number of neutrons/str/MeV/micropulse. The number of neutrons/sec over the area of the sample is the product of the intensity given in fig. 1, the solid angle subtended by the sample, the micropulse rate and the neutron energy bin width. A similar plot for the 90° flight path would show orders of magnitude less intensity above 200 MeV but approximately a factor of 2 greater intensity below 20 MeV. Lighter mass target materials (eg., copper) would show generally less neutron intensity over the entire range with a greater reduction occurring at lower energies. Thus the flux would be more nearly constant as a function of energy for these materials. The neutron flux is monitored during an experiment using a fission ionization chamber operated in the TOF mode with deposits of ^{235}U and ^{238}U.

Gamma-ray measurements

We will separate the experimental program into three gamma-ray energy ranges. The gamma rays in the energy range from several hundred keV to approximately 15 MeV are from decays of bound state levels. The gamma rays in the energy range from 5 to 40 MeV are from the decay of capture states with the giant dipole resonance being dominant. Very hard photons in the energy range above 50 MeV are from bremsstrahlung processes, and π^0 decay.

5 CRYSTAL BGO GAMMA-RAY SPECTROMETER

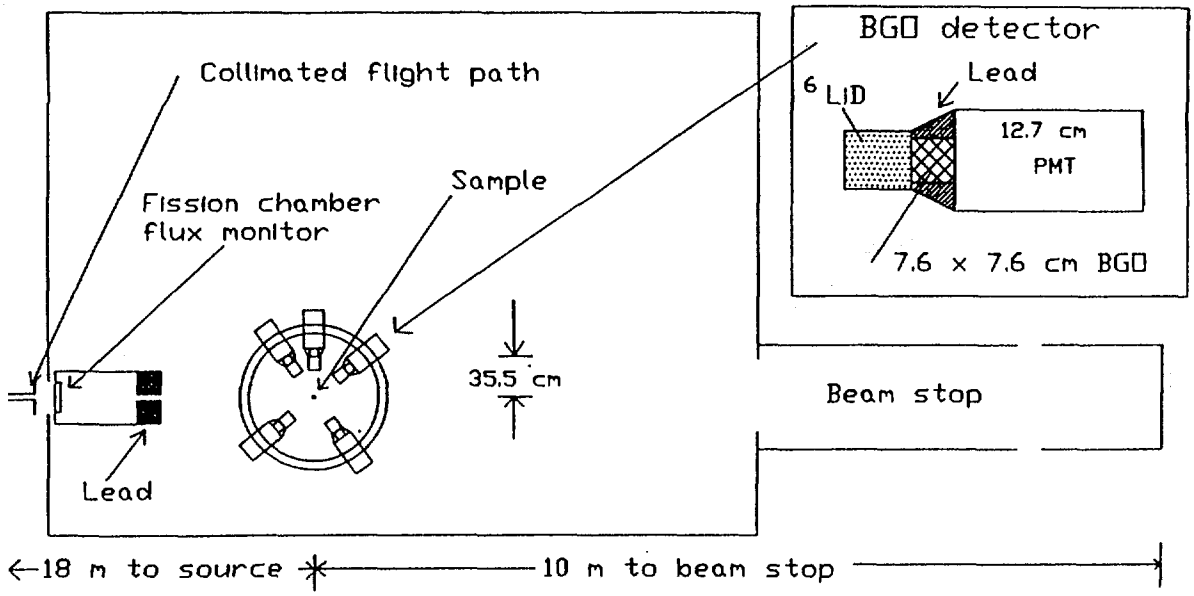

2. Diagram of the 5 crystal BGO detector system at the white neutron source. The detectors are located at 39^0, 55^o, 90^o, 125^o, and 145^o.

Two detector systems are used for measuring low energy gamma rays. The first consists of an array of five 7.6 cm long x 7.6 cm diam BGO scintillators as shown in fig. 2. These detectors are characterized by high efficiency, low sensitivity to neutrons, timing on the order of 1-2 nsec and gamma-ray energy resolutions of approximately 5-10 %. These detectors have been used for measurements of gamma rays both from light nuclei where the transition energies are large and the level density is small, and from rare earth elements where the density of gamma-ray transitions is so large that only continuum measurements are possible. Because we have 5 detectors, angular distribution coefficients can be obtained up to order a_4 in the usual Legendre polynomial expansion.

As an example of the data obtained with this system, fig. 3 shows typical data from the $^{12}C(n,n'\gamma)$ reaction. In fig. 3a, we have gated on neutrons between 4 and 15 MeV, in fig. 3b, we have gated on neutrons from 15 MeV to 200 MeV. As can be seen from the figure, the decay of the first excited state at 4.44 MeV dominates the low-energy-neutron spectrum while in the higher-energy-neutron spectrum gamma rays from the decay of the 15 MeV state are also seen. Fig. 4 shows the preliminary results for the a_2 angular distribution coefficients for the 4.44 MeV state as data points. Also shown in fig 4 are the evaluated a_2 coefficients (solid line) which were obtained with only two detectors. The reason for the large discrepancy between the two data sets is that in fitting our data we did not assume that the a_4 coefficients were zero as in the evaluated data. In fact our measurements show that the a_4 coefficients are often large.

Continuum measurements are much more difficult than measurements involving discrete lines for two reasons. First, it is essential that the detector response be

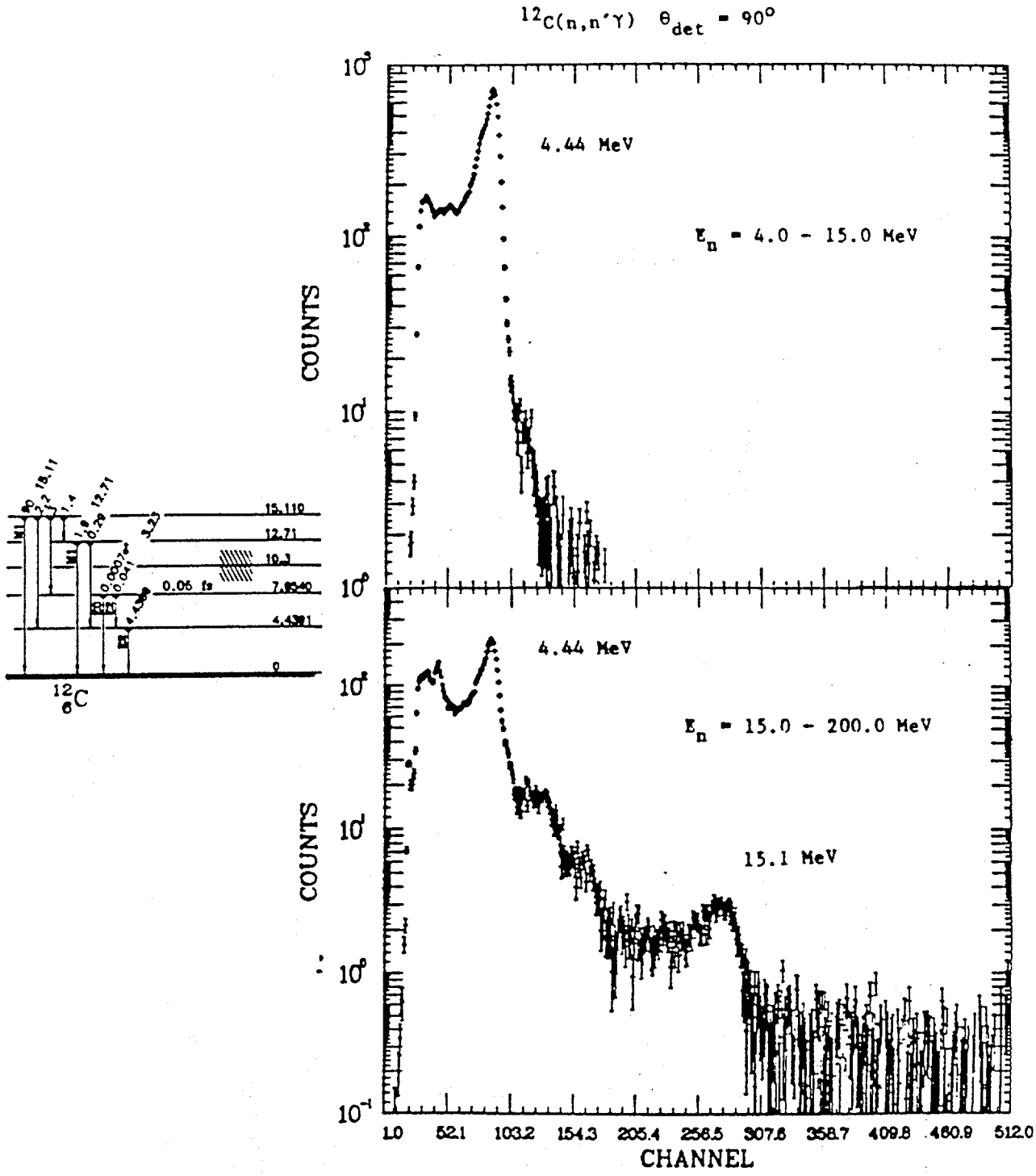

3. Pulse height spectrum measured for the $^{12}C(n,n'\gamma)$ reaction for neutrons in the energy bin a) 4 to 15 MeV, and b) 15 to 200 MeV.

unfolded from the pulse height spectrum and second, accurate determination of backgrounds becomes a major problem. Considerable effort has been put into measuring the response functions[3] of the BGO detectors and unfolding the response from the data. There are many components to the background which have to be removed from the data. Time uncorrelated background may be determined from data preceeding the beam pulse. Sample-independent, time-dependent backgrounds can be measured by running without a sample. Backgrounds associated with target containers may be determined from "empty-can" runs. The background most difficult to

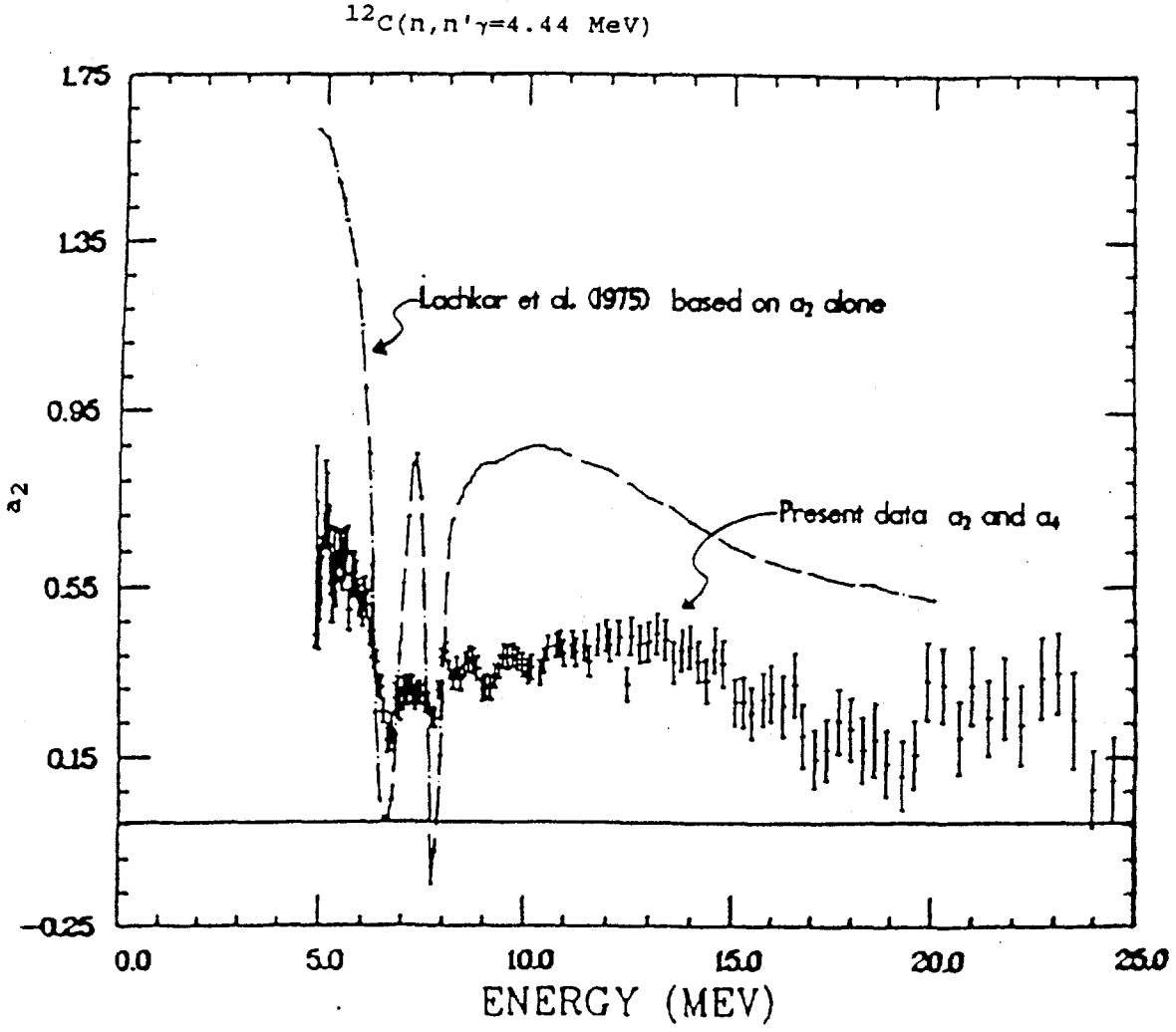

4. Preliminary a_2 angular distribution coefficients (data points) for the 4.44 MeV state in ^{12}C as a function of neutron energy measured in the $^{12}C(n,n'\gamma)$ reaction. The solid curve is the evaluated a_2 angular distribution coefficients assuming $a_4 = 0$.

determine comes from neutrons scattered from the sample depositing energy in the detectors. The data have been corrected for this background by measuring the pulse-height spectra for a Beryllium sample and determining the normalizing factor with a Monte-Carlo computer code.[4]

The second detector system for low energy gamma-rays consists of two Ge detectors at 90° and 125°. These detectors have excellent gamma-ray energy resolution so that it is possible to identify particular reactions by the energy of the gamma rays detected. The time resolution is on the order of 5 nsec, and their efficiency is typically 10% that of a 7.6 x 7.6 cm NaI detector. Fig. 5 shows the pulse height spectrum for the $^{nat}Fe(n,x\gamma)$ reaction for neutron energies between a) 26.8 and 29.8 MeV, and b) for neutron energies between 38.7 and 41.2 MeV. Identified on the plots are the (n,n'), (n,2n'), (n,p) etc. reactions that are observed. Fig. 6 shows preliminary results for the excitation function of the second excited state in ^{55}Fe (E_γ = 931 keV) excited in the (n,2n) reaction. The curve in fig 6 is a preliminary GNASH calculation[5] and the circles are data from Oak Ridge[6]. This type of measurement is very useful for checking calculational models as well as providing excitation function data for specific elements.

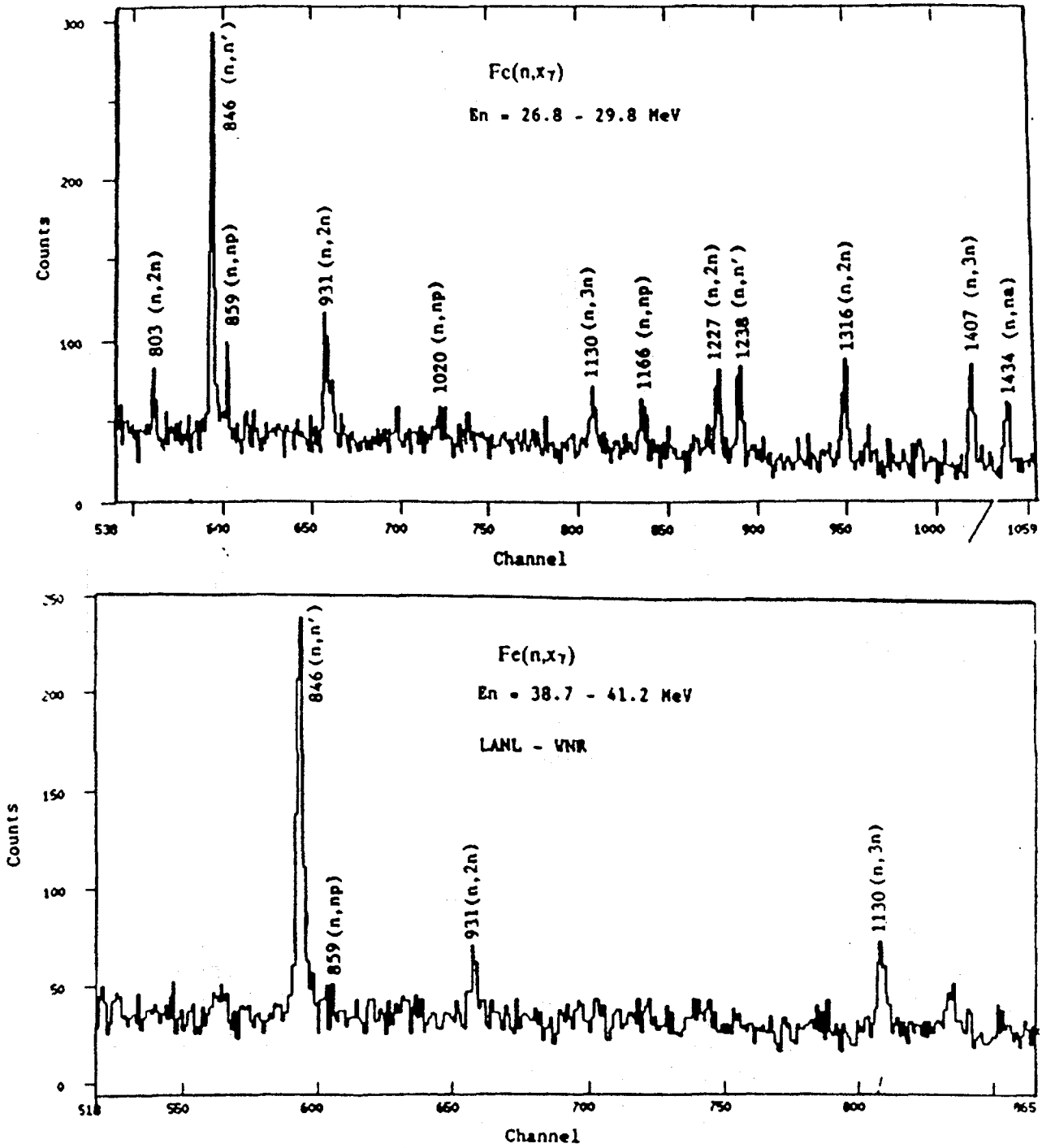

5. Pulse height spectrum for the $^{nat}Fe(n,x\gamma)$ reaction obtained using a Ge detector for a) 26.8-29.8 MeV and, b)38.7-41.2 MeV incident neutrons. The gamma rays are labeled by their energies (keV) and reactions.

For the energy range between 5 and 40 MeV we are using an actively shielded 10.2 cm diam by 15.2 cm long BGO detector. The detector and its 8.5 cm thick plastic anti-coincidence shield are surrounded by 10 cm of lead, approximately 5 cm of borated polyethylene and approximately 20 cm of polyethylene.

The goal of the experiments in the 5 to 40 MeV energy range is to measure the strengths, widths and locations of higher multipole resonances. In particular, we plan to measure the isovector giant quadrupole resonance (IVGQR) in

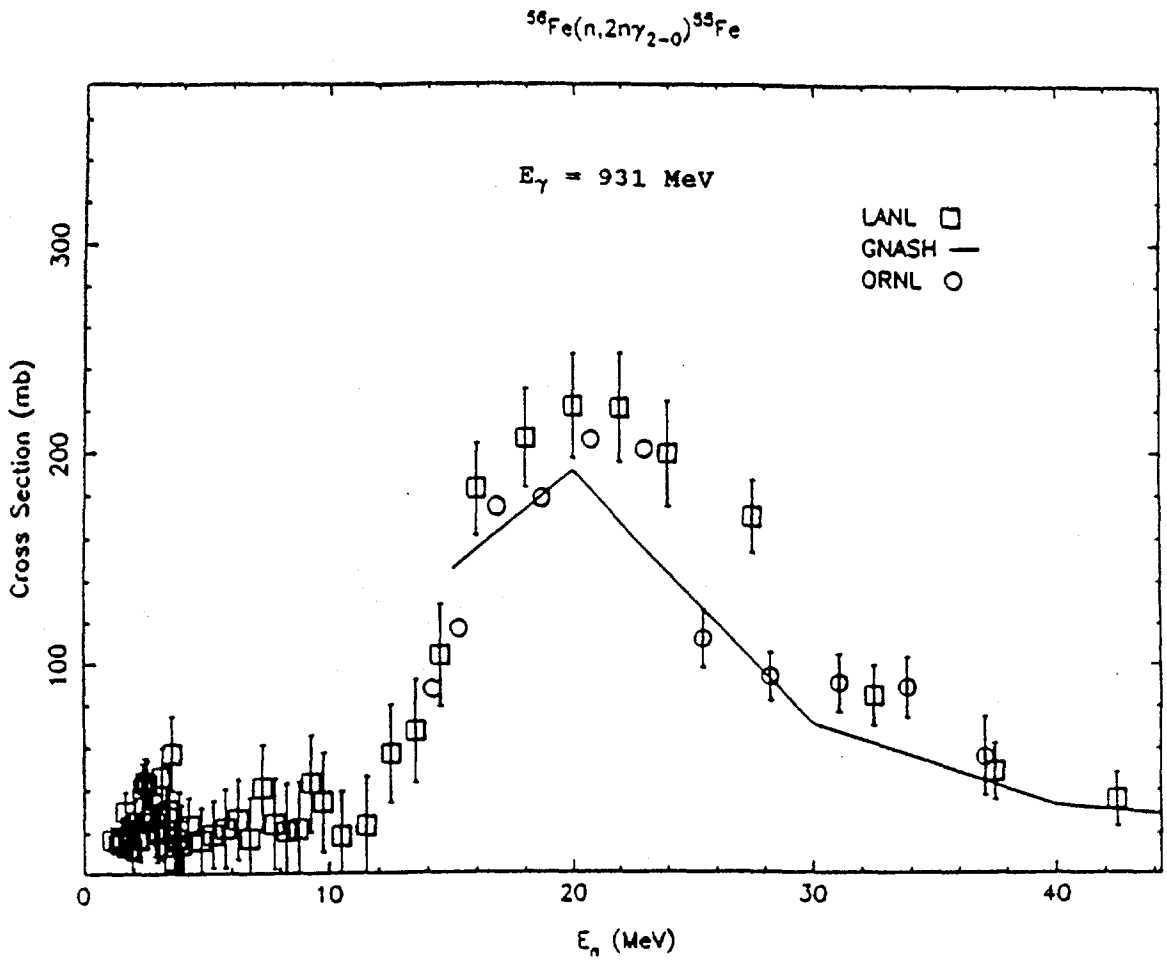

6. Preliminary values for the cross section as a function of neutron energy for the second excited state (E_γ=931 keV) in ^{55}Fe following the $^{56}Fe(n,2n)$ reaction. Also shown is data from Oak Ridge, and a preliminary calculation using the code GNASH.

^{40}Ca which is reported to be located at 34 MeV excitation energy. Because the neutron is uncharged, the effective charge, which multiplies the direct part of the capture amplitude, is small for multipoles greater than 1 (see ref. 8). The collective, or resonant, part of the capture amplitude is therefore not obscured by the direct part as is the case for proton capture. Evidence for E-2 strength is seen through its interference with the dominant electric-dipole radiation amplitude. This interference manifests itself as an asymmetry about 90° in the gamma-ray angular distribution. Fig. 7 shows pulse height spectra measured at 90° for several incident neutron energies obtained during a 33 hour run last year. The vertical lines bracket the expected location of the ground state gamma ray. As seen from this series of plots, the yield is good in the region of the giant dipole resonance (E_n=11 MeV). At higher energies, where the flux and cross section are lower, longer runs will be required to obtain better statistics. We are planning to continue this experiment in the 1990 run cycle to measure the fore-aft asymmetries and map out the IVGQR in ^{41}Ca.

There has recently been considerable interest in measuring the cross sections for neutron-proton bremsstrahlung (NPB) processes. In particular, the gamma-rays observed in heavy-ion reactions have been attributed to

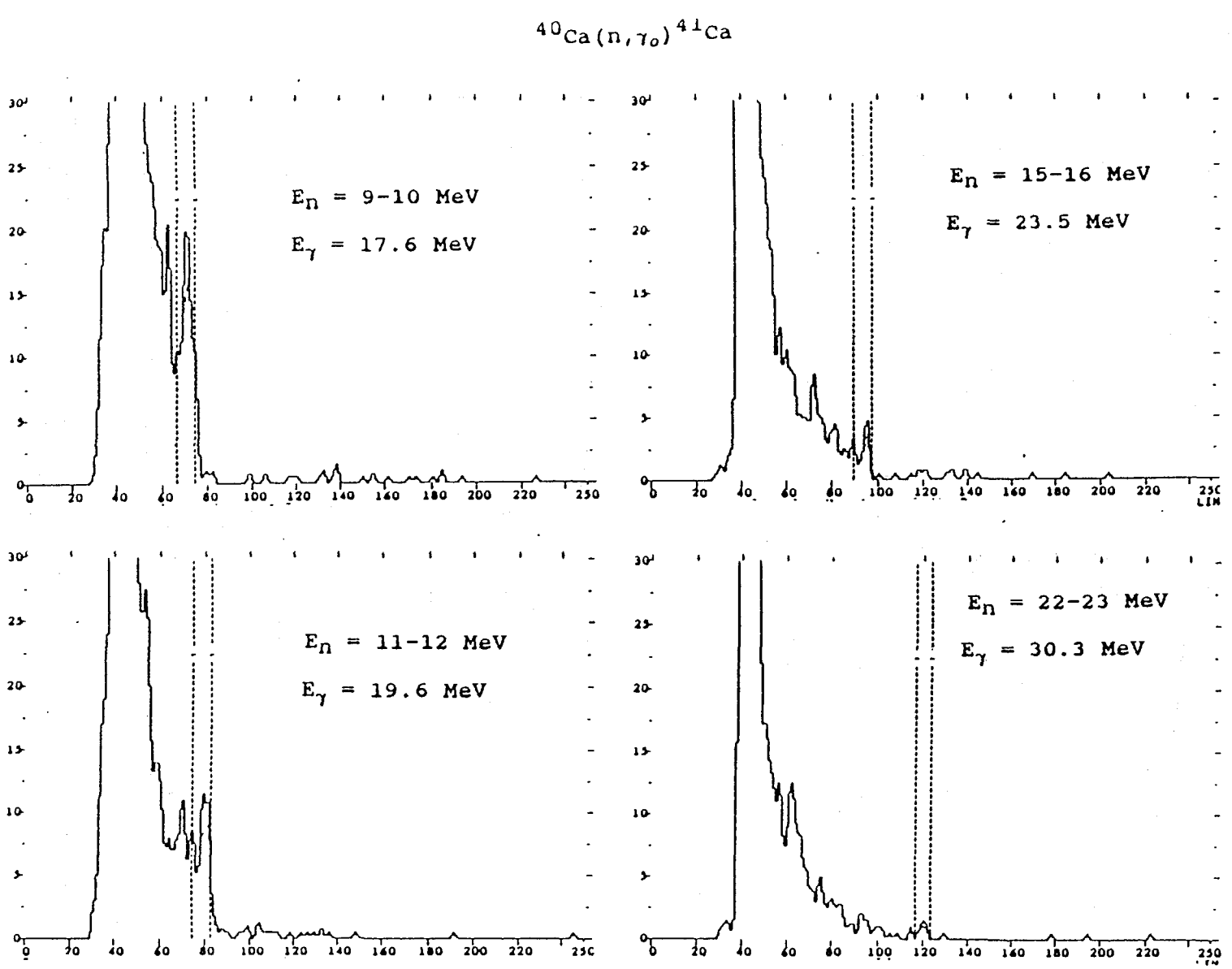

7. Pulse height spectra for various incident neutron energies on a natural Ca target. The vertical lines show the location of the expected ground state gamma ray.

NPB processes but the data are very sparse and it appears that some of the data may be in error. NPB provides a simple system for studying off-shell effects in the nucleon-nucleon potential. Meson-exchange currents have been calculated to be large and it has been suggested that contributions from heavier mesons may also be observed. For these reasons, we are considering performing a NPB measurement at the white neutron source.

Presently, we are studying two approaches to these measurements. The first involves measuring the scattered neutron and the recoil proton in calorimetric detectors. The second approach involves detecting the hard photons directly using a multi-element gamma-ray telescope. Such a detector is very insensitive to neutrons and therefore will have low background rates. This detector should be useful for detecting NPB events below the pion production threshold. Above the pion threshold it will be necessary to demand a coincidence with the recoil proton to unambiguously identify NPB events. The best experiment will probably involve measuring all three particles in coincidence. The goal for the 1990 run cycle is to install a multi-element gamma-ray detector at 90° and improve on a recent experiment done by the Grenoble group at SATURNE.

Conclusion

The white neutron source at LAMPF is an excellent tool for measuring photon-production cross sections for discrete gamma-ray lines over a wide gamma-ray and neutron energy range. Continuum measurements are somewhat more difficult because of the uncertainties in the backgrounds. Medium energy neutron physics experiments are made possible by the high energy component of the beam.

References

1. "The Los Alamos National Laboratory Spallation Neutron Sources", P.W. Lisowski, C.D. Bowman, S.A. Wender, and G.J. Russell, Nucl. Sci. and Eng. to be Published.

2. S. A. Wender, S.J. Seestrom-Morris, and R.O. Nelson, "A White Neutron Source From 1 to 400 MeV", J. of Phys. G 14(1988)S417.

3. S.A. Wender, G.F. Auchampaugh, H. Hsu, P.T. Debevec, S.F. LeBrun and S.D. Hoblit, Nucl. Instr. and Meth. A258 (1987) 225.

4. P. Ramakrishnan, G.E. Mitchell, C.R. Gould, S.A. Wender, and G.F. Auchampaugh, Nucl. Sci. and Eng. 98 (1987) 357.

5. P.G. Young, Private communication.

6. D.C. Larson in "Proceedings of the International Conference on Nuclear Data for Basic and Applied Science, May 13, 1985", Gordon and Breach, New York, NY. pg. 71

7. I. Bergqvist, R. Zorro, A. Hakansson, A. Lindholm, L. Nilsson, N. Olsson, and A. Likar, Nucl. Phys. A419 (1984) 509.

8. S.A. Wender, H.R. Weller, N.R. Roberson, D.R. Tilley, and R.G. Seyler, Phys. Rev. C25 (1982) 89.

Measurements of γ-ray production from $^{52}Cr(n,x\gamma)$ reactions at 14.6 MeV

S. Hlaváč and P. Obložinský

Institute of Physics of the Slovak Academy of Sciences
842 28 Bratislava, Czechoslovakia

Abstract: Highly enriched sample of ^{52}Cr was irradiated by 14.6 MeV neutrons. Measured were discrete γ ray production cross sections, total γ ray spectrum as well as coincident data such as average γ ray multiplicities.

1. Introduction

Chromium is among basic elements of constructional materials and its interactions with neutrons are of interest for both the fusion and fission reactor technology. Among these interactions a specific role is played by $(n,x\gamma)$ reactions. To study in more detail various γ emission modes in these reactions as well as to measure relevant γ ray production cross sections we have developed a multidetector system associated with a compact 14 MeV neutron generator.[1)]

In this report we summarize a set of quite complete measurements of γ ray production in $^{52}Cr(n,x\gamma)$ reactions at the incident neutron energy of 14.6 MeV. These include discrete γ ray production cross sections together with their angular distributions, total γ ray spectrum up to the maximum spectral energy possible, and also average γ ray multiplicities for cascades defined by specific discrete γ ray or by energy of emitted neutron. For more detail reports the reader is referred to Refs.2-4.

2.Experimental procedure

The multidetector system utilizes fully the advantage of associated α particles from D-T reaction for timing as well as mechanical collimation of neutron beam. Both timing and collimation resulted in low background in γ and neutron spectrometers. The whole system is described in detail elsewhere[1)], therefore only brief description of the whole setup will be given here.

Schematic drawing of the experimental set-up is shown in fig.1. Deuteron beam from a small compact accelerator impinges on the TiT target. Part of the neutrons flow through

---

*) Contribution presented by S. Hlaváč

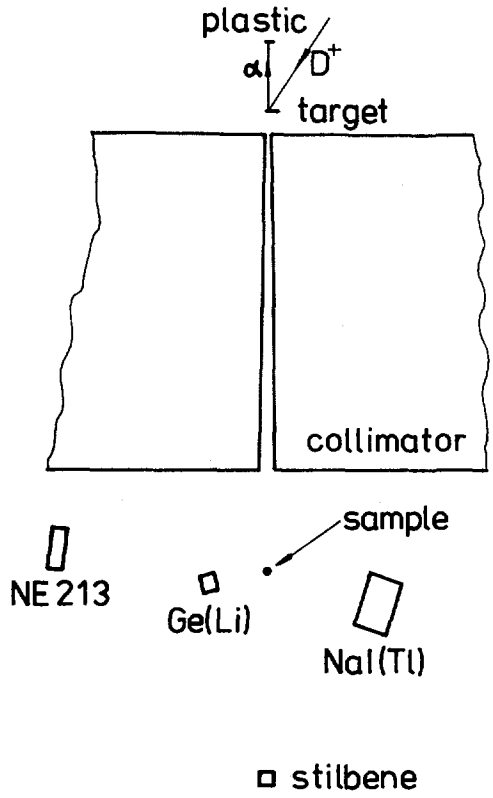

Fig.1. Simplified drawing of the experimental arrangement.

a massive collimator with length of 155 cm and solid angle of $4\pi \times 2.2 \times 10^{-4}$. Energy of the collimated neutrons is 14.6(0.2) MeV. Associated α particles are detected by a carefully positioned fast plastic scintillation detector. Solid angle of the α particle detector is slightly greater than the solid angle of the neutron collimator.

Collimated neutrons reach the scattering sample, which is located on the collimator axis at the typical distance of 200 cm from the TiT target. In this experiment we used enriched ^{52}Cr sample (enrichment 99.8 %, weight 119.8 g) in metallic powder form borrowed from the Techsnabexport, Moscow. The sample was filled in a thin polyethylene bag (weight 1.5 g) of cylindrical shape (Φ 3.5 cm x 6.5 cm). Its average thickness was 0.061 at/barn.

Gamma rays as well as scattered neutrons from the sample were observed by spectrometers located around it. Discrete γ rays were detected by a 70 cm^3 Ge(Li) spectrometer at 6 angles, ranging from 42° to 156° towards the collimated neutron beam. Detector distance from the sample was 20 cm (15 cm at 90°). Absolute cross section measurement was performed at 90°, at all other angles cross sections relative to this value was measured. Absolute detector efficiency was measured and in situ checked for all angles. Time resolution of the Ge(Li) detector with respect to the α particle detector was 9.8 ns FWHM.

The total γ ray spectrum from the threshold of .18 MeV up to 25 MeV was observed by Φ 16cm x 10 cm NaI(Tl)

spectrometer. The spectrometer was placed at the first minimum of the elastic scattering of 14 MeV neutrons on ^{52}Cr, at 70° towards the incident beam, in order to suppress the fraction of neutrons detected by the NaI(Tl). The neutrons were further discriminated by time of flight technique. The distance between the front face of the spectrometer and the center of the scattering sample was 30.4 cm. Time resolution of the detector was 7.5 ns FWHM.

In n-γ coincidence measurements in addition to γ spectrometersa NE213 liquid scintillation neutron spectrometer was utilized. Dimensions of the scintillator were Φ 12cmx4 cm. Detector was placed at the distance of 60 cm from the center of the sample at an angle of 100° towards the neutron beam. The time of flight method was used for neutron spectrometry with pulse shape discrimination against unwanted detection of γ rays. The time resolution of neutron spectrometer was 2.4 ns.

Absolute neutron flux was determined by α particle counting provided by the associated particle detector. Another neutron monitor based on stilbene scintillator with dimensions of Φ 4cm x 4 cm was placed on the collimator axis at the distance of 180 cm behind the scattering sample. From this detector singles as well as coincidences with the associated particle detector were recorded. Ratio of coincidence to single counts observed with stilbene monitor provided a correction factor for geometrical efficiency of the whole setup. In an ideal case this ratio is unity but finite dimension of deuteron beam spot and geometrical misallignement make it lower. Our typical value during the measurement was close to 0.8.

2.1. Discrete γ ray production cross sections

Cross sections and angular distributions of discrete γ rays produced in $^{52}Cr(n,x\gamma)$ reaction were determined from the γ ray spectra observed by the Ge(Li) detector.Only prompt γ rays were recorded in multichannel analyzer as determined by coincidence tagg provided by the associated particle detector.

The γ ray spectra were analysed using nonlinear least square code GWENN[5]. Corrections for neutron and γ ray absorption as well as for voluminous sample, but not for multiple scattering, were applied. Uncertainties were obtained assuming independent contribution from the Ge(Li) absolute efficiency (typical value 8 %), peak area (1 - 15 %) and neutron fluence (3 %).

Angular distribution of γ rays can be described by the expression

$$d\sigma/d\omega = \sigma/4\pi \ (\ 1 + a_2 P_2(\cos \vartheta) + a_4 P_4(\cos\vartheta)).$$

The angle integrated cross sections as well as the Legendre coefficients a_2, a_4 were extracted from the observed angular distributions using weighted linear least squares method.

Tab.1. Angle-integrated production cross sections and Legendre coefficients for angular distributions of discrete γ rays emitted from $^{52}Cr(n,x\gamma)$ reactions at 14.6 MeV.

E_γ(keV)	Reaction	a_2	a_4	$\sigma_{4\pi}$(mb)
647.4	(n,n'γ)	0.33(14)	-0.02(17)	70(4)
704.6	(n,n'γ)	-0.19(11)	-0.11(15)	42(3)
744.2	(n,n'γ)	0.39(13)	-0.01(18)	71(4)
749.1	(n,2nγ)	0.42(13)	0.26(20)	42(1)
848.2	(n,n'γ)	0.60(16)	0.60(20)	38(3)
935.5	(n,n'γ)	0.31(09)	0.12(12)	237(9)
1164.4	(n,2nγ)	-0.52(19)	0.13(20)	36(4)
1246.2	(n,n'γ)	-0.59(17)	0.10(19)	39(4)
1333.6	(n,n'γ)	0.31(09)	0.04(12)	205(8)
1434.1	(n,n'γ)	0.12(08)	0.04(11)	783(30)
1530.7	(n,n'γ)	0.04(15)	0.74(18)	40(3)
1727.5	(n,n'γ)	-0.90(30)	0.32(28)	26(4)

Uncertainties were obtained by normal matrix inversion. The angle integrated cross sections and Legendre coefficients are given in tab. 1.

2.2 Total γ ray spectrum

Total γ ray spectrum from the $^{52}Cr(n,x\gamma)$ reactions was determined from pulse height spectrum observed by the NaI(Tl) spectrometer. In order to subtract background from the continuous pulse heigth spectrum a two-parametric spectrum energy (256 channels) x time(32 channels) was recorded. The whole matrix was processed so that neutron component and random background were subtracted to get the net γ ray energy pulse height spectrum.

The net pulse height spectrum was unfolded by means of the code UNFOLD[6]. Response matrix for the monoenergetic γ rays incident on the NaI(Tl) was deduced from the experimentally observed lineshapes for a number of discrete γ lines. They were measured using standard radionuclides for γ rays up to E_γ < 3 MeV. For higher energies we used reactions $^{12}C(n,n'\gamma)$, $^{11}B(p,\gamma)$ and $^{3}He(p,\gamma)$. The absolute efficiency was determined by the coincidence technique.[1]

The resulting γ ray energy spectrum is still distorted by interactions of primary γ rays in the sample itself. Only part of these interactions led to γ ray absorption since major interactions for γ rays with energy of several MeV proceed via the Compton scattering and pair production. To account for the above effects we applied the second unfolding. The response matrix refered now to the distortion of primary γ rays by interactions in the voluminous sample. The response was calculated using realistic γ ray absorption coefficients and theoretical prescriptions for the Compton scattering and pair production. Bremsstrahlung radiation was assumed to follow the low frequency approximation that

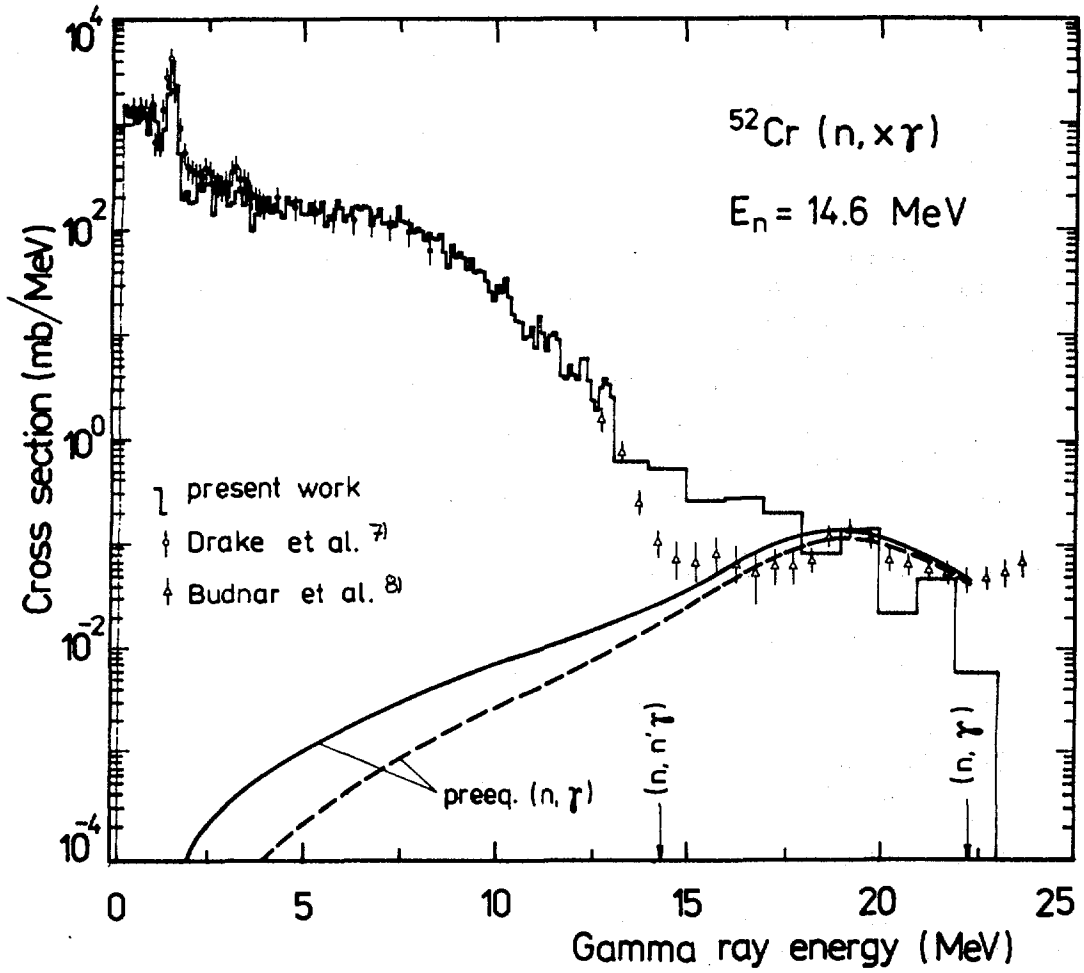

Fig.2. Observed total γ ray spectrum from ^{52}Cr(n,xγ) at14.6 MeV. Shown for comparison is the spectrum by Drake et al.[7] and at the high energy part the spectrum by Budnar et al.[8]

implies $1/E_\gamma$ distribution function, where E_γ is the energy of created γ ray. Efficiences were calculated as the number of γ rays emitted from the sample relative to the number of primary γ rays. This procedure changed the spectrum in average by several percent (-7.5% at 2 MeV and +3% at 10 MeV).

Differential cross sections of γ ray production from ^{52}Cr(n,xγ) reaction at ϑ = 70° are summarized in ref. 4.Total γ ray production spectrum is obtained by multiplying the observed 70° spectrum by a factor of 4π, neglecting thus a possible angular anisotropy of emitted γ rays. The final spectrum is shown in fig. 2. Comparison is made with the spectrum as measured by Drake et al[7] for ^{nat}Cr at 14.2 MeV under 90° in the spectral energy range E_γ=0.4-8.5 MeV. Accord of the spectra seems good in view of the differences in the experimental conditions. Peaks in the low energy region of our spectrum are less pronounced because of the modest energy resolution of our spectrometer.

Further comparison is made with the high energy part of the spectrum (E > 12.5 MeV) measured by Budnar et al[8] for

^{nat}Cr at 14.6 MeV. The accord is reasonable except for the energy range E_γ = 14 - 18 MeV, where our spectrum exceeds the data of ref.8 by about a factor of 3. A possible explanation might be in contribution from the strong (n,n'γ) channel via high energy tails in the response functions of about 10 - 12 MeV γ rays.

Two integral quantities are of special interest, the energy- angle integrated total γ ray production cross section and the average energy per γ ray emitted. Integration of our spectrum over the entire spectral energy range of 0.2-22.3 MeV yields σ_γ^{tot} = 3540(230) mb, while the energies 0.2-0.5 MeV contribute by 430(30) mb and the energies above 8.5 MeV by 101(11) mb. The centroid of the spectrum means the average γ ray energy. Our spectrum yields E_γ(n,xγ) = 2.49(0.15) MeV.

2.3. Coincidence measurements

In this section we present complete set of our experimental data for the ^{52}Cr sample obtained by γ-γ and n-γ coincident in-beam techniques. This data are of two types, first average length of γ ray cascades were determined. These γ ray multiplicities refer either to cascades selected by presence of discrete γ ray transition or to γ cascades selected by entry energy of the cascade, determined by the energy of scattered neutron.

The coincidence measurements were performed with Ge(Li), NaI(Tl) and NE213 spectrometers. Their distances from the center of the ^{52}Cr sample and angular positions with respect to the incoming neutron beam were (15cm,-70°), (30cm,70°) and (60cm,100°) for the Ge(Li), NaI(Tl) and NE213 detectors, respectively. First, we measured two spectra of Ge(Li) and NE213 spectrometers in coincidence with another γ ray detected by the NaI(Tl) spectrometer. Second, two parametric spectrum comprising of neutron tof events as observed by the NE213 in coincidence the with energy of γ ray events observed by the NaI(Tl). In addition, we recorded singles spectra from all the spectrometers. Data were collected by means of standard analyzers and low rate CAMAC based two-parametric data acquisition system.

Average γ ray multiplicities were obtained by comparing coincident to singles Ge(Li) yields and by comparing coincident to singles neutron tof spectra[1]. Absolute scale was retained by using measured total efficiency of the NaI(Tl). Energy -angle differential cross sections for exclusive neutron spectrum were obtained under the assumption that the angular correlation between neutron and discrete γ ray transition (predominantly 1434.1 keV, $2^+ \rightarrow 0^+$(g.s.)) is weak. We used relation

$$d^2\sigma/dE_n d\omega_n = 4\pi\, d^3\sigma / dE_n d\omega_n d\omega_\gamma = N_{n\gamma} / 4\pi\Phi A\Omega_n \Omega_\gamma^{phot},$$

where $N_{n\gamma}$ is the observed intensity per 1 MeV in the neutron spectrum as measured in coincidence with discrete γ

transitions detected by the NaI(Tl), Φ stands for neutron fluence, A is the number of target nuclei, Ω_n is the absolute NE213 efficiency including solid angle and Ω_γ^{phot} is the absolute photopeak efficiency of the NaI(Tl).

Average γ ray multiplicities of cascades passing through specific low lying discrete transitions were observed in 8 instances in the $(n,n'\gamma)$ channel. The results are summarized in tab.2. Included in the uncertainties are statistical error in determining the peak area of coincident as well as singles Ge(Li) spectra, 5% uncertainty of the NaI(Tl) total efficiency and estimated 3% uncertainty of applied corrections.

Tab.2. Average γ ray multiplicities of cascades passing through specific discrete γ transitions in $^{52}Cr(n,x\gamma)$.

Transition (keV)	Multiplicity
647.4, $4^+ \Rightarrow 4^+$	5.6(0.6)
704.6, $(3^+) \Rightarrow 4^+$	6.8(0.7)
744.2, $6^+ \Rightarrow 4^+$	5.8(0.6)
848.2, $5^+ \Rightarrow 4^+$	4.8(1.5)
935.5, $4^+ \Rightarrow 2^+$	3.7(0.3)
1246.2, $5^+ \Rightarrow 4^+$	4.4(1.4)
1333.6, $4^+ \Rightarrow 2^+$	3.7(0.4)
1434.1, $2^+ \Rightarrow 0^+$	3.7(0.2)

Average γ ray multiplicities of cascades following emission of a neutron with specific energy are summarized in fig.5. Multiplicities were extracted from ratios of given bins of coincident and singles neutron tof spectra. Background was subtracted from the raw spectra by the procedure devised by Klein et al[9]. The uncertainties quoted are basically due to statistical error in coincident neutron spectrum. Uncertainties in neutron energies run from about 20% at 1.5 MeV up to about 35% at 10 MeV. In the energy region where the (n,2n) channel is open long $(n,n'\gamma)$ cascades are mixed with much shorter ones from $(n,2n\gamma)$. Most of the secondary neutrons observed from (n,2n) channel in the present experiment, however, refer to process leading directly to the ground state of ^{52}Cr.

The two-parametric spectrum n_{tof} versus γ_{energy} was used to extract neutron spectrum in coincidence with 1434 keV γ rays. These refer to the strong $2^+ \rightarrow 0^+$ g.s. transition in ^{52}Cr which cumulates almost all $(n,n'\gamma)$ cross section. Pertinent neutrons, therefore, represent practically complete (n,n') component with no admixture from the (n,2n) channel. In our case the 1434.1 keV peak should contain small contribution from nearby 1333.6 keV and perhaps also from 1246.2 keV γ lines. This admixture was taken into account using our singles Ge(Li) data and thus double counting of coincident neutrons was eliminated. The resulting exclusive neutron spectrum is shown in fig.4.

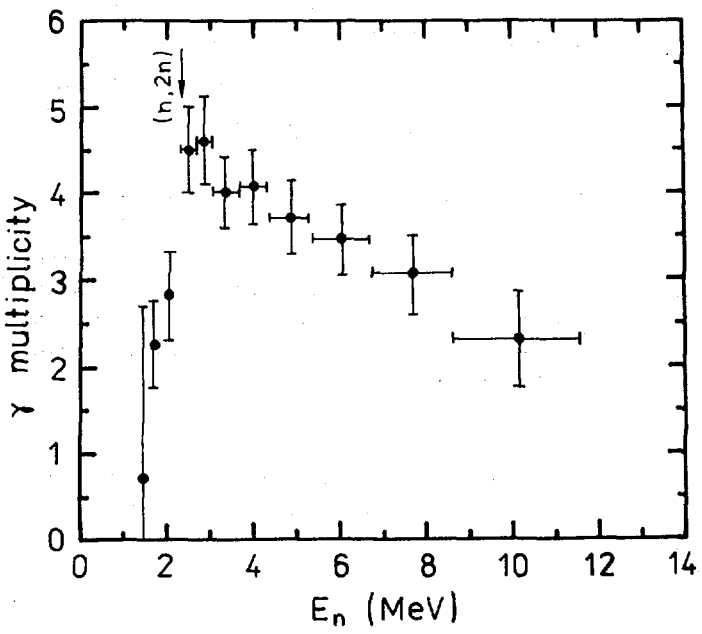

Fig.3. Average γ ray multiplicity as the function of observed energy of emitted neutron in the laboratory frame. Shown by an arrow is the (n,2n) threshold.

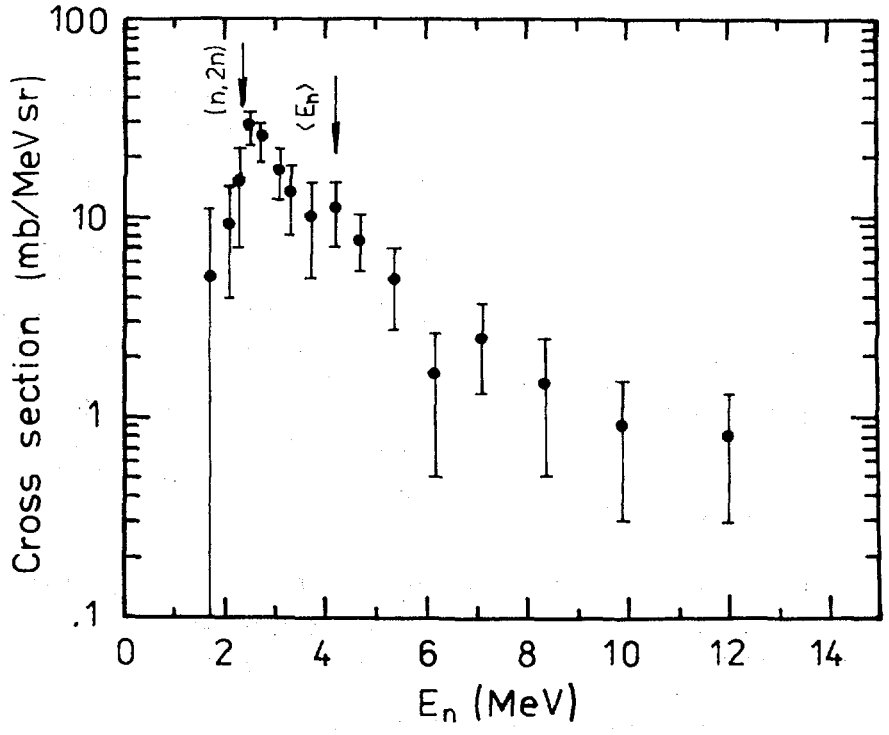

Fig.4. Exclusive spectrum of neutrons from the ^{52}Cr(n,n') channel. Average neutron energy indicated by arrow is 4.19(.17) MeV.

3. Discussion

Experimental data on γ ray production measured in this work, i.e., discrete γ ray production, total γ ray production spectrum and the coincident γ-γ and γ-n data provide rather complete information related to γ production. Since an overlap between them exists one can check internal consistency of the whole data set. The three pieces of data were obtained in independent, slightly different experimental conditions and in fact in different experimental runs. By cross checking of the data one can identify a possible systematical error in one piece of the data and to achieve higher reliability of the whole set.

The γ ray production cross section integrated over the peak in the spectral energy range 1.2-1.6 MeV is 937(70) mb. This can be compared with the γ production cross section as measured with Ge(Li) spectrometer. Four discrete γ lines were observed int his energy range. Major contribution comes from the dominant 1434.1 keV γ line that amounts to 783(30) mb. By adding the cross sections of the 1246.2, 1333.6 and 1530.7 keV γ lines one gets 1067(41) mb in good accord with the above value.

The total γ ray production cross section, 3540(230) mb, can be compared with that deduced from the discrete γ ray production cross sections and the average γ multiplicities. It holds

$$\sigma_\gamma^{tot} = \sigma(n,n'\gamma)M(n,n'\gamma) + \sigma(n,2n\gamma)M(n,2n\gamma) + \sigma(n,ch.p.\gamma)M(ch.p.,\gamma),$$

where $\sigma(n,n'\gamma)$ is the cross section of neutron inelastic scattering, $M(n,n'\gamma)$ is the average γ ray multiplicity in the same channel and similar notation is used for the $(n,2n\gamma)$ channel and the sum of channels involving charged particles. Using our data for $(n,n'\gamma)$ channel, data of refs.10,11 for n(n,2n) and (n,ch.p.) channels one gets

$$\sigma_\gamma^{tot} = \frac{1}{.918}(783\pm30)(3.7\pm.2) + (78\pm6)1 + (134\pm8)(2.5\pm.5) =$$

$$= 3570 \pm 250 \text{ mb.}$$

This cross section agrees well with the value obtained from the total γ production spectrum.The factor 1/.918 accounts for the γ cascades that do not pass through the first 2_1^+ state.

Our final check concerns the average energy per one γ ray emitted. The total γ ray spectrum yields $E_\gamma(n,x\gamma) = 2.49$ (.15) MeV. In the $(n,n'\gamma)$ channel itself one should thus have somewhat higher energy $E_\gamma(n,n'\gamma) \cong 2.6(.2)$ MeV. This average can be compared with that deduced from our coincident data. Exclusive neutron spectrum gives for the average energy of inelastic neutrons $E_{n'} = 4.19(.17)$ MeV. This implies that the

energy left for γ cascades in the (n,n'γ) channel is

$$E_{exc}(n,n'\gamma) \cong [(14.6\pm.2) - (4.19\pm.17)\ 52/53 \cong 10.20 \pm .25 \text{ MeV}.$$

Using $M(n,n'\gamma) \cong M_{1434} = 3.7(.2)$ one gets

$$E_{\gamma}(n,n'\gamma) = 10.20(.25)/3.7(.2) = 2.76(.16) \text{ MeV}.$$

in agreement with the value obtained from the total γ ray spectrum.

Integrated cross section of the total γ ray spectrum for spectral energies in excess of 14.6 MeV yields the value

$$\sigma(n,\gamma) = 1310\ (160)\ \mu b,$$

where the uncertainty does not include the contribution from the unfolding procedure. This cross section seems to be higher than that reported by Budnar et al.[8], who give 750(110) μb. Their value, though refers to ^{nat}Cr rather than ^{52}Cr and to 14 MeV neutrons rather than 14.6 MeV ones.

In conclusion we stress that, to the best of our knowledge, the above data represent the most comprehensive γ emission data set at 14 MeV neutron incident energy ever measured for one isotope.

References

1. S. Hlaváč and P. Obložinský, Nucl. Instr. Meth. 206 (1983) 127.
2. P. Obložinský and S. Hlaváč, in Report INDC(CSR)-6/GI (IAEA, Vienna 1985) pp.17-25.
3. S. Hlaváč and P. Obložinský, Report INDC(CSR)-011/GI (IAEA, Vienna 1989).
4. P. Obložinský and S. Hlaváč, Report INDC(CSR)-013/GM, (IAEA,Vienna 1988).
5. Š. Gmuca and I. Ribanský, Jaderná energie 29(1983 6.
6. R. S. Simon, code UNFOLD, GSI Darmstadt 1978 (unpublished).
7. D. M. Drake, E. D. Arthur and M. G. Silbert, Report LA-5893-MS (LASL, Los Alamos 1975).
8. M. Budnar, F. Cvelbar, E. Hodgson et al., Report INDC(YUG)-6/L (IAEA, Vienna 1979).
9. H. Klein et al. Report INDC(NDS)-146, (IAEA, Vienna 1983) p.191.
10. I. Ribansky, T. Pantelejev and L. Stoeva, Report INDC(CSR)-6/GI, (IAEA, Vienna 1985) p.1.
11. S. M. Grimes, R. C. Haight, K. R. Alvar, H. H. Barshall and R. R. Borchera, Phys. Rev.C19 (1979) 2127.

PROMPT γ-RAYS FROM ^{232}Th, ^{235}U, AND ^{238}U FISSION FRAGMENTS

A.A.Filatenkov, S.V.Chuvaev

V.G.Khlopin Radium Institute, Leningrad, USSR

Abstract: An analysis of spectra of prompt γ-rays emitted at the ^{232}Th, ^{235}U, and ^{238}U fission induced by 3 MeV and 15 MeV neutrons is presented. Energies and yields of about 30 γ-transitions have been determined in the time interval of 25 ns. An availability of the method used is discussed for investigation of the induced fission and for obtaining of the spectroscopic information on nuclei laying far from the beta-stability valley.

Introduction

The spectra of γ-radiation, which arise at interaction of fast neutrons with fissile nuclei, contain usually a remarkable contamination of γ-rays emitted by fission fragments. Its share of the total γ-ray production cross section may exceed 50% . In the spectra the fission γ-rays appear mainly in the form of an intense component with a continuous, exponentially failed energy distribution. At the same time, it is also possible to observe some individual γ-peaks from fission fragments having high yields, because their cross sections are of order of tens millibarns. The presence of these peaks essentially complicate the spectra treatment and increase the uncertainty of results (for examples, at the (n, n'γ)-reaction study). On the other side, these peaks contain an important information on γ-transitions occuring in fission fragments in time interval of 10^{-14} - 10^{-8} s, i.e. just after neutron emission and before beta-decays, and, therefore, they may be used for a more detailed investigation of fission dynamics and for obtaining a new spectroscopic data on short-living neutron-enriched nuclei.

Recently, at the analysis of the ^{232}Th, ^{235}U, and ^{238}U γ-spectra measured in-beam at neutron energy 3 MeV about 30 γ-transitions have been interpreted as being the fission fragment ones /1/. The identification have been done by a comparison of the experimental energy values and excitation cross sections of the γ-transitions with the corresponding values obtained from the available data on fission cross sections /2, 3/, on fission fragment yields /4/, and on level schemes of nuclei /5, 6/. The present work is a development of the work /1/. In this the results obtained at 3 MeV are considered together with results obtained at neutron energy about 15 MeV where the fission γ-rays become predominant.

Experiment

The measurements have been performed at the neutron generator NG-400 working in a pulse mode. Neutrons were produced in the ^{2}H(d, n)^{3}He and ^{3}H(d, n)^{4}He-reactions at the deuteron

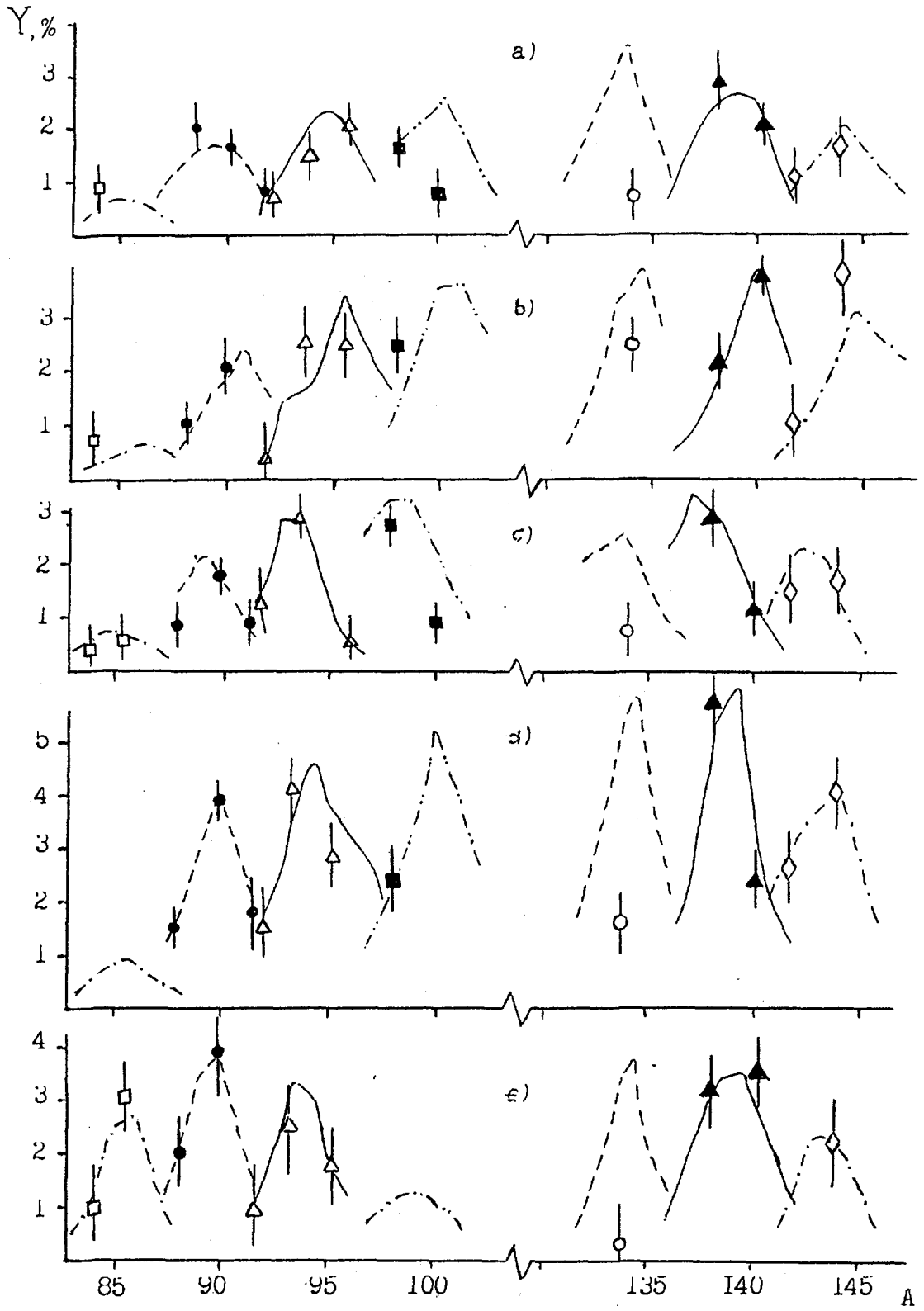

Fig. 1. The yields of the $2^+ - 0^+$ γ-transitions of even-even fragments. a) ^{238}U, E_n=15 MeV, b) ^{238}U, E_n=3 MeV, c) ^{235}U, E_n=15 Mev, d) ^{235}U, E_n=3 MeV, e) ^{232}Th, E_n=15 MeV. ◻ - Se isotopes , ◆ - Kr, △ - Sr, ● - Zr, ◇ - Te, ▲ - Xe, ◊ - Ba. Lines are the evaluated fission fragment yields /4/. At neutron energy 3 MeV the evaluation was used for "fast" neutrons.

energy 300 keV. The metallic cylindrical samples made of monoisotopes were used. Its weights were 117, 100 and 187 g respectively for ^{232}Th, ^{235}U and ^{238}U. The background was measured with a carbon sample and without the sample. The γ-rays were registered in the time interval of 25 ns with a Ge(Li)-detector, which was surrounded by a shield consisting of iron, borated polyethylene and lead. The neutron flux was determined by three scintillator counters, placed at 0, 30, and 90 degrees with respect to the beam.

The corrections for neutron field distorsion and γ-rays self-absorption, occuring in thick samples were calculated by Bthe Monte-Carlo method. To check its correctness the additional measurements have been carried out with a thin plate made of ^{238}U, and with an iron cylinder of the same dimensions as the ^{238}U-cylinder. The experimental set-up and the data treatment were described in more detail elsewhere /1, 7, 8/.

Results

In the six mesured γ-spectra several hundreds of γ-peaks have been revealed. The most of them had an individual character for each spectrum and were related to the (n, n$'\gamma$)-, (n, 2nγ)-, and (n, 3nγ)-reactions. The full spectra were carefully analysed at neutron energy 3 MeV /9/. Besides, in all the six spectra the γ-transitions were observed, that had coinciding energies and were absent in the background spectra. Naturally, these γ-transitions were assigned to the fission fragments.

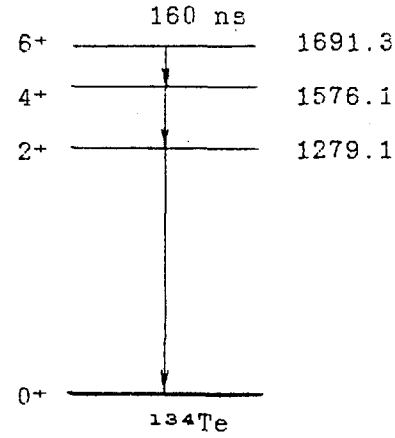

Fig. 2. The level scheme of ^{134}Te.

Among them the γ-transitions $2^+ - 0^+$ of even-even fission fragments were exhibited most clearly. In Fig. 1 its measured yields are compared with the evaluated independent yields of the corresponding fission fragments that were taken from /4/. Generally, the agreement is quite satisfactory.

The only remarkable exception is the γ-transition 1279.1 keV of ^{134}Te whose yield is noticeably lower. It may be explained by a peculiarity of the level scheme of this nucleus (Fig. 2). The level 1691.3 keV 6^+ is isomeric, its lifetime is 160 ns. Since in the experiment the γ-rays were measured that were

emitted in a time interval of 25 ns, then only 10% of γ-cascades going through this level could be registered. Thus, the observed low intensity of the γ-transition 1279.1 keV presents evidence for a large contribution of high spin states at forming of fission fragments.

Another confirmation of high angular momenta of fragments is observation of the γ-transitions $4^+ - 2^+$ and $6^+ - 4^+$ for some nuclides (e.g. ^{138}Xe, ^{140}Xe, ^{142}Ba, ^{144}Ba). The average intensities of these transitions were, in units of independent fragment yield, 0.8 and 0.6, respectively.

Assuming that the fragment spin distribution is described in this case by

$$N(J) \sim (2J+1) \cdot \exp[-J(J+1)/2\beta^2]$$

the average fragment spin β may be deduced. It proved to be (5.5 + 1.5) h.

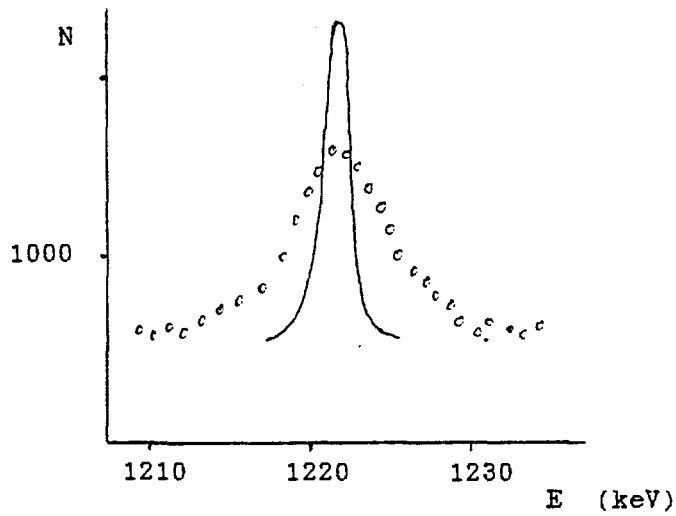

Fig. 3. The γ-peak 1222.8 keV region (^{235}U, E_n=15 MeV) The full line - the energy resolution of the spectrometer.

There was also a possibility found to deduce the level lifetime. In Fig. 3 the region of the γ-line 1222.8 keV is shown, that appears to correspond to the transition $2_1^+ - 0_1^+$ of ^{98}Zr. There was no other relevant candidate found for this transition. In all spectra the peak intensities proved to agree with the expected yields of the ^{98}Zr. At the same time, the line width exceded considerably the energy resolution of the spectrometer in this region. Therefore, we have assumed, this is due to the Doppler broadening of the γ-line emitted from the not entirely stopped fragment. Using the stopping power tables for heavy ions /10/ we evaluate the lifetime of the state 1222.8 keV 2^+ of the ^{98}Zr 2.0 ps. Then, the quadrupole momentum and the deformation parameter of the ^{98}Zr may be deduced. For this we have used the following relations:

$$(\tau)^{-1} = 1.22 \cdot 10^{9} (E)^{5} \cdot B(E2)$$

$$B(E2; K I_1 \to K I_2) = \frac{5}{16\pi} e^2 Q_0^2 \langle I_1 K_2 20 | I_2 K \rangle^2$$

$$Q_0 = \frac{4}{3} \langle \sum_{K=1}^{Z} r_K^2 \rangle \cdot \delta$$

Table 1.

A Z	^{84}Zr	^{86}Zr	^{88}Zr	^{90}Zr	^{92}Zr	^{94}Zr	^{96}Zr	^{98}Zr	^{100}Zr	^{102}Zr
δ	0.250	0.149	0.187	0.091	0.103	0.090	0.081	**0.12**	0.321	0.421

In table 1 the evaluted deformation parameters of zirconium isotopes are listed /11/. The parameter obtained by us for the ^{98}Zr (that was not presented in /11/) agrees well with a given systematic showing the ^{98}Zr-nucleus occupying the intermediate place between the round ^{96}Zr and the deformed ^{100}Zr.

Conclusion

In the present work the energie and yields of about 30 γ-transitions have been determined that were emitted by fission fragments in the time interval less than $2*10^{-8}$ s. The $2^+ - 0^+$ transition yields are shown to be close to the independent yields of the corresponding fission fragments. The insufficient intensity of the 1279.1 keV γ-transition of ^{134}Te is due to the large lifetime of the 1691.3 keV 6^+ state, through that the main part of γ-cascades appear to go. The observation of some γ-transitions $6_1^+ - 4_1^+$ and $4_1^+ - 2_1^+$ indicate also that the fission fragments have spins of order of 5.5 h. Using the observed Doppler broadening of the 1222.8 keV line the lifetime of the ^{98}Zr corresponding state was obtained and then the deformation parameter was deduced that agree satisfactorily with available systematic. All these facts point out that the high resolution in-beam γ-spectroscopy may be used for investigation of fission fragments γ-rays even when the fission act is not registered.

Literature

1. Filatenkov A.A. et al. VANT, Ser.: Yadernye constanty, 1988, vyp.2, s.56-60 (in russian).
2. Body Z. In: Handbook on Nuclear Activation Data, IAEI, Vienna, 1987.
3. Blons J. et al. Nucl. Phys., 1984, v. A414, No. 1, p. 1-41.
4. Crouch E.A.C. AD and NDT, 1977, v. 19, No. 5, p. 500-520.
5. Sakai M. AD and NDT, 1984, v. 31, p. 399-433.

6. Lederer M.C. and Shirleg V. Tables of Isotopes. 7-th ed., N.-Y., 1978.
7. Blinov M.V. et al. VANT, Ser.: Yadernye constanty, 1984, vyp.3(57), s.3-12 (in russian).
8. Dushin V.N., Filatenkov A.A. In: Nejtronnaya fizika, 5-ya Vses. konf. M., 1980, ch.4, s.242-244 (in russian).
9. Filatenkov A.A. et al. In: Proc. of Intern. Conf. on Nuclear Data for Science and Technology, MITO, 1988, p. 79-82.
10. Northcliffe L.C. and Shilling R.F. NDT, 1970, v. A7, p. 233-463.
11. Raman S. et al. AD and NDT, 1987, v. 36, No. 1, p. 20-24.

SESSION II: CALCULATION OF PHOTON CROSS-SECTIONS

Chairman: J. Kopecky

PRE-EQUILIBRIUM GAMMA EMISSION IN NUCLEAR REACTIONS

E. Běták and P. Obložinský
Institute of Physics, Slovak Academy of Sciences,
Dúbravská cesta 9, CS-84228 Bratislava, Czechoslovakia

ABSTRACT

The present status of the single-particle mechanism for the pre-equilibrium gamma emission mechanism is outlined shortly, and its place among other models of the γ emission is shown. The main attention is devoted to the exciton model, but also other ones are treated.

1. INTRODUCTION

The first decade of the existence of the pre-equilibrium model of nuclear reactions (if we take Griffin [1] as its starting point, as is usually accepted *) did not care about the pre-equilibrium γ emission. At present, however, a large variety of the approaches to the pre-equilibrium γ emission emerged. Very roughly, they can be classified in accord with the basic mechanism responsible for the γ emission. In this way, this can be:

i) Single-particle transition, where a single nucleon changes its position (energy), and the amount of energy released is carried out by a γ. This picture is rather popular in the exciton and the hybrid models (see below).

ii) Two-particle transition, also called as a quasideuteron mechanism, which assumes two correlated nucleons (a quasideuteron) to be responsible for the γ emission. It is a resurrection of the quasideuteron idea used in Levinger's model [4] for the photon absorption. For more details, see the original paper [5] or elsewhere in these Proceedings [6].

iii) A wide range of the bremsstrahlung models. The bremsstrahlung concept (in the limit of low energies [7]) can be applied either to the individual nucleons and/or their collisions, or to the nuclei as wholes; the components may be added together either in a coherent way or incoherently. The details of calculations, especially the method describing the evolution of a reaction, are quite different (Boltzmann master equation, TDHF, nuclear molecular dynamics, etc.). Anyway, the resulting γ spectra manifest some similar features: they decrease slowly with the increasing energy, and describe reasonably the experimental data within the range of about 30 to several hundreds MeV of γ energy. This group of models is rather successful nowadays. Recently, a review on high-energy gammas from heavy ions appeared [8]. Therein, the bremsstrahlung mechanisms serve as a main interpretation basis. Also, the reader is referred to the original papers [9-14].

iv) Different thermal models are somewhat aside of the main stream of interest. In practice, they are used only in heavy-ion physics, and even there seldom (see, e.g., the review on γ's from heavy-ion reactions [15]).

---

* The pioneering works of Serber [2] and Goldberger [3] did not initialize such a boom as that of Griffin [1].

As the other models are sufficiently covered by available reviews (see above), we'll restrict ourselves to the single-particle radiative transitions below.

2. SINGLE-PARTICLE TRANSITIONS

Briefly, we'll illustrate this group of approaches on the case of the exciton model first. At the end of this section, necessary changes needed for the hybrid model will be given.

2.1 Exciton model in its spin-independent form

The first intentions to include the pre-equilibrium γ emission can be traced in the thesis of Wu [16], followed by an unsuccessful attempt by Plyuyko and Prokopets [17]. Both the papers identify the densities of the final states with the total densities of the states with properly reduced excitation energy and given exciton number. Wu considers the $\Delta n=0$ transitions only (n being the exciton number), but does not calculate the γ emission itself (gamma emission stands only in the total emission widths in his work); Plyuyko and Prokopets ignore all the details of the γ emission, and take into account three processes responsible for the γ emission, Δn = -2, 0, +2, and they conclude that the last one is the dominant term. As a result, the authors [17] are not able to describe the observed γ spectra, and they must therefore add (at least) the direct-semidirect contribution. A breakdown in the calculations of γ emission came with the work of Běták and Dobeš [18], who derived the emission rates and pointed out that the term of $\Delta n=+2$ is forbidden in a classical exciton model picture, which was used also by the preceding authors [17]. The agreement of ref. [18] to the data is rather good (very good reproduction of shape and the absolute value up to a factor of 2 with respect to the data), even with a global set of parameters for the γ emission. Finally, Akkermans and Gruppelaar [19] improved both the philosophy and the equilibrium limit, using another interpretation of the Brink-Axel hypothesis. However, their total γ spectra are very close to that of ref. [18] (but the primary γ spectrum is lower by about a factor of 2 at equilibrium, which corresponds to low energies of gammas).

The approach initiated by Běták and Dobeš [18] and Akkermans and Gruppelaar [19] is used mainly within the frame of the exciton model, with a small portion of publications concerning the hybrid model (see a subsection below). We assume the single-particle mechanism, i.e. only one particle can change its position. Consequently, two processes responsible for the γ emission may occur: $\Delta n=0$ and $\Delta n=-2$ (Fig. 1).

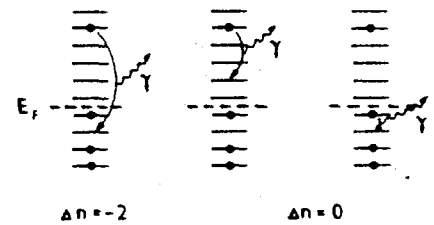

Fig. 1. Scheme of possible processes in single-particle picture.

The corresponding γ energy spectrum can be expressed as

$$\frac{d\sigma}{d\varepsilon_\gamma} = \sigma_R \sum_n \tau_n \lambda_\gamma^c(n,E,\varepsilon_\gamma) \qquad (1)$$

with σ_R denoting the reaction cross section (creation of a composite system) and

$$\tau_n = \int_0^\infty P(n,t)\, dt \qquad (2)$$

being the total time spent by a nucleus in the n-exciton state, and $P(n,t)$ is the probability of finding a nucleus in an n-exciton state at time t. The γ emission rates can be written as [20]

$$\lambda_\gamma^c(n,E,\varepsilon_\gamma) = \frac{\varepsilon_\gamma^2 \sigma_a(\varepsilon_\gamma)}{\pi^2\hbar^3c^2} \frac{\sum_{m=n,n-2} b(m,\varepsilon_\gamma)\,\omega(m,\varepsilon_\gamma)}{\omega(n,E)}, \qquad (3)$$

where b is the branching ratio for the two possible processes, and $\sigma_a(\varepsilon\gamma)$ is the photo-absorption cross section. Here, the experimental data are preferred, but the Lorentzian shape (or a sum of Lorentzians) is rather frequently taken, which reads [21]

$$\sigma_a(\varepsilon_\gamma) = \frac{4\pi\, e^2\,\hbar}{M\,c} \frac{N\,Z}{A}(1+0.8x) \frac{\Gamma_G\,\varepsilon_\gamma^2}{[\,(\varepsilon_\gamma^2-E_G^2)^2 + (\Gamma_G\varepsilon_\gamma)^2\,]}, \qquad (4)$$

where E_G and Γ_G are the energy and the width of the GDR ($E_G \approx 80\ A^{-1/3}$ MeV, $\Gamma_G \approx 5$ MeV). The existing tables (e.g. [20]) provide the individual widths, energies and peak cross sections for various nuclei. The branching ratios $b(m,\varepsilon\gamma)$, as given by [19], are

$$b(n-2,\varepsilon_\gamma) = \frac{\omega(1,1,\varepsilon_\gamma)}{g(n-2) + \omega(1,1,\varepsilon_\gamma)}$$

$$b(n,\varepsilon_\gamma) = \frac{g\,n}{gn + \omega(1,1,\varepsilon_\gamma)}. \qquad (5)$$

Here, the difference with respect to the earlier work [18] is rather tiny for high-energy ("typically pre-equilibrium") gammas, and close to a factor of 2 for low-energy (practically equilibrium) ones. Such is also the difference for the first-chance γ emitted in a reaction (see the figure in the Akkermans paper [19]). However, the differences in the total γ spectra (and the first-chance γ spectrum is never separated experimentally) are again very little, as the main contribution to the region of low-energy gammas comes from nuclei with low excitation energy, where nothing else but γ can be emitted - and the spectral shapes of both [18] and [19] are very similar, the only thing they differ in is their absolute value in low energies.

For the γ emission from the nucleon-induced reactions, one must start from a state of $n_0=1$ ($1p0h$). In the case of no gamma emission, such a state transforms completely into the $n=3$ ($2p1h$) state, and we can assume the latter one being the initial state. However, the γ emission from $n=1$ is essential. Fig. 2 brings the relative γ intensities versus the exciton number, as obtained for a "model nucleus" (A=90, g=7 MeV^{-1}, E_{exc}=22 MeV). The presented relative γ intensities are insensitive to the model parameters and to the details of the equilibration process. To convert them to the γ spectra, one has to multiply them by the total lifetimes of n-exciton states, τ_n. As seen from the picture, we do not agree with the conclusions of Reffo et al. [23], who declare the emission from the $n=3$ state being the most important one in these reactions.

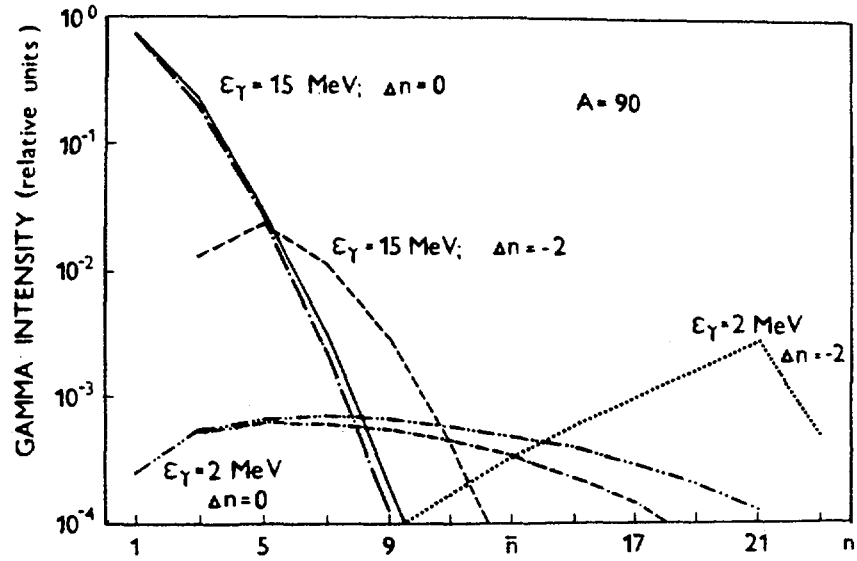

Fig. 2. Relative γ intensities versus the exciton number. The two possible processes are depicted, and for the case of $\Delta n=0$ both the contribution without (the upper line) and that with the Pauli principle correction in the γ emission rates (lowe line) is given.

Obviously, one has to have a possibility to include the successive γ's (interspersed by nucleons as needed) in the equations to get the total γ production. The enlarged set of master equations reads [24]

$$\frac{dP(n,t,E,i)}{dt} = P(n-2,t,E,i)\,\lambda^{+}(n-2,E,i) + P(n+2,t,E,i)\,\lambda^{-}(n+2,E,i) - P(n,t,E,i)\,[\lambda^{+}(n,E,i) + \lambda^{-}(n,E,i) + L(n,E,i)] + \sum_{j,m,x} \int_{\varepsilon} P(m,t,E',j)\,\lambda_x^{c}(m,E',j,\varepsilon)\,d\varepsilon \qquad (6)$$

Here, the excitation energy E and time t are written explicitly, as well as the index i, which is to denote different nuclei in a sequence of emissions. Further on, λ's are the transition rates (per unit time) to the neighbour states, and L is the total emission rate (including particles and gammas, integrated over the outgoing energy and summed over all possible emission channels) of the specified exciton state,

$$L(n,E,i) = \sum_{x} \int_{\varepsilon} P(n,t,E,i)\,\lambda_x^{c}(n,E,i,\varepsilon)\,d\varepsilon \qquad (7)$$

The last term in eq. (6) ensures the coupling of different nuclei and various excitation energies. Whereas the "pre-γ-era" set of master equations was of a size (typically) 20 or 30 equations, eq. (6) represents usually thousands (or tens of thousands) coupled equations. They are incorporated in the computer code PEQGM [24] and its updated PC versions [25].

The form of branching ratios (5) was derived neglecting the influence of the Pauli principle. If one takes it into account,

there is no change for the $\Delta n=-2$ processes (if there is a particle-hole pair, it can annihilate), but the $\Delta n=0$ radiation transition is reduced (not every level is empty) effectively by a factor [26]

$$1 - \frac{a_{ph}}{E - \varepsilon_{\gamma}} , \qquad (8)$$

where a_{ph} is the minimal energy needed to create a state of p particles and h holes. Anyway, the influence of the Pauli principle correction is reduced, if one considers full γ cascades, and not only the first emitted γ.

An example of the force of the model to predict the γ spectra is in Fig. 3, where we present *a priori* calculations (i.e. without any fit of the parameters for the γ emission) [27] compared to the data.

With the appearance of the so-called realistic exciton state densities [28], i.e. the densities of states with specified exciton number, based not on the equidistant-spacing scheme, but on the realistic single-particle one (e.g. that of Nilsson) and the codes capable to handle them, also the γ spectra were calculated within this approach. Though the results are encouraging, and sometimes (by a chance) even excellent (as is that in Fig. 4), the final understanding of the problem is still

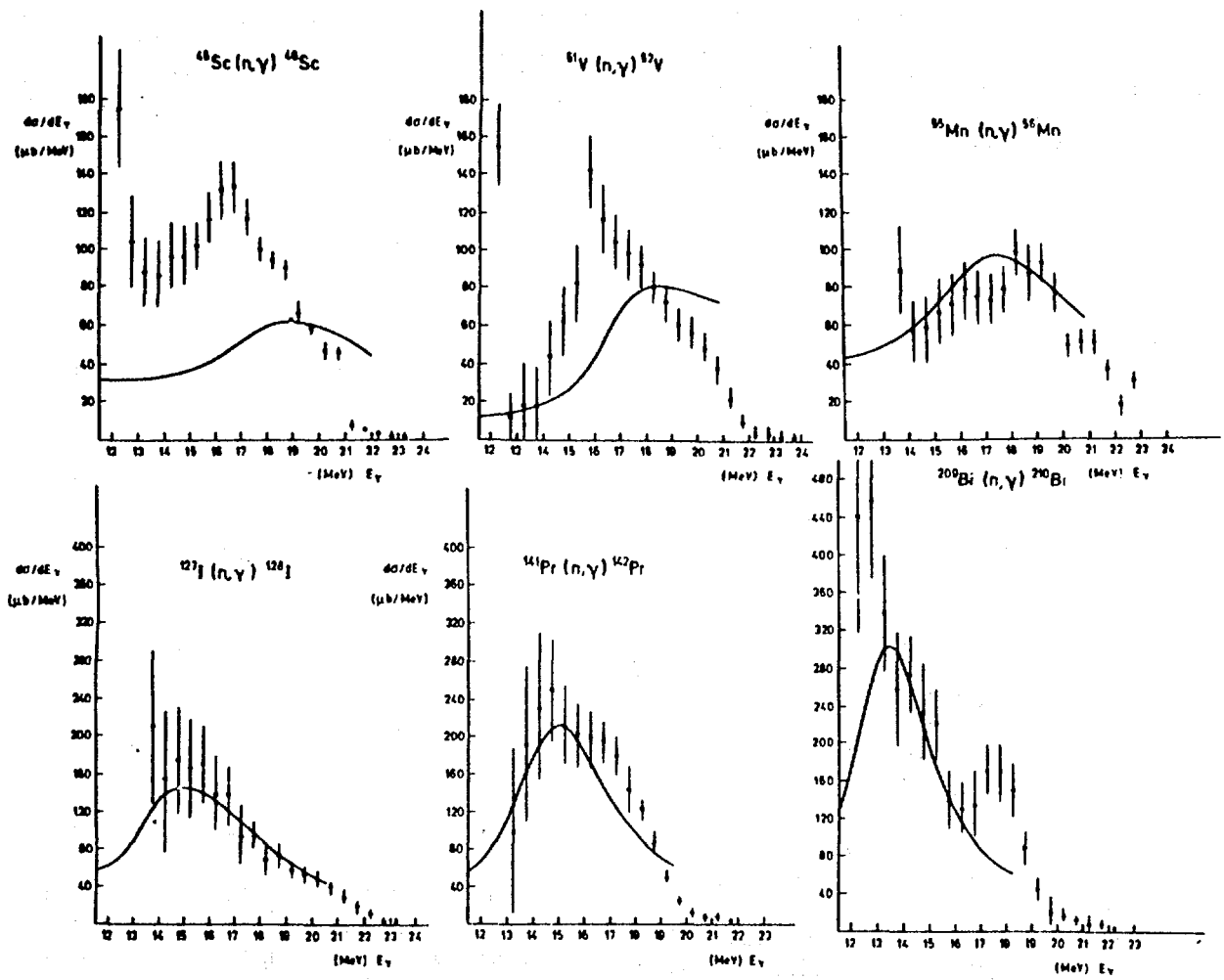

Fig. 3. The γ spectra from several 14 MeV neutron induced reactions, as obtained without any fit of the parameters for the γ emission. From [27].

beyond this picture. Some further step may be performed with the so-called realistic exciton state densities with specified spin and parity [30].

Apart of the γ spectra and corresponding integrated cross sections, also other quantities (even the correlation ones!) depending on the γ emission can be calculated (see ref. [31]).

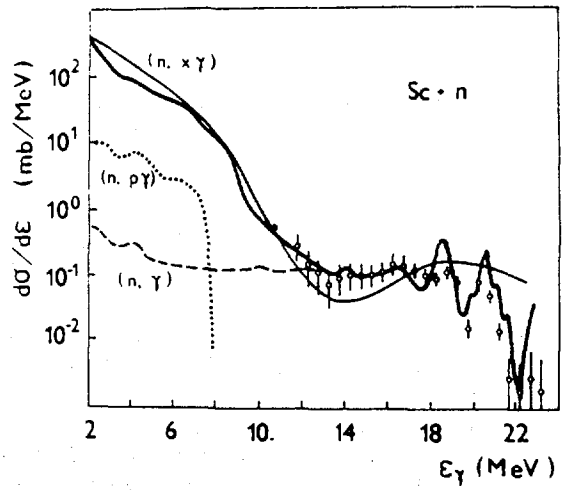

Fig. 4. Example of an attempt to get the γ spectra using the so-called realistic exciton state densities. The thin line is usual equidistant-spacing-model; the heavy line comes from the "realistic" densities. Code PEQGM [24,25], densities by [29].

2.2 Heavy-ion reactions

The main problem here is the initial stage of the reaction. In the heavy-ion collisions, the initial stage for the pre-equilibrium decay itself is time-dependent, and was described by Blann [32] and later on in a more refined way by a Japanese group [33]. Surprisingly, if we plot the initial exciton number versus the projectile energy above the Coulomb barrier, we get a pretty reasonable systematics [34], as is presented in Fig. 5.

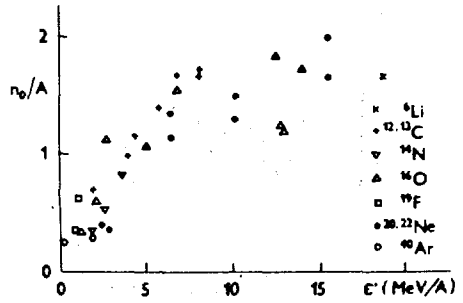

Fig. 5. Systematics of n_0 in heavy-ion reactions. Taken from [34].

Today, some understanding of such a behaviour is emerging [35]. An example of γ spectra from heavy-ion reactions, namely from the decay of ^{132}Nd, created once by ^{64}Zn+^{68}Zn, and by ^{20}Ne+^{112}Sn in the second case (at roughly the same excitation energy), is presented in Fig. 6. We see that the calculation (with *a priori* parameters for γ's) reproduces the main features observed in the experiment, especially the structure near 12 MeV.

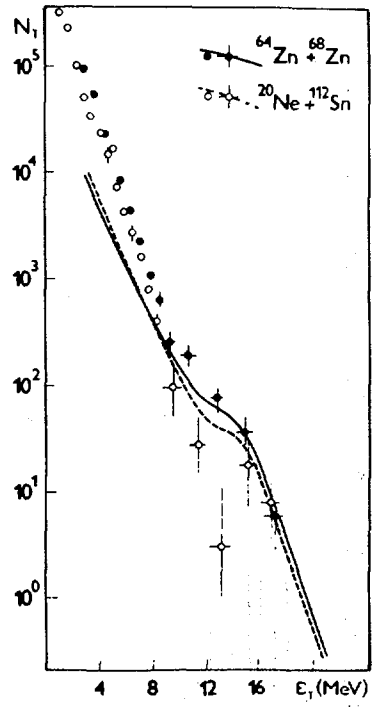

Fig. 6. The γ spectra from the decay of ^{132}Nd. The creation of a composite system was verified by a coincidence with X-rays. Data from [36], calculation from [37].

2.3 Exciton model; spin-dependent description

The angular momentum has been introduced into the pre-equilibrium formulation of the γ emission by Obložinský [38]. It was shown that no simple solution, like adding of the angular momentum part of the level densities is sufficient. Rather, the angular momentum coupling terms are complicated expressions, where one has to take into account the angular momentum structure of the electric dipole matrix elements, perform the summation over available single-particle states and averaging over the initial states. The structure of eqs. (5) is still preserved, but three coupling terms appear in the branching ratios. For example, one has

$$b_{ns}^{nJ} = \frac{g\, n\, x_{ns}^{nJ}}{g\, n\, x_{ns}^{nJ} + g^2\, \varepsilon_\gamma\, x_{ns}^{n+2,J}} \qquad (9)$$

for the emission $J \to s$ (or absorption $s \to J$) instead of $b(n,\varepsilon\gamma)$. Here, J and s are the spins (see Fig. 7), and

$$x_{ns}^{nJ} = \frac{3\,(2J+1)}{R_n(s)} \sum_{j_1 j_2 j_3} (2j_1+1)\, R_1(j_1)\, (2j_2+1)\, R_1(j_2)\, R_{n-1}(j_3)\, \cdot$$

$$\begin{pmatrix} j_2 & 1 & j_1 \\ \frac{1}{2} & 0 & -\frac{1}{2} \end{pmatrix}^2 \quad \begin{Bmatrix} j_2 & j_3 & s \\ J & 1 & j_3 \end{Bmatrix}^2 , \qquad (9)$$

where the notation is explained in Fig. 7 and $R_n(s)$ stands for the spin part of the level density. Importantly, the consistency is again achieved with the equilibrium statistical result.

Without going into further details, we show in Fig. 8 that the effect of the angular momentum coupling on the $^{56}Fe(n,\gamma)$ spectrum at 14.6 MeV is rather small. We note, however, that the matrix element $|M_{nJ}|^2$ appearing in the spin-dependent exciton model was, after averaging over J, adjusted to the non-spin matrix element $|M_n|^2$ so that

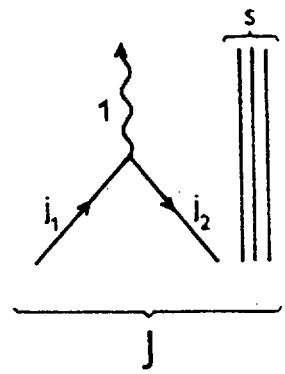

Fig. 7. Scheme of angular momenta for the γ emission.

$$\langle |M_{nJ}|^2 \rangle = |M_n^{n+2}|^2 \langle X_{nJ}^{\downarrow} \rangle = |M_n|^2 , \qquad (10)$$

where $\langle X_{nJ}^{\downarrow} \rangle$ is the averaged coupling term for intranuclear transitions and it was evaluated as 0.0208 in the reaction studied [38].

2.4 Hybrid model

In the hybrid model, the energy of one specified particle exciton is explicitly followed, and - as a rule - the never-come-back approximation is used. In this way, one has [39]

$$\frac{d\sigma}{d\varepsilon_\gamma} = \sigma_R \sum_x \sum_n \int_0^E \left[\frac{n^p x}{p} \frac{\omega_{n-1}(E-\varepsilon)\, g\, d\varepsilon}{\omega_n(E)} \right] \left[\frac{\lambda_\gamma(\varepsilon,\varepsilon_\gamma)}{\lambda_\gamma(\varepsilon)+\lambda_c(\varepsilon)+\lambda^+(\varepsilon)} \right] D_n . \qquad (12)$$

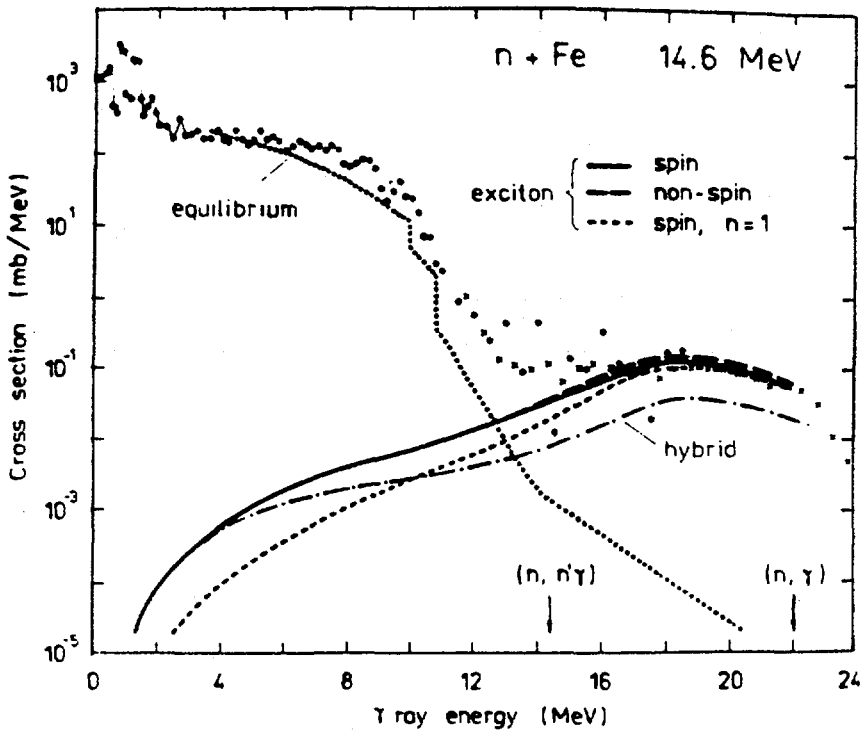

Fig. 8. Influence of angular momentum on the γ spectrum from ^{56}Fe + n at 14 MeV. Figure taken from ref. [38].

Here, D_n is the depletion factor, and the first term in the first pair of brackets is to ensure the proper charge composition of the particle ejectile. Note, that all the transition as well as the emission rates refer to a state with exciton of a specified energy ε. In this picture, obviously, one has some restrictions on the possible γ energy, namely

$$\lambda_\gamma(\varepsilon,\varepsilon_\gamma) = \begin{cases} \lambda_\gamma^-(\varepsilon,\varepsilon_\gamma) & \text{for } \varepsilon_\gamma > \varepsilon \\ \lambda_\gamma^0(\varepsilon,\varepsilon_\gamma) & \text{for } \varepsilon_\gamma < \varepsilon\ , \end{cases} \tag{13}$$

as just the specified particle may be involved in the γ transition. This is a significant difference with respect to the exciton model, where an arbitrary one could undergo the radiative transition. The γ emission rates themselves remind those used in the exciton model, as given by eqs. (3) and (5). In full,

$$\lambda_\gamma^0(\varepsilon,\varepsilon_\gamma) = \frac{\varepsilon_\gamma^2 \sigma_a(\varepsilon_\gamma)}{\pi^2\hbar^3c^2} \frac{g}{gn + g^2\varepsilon_\gamma}$$

$$\lambda_\gamma^-(\varepsilon,\varepsilon_\gamma) = \frac{\varepsilon_\gamma^2 \sigma_a(\varepsilon_\gamma)}{\pi^2\hbar^3c^2} \frac{g}{g(n-2) + g^2\varepsilon_\gamma} \frac{\omega_{n-2}(E-\varepsilon_\gamma)}{\omega_{n-1}(E-\varepsilon)}\ . \tag{14}$$

(Note that we have put explicitly $\omega(1,1,\varepsilon\gamma)=g^2\varepsilon\gamma$.) The spectral shape is rather close to that of the exciton model. On the other hand, however, the hybrid model gives the intranuclear transition rates without any ambiguities, what was not the case of the exciton model. Therein, the value of the effective matrix element

of the residual interaction is fixed for the 3-exciton state (the dominant one for nucleon emission), and some model assumptions are used to obtain its value for all other states. Especially in the case of γ emission, where n=1 state is the dominant one, such a process is not unique [40].

3. CONCLUSIONS

We dealt with the one-particle radiative mechanism within the pre-equilibrium models. It is capable to describe many features of the observed γ spectra (and of other quantities dependent on the γ emission) as well, especially the manifestation of the giant dipole resonance. A special branch of the one-particle mechanism, namely the γ emission within the multistep compound reactions, was not touched here, as it is a subject of a separate paper within this Meeting [41].

The one-particle mechanism serves well for the excitation and γ energies below 30 or 50 MeV (see also [31]). Higher energies, however, call also for the presence of other mechanisms mentioned in the Introduction (see especially refs. [6], [8], and [15] for better impression).

The work has been supported in part by International Atomic Energy Agency contract No. 5148/RB.

REFERENCES

[1] J.J. Griffin, Phys. Rev. Lett. *17* (1966), 478.
[2] R. Serber, Phys. Rev. *72* (1947), 1114.
[3] M.L. Goldberger, Phys. Rev. *74* (1948), 1268.
[4] J.S. Levinger, Phys. Rev. *84* (1951), 43.
[5] P. Obložinský, Phys. Rev. *C40* (1989), 1591.
[6] P. Obložinský, *this Meeting*.
[7] J.D. Jackson, Classical Electrodynamics (Wiley, NY 1975); L.D. Landau, E.M. Lifshitz, Teoriya polya (Field theory, *in Russian*) (Nauka, Moscow 1967).
[8] H. Nifenecker, J.A. Pinston, Prog. Part. Nucl. Phys. *23* (1989), 271.
[9] D. Vasak et al., Nucl. Phys. *A428* (1984), 291c.
[10] H. Nifenecker, J. Bondorf, Nucl. Phys. *A442* (1985), 478.
[11] B.A. Remington et al., Phys. Rev. *C35* 1987), 1720.
[12] D. Neuhauser, S.E. Koonin, Nucl. Phys. *A462* (1987), 163.
[13] R. Heuer et al., UFTP Preprint 204/1987 (Frankfurt 1987).
[14] K. Niita et al., Nucl. Phys. *A504* (1989), 391.
[15] V.V. Kamanin et al., Paricles and Nuclei *20* (1989), 741.
[16] J.R. Wu, PhD Thesis, Univ. Maryland (1977), PP-77-275.
[17] V.A. Plyuyko, G.A. Prokopets, Yad. Fiz. *27* (1978), 1487; *practically identical paper also* Phys. Lett. *76B* (1978), 253.
[18] E. Běták, J. Dobeš, Phys. Lett. *84B* (1979), 368.
[19] J.M. Akkermans, H. Gruppelaar, Phys. Lett. *157B* (1985), 91.
[20] E. Běták, J. Dobeš *in* Neutron Induced Reactions, Proc. 4 Int. Symp., Smolenice 1985 (D. Reidel, Dordrecht and VEDA, Bratislava 1986), p. 294.
[21] G.A. Bartholomew et al., Adv. Nucl. Phys. 7 (1973), 229.
[22] B.L. Berman, At. Data Nucl. Data Tbl. *15* (1975), 319.
[23] G. Reffo et al., *in* Proc. IAEA Res. Coord. Meeting, Bologna 1986 (INDC(NDS)-193/L, IAEA Vienna 1988), p. 73.
[24] E. Běták, J. Dobeš, Report IP EPRC SAS 43/1983 (Bratislava 1983).
[25] E. Běták, Reports INDC(CSR)-016/LJ (IAEA Vienna 1989) and FU SAV 89/5 (Bratislava 1989) (*code available on request*).

[26] E. Běták, Comm. Theor. Phys. *12* (1989), 291.
[27] E. Běták, F. Cvelbar, Z. Phys. *A332* (1989), 163.
[28] F.C. Williams et al., Nucl. Phys. *A207* (1973), 619;
K. Albrecht, M. Blann, Phys. Rev. *C8* (1973), 1481.
[29] E.J. Käbin et al., VINITI 613-81 (Moscow 1981);
A.M. Blekhman et al., Report INP AN KSSR 6-83 (Alma-Ata 1983)
[30] V.Y. Galkin et al.,*in* Matem.Metody Obrab.(Moscow 1984),p.110;
M. Herman, G. Reffo, Comp. Phys. Comm. *47* (1987), 103.
[31] E. Běták, F. Cvelbar, *This Meeting*
[32] M. Blann, Phys. Rev. *C23* (1981), 205.
[33] T. Otsuka, K. Harada, Phys. Lett. *121B* (1983), 106;
K. Niita, Z. Phys. *A316* (1984), 309.
[34] E. Běták, Cz. J. Phys. *B34* (1984), 850; *and* Jaderné reakcie s ťažkými iónmi (Heavy-ion reactions., *in Slovak*) (VEDA Bratislava 1989).
[35] J.J. Griffin et al., *to be published.*
[36] V.V. Kamanin et al., Z. Phys. *A327* (1987), 109; *and in* Int. School-Seminar HI Phys., Dubna 1986 (D7-87-68, Dubna 1987), p. 489.
[37] E. Běták, Fizika *19* (1987), Suppl. 1, p. 49.
[38] P. Obložinský, Phys. Rev. *C35* (1987), 407.
[39] P. Obložinský, Phys. Lett. *215B* (1988), 597.
[40] A. Mussachio Lasa, Diplom Work, Comenius University, Bratislava 1989.
[41] M. Chadwick, P. Obložinský, *This Meeting*

γ-Emission within a Statistical Multistep Reaction Model

H. Kalka
Technische Universität Dresden, Sektion Physik, Dresden 8027, G.D.R.

1. Introduction

A unique description of (a,xb) emission spectra where a,b = n,p,α, and γ (neutron, proton, alpha, and γ-ray) as well as excitation functions (activation cross sections) is proposed within a pure statistical multistep approach /1-3/. This approach is based on random matrix physics /4,5/ and was derived from Green's function formalism /6/. In this model the total emission spectrum of the process (a,xb) is divided in three main parts,

$$\frac{d\sigma_{a,xb}(E_a)}{dE_b} = \frac{d\sigma^{SMD}_{a,b}(E_a)}{dE_b} + \frac{d\sigma^{SMC}_{a,b}(E_a)}{dE_b} + \frac{d\sigma^{MPE}_{a,xb}(E_a)}{dE_b} \quad . \tag{1}$$

The first term denotes the statistical multistep direct (SMD) part and contains one- and two-step contributions. The second term symbolizes the statistical multistep compound (SMC) emission. Both terms together represent the so-called first-chance emission process. Otherwise, the multiple particle emission (MPE) reactions which include the second-chance, third-chance emissions, etc. are summarized in the last term, i.e.,

$$\frac{d\sigma^{MPE}_{a,xb}(E_a)}{dE_b} = \sum_c \frac{d\sigma_{a,cb}}{dE_b} + \sum_{c,d} \frac{d\sigma_{a,cdb}}{dE_b} + \ldots \quad . \tag{2}$$

The following (model-independent) relations between the optical-model (OM) reaction cross section and the integral partial cross sections should be satisfied (at incident energy E_a)

$$\sigma^{OM}_a = \sum_b \sigma_{a,b} \quad , \tag{3a}$$

$$\sigma_{a,b} = \sum_c \sigma_{a,bc} \quad \text{and} \quad \sigma_{a,bc} = \sum_d \sigma_{a,bcd} \quad , \text{ etc.,} \tag{3b}$$

with $\sigma_{a,b} = \sigma^{SMD}_{a,b} + \sigma^{SMC}_{a,b}$ as the total first-chance emission cross section. In this context, activation cross sections are given by

$$\sigma_{a,b\gamma} = \sigma_{a,b} - \sum_{c\neq\gamma} \sigma_{a,bc} \quad , \tag{4a}$$

$$\sigma_{a,cb\gamma} = \sigma_{a,cb} - \sum_{d\neq\gamma} \sigma_{a,cbd} \quad , \tag{4b}$$

where b,c,d $\neq \gamma$. More explicitly, the (n,p)-, (n,α)-, and (n,2n)-excitation functions have the form

$$\sigma_{n,p\gamma} = \sigma_{n,p} - \sigma_{n,pn} - \sigma_{n,2p} - \sigma_{n,p\alpha} \quad , \tag{5a}$$

$$\sigma_{n,\alpha\gamma} = \sigma_{n,\alpha} - \sigma_{n,\alpha n} - \sigma_{n,\alpha p} - \sigma_{n,2\alpha} \quad , \tag{5b}$$

$$\sigma_{n,2n\gamma} = \sigma_{n,2n} - \sigma_{n,3n} - \sigma_{n,2np} - \sigma_{n,2n\alpha} \quad . \tag{5c}$$

2. Model Parameters

The most important parameters in statistical multistep (and preequilibrium) models are the single-particle state density g and the mean squared matrix elements, $\overline{I^2}$. Both quantities we define *outside* the model to perform all calculations *without* any parameter-fit.

The state density of (free) particles c = n,p,α with mass μ_c inside the nucleus volume $\mathcal{V} = 4\pi R^3/3$ is given by

$$\rho(E_c) = \frac{4\pi\,\mathcal{V}\,\mu_c k_c}{(2\pi)^3\hbar^2} = \frac{r_o^3\,A\,E_c^{1/2}}{893.3} \quad \text{in MeV}^{-1} \tag{6a}$$

with $R = r_o A^{1/3}$ in fm and E_c is the kinetic energy in MeV. We set r_o= 1.40 fm which leads to the single-nucleon state density

$$g = 2\,(2s+1)\,\rho(E_F) = A/13 \quad \text{in MeV}^{-1} \tag{7}$$

at Fermi energy $E_F \simeq$ 40 MeV. The factor 2 in (7) represents the isospin degeneracy.

Otherwise, the state density of (free) photons is given by

$$\rho(E_\gamma) = \frac{4\pi\,\mathcal{V}\,k_\gamma}{(2\pi)^3 c\hbar} = 2.76\ 10^{-8}\ r_o^3\,A\,E_\gamma^2 \quad \text{in MeV}^{-1} \quad . \tag{6b}$$

To define the *nuclear* mean squared matrix element assumptions about the shape and strength of the residual interaction are

necessary. We restrict ourselves to a (spin- and isospin-independent) surface-delta interaction /7/,

$$V(\vec{r}_1,\vec{r}_2) = - V_o \frac{4\pi}{3} r_o^4 \delta(\vec{r}_1-\vec{r}_2) \delta(r_1-R) \quad . \tag{8}$$

In contrast to a simple (volume) delta-interaction $V(\vec{r}_1,\vec{r}_2) = -V_o 4\pi r_o^3 \delta(\vec{r}_1-\vec{r}_2)/3$ used in Refs./8,9/ the surface-delta interaction can be interpreted as an idealized (density-dependent) Migdal force and thus it is more realistic. Using (8) and performing an average over angular momentum we obtain a closed expression for the mean squared matrix element,

$$\overline{I^2}(E) = \frac{1}{2s+1} \frac{1}{(kR)^2} \left(\frac{r_o}{R}\right)^2 \left(\frac{V_o}{A}\right)^2 = 5.29\, V_o^2\, E^{-1}\, A^{-10/3} \tag{9a}$$

(in MeV^2) for bound-bound transitions, $\overline{I^2_{BB}} \equiv \overline{I^2}(E)$. They will enter the damping widths $\Gamma_{m\downarrow}$. The corresponding quantities which enter the escape widths $\Gamma_{m\uparrow}$ (bound-unbound transitions) and the OM reaction cross section (unbound-bound transitions) are given by

$$\overline{I^2_{BU}} = \overline{I^2}(E)\ (2s_b+1)\ \rho(E_b) \quad \text{and} \quad \overline{I^2_{UB}} = \rho(E_a)\ \overline{I^2}(E) \quad . \tag{9b}$$

Finally, the expression for unbound-unbound transitions (SMD processes) will be written as

$$\overline{I^2_{UU}} = \rho(E_a)\ (E/E_a)\ \overline{I^2}(E)\ (2s_b+1)\ \rho(E_b) \quad . \tag{9c}$$

The strength V_o was determined from the assumption that the (neutron) OM reaction cross section is equal to the formation of the 2p1h-doorway state,

$$\sigma_n^{OM}(E_n) = \sigma^{2p1h}(E_n) = \frac{4\pi^3}{k_n^2} \overline{I^2_{UB}} \frac{g^3E^2}{4} = \frac{2\pi\mathcal{V}}{\hbar v_n} \overline{I^2}(E) \frac{g^3E^2}{4} \quad . \tag{10}$$

This assumption holds in the incident-energy range $E_n = 3...7$ MeV where SMC processes dominate and leads to the value $V_o \simeq 20$ MeV.

The γ-emission is assumed as pure dipole emission. Adopting the Brink hypothesis /10/ the *electro-magnetic* mean squared matrix element $\overline{D^2}(E)$ can be obtained directly from the formation cross section of a 1p1h-doorway state,

$$\sigma_\gamma^{GDR}(E_\gamma) = \sigma^{1p1h}(E_\gamma) = \frac{2\pi\mathcal{V}}{\hbar c} \overline{D^2}(E)\ g^2E_\gamma \quad . \tag{11}$$

For σ_γ^{GDR} the Lorentzian form of Ref./11/ was used with β=0.

3. SMD Cross Section

For the incident-energy range below 30 MeV we restrict ourselves to one- and two-step contributions since the SMD process terminates after few collisions. According to the distinction between non-collective particle-hole excitations [ex] and collective vibrational states [vib] the SMD cross section becomes a sum of 2 one-step and 4 two-step contributions (b = n,p),

$$\frac{d\sigma^{SMD}_{a,b}(E_a)}{dE_b} = \sum_{[y]} \left(\frac{\mu_a \mathcal{V}}{2\pi\hbar^2} \right)^2 \frac{4\pi}{(k_a R)^2} [\, y \,] \frac{k_b}{k_a} \mathcal{P}_a(E_a)\mathcal{P}_b(E_b) \quad , \qquad (12)$$

where [y] symbolizes the individual contributions denoted according to the sequence of exciton and phonon excitations,

$$[ex] = (1+\delta_{ab})\,(V_o A^{-4/3} g/2)^2\, U \quad , \qquad (14a)$$

$$[vib] = \delta_{ab} \sum_{\lambda} \hat{\beta}_\lambda^2\, V_R^2\, \delta(U-\omega_\lambda) \quad , \qquad (13b)$$

$$[2ex] = (1+\delta_{ab})\, 2\, (V_o A^{-4/3} g/2)^4\, q_1 U^3/6 \quad , \qquad (13c)$$

$$[ex,vib] = (1+\delta_{ab})\,(V_o A^{-4/3} g/2)^2\, q_1 \sum_{\lambda} \hat{\beta}_\lambda^2\, V_R^2\, (U-\omega_\lambda) \quad , \qquad (13d)$$

$$[vib,ex] = \delta_{ab}\, [ex,vib] \quad , \qquad (13e)$$

$$[2vib] = \delta_{ab} \sum_{\lambda,\lambda'} \hat{\beta}_\lambda^2\, \hat{\beta}_{\lambda'}^2\, V_R^4\, q_1\, \delta(U-\omega_\lambda-\omega_{\lambda'}) \quad . \qquad (13f)$$

The following abbreviations are used: $U=E_a+B_a-B_b-E_b$ is the residual excitation energy; B_c and $E_c=\hbar^2 k_c^2/2m$ are the binding and kinetic energies. The real OM potential depth is taken as V_R = 48 MeV. Otherwise, the quantities ω_λ and $\beta_\lambda^2 = 4\pi(2\lambda+1)\hat{\beta}_\lambda^2$ denote the energy and deformation parameters of a phonon with multipolarity λ. Here, we restrict ourselves to two low-lying vibrational states of multipolarity $\lambda^\pi = 2^+$ and 3^- taken from nuclear tables /12,13/. For odd-mass nuclei the weak coupling model /14/ was adopted. All delta functions are replaced by Gaussians of width 0.7 MeV simulating both the limited (exit channel) energy resolution in experiments and the spreading of spectroscopic strength. Further, $q_1 = (\pi/2)(\rho(E_c)/k_c R)^2 = 4.12\ 10^{-5}\ r_o^4 A^{4/3}$ MeV^{-2}.

The phenomenological penetration factors in (13),

$$\mathcal{P}_c(E_c) = (\sigma_c^{OM}(E_c)/\sigma_n^{OM}(E_c))\ (1-\exp(-E_c/C)) \quad , \tag{14}$$

will also enter the SMC formulas (c=n,p,α). They consist of two factors which both influence the low (incident and/or emission) energy region. The first factor simulates the penetrability through the Coulomb barrier and is 1 for neutrons. The second factor simulates the penetrability through the centrifugal barrier ($C \simeq 1$ MeV).

The label "SMD" will be used here also for a kind of γ-emission processes which are *not* proceed via SMC-mechanism. Here we consider two-step processes (first a nuclear interaction and second an electromagnetic interaction) given by (preliminary)

$$\frac{d\sigma_{a,\gamma}^{SMD}(E_a)}{dE_\gamma} = \frac{4\pi^3}{k_\gamma^2} \int \frac{dE_1}{4\pi}\, \overline{I_{UB}^2}\, 2\rho(E_1)\, g^2(E-E_1)\, 2\pi^2\rho(E_1)\, \overline{D^2}(E_\gamma)\, \rho(E_\gamma)\, g.$$

After the first collision the nucleon occupies states of density $\rho(E_1) \equiv \rho_a(E_F+E_1) = g(1+E/E_F)^{1/2}/4$. Performing the integral between 0 and E we obtain the simple expression

$$\frac{d\sigma_{a,\gamma}^{SMD}(E_a)}{dE_\gamma} = \frac{2\pi\mathcal{V}}{\hbar v_a}\, \overline{I^2}(E)\, \frac{g^3E^2}{4} \left[\, 1 + \frac{E}{3E_F} \,\right] \frac{\pi}{8}\, \overline{D^2}(E_\gamma)\ \rho(E_\gamma)\, g \ . \tag{15}$$

Finally, we consider a factor of 2 for the degeneracy of two photon-polarizations (right and left).

4. SMC Cross Section

The SMC cross section has the familiar form (b = n,p,α,γ)

$$\frac{d\sigma_{a,b}^{SMC}(E_a)}{dE_b} = \sigma_a^{SMC}(E_a) \sum_{m=m_o}^{m'} \frac{\tau_m(E)}{\hbar}\, \Gamma_{mb}(E,E_b)\uparrow \quad , \tag{16}$$

where $\tau_m(E)$ satisfies the time-integrated master equation,

$$-\hbar\,\delta_{mm_o} = \Gamma_{m-2}^{(+)}(E)\downarrow \tau_{m-2}(E) + \Gamma_{m+2}^{(-)}(E)\downarrow \tau_{m+2}(E) - \Gamma_m(E)\tau_m(E) \quad , \tag{17}$$

for each exciton number m=p+h. The sum runs from m_o up to $m' = (2gE)^{1/2}$ which includes the equilibrium stage $\bar{m} \simeq (1.4gE)^{1/2}$. The

initial exciton number is m_o= 2, 3, or 6 for photon-, nucleon-, or α-induced reactions. Here, $E=E_a+B_a^{eff}$ is the (effective) excitation energy of the composite system and B_a^{eff} is the effective binding energy. For a system of A=N+Z nucleons the effective neutron (proton) binding energy is defined as /2/

$$B_{n(p)}^{eff} = \begin{cases} B_{n(p)}+\Delta \\ B_{n(p)}-\Delta \end{cases} \quad \text{for} \quad \begin{matrix} \text{odd} \\ \text{even} \end{matrix} \quad N\ (\ Z\ )\ , \tag{18}$$

where $B_{n(p)}$ is the exact neutron (proton) binding energy, and Δ = 12 $A^{-1/2}$ MeV. In this way, pairing effects are considered within the SMC description. For α- and γ-emissions we use B_α^{eff}= B_α and B_γ^{eff}= 0.

In (18) the damping widths are given by

$$\Gamma_m^{(+)}(E)\downarrow = 2\pi\ \overline{I^2}(E)\ \frac{g^3(E-A_{p+1,h+1})^2}{2(m+1)}\ , \tag{19a}$$

$$\Gamma_m^{(-)}(E)\downarrow = 2\pi\ \overline{I^2}(E)\ g\ ph(m-2)/2\ , \tag{19b}$$

where A_{ph}= $(p^2+h^2+p-3h)/4g$ is a correction for Pauli-principle. Otherwise, for the (differential) escape widths we have (b = n,p,α)

$$\Gamma_{mb}(E,E_b)\hat{\uparrow} = 2\pi\ \overline{I^2}(E)\ (2s_b+1)\ \rho(E_b)\ \mathcal{P}_b(E_b) \sum_{\Delta m} \rho_m^{(\Delta m)}(E-B_b^{eff}-E_b) \tag{20}$$

where the sum runs over three escape modes defined by the final state densities of the *residual* system,

$$\rho_m^{(+)}(U) = \frac{h}{m}\ g^2\ E_{ph} \left[\frac{U_{p,h+1}}{E_{ph}}\right]^m\ , \tag{21a}$$

$$\rho_m^{(0)}(U) = p(h+\frac{p-1}{2})g \left[\frac{U_{p-1,h}}{E_{ph}}\right]^{m-2} \left[(m-1)-(m-2)\left[\frac{U_{p-1,h}}{E_{ph}}\right]\right], \tag{21b}$$

$$\rho_m^{(-)}(U) = \frac{p(p-1)h}{4E_{ph}}\ \frac{(m-1)!}{(m-4)!} \left[\frac{U_{p-2,h-1}}{E_{ph}}\right]^{m-4} \left[1-\left[\frac{U_{p-2,h-1}}{E_{ph}}\right]\right]^2 \tag{21c}$$

Here, for the (Pauli-corrected) excitation energies of the composite and residual systems the abbreviations E_{ph} = $E-A_{ph}$ and U_{ph} = $E-A_{ph}-B_b^{eff}-E_b$ are used. If, for example, the Pauli-

correction A_{ph} would be ignored, then the final state densities in (21) turn to those proposed in /8/. Note, however, the factor h/m in (21a) which excludes pair-creation by *particle*-scattering.

For α-particles (b=α) Eq.(20) should be multiplied by the form factor /15/

$$F_{is}(E_\alpha) = 0.28144 - 0.01113\ E_\alpha + 1.34\ 10^{-4}\ E_\alpha^2 \quad , \tag{22}$$

which plays the dominant role for emission energies below 20 MeV. Additionally, a factor of 2 (spin-degeneracy of the active nucleon in the formation mode [1,3] of the α-particle) is considered.

The escape width for γ-emission (b=γ) are defined by

$$\Gamma_{m\gamma}(E,E_\gamma)\hat{\uparrow} = 2\pi\ \overline{D^2}(E)\ \rho(E_\gamma) \sum_m \rho_{m\gamma}^{(\Delta m)}(E-E_\gamma) \quad , \tag{23}$$

where the sum runs over two escape-modes defined by the final state densities

$$\rho_{m\gamma}^{(0)}(U) = m\ g\ (\ U_{ph}/E_{ph}\ )^{m-1} \quad , \tag{24a}$$

$$\rho_{m\gamma}^{(-)}(U) = ph\ (m-1)(m-2)\ (E_\gamma/E_{ph}^2)\ (\ U_{p-1,h-1}/E_{ph}\ )^{m-3} \quad . \tag{24b}$$

Finally, the total width in (17) is defined by

$$\Gamma_m(E) = \Gamma_m^{(+)}(E)\downarrow + \Gamma_m^{(-)}(E)\downarrow + \sum_b \int dE_b\ \Gamma_{mb}(E,E_b)\hat{\uparrow} \quad , \tag{25}$$

where the sum runs over all particle-types b = n,p,α, and γ.

According to (3a) the normalization constant in (16) is chosen as

$$\sigma_\alpha^{SMC}(E_\alpha) = \sigma_\alpha^{OM}(E_\alpha) - \sum_{b=n,p,\gamma} \sigma_{\alpha,b}^{SMD}(E_\alpha) \quad . \tag{26}$$

Shell-structure effects in SMC processes are considered by an energy-dependent single-particle state density /18/,

$$g(\mathcal{E}) = g\ (\ 1 + \frac{\delta W}{\mathcal{E}}\ (1-\exp(-0.05/\mathcal{E}))) \quad , \tag{27}$$

with δW as the mass excess taken from tables. The quantity $\mathcal{E}$ = E or U denotes here the excitation energy of the composite or residual systems.

5. MPE Cross Section

The MPE is treated as a pure SMC approach. Thus, for second-chance processes (a,cb) with $c \neq \gamma$, i.e., the first term in (2), we write

$$\frac{d\sigma_{a,cb}(E_a)}{dE_b} = \int dE_c \, \frac{d\sigma_{a,c}(E_a)}{dE_c} \, \mathcal{N}_{a,cb}(E_1,E_b) \quad , \tag{28}$$

with $E_1 = E - B_c^{eff} - E_c$ as the intermediate energy. Here, the emission probability is given by

$$\mathcal{N}_{a,cb}(E_1,E_b) \equiv \sum_{m=m_o}^{m'} \frac{\tau_{m-1}(E_1)}{\hbar} \, \Gamma_{m-1,b}(E_1,E_b) \hat{\Gamma} \quad , \tag{29}$$

which is normalized according to

$$\sum_b \int dE_b \, \mathcal{N}_{a,cb}(E_1,E_b) = 1 \quad . \tag{30}$$

The escape widths in (29) are calculated by Eqs.(20) and (21) using the residual excitation energy (including the Pauli-correction)

$$U_{ph} = E_1 - A_{ph} - E_b - B_b^{eff} - k\Delta \tag{31}$$

with k = 1. (In general, e.g., if we consider magic-number nuclei, we have k = -1, 0, or 1 depending on the reaction channel.)

The above MPE-formalism is more general than the MPE-expressions reported earlier in /1,2/. As obvious from (28) and (29) the master equation (17) should be solved for each intermediate energy E_1. An extension of this formalism to higher-chance emission processes like (a,cdb), etc. is straightforward.

6. Results

Calculations of activation and double-differential cross-sections for 58 nuclei (mainly structural materials) up to 26 MeV are performed in /17/ with code EXIFON /18/.

The γ-production cross section (n,nγ) can only be discussed together with all other competitive reaction channels (neutron, proton, alpha). This will be demonstrated for the neutron-induced reaction on 56-Fe at about 14 MeV incident energy in Figs. 1-4.

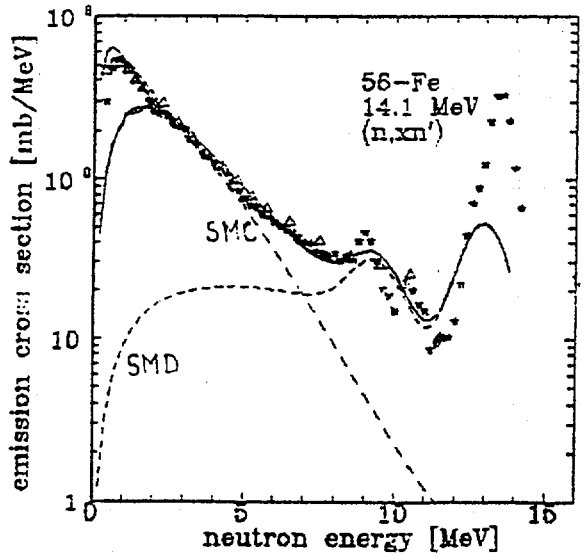

Fig.1 Experiments from /19,20/

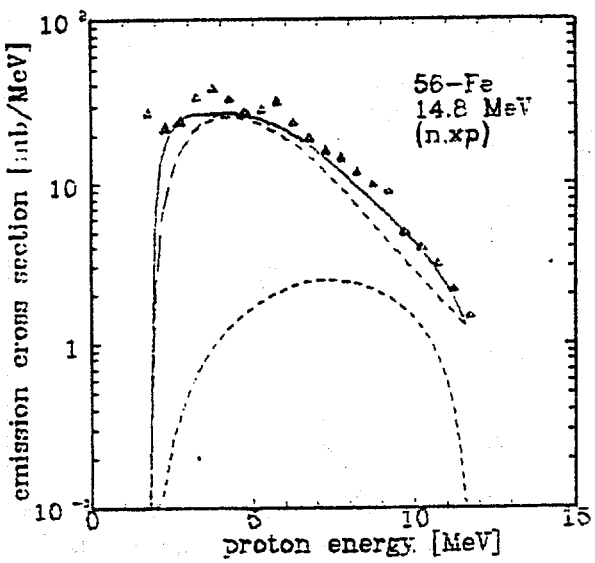

Fig.2 Experiments from /21/

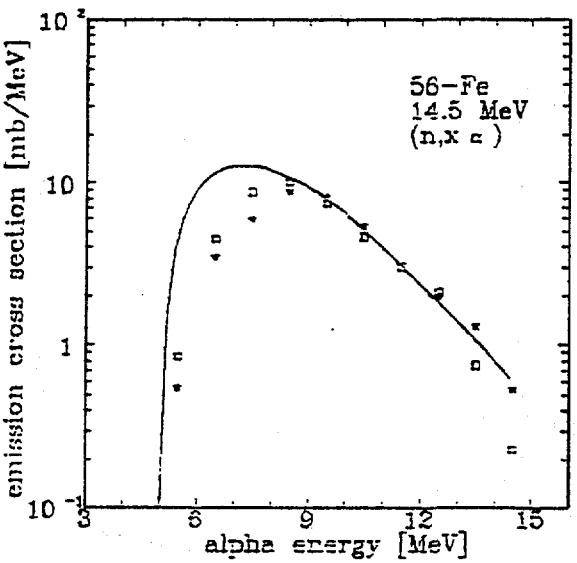

Fig.3 Experiments from /22,23/

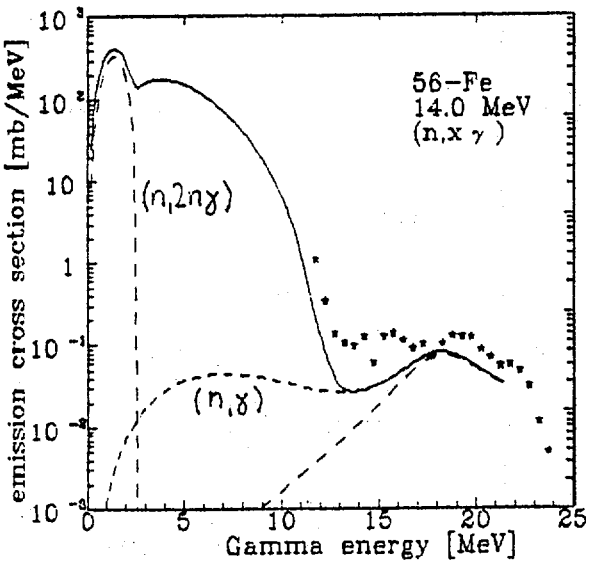

Fig.4 Experiments from /24/

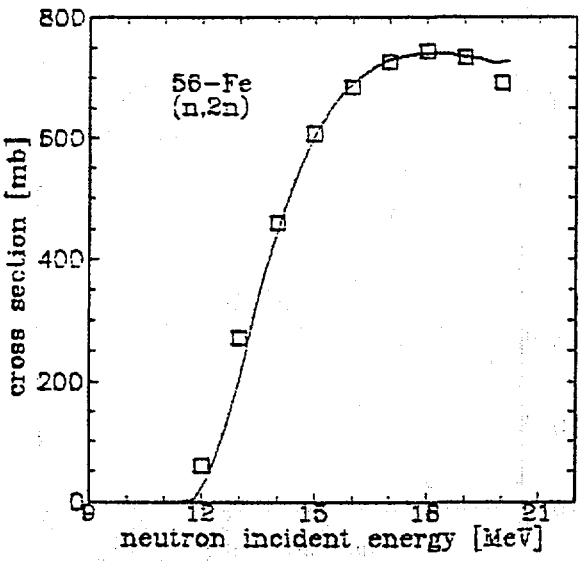

Fig.5 Experiments from /25/

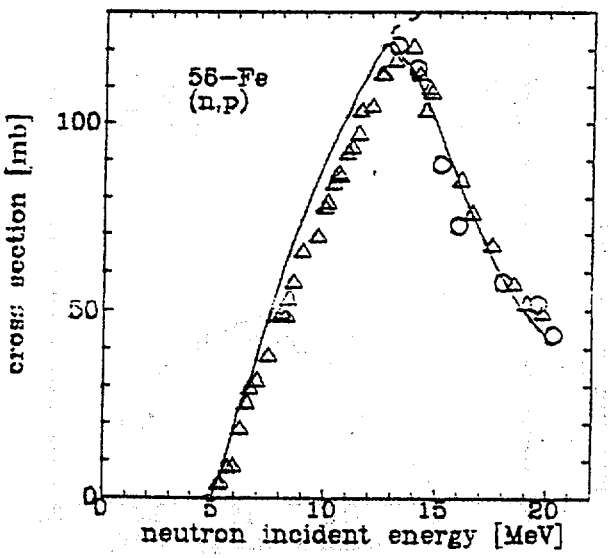

Fig.6 Experiments from /26,27/

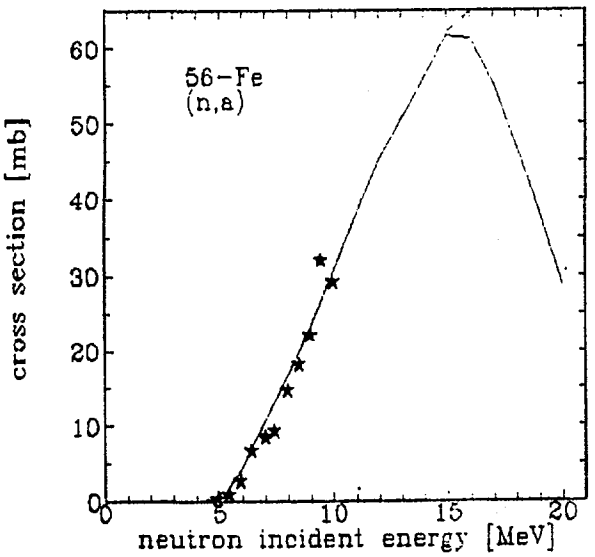

Fig.7 Experiments from /28/

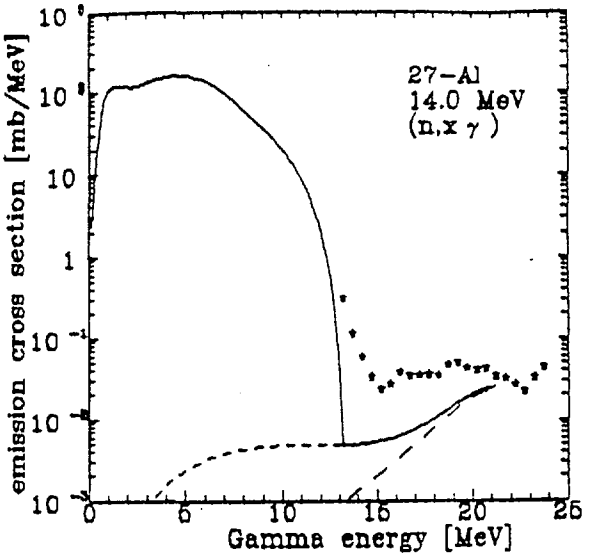

Fig.8 Experiments from /24/

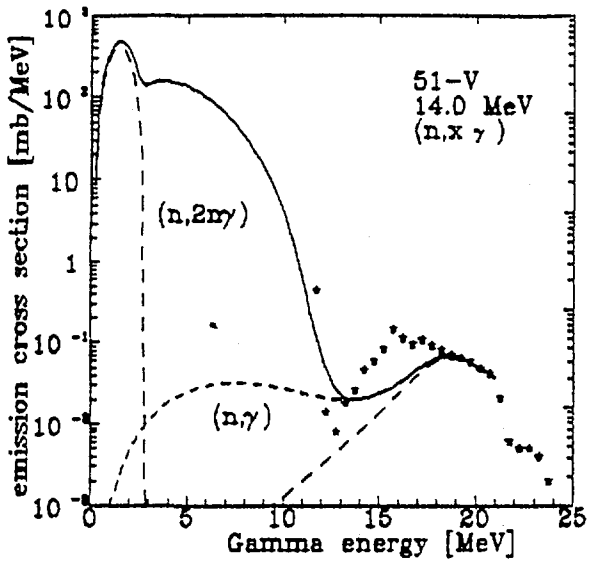

Fig.9 Experiments from /24/

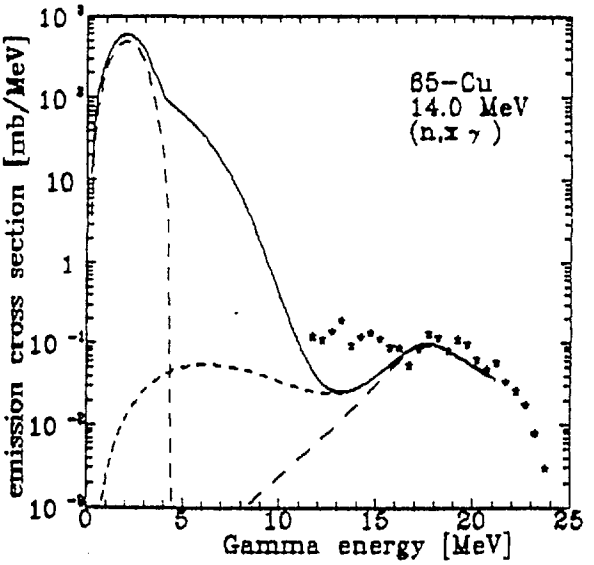

Fig.10 Experiments from /24/

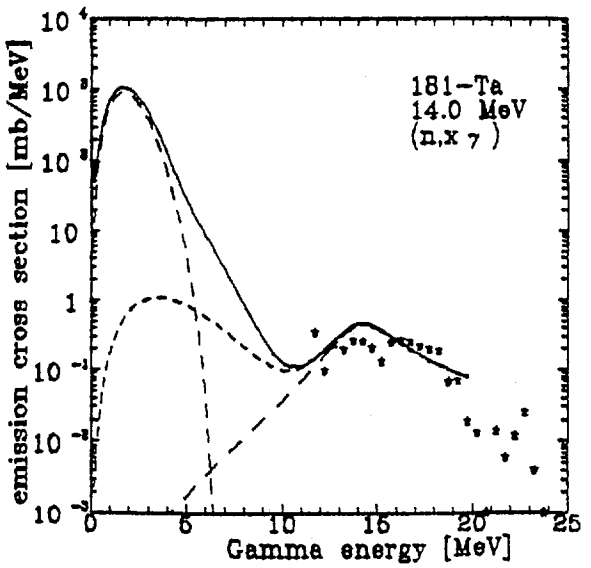

Fig.11 Experiments from /24/

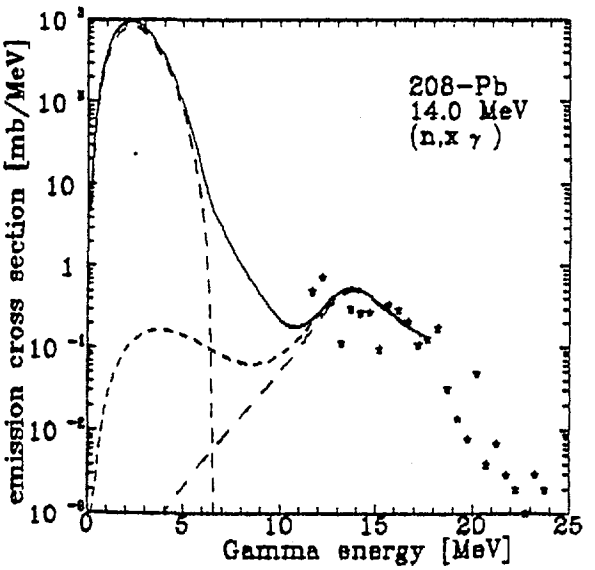

Fig.12 Experiments from /24/

Here the total emission spectra (full line) according to Eq.(1) are supposed of three main parts which are drawn separately: the SMD- and SMC-processes (broken lines) as well as the MPE-processes. There are big differences in the shape and magnitude of the different emission spectra. Thus, in contrast to the particle-emission processes the first-chance γ-emission (short-broken line in Fig.4) is very small, $\sigma_{n,\gamma} < 1$ mb. The high-energy part of the γ-spectrum is described by the "SMD"-process (long-dashed line) in Eq.(15) and shows a maximum at the GDR-energy of about 17 MeV. The bulk of the γ-production comes, however, from the $(n,n\gamma)$-processes. In Fig.4 also the $(n,2n\gamma)$-processes in the low-energy region are depicted as a short-dashed line. For some nuclei the different processes which are built up the total γ-production $(n,x\gamma)$ are summarized in Table 1.

Table 1. Partial γ-cross sections in mb for neutron-induced reactions at incident energy E_n

Target	E_n/MeV	$\sigma^{SMD}_{n,\gamma}$	$\sigma_{n,\gamma}$	$\sigma_{n,n\gamma}$	$\sigma_{n,p\gamma}$	$\sigma_{n,\alpha\gamma}$	$\sigma_{n,2n\gamma}$
27-Al	14.0	0.07	0.1	710.2	56.2	251.6	0.2
51-V	14.0	0.3	0.6	745.9	32.4	21.4	555.8
56-Fe	14.0	0.4	0.8	789.8	113.2	56.0	447.6
65-Cu	14.0	0.4	0.9	559.2	26.9	12.6	909.3
181-Ta	14.0	2.1	7.5	530.5	5.3	0.7	1868.7
208-Pb	14.0	2.2	3.2	394.3	0.3		2174.8
93-Nb	4.5	0.03	16.0	2057.	0.9	2.2	
93-Nb	13.0	0.8	2.3	579.7	29.8	25.8	1138.9
93-Nb	15.5	0.9	2.1	323.2	29.8	13.1	1307.0
93-Nb	18.5	1.0	1.9	245.2	30.9	7.1	1258.6

The (n,2n)-, (n,p)- and (n,α)-activation cross sections for 56-Fe are shown in Figs. 5-7. They are calculated according to Eqs.(5). The inclusion of the γ-channel mainly influences the (n,2n)-cross section. This will be shown in Figs. 13 and 14 for 65-Cu and 181-Ta where calculations with (full line) and without the $(n,n\gamma)$-processes (broken line) are depicted. As obvious from the figures the influence of the $(n,n\gamma)$-channel rises with mass number.

Further, in Figs. 8-12 the high-energy part of the γ-spectra are compared with experimental data /24/ at 14 MeV incident energy for different nuclei including the double-magic nucleus 208-Pb. Otherwise, the low-energy part of the γ-spectra are shown for 93-Nb in Figs. 15-18 at different incident energies (taken as the

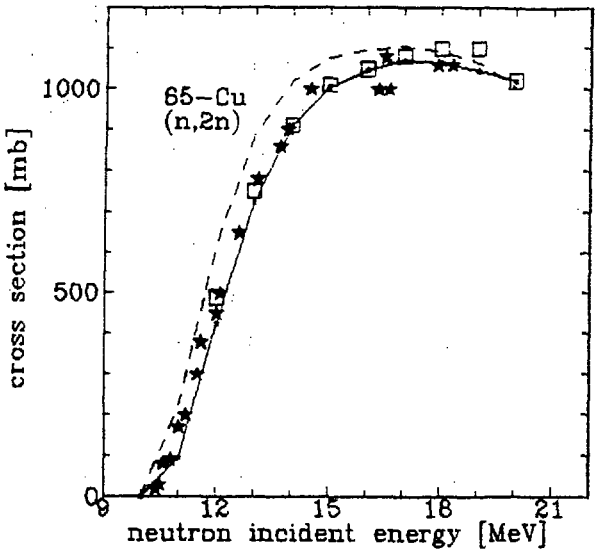

Fig.13 Experiments from /25,29/

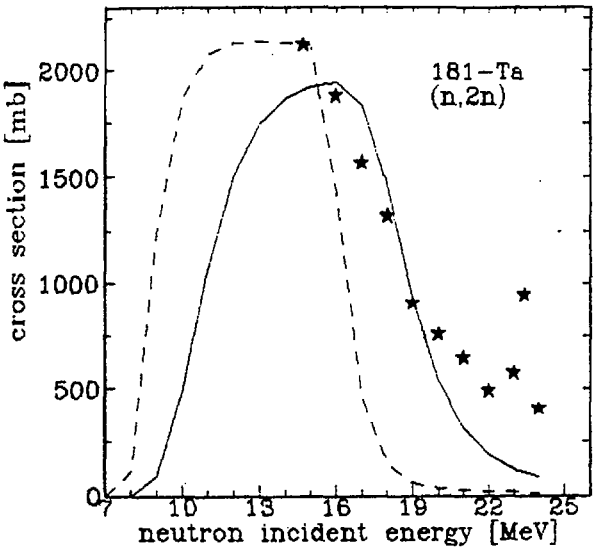

Fig.14 Experiments from /30/

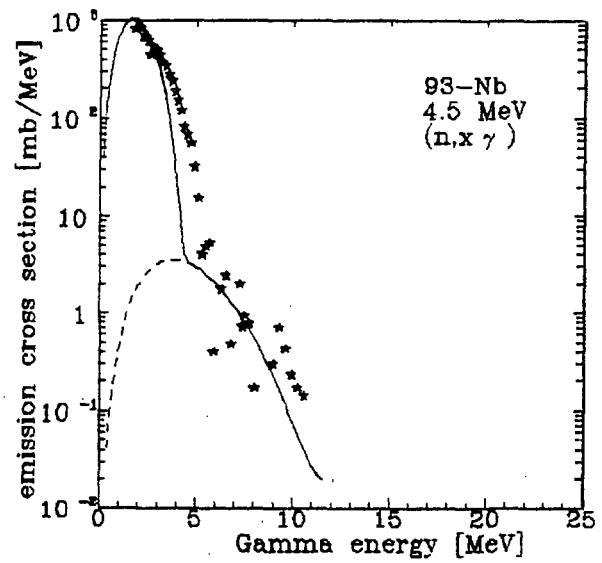

Fig.15 Experiments from /31/

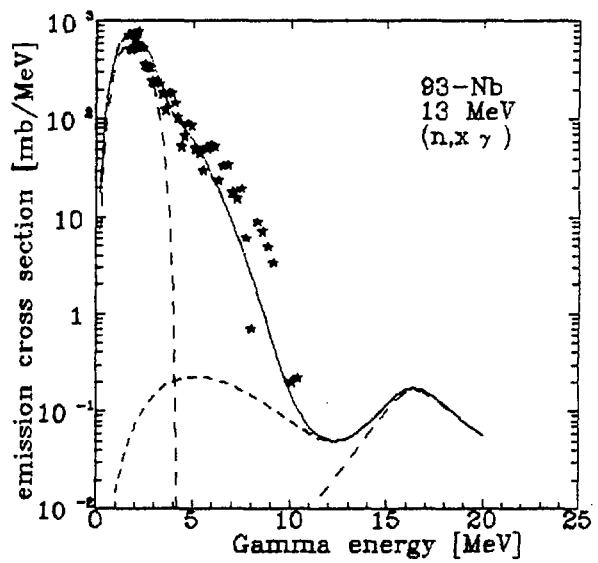

Fig.16 Experiments from /31/

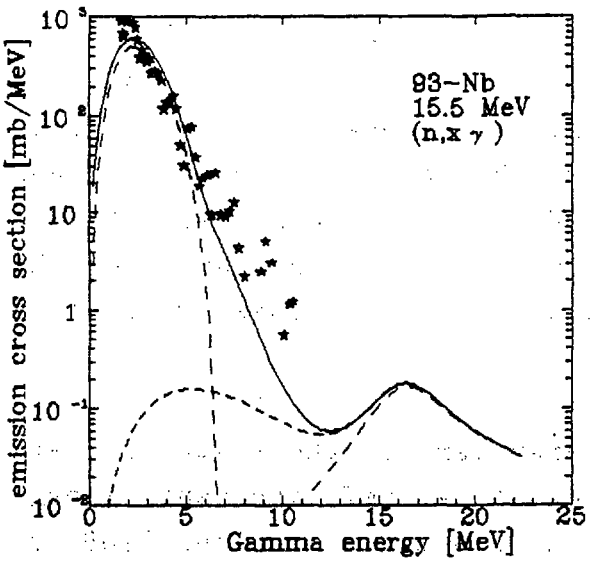

Fig.17 Experiments from /31/

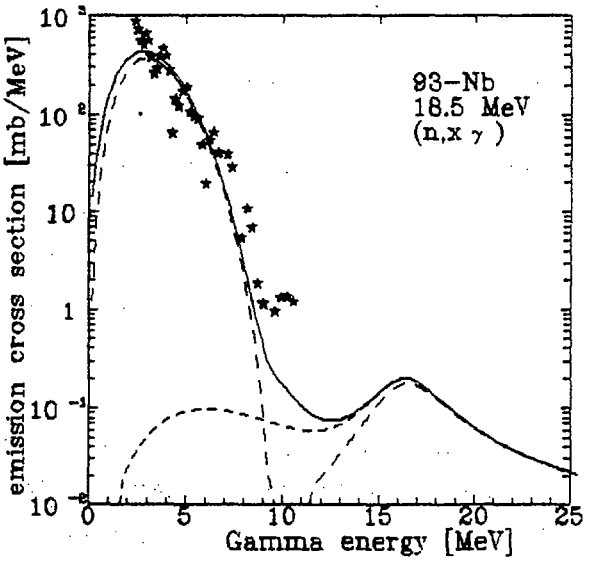

Fig.18 Experiments from /31/

mid-points of the experimental incident-energy bins). Here the double-differential experimental data at 90° are multiplied by 4π. However, a γ-multiplicity of M=1 was used (neglection of cascade decay). Thus, especially in the low-energy region, $E_\gamma \lesssim 3$ MeV, the calculation underpredicts the experimental data (see. Figs. 17-18).
In summary, the proposed statistical multistep reaction model predicts emission spectra which are in good agreement with experimental data. The calculation time of code EXIFON on PC/AT for 56-Fe at 14 MeV (including neutron, proton, alpha, and γ-spectra as well as angular distributions for nucleons) is about 70 secs, where 80% of the running time is used for MPE.

In the following over-simplified scheme code EXIFON (880 lines, 180 kByte) is compared with other codes /32-34/ in regard of reaction mechanisms considered

<table>
<tr><td>ECIS</td><td colspan="3">ALICE or STAPRE</td></tr>
<tr><td>DI</td><td colspan="2">PEQ</td><td>EV</td></tr>
<tr><td>collect.</td><td colspan="3">non-collective excitations</td></tr>
<tr><td>[vib]</td><td>[ex]</td><td colspan="2" rowspan="2">SMC</td></tr>
<tr><td colspan="2">SMD</td></tr>
<tr><td colspan="4">EXIFON</td></tr>
</table>

Here MPE and two-step direct processes are neglected. (The abbreviations: DI - direct reaction, PEQ - preequilibrium, EV - equilibrium mechanisms.) However, whereas the ECIS-code is based on a pure microscopic description the code EXIFON predicts direct collective excitations in a rather phenomenologic way.

7. References

1. Kalka,H., Torjman,M., Seeliger,D.: Phys.Rev.C 40, 1619 (1989)
2. Kalka,H., Torjman,M., Lien,H.N., Lopez,R., Seeliger,D.: Z. Phys.A (in press); (Report INDC(GDR)-055/LJ)
3. Kalka,H., Seeliger,D.: In: *Proceed. of the 5th Int. Symp. on Nucleon Induced Reactions*, Smolenice 1988, p.206
4. Agassi,D., Weidenmüller,H.,A., Mantzouranis,G.: Phys.Rep. 22, 145 (1975)
5. Brody,T.A., Flores,J., French,J.B., Mello,P.A., Pandey,A., Wong ,S.M.: Rev.Mod.Phys. 53, 385 (1981)
6. Zhivopistsev,F.A., Sukharevsky,V.G.: Phys. Elem. Part. Nucl., Dubna 15, 1208 (1984)
7. Ring,P., Schuck,P.: The Nuclear Many-Body Problem, New York: Springer-Verlag 1980

8. Feshbach,H., Kerman,A., Koonin,S.E.: Ann.Phys.(N.Y.) **125**, 429 (1980)
9. Field,G.M., Bonetti,R., Hodgson,P.E.: J.Phys. G12, 93 (1986)
10. Brink,D.M.: Thesis, Oxford University, 1955
11. Wisshak,K., Wickenhauser,J., Käppler,F., Reffo,G., Fabbri,F.: Nucl.Sc.Eng. **81**, 396 (1982)
12. Raman,S., et al.: At. Data Nucl. Data Tables **36**, 1 (1987)
13. Spear,R.H.: At. Data Nucl.Data Tables **42**, 55 (1989)
14. Bohr,A., Mottelson,B.R.: Nuclear Structure, Vol. II. Reading: Benjamin 1975
15. Iwamoto,A., Harada,K.: International Conference on Nuclear Data for Science and Technology, Mito (Japan) 1988, p. 485
16. Ando,Y., Uno,M., Yamada,M.: Report JAERI-M83-025 (1983)
17. Torjman,M.: PhD-thesis, TU Dresden 1990.
18. Kalka,H.: code EXIFON, unpublished
19. Pavlik,A., Vonach,H.: Physics Data 13-4 (1988), Fachinformationszentrum Karlsuhe.
20. Baba,M., et al.: International Conference on Nuclear Data for Science and Technology, Mito (Japan) 1988, p. 291
21. Grimes,S.M., et al.: Phys.Rev. C **1**, 2127 (1979)
22. Grimes,S.M., et al.: Phys.Rev. C **17**, 508 (1987)
23. Fischer,R., et al.: Ann. Nucl. Eng. **9**, 409 (1982)
24. Budnar,M., et al.: INDC(YUG)-6/L.
25. Manokhin,V.N., et al.: *Hand Book on Nuclear Activation Data*, p. 305 (1987)
26. Santry,D.C., Butler,J.P.: Can.J.Phys. **42**, 1030 (1964)
27. Bormann,M., et al.: Z.Phys. **166**, 477 (1962)
28. Paulsen,A., et al.: Nucl.Sc.Eng. **78**, 377 (1981)
29. Nagel.,W., Aten,A.H.W.: Jr.Physica **31**, 1091 (1965).
30. Veeser,L.R., et al.: Phys.Rev. C **16**, 1792 (1977)
31. Dickens,J.K., Morgan,G.L., Newmann,E.: ORNL-TM-4972 ENDF-219
32. Raynal,J.: "Optical Model and Coupled Channel Calculations in Nuclear Physics", in Computing as a Language of Physics (IAEA, Vienna, 1972)
33. Blann,M.: "OVERLAID ALICE: A Statistical Model Computer Code Including Fission and Pre-equilrium Models", COO-3494-29, 1976
34. Uhl,M., Strohmaier,B.: "STAPRE: A Computer Code for Particle Induced Activation Cross Sections and Related Quantities". IRK 76/01 (1976, Upd. 1981)

Gamma ray emission from multistep compound reactions*

P. Obložinský[1,2] and M. B. Chadwick[1]

[1]Nuclear Physics Laboratory, University of Oxford,
Oxford OX1 3RH, United Kingdom
and
[2]Institute of Physics, Slovak Academy of Sciences,
842 28 Bratislava, Czechoslovakia

Abstract

The multistep compound formalism of Feshbach, Kerman,and Koonin has been extended to include γ ray emission. By allowing the first few simple preequilibrium bound states to decay via electromagnetic transitions rather than particle emission, the large number of high-energy γ rays observed in the experimental data can be understood. It is assumed that single-particle and hole transitions lead to the emission of γ rays, and radial matrix elements for such transitions are estimated by exploiting the inverse process, photoabsorption. Reactions of 14 MeV neutrons with ^{59}Co, ^{93}Nb, and ^{181}Ta are analyzed and it is found that between twenty and fifty percent of cross sections for high-energy γ ray emission can be accounted for by the multistep compound mechanism.

I. INTRODUCTION

The statistical theory of multistep compound and multistep direct reactions developed by Feshbach, Kerman,and Koonin[1] (FKK) in 1980 was subsequently improved[2] and applied to explain particle emission spectra in a number of nuclear reactions (for surveys see Ref.3). Until now, γ ray emission has not been considered in this theory. Yet there is ample evidence from the high-energy parts of observed γ ray spectra, notably from those falling in the giant dipole resonance range, suggesting the presence of direct and preequilibrium radiative processes.[4] It seems therefore worthwhile to extend the FKK theory by including γ ray emission, particularly since the basic ideas regarding how to proceed in this direction are already available. The direct-semidirect model for γ ray emission developed by Brown et al.[5-7] should probably be adapted to serve as the first two terms of the multistep direct model. The theory of

* Talk delivered by M.B. Chadwick

multistep compound γ ray emission, on the other hand, should benefit from the treatment of one-body radiative transitions as included recently into the preequilibrium exciton[9-11] as well as hybrid[12,13] models. The purpose of the present work is to examine this latter possibility and include γ ray emission into the multistep compound theory of nuclear reactions.

II. THE MULTISTEP COMPOUND THEORY INCLUDING γ RAY EMISSION

In the FKK theory of multistep compound reactions[1] it is assumed that the interaction between the incident nucleon and the target nucleus takes place in a number of stages of increasing complexity. The process continues until the energy is spread through the nucleus to produce a fully equilibrated system, which then decays statistically. At each stage of the excitation there are three possibilities: excitation of an additional particle-hole pair to produce a more complex stage; particle emission via a two-body interaction into the continuum; and radiative transitions producing γ rays.

Following preequilibrium models,[9-13] we assume that radiative processes are electric dipole and one-body in character. The multistep compound theory for γ ray emission presented in this work follows the usual FKK formalism for calculating the matrix elements for escape processes, but instead of determining the radial part of radiative matrix elements by considering the overlap integral of the electrical dipole operator between single-particle states, we estimate these matrix elements by invoking detailed balance.

The differential cross section for multistep compound γ ray emission can be expressed as the product of three factors, namely the cross section for the formation of the composite system, the probability of γ ray escape from particular reaction stage, and the probability of reaching that stage. This product should be summed over all reaction stages prior to reaching equilibrium and over all the quantum numbers involved. The γ ray emission cross section is thus given by

$$\frac{d\sigma}{d\varepsilon_\gamma} = \pi\lambda^2 \sum_J \frac{2J+1}{(2i+1)(2I+1)} \frac{2\pi < \Gamma_J^{in} >}{< D_J >} \sum_{N=1}^{r-1} \frac{\Sigma_{s,\nu} < \Gamma_{\gamma n_J}^{\nu s}(U)\rho_{\nu s}(U) >}{< \Gamma_{n_J} >} \times \prod_{M=1}^{N-1} \frac{< \Gamma_{m_J} >}{< \Gamma_{m_J} >} \qquad (1)$$

$2\pi < \Gamma_J^{in} > / < D_J >$ is the entrance channel strength function for the formation of a bound $2p1h$ state. Further, λ is the projectile wavelength, and i, I, and J are the spins of the projectile, target, and composite nucleus, respectively. The probability that a γ ray will be emitted into the continuum from the reaction stage N is given by the γ escape width

divided by the total width of the stage,

$$\frac{\langle \Gamma^{\nu s}_{\gamma n J}(U)\rho_{\nu s}(U) \rangle}{\langle \Gamma_{nJ} \rangle} \qquad (2)$$

The exciton number, $n = p + h$, is related to the reaction stage N by $n = 2N + 1$. The index $\nu = n, n-2$ labels the different exit modes allowed in γ emission which, because of the single-particle nature of the transitions, involve changes in the exciton number of $\Delta n = 0$ or -2. The residual nucleus spin after γ emission can be $s = J-1$, J or $J+1$, the residual excitation energy is U, and the respective level density is denoted as $\rho_{\nu s}(U)$. The last term to the right of Eq.(1) gives the probability that a system survives to the stage of interest without particle emission. Summation over N in Eq.(1) is terminated at the $(r-1)$-stage, which is still considered to be preequilibrium. The r-stage then contains a statistical description of all the following stages.

The entrance channel strength function can be evaluated from the optical-model strength function, reduced to account for flux in the multistep direct chain.

The particle-hole level density can be written in a form with energy and spin separated

$$\rho_{nJ}(E) = \omega(p,h,E)R_n(J). \qquad (3)$$

The energy dependent part, $\omega(p,h,E)$, is the particle-hole state density, and can be evaluated within the equidistant-spacing model under the constraint that all particles are bound.[17] One has

$$\omega(p,h,E) = \frac{g^n}{p!h!(n-1)!}\sum_{i=0}^{p}(-1)^i\binom{p}{i}\left[E-\Delta-A_{ph}-iB\right]^{n-1} \times\Theta\left[E-\Delta-A_{ph}-iB\right], \qquad (4)$$

where g is the single-particle state density, Δ is the pairing energy, B is the nucleon binding energy, and A_{ph} is the Pauli blocking term. The unit step function, Θ, is unity for positive arguments and zero otherwise. The angular-momentum distribution part of the level density can be represented by a Gaussian function

$$R_n(J) = \frac{2J+1}{2\sqrt{2\pi}\,\sigma_n^3}\exp\left[-\frac{(J+1/2)^2}{2\sigma_n^2}\right], \qquad (5)$$

where $\sigma^2 = n\sigma^2$ is the spin cut-off parameter. Combinatorial calculations using the shell model single-particle states yield[18] $\sigma^2 = 0.28\,A^{2/3}$.

III. γ RAY ESCAPE WIDTHS
A. Formalism

We consider single-particle electric dipole radiative transitions between an initial particle-hole bound state of energy E and spin J, and a final state of energy U and spin s. Neutrons as well as protons induce radiative transitions because of their dipole effective charge. Since the square of the neutron dipole effective charge differs only slightly from that of the proton,[19] we shall neglect neutron-proton distinguishability. Also, we shall not consider parity explicitly, since parity can be, to first order, neglected in the semi-classsical theories of preequilibrium γ ray emission[20] and the same applies in the multistep compound case.

The coordinates of only one nucleon are changed in the single-particle transition, and this leads to the selection rule $\Delta n = 0, -2$. Because of the energy-angular momentum factorization of the single-particle level density as well as of the electromagnetic operator, the γ ray escape width is of the factorized form and has the structure

$$<\Gamma^{\nu s}_{\gamma nJ}(U)\rho_{\nu s}(U)> = X^{\nu s}_{\gamma nJ} Y^{\nu}_{\gamma n}(U), \qquad (6)$$

where $\nu = n, n-2$. The functions X_γ and Y_γ have similar meaning as the X and Y functions in the nucleon escape widths. For the details of evaluating these functions we refer the reader to recent thesis by Chadwick.[8] Below we briefly remind only few importants results.

The electric dipole transition matrix element can be obtained in a way outlined in Ref.11 using standard theoretical methods.[21] The particle-hole system with the total spin J is divided into the core of spin j_3 and the single-particle excitation j_1 that makes a transition $j_1 \Rightarrow j_2$, while the spin j_2 couples to the spin j_3 to give the final spin s. The X^0_γ function is

$$X^0_\gamma \equiv X^{nS}_{\gamma nJ} = \frac{e^2}{2}|<j_2|r|j_1>|^2 \omega(\varepsilon_\gamma) \mathcal{X}^{nS}_{nJ}, \qquad (7)$$

where the radial matrix element is averaged over single-particle states, the state density of free γ rays

$$\omega(\varepsilon_\gamma) = \frac{V}{\pi^2 \hbar^3 c^3} \varepsilon^2_\gamma \qquad (8)$$

comes from the summation over final states (V is the nuclear volume), and $\mathcal{X}^{nS}_{nJ}$ is the angular momentum coupling term

$$\mathcal{X}^{nS}_{nJ} = \frac{3(2s+1)}{R_n(J)} \sum_{j_1 j_2 j_3} (2j_1+1)R_1(j_1)(2j_2+1)R_1(j_2)R_{n-1}(j_3)$$

$$\times \begin{pmatrix} j_1 & 1 & j_2 \\ \frac{1}{2} & 0 & -\frac{1}{2} \end{pmatrix}^2 \begin{Bmatrix} j_1 & j_3 & J \\ s & 1 & j_2 \end{Bmatrix}^2 . \qquad (9)$$

The radial matrix elements are evaluated using the inverse process. Though such a procedure is dictated by practical reasons, it seems to be justifiable because we need only average squared values of these matrix elements. The rate of γ ray absorption per second can be expressed by means of the golden rule[11]

$$\frac{c}{V}\sigma_n^{abs}(U,s \overset{\varepsilon_\gamma}{\Rightarrow} E,J) = \frac{e^2}{2h}|\langle j_2 | r | j_1 \rangle|^2 \left[y_n^n x_{ns}^{nJ} + y_n^{n+2} x_{ns}^{n+2J} \right], \qquad (10)$$

where the squared radial matrix element is already averaged over single-particle states and σ_n^{abs} is the photoabsorption cross section for a nucleus in a state with n excitons. The y functions give the energy dependence of the accessible level densities in the γ absorption. The x functions contain the angular momentum part of the accessible level densities. In terms of $x_{nJ}^{\nu s}$ one has

$$x_{\nu s}^{nJ} = \frac{(2J+1)\ R_n(J)}{(2s+1)\ R_\nu(s)}\, x_{nJ}^{\nu s} . \qquad (11)$$

The photoabsorption cross section can be obtained from the Brink-Axel hypothesis which states that the giant dipole resonance can be built on any excited state. The corresponding photoabsorption cross section is related to that on the ground state by[22]

$$\sigma_n^{abs}(U,s \overset{\varepsilon_\gamma}{\Rightarrow} E,J) = \frac{(2J+1)}{3(2s+1)}\sigma_{g.s.}^{abs}(\varepsilon_\gamma) . \qquad (12)$$

This latter cross section can be conveniently expressed as the sum of two Lorentzian functions

$$\sigma_{g.s.}^{abs}(\varepsilon_\gamma) = \sum_{q=1,2} \sigma_q \frac{\varepsilon_\gamma^2 \Gamma_q^2}{(\varepsilon_\gamma^2 - E_q^2)^2 + \varepsilon_\gamma^2 \Gamma_q^2} , \qquad (13)$$

where σ_q , Γ_q , and E_q are the peak cross section, width, and energy, respectively. The final result for X_γ^o is

$$X_\gamma^o = \frac{\varepsilon_\gamma^2 \sigma_{g.s.}^{abs}(\varepsilon_\gamma)}{3\pi^2 h^2 c^2} \frac{\frac{R_n(s)}{R_n(J)}\, x_{ns}^{nJ}}{y_n^n\, x_{ns}^{nJ} + y_n^{n+2}\, x_{ns}^{n+2J}} . \qquad (14)$$

Similarly, for $X_\gamma^- \equiv X_{\gamma nJ}^{n-2s}$ one gets

$$\varkappa_{nJ}^{n-2s} = \frac{R_{n-2}(s)}{R_n(J)} \sum_{j_1 j_2} (2j_1+1)R_1(j_1)(2j_2+1)R_1(j_2)$$

$$\times \begin{Bmatrix} j_1 & j_2 & 1 \\ \frac{1}{2} & -\frac{1}{2} & 0 \end{Bmatrix}^2 \Delta(s1J), \qquad (15)$$

and

$$X_\gamma^- = \frac{\varepsilon_\gamma^2 \sigma_{g.s.}^{abs}(\varepsilon_\gamma)}{3\pi^2 h^2 c^2} \frac{\frac{R_{n-2}(s)}{R_n(J)} \varkappa_{n-2s}^{nJ}}{y_{n-2}^{n-2} \varkappa_{n-2s}^{n-2J} + y_{n-2}^{n} \varkappa_{n-2s}^{nJ}} . \qquad (16)$$

Diagrams for Y_γ functions are self-evident. For the function Y_γ^o one has

$$Y_\gamma^o \equiv Y_n^n(U) = {}_pY_\gamma^o + {}_hY_\gamma^o \qquad (17)$$

since the transition can be made either by a particle or a hole. Considering higher γ ray energies, $\varepsilon_\gamma > B$, only the ${}_hY_\gamma^o$ term contributes to Y_γ^o. In this case, which is of most interest to us one obtains

$$Y_\gamma^o \cong {}_hY_\gamma^o \cong gh\frac{\omega(p,h,U)}{\omega(p,h,E)} , \qquad (18)$$

The function Y_γ^- is simply the probability of finding a particle-hole pair of energy $\varepsilon_\gamma = E - U$,

$$Y_\gamma^- \equiv Y_n^{n-2}(U) = \frac{\omega(p-1,h-1,U)}{\omega(p,h,E)} \omega(1,1,\varepsilon_\gamma) . \qquad (19)$$

Here,

$$\omega(1,1,\varepsilon_\gamma) = \begin{cases} g^2\varepsilon_\gamma & \text{if } \varepsilon_\gamma \le B \\ g^2 B & \text{if } \varepsilon_\gamma \ge B \end{cases} \qquad (20)$$

as follows from Eq.(3).

The y_n^n and y_n^{n+2} functions for the photoabsorption are obtained easily as inverse to emission, though, with no restrictions to bound states. This yields $y_n^n = gn$ and $y_n^{n+2} = g^2\varepsilon$.

B. Summary and discussion of γ ray escape widths

We summarize the above results as follows. Considering transitions of energies $\varepsilon_\gamma \geq B$ one has

$$\langle \Gamma^{nS}_{\gamma nJ}(U)\rho_{nS}(U)\rangle = X^{0}_{\gamma}Y^{0}_{\gamma} = \frac{\varepsilon_\gamma^2\ \sigma^{abs}_{g.s.}(\varepsilon_\gamma)\ \rho_{nS}(U)}{3\pi^2\hbar^2c^2\quad \rho_{nJ}(E)}\beta^{nJ}_{nS}\ , \tag{21}$$

where

$$\beta^{nJ}_{nS} = \frac{gh\ \varkappa^{nJ}_{nS}}{gn\ \varkappa^{nJ}_{nS} + g^2\varepsilon_\gamma\ \varkappa^{n+2J}_{nS}}\ . \tag{22}$$

Similarly,

$$\langle \Gamma^{n-2S}_{\gamma nJ}(U)\rho_{n-2S}(U)\rangle = X^{-}_{\gamma}\ Y^{-}_{\gamma} =$$

$$= \frac{\varepsilon_\gamma^2\ \sigma^{abs}_{g.s.}(\varepsilon_\gamma)}{3\pi^2\hbar^2c^2}\ \frac{\rho_{n-2S}(U)}{\rho_{nJ}(E)}\beta^{nJ}_{n-2S}\ , \tag{23}$$

where

$$\beta^{nJ}_{n-2S} = \frac{\omega(1,1,\varepsilon_\gamma)\varkappa^{nJ}_{n-2S}}{g(n-2)\ \varkappa^{n-2J}_{n-2S} + g^2\varepsilon_\gamma\ \varkappa^{nJ}_{n-2S}} \tag{24}$$

The multistep compound γ ray escape widths have the same structure as the γ emission widths in the exciton model.[11] The essential difference is that the multistep compound radiative processes are confined to transitions between bound states rather than between unconditional states as is the case in the exciton model. The factor $\beta^{nJ}_{\nu S}$ represents the branching ratio for photoabsorption, i.e., the fraction of the total photoabsorption cross section for a state with ν excitons and spin s leading to bound state with n excitons and spin J. Since photoabsorption also includes transitions to unbound states, the sum of the branching ratios is smaller than unity,

$$\beta^{nJ}_{nS} + \beta^{n+2J}_{nS} < 1 \tag{25}$$

rather than equal to unity as found in the exciton model. By releasing the constraint on bound states Eqs.(21)-(24) become identical with the respective results in the exciton model.

IV. RADIATIVE CAPTURE OF FAST NEUTRONS

The presence of multistep compound processes in reactions of 14 MeV neutrons is now well established via analyses of the emission spectra of nucleons.[14,15] It seems therefore

worthwhile to apply our γ emission formalism to study radiative capture of fast neutrons. Below we examine the (n,γ) reactions at 14 MeV on target nuclei ^{59}Co, ^{93}Nb, and ^{181}Ta and focus our attention on the spectra of primary γ rays in the giant dipole resonance region.

The multistep compound calculations were performed, whenever possible, along the lines described by Chadwick et al.[14] and by Herman et al.[16]. The entrance channel strength functions were calculated from the optical model transmission coefficients corrected to account for multistep direct processes. The corresponding reduction factor was taken as R = 0.90, 0.86, and 0.90 for ^{59}Co, ^{93}Nb, and ^{181}Ta, respectively.[16] The nucleon escape and damping widths were calculated using harmonic oscillator wave functions for the bound nucleons and optical model scattering wave functions for the unbound nucleons.[14] The level density parameters were those of Ref. 14 and the parameterization of the giant dipole resonance photoabsorption cross section was taken from Ref. 23.

The calculations in the Hauser-Feshbach statistical model were replaced by much more simple ones using the Weisskopf-Ewing evaporation model.[24] A close equivalence with the Hauser-Feshbach formulation for (n,γ) reactions was retained by applying relatively simple correction factors to the Weisskopf-Ewing results, as discussed by Gruppelaar.[25]

The approach adopted in this paper for multistep compound emission makes use of the approximate equivalence of the r-stage widths for nucleon escape with the nucleon emission widths in the (equilibrium) statistical model. An essential point is that by equating the two widths one determines the residual nucleon-nucleon interaction strength V_0. This approach has two advantages: our calculation becomes essentially parameter-free; and in equilibrium the γ ray spectra are matched with the established statistical model results.

We proceed by comparing in Figs. 1 - 3 the calculated spectra of primary γ rays with the experimental data[26,27] for the three (n,γ) reactions. The multistep compound spectrum consists of contributions from the initial reaction stages N = 1, 2, and 3, and from the r-stage. The spectrum shows two peaks. The high energy peak is close to the maximum energy of the giant dipole resonance (note the double peak for ^{181}Ta because of two GDRs) and is due to preequilibrium γ rays coming from the early reactions stages. A low energy peak is in the energy range of a few MeV and corresponds to the r-stage contribution. Shown for comparison is the equilibrium spectrum as calculated by the statistical model. This spectrum has a shape quite similar to, but considerably stronger than, the r-stage spectrum. The different intensities of the two spectra is due to the depletion factor, which is included in multistep compound emission but not in the statistical model.

Comparison of the primary γ rays as calculated by the multistep compound formalism with the experimentally observed

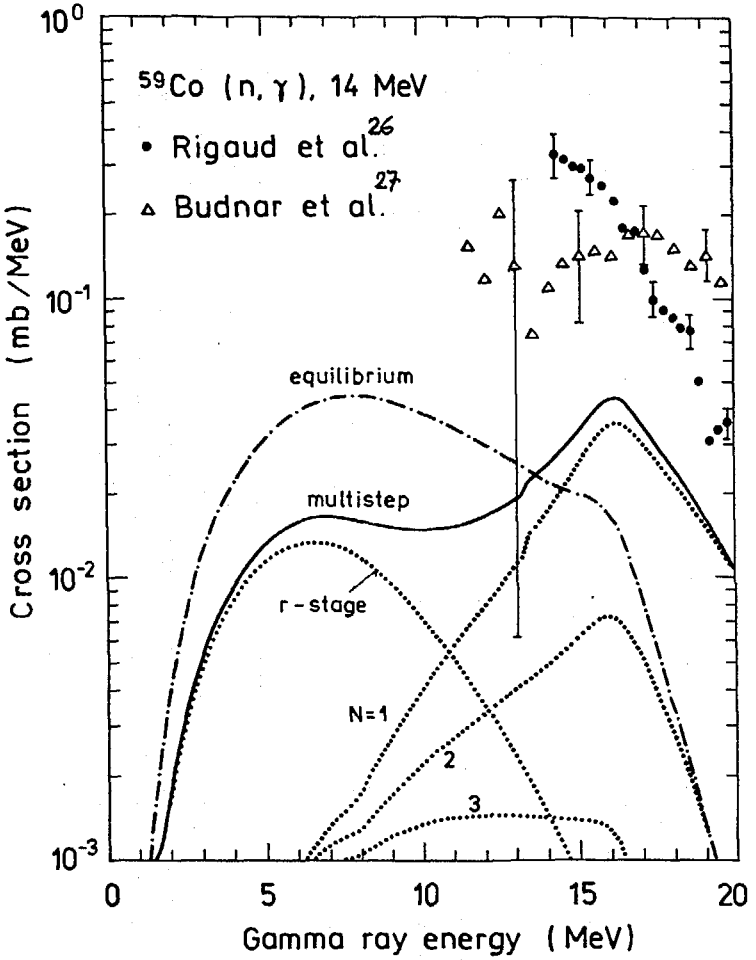

Fig.1 ^{59}Co(n,γ) at E_n = 14 MeV compared with experimental data. The full curve represents the multistep compound spectrum, dotted lines being the contributions from stages N = 1, 2, 3, and from the r-stage. The dashed-dotted curve is the γ ray spectrum calculated within the (equilibrium) statistical model.

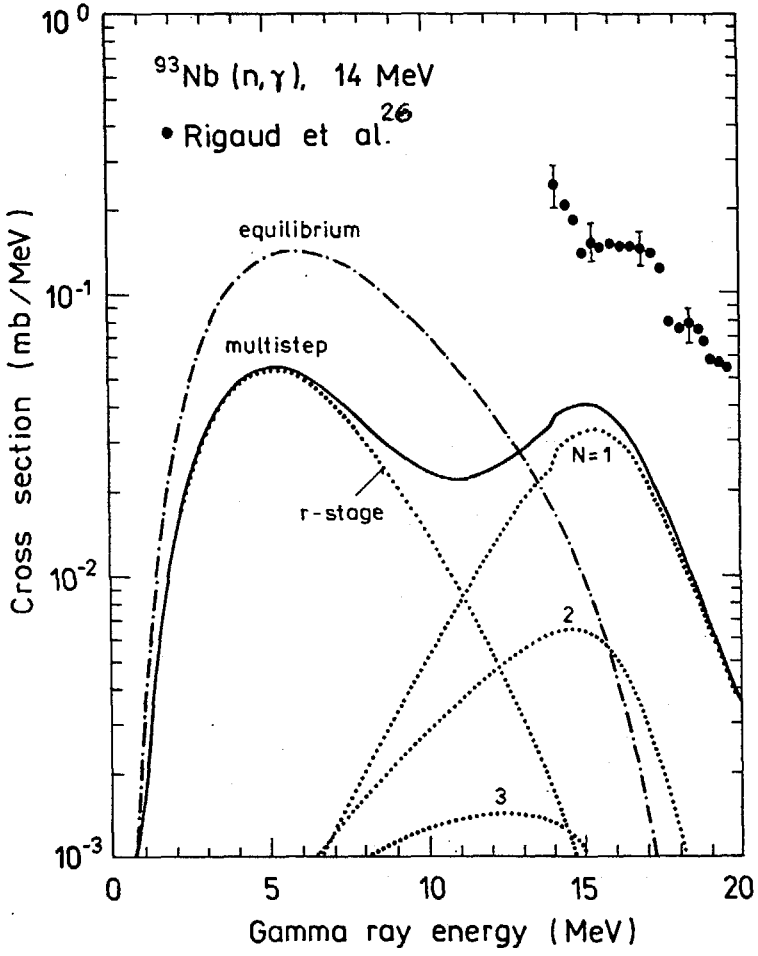

Fig.2. Calculated spectra of primary γ rays from the reaction ^{93}Nb(n,γ) at E_n = 14 MeV compared with experimental data. For further explanation see Fig.1.

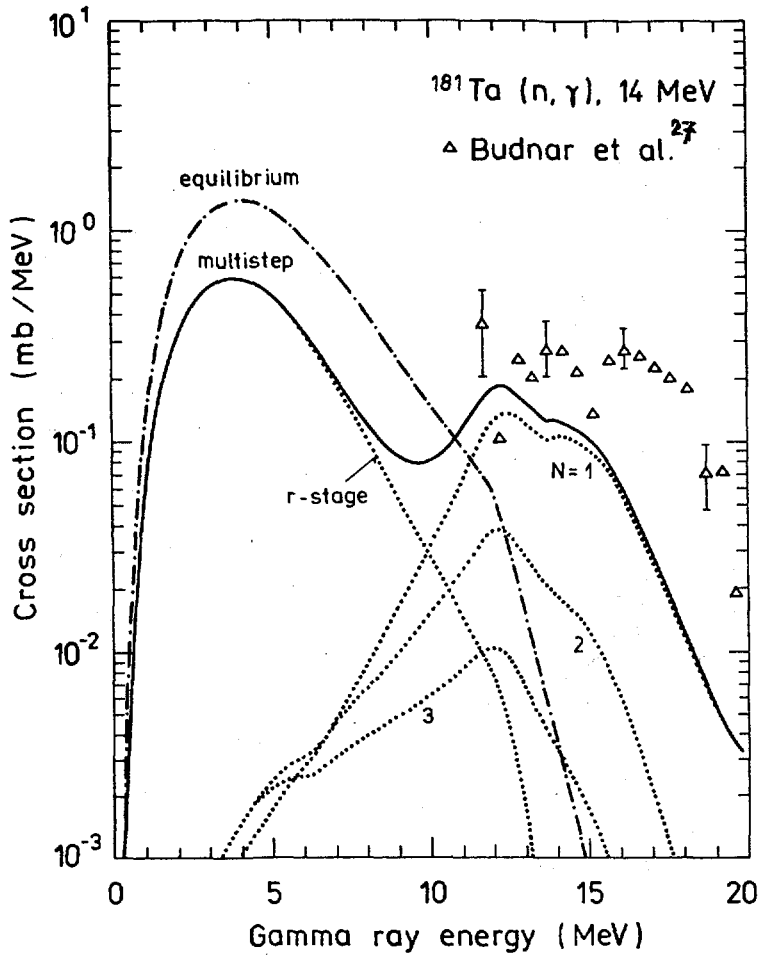

Fig.3. Calculated spectra of primary γ rays from the reaction ^{181}Ta(n,γ) at E_n = 14 MeV compared with experimental data. For further explanation see Fig.1.

spectra is meaningful only in the spectral range of high energies, ε_γ > 14 MeV. At lower emission energies the primary γ rays from radiative capture are masked by order of magnitudes stronger (n,n'γ) component. It is seen that the multistep compound γ emission accounts for about 20% of the observed intensity of high energy γ rays for ^{59}Co, some 30% for ^{93}Nb, and almost 50% for ^{181}Ta. This can be considered as an encouraging result since the rest of the observed γ rays may be related to multistep direct processes. Unfortunately, at present there is no theory for the multistep direct γ emission which would allow a more complete comparison of our results with the data.

The authors wish to express their gratitude to Peter Hodgson for his support of this work and for many valuable comments and suggestions. One of us (P.O.) is most grateful to Oxford University for its hospitality. This work was partly supported by the International Atomic Energy Agency under the research contracts No. 4997/RB and 5148/RB.

References

1 H. Feshbach, A. Kerman, and S. Koonin, Ann.Phys. (NY) 125, 429 (1980).
2 R. Bonetti, L. Colli Milazzo, and M. Melanotte, Phys. Rev. C 27, 1003 (1983).
3 H. Gruppelaar, P. Nagel, and P.E. Hodgson, La Rivista del Nuovo Cimento 9, 1 (1986);
4 K.A. Snover, Annu. Rev. Nucl. Part. Sci. 36, 545 (1986).
5 G.E. Brown, Nucl. Phys. 57, 339 (1964).
6 A.A. Lushnikov and D.F. Zaretsky, Nucl. Phys. 66, 35 (1966).
7 C.F. Clement, A.M. Lane, and J.R. Rook, Nucl. Phys. 66, 273 (1965); 66, 293 (1965).
8 M.B. Chadwick, PhD Thesis, Oxford University (1989), unpublished.
9 E. Běták and J. Dobeš, Phys. Lett. 84B, 368 (1979).
10 J.M. Akkermans and H. Gruppelaar, Phys. Lett. 157B, 95 (1985).
11 P. Obložinský, Phys. Rev. C 35, 407 (1987).
12 G. Reffo, M. Blann, and B.A. Remington, Phys. Rev. C 38, 1190 (1988); 39, 1188(E) (1989).
13 P. Obložinský, Phys. Lett. 215B, 597 (1988).
14 M.B. Chadwick, R. Bonetti, and P.E. Hodgson, J. Phys. G15, 237 (1989);
15 N. Koumdijeva and P. E. Hodgson, J. Phys. G15, 1689 (1989).
16 M. Herman, A. Marcinkowski, and K. Stankiewicz, Nucl. Phys. A430, 69 (1984); 435, 859(E) (1989).
17 P. Obložinský, Nucl. Phys. A453, 127 (1986).
18 G. Reffo and M. Herman, Lett. Nuovo Cimento, 34, 261 (1982).
19 R. Chrien, A. Hofmann, and A. Molinary, Phys. Rep. 64, No.5, 295 (1980).
20 P. Obložinský, Phys. Rev. C 41, 401 (1990).
21 A. Bohr and B.R. Mottelson, Nuclear Structure (Benjamin, New York, 1969) vol.1, pp. 83, 84, and 387.
22 G.A. Bartholomew, E.D. Earle, A.J. Ferguson, J.W. Knowles, and M. A. Lone, Adv. Nucl. Phys. 7, 229 (1973).
23 S. S. Dietrich and B. L. Berman, Atomic Data and Nuclear Data Tables, 38, 199 (1988).
24 V. F. Weisskopf and D. E. Ewing, Phys. Rev. 57, 472 (1940); 57, 935 (1940).
25 H. Gruppelaar, Energieonderzoek Centrum Nederland, Report ECN-83-064, Petten 1983.
26 F. Rigaud, J. L. Irigaray, G. Y. Petit, G. Longo, and F. Saporetti, Nucl. Phys. A173, 551 (1971).
27 M. Budnar et al., International Atomic Energy Agency, Report INDC(YUG)-6/L, Vienna 1979.

Preequilibrium emission of hard photons in proton-nucleus reactions

P. Obložinský
Institute of Physics of the Slovak Academy of Sciences,
842 28 Bratislava, Czechoslovakia

The preequilibrium hybrid model is extended to account for emission of hard photons using the quasideuteron radiative concept and detailed balance. We analyse proton-nucleus reactions, find good accord with the observed photon spectra at 72 MeV incident energy and predict two times higher spectra than the observed ones at 140 MeV.

I. INTRODUCTION

The theory of preequilibrium decay proved useful in interpretation of particle spectra in a variety of nuclear reactions, especially in those induced by nucleons. Particularly, proton-nucleus reactions were studied in detail over a broad incident energy range in the framework of the hybrid model.[1] Recent interest in medium (giant dipole resonance) and hard photon emission was triggered by observations of these photons in heavy-ion collisions, followed by vigorous activity in the field (for surveys see, e.g., Snover[2] and Metag[3]). The hybrid model was extended quite recently to account for preequilibrium photon emission of moderate energies by incorporating single-particle radiative transitions. Applications to light-ion induced reactions have met with considerable success.[4,5] It seems therefore natural to extend further the hybrid model to account for the hard photon emission. To this end, however, another radiative mechanism must be considered.

There is growing evidence that hard photons come from incoherent proton-neutron collisions in the initial stages of nuclear reactions.[6,3] This two-particle radiative mechanism, usually identified with bremsstrahlung, is firther supported by the photoabsorption, an inverse process well described by the quasideuteron model of Levinger.[7] This model opens up the possibility to aaply detailed balance to hard photon emission, an idea raised recently by several authors.[8,9,10] Another clue in favour of the quasideuteron picture comes from the photonucleon spectral studies.[11]

The main goal of the present contribution (see also Ref.17) is to remind how one can incorporate the quasideuteron radiative mechanism via detailed balance into preequilibrium hybrid model. We show that the resulting formalism of preequilibrium hard photon emission is very

transparent and its application to proton-nucleus reactions is straightforward. We perform analysis of the photon spectra measured recently by Kwato Njock et al.[12] at 72 MeV and also compare our prediction with the Edgington and Rose data at 140 MeV.[13] This is of interest in view of possible incosistencies between these two measurements that show up as a bias of the 140 MeV data in the emerging systematics of hard photon production in heavy-ion collisions.[3]

II. FORMALISM

The hybrid model[4,5] for the photon emission can be formulated as

$$\frac{d\sigma}{d\varepsilon_\gamma} = \sigma_a \sum_x \sum_{\substack{n=n_0 \\ \Delta n=+2}}^{\bar{n}} \int_0^E \left[\frac{\omega_{n-1}(E-\varepsilon)\, g_x\, d\varepsilon}{\omega_n(E)}\right] \left[\frac{\lambda_\gamma(\varepsilon,\varepsilon_\gamma)}{\lambda_\gamma(\varepsilon)+\lambda_c(\varepsilon)+\lambda_+(\varepsilon)}\right] D_n\,, \quad (1)$$

where σ_a is the reaction cross section. The expression in the first set of square brackets represents the fraction of particles of type x (neutrons or protons) with energy in the range ε, $\varepsilon+d\varepsilon$ in a state with n excitons and energy E. The quantity $\omega_n(E)$ is the state density and g_x means the single-particle state density. The expression in the second set of square brackets gives the relative rate of the particle ε to undergo a two-particle interaction and to emit a photon with the energy ε_γ. The denominator is given by the sum of the total photon emission rate (this part can be neglected), particle emission rate into continuum and nucleon-nucleon collision rate. The last term to the right is the depletion factor, n_0 and $\bar{n}$ are the initial and the equilibrium exciton numbers, respectively.

The state density should be given for a two-component gas with a constraint on the finite potential well. Using the technique outlined in Ref.14 and considering the same potential well depth for neutrons as well as protons, one has

$$\omega_n(E) \equiv \omega_{p_\nu p_\pi h_\nu h_\pi}(E) = \frac{g_\nu^{p_\nu+h_\nu} g_\pi^{p_\pi+h_\pi}}{p_\nu!\, p_\pi!\, h_\nu!\, h_\pi!\, (n-1)!} \sum_{\ell=0}^{h_\nu+h_\pi} (-1)^\ell \binom{h_\nu+h_\pi}{\ell} \cdot$$

$$\cdot\, (E-\ell\varepsilon_F)^{n-1}\, \Theta(E-\ell\varepsilon_F)\,. \quad (2)$$

Here, ν stands for neutrons and π for protons, p is the number of excited particles, h is the number of holes and $n = p_\nu + p_\pi + h_\nu + h_\pi$. The Fermi energy is denoted by ε_F and $\theta(t)$ is the unit step functions (1 for $t > 0$ and 0 otherwise). The single-particle state densities were taken in the present work conventionally as $g_\nu = N/14$, $g_\pi = Z/14$, and $\varepsilon_F = 40$ MeV.

Our essential task is to develop an expression for the photon emission rate. To do this we start with the Levinger

quasideuteron model for the photoabsorption of hard photons (30 - 150 MeV). In this model the photoabsorption proceeds via disintegration of proton-neutron pairs, (quasideuterons) in the nucleus and the cross sections reads[7]

$$\sigma_{qd}(\varepsilon_\gamma) = L \frac{N Z}{A} \sigma_d(\varepsilon_\gamma) e^{-D/\varepsilon_\gamma}, \qquad (3a)$$

where L is the Levinger parameter, NZ/A is the number of proton-neutron pairs per unit volume, σ_d is the free deuteron photodisintegration cross section and the last term is a damping factor which accounts for Pauli blocking. We use the value L = 6 which is somewhat smaller than the one recommended by Levinger[7] and somewhat higher than the one adopted recently by Prakash er al.[9] We use D = 60 MeV in accord with these two latter works. The cross section σ_d is conveniently expressed, as [11]

$$\sigma_d(\varepsilon_\gamma) = 61.2 \frac{(\varepsilon_\gamma - 2.224)^{3/2}}{\varepsilon_\gamma^3} \qquad (3b)$$

with ε_γ in MeV and σ_d in mb. The photoabsorption cross section on an excited state is obtained by assuming that it can be identified with the cross section on the ground state.[5] Although σ_{qd} decreases somewhat with the excitation energy, this decrease should not exceed several percent in reaction considered in the present paper and we neglect it hroughout this work.

Prior to using detailed balance, one should evaluate the photoabsorption cross section available for one way of exciting a particle x to the energy ε. This is performed in terms of branching ratios for the photoabsorption using phase space considerations, an idea applied already in Ref.5.

The two-particle nature of the quasideuteron photoabsorption implies for the nuclear ground state that a 4-exciton, more strictly $1p_\nu 1p_\pi 1h_\nu 1h_\pi$, state is excited.[11] Considering a particle of type x, there are $\omega_4(\varepsilon_\gamma)/g_x$ ways the excitation is realized. Assuming equal probability for all these ways, the branching ratio for one way, including the one we are interested in, is $g_x/\omega_4(\varepsilon_\gamma)$. For photoabsorption on an excited state with energy $E-\varepsilon_\gamma$ an additional to ω_4 phase space should be considered. Its major part comes from the photon striking a quasideuteron with one nucleon above (it can also be a hole) and another one below the Fermi level. A new particle-hole pair is created and the additional phase space is

$$n\omega_3\left[\varepsilon_\gamma + \frac{E - \varepsilon_\gamma}{n}\right],$$

where the energy to shared by three excitons after absorption includes the average energy of the excited nucleon. Then the

photoabsorption cross section available for exciting a particle of type x to energy ε can be written as

$$\sigma_n^{abs}(\varepsilon_\gamma, \varepsilon) = \sigma_{qd}(\varepsilon_\gamma) \frac{g_x}{\omega_4(\varepsilon_\gamma) + n\omega_3\left(\varepsilon_\gamma + \frac{E - \varepsilon_\gamma}{n}\right)} \qquad (4)$$

independent of ε.

The two-particle nature of the hard photon emission implies for the change of the exciton number a selection rule $\Delta n = +2, 0, -2, -4$. Detailed balance should be therefore applied to each process n n + Δn separately. In this notation the inverse reaction is the photoabsorption that proceeds on a state n + Δn and leads to a state n with a particle x having energy ε. As the inverse cross section we thus use $\sigma^{abs}_{n+\Delta n}(\varepsilon, \varepsilon_\gamma)$ defined by Eq.(4). This is justified since the hybrid model already chooses the particle ε according to the number of ways in which it can be selected among n excitons with the full energy E (the term $\omega_{n-1}(E-\varepsilon)$ in Eq.(1)). The final state density for the $\Delta n = +2$ emission is obviously $\omega_3(\varepsilon - \varepsilon_\gamma)$. Generally much smaller state density is available for the $\Delta n = 0$ emission as given by the interaction of the particle ε with another excited particle (or hole) ε' of the proper type to form a quasideuteron. This leads to $(1/2)(n-1)\omega_2(\varepsilon + <\varepsilon'> - \varepsilon_\gamma)$ possibilities, expressed as a product of the number of quasideuteron and their state density after photon emission. The average energy of the second particle is

$$<\varepsilon'> = \frac{E - \varepsilon}{n - 1} \quad \text{for } \varepsilon < \varepsilon_\gamma$$

and somewhat more complicated expression is needed otherwise. If one neglects small contributions from $\Delta n = -2, -4$, the photon emission rate for a particle with energy ε with the initial state density g_x reads

$$\lambda_\gamma(\varepsilon_\gamma, \varepsilon) = \frac{\varepsilon_\gamma^2}{\pi^2\hbar^3c^2}\left[\sigma^{abs}_{n+2}(\varepsilon_\gamma, \varepsilon)\frac{\omega_3(\varepsilon - \varepsilon_\gamma)}{g_x} + \right.$$

$$\left. + \sigma_n^{abs}(\varepsilon_\gamma, \varepsilon)\frac{\frac{1}{2}(n-1)\omega_2(\varepsilon + <\varepsilon'> - \varepsilon_\gamma)}{g_x}\right], \qquad (5)$$

where $\varepsilon_\gamma^2 / \pi^2\hbar^3c^2$ is related to the state density of free photons. Using (4) and considering small n, one can approximate Eq.(5) by

$$\lambda_\gamma(\varepsilon, \varepsilon_\gamma) \cong \frac{\varepsilon_\gamma^2}{\pi^2\hbar^3c^2}\sigma_{qd}(\varepsilon_\gamma)\frac{\omega_3(\varepsilon - \varepsilon_\gamma)}{\omega_4(\varepsilon_\gamma)}. \qquad (6)$$

III. ANALYSIS AND DISCUSSION

We now apply the above formalism to proton-nucleus reactions, where all the key parameters to be used in describing the preequilibrium cascade are well established in the hybrid model.[1] Thus, the intranuclear transition rates are calculated from the nucleon-nucleon collision rate in the nuclear matter corrected for Pauli blocking[15] with the mean free path adjustment factor k = 2 to account for surface effects. The initial exciton number is $n_0 = 1$, reaction and inverse cross sections for nucleons are close to those adopted in Ref.1, and the parametrization of ω_n/ and σ_{qd} was already specified.

We start with the reaction p + Au at 72 MeV incident proton energy and show in Fig. various components of the hard photon spectrum. It is seen that the dominant contribution comes from the initial stage of the reactions (n = 1), much in line with the present understanding of the process.[12] Also shown is the spectrum obtained by the simplified photon emission rate of Ed.(6). Good validity of this approximation makes it possible to deduce easily a scaling factor for the hard photon production cross sections. Considering only the n =1 term in Eq.(1) and inserting the photon emission rate (6) into it, one obtains

$$\frac{d\sigma}{d\varepsilon_\gamma} \propto \sigma_a \sigma_{qd} \frac{\omega_3}{\omega_4} \propto \frac{N}{A^{1/3}}, \qquad (7)$$

since $\sigma_a \propto A^{2/3}$, $\sigma_{qd} \propto NZ/A$ and $\omega_3/\omega_4 \propto g_\nu^2 g_\pi / g_\nu^2 g_\pi^2 \propto 1/Z$. The scaling factor $N/A^{1/3}$ is exactly the same as proposed originally by Edgington and Rose for their 140 MeV data[13] and it proved to follow also the 72 MeV data.[12]

The calculated photon spectrum can be compared with experimental data after it is transformed into the laboratory system. In our model a photon is emitted from a neutron-proton pair which virtually moves in the laboratory system with a velocity close to 1/2 of that of the incident proton. There can be a considerable Doppler shift in the observed photon energy depending on the emission angle. Following Ref.9, we transform the calculated cross sections, which refer to the quasideuteron center of mass system, into the laboratory system. One has[16]

$$\frac{d^2\sigma}{d\varepsilon_\gamma^{lab}\, d\omega_\gamma^{lab}} = \frac{p_\gamma^{lab}}{p_\gamma^{cm}} \frac{d^2\sigma}{d\varepsilon_\gamma^{cm}\, d\omega_\gamma^{cm}}, \qquad (8)$$

where $p_\gamma = \varepsilon_\gamma / c$ is the photon momentum. The photon energies are related as

$$\varepsilon_\gamma^{lab} = \varepsilon_\gamma^{cm} \frac{\sqrt{1-\beta^2}}{1-\beta\cos\theta_\gamma^{lab}}, \qquad (9)$$

where β is the quasideuteron velocity in the laboratory system and Θ_γ^{lab} measn the emission angle. In the present

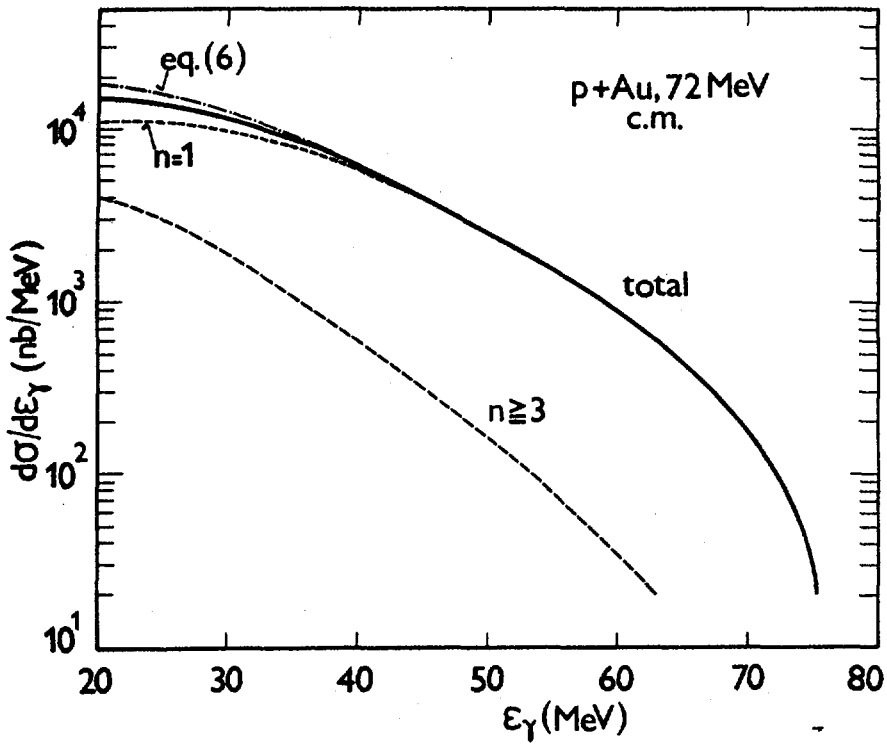

Fig.1. Calculated photon spectra for the reactions p + Au at 72 MeV. Shown by dashed curves is the contribution for the exciton number n = 1 and the sum of contributions for n ≥ 3. Full curve represents the total spectrum. Dashed-dotted curve is the total spectrum calculated by the approximate emission rate, Eq.(6).

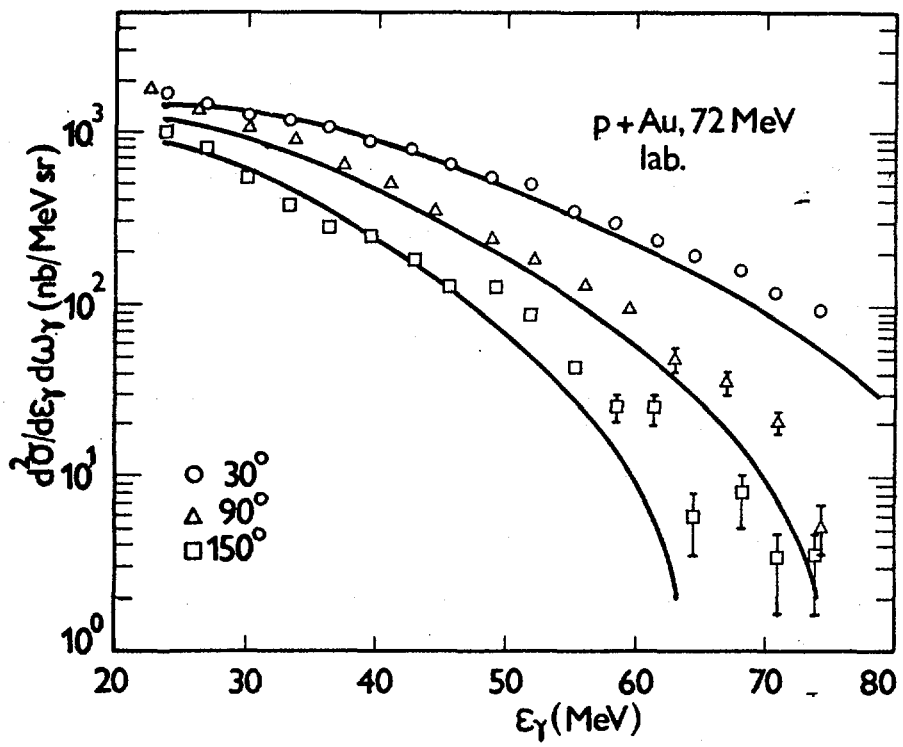

Fig.2. Calculated photon spectra for the reaction p + Au at 72 MeV are transformed into the laboratory system and compared with the data of Kwato Njock et al.[12] at θ_γ^{lab} = 30°, 90° and 150°.

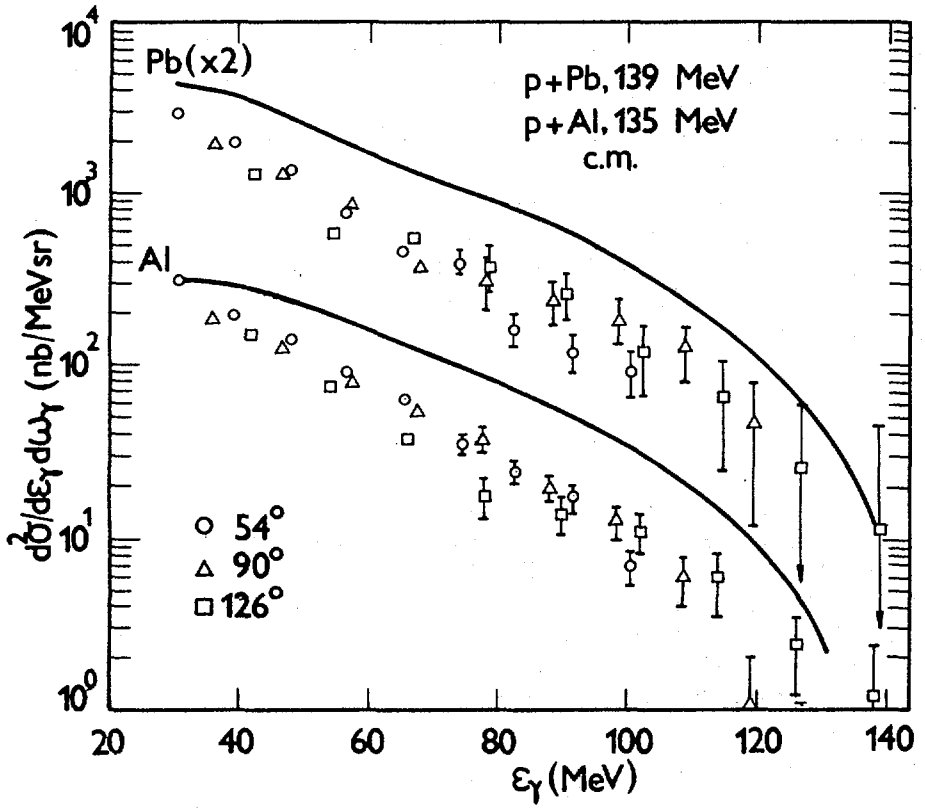

Fig.3. Calculated photon spectra for the reactions p + Pb at 139 MeV and p + Al at 135 MeV are compared with the data of Edgington and Rose.[13] The data at θ_γ^{lab} = 54°, 90° and 126° are transformed into the quasideuteron center of mass system. (All results for Pb are multiplied by a factor of two for better distinquishing from Al.)

approach, the angular distribution of emitted photons is isotropic in the quasideuteron center of mass system.

Using Eqs.(8) and (9), we transformed the calculated photon spectrum for the reaction p + Au into the laboratory system at θ_γ^{lab} = 30°, 90° and 150°. This is possible in view of the dominant n = 1 term which implies that the quasideuteron velocity vector is sufficiently parallel with the incident proton beam. The transformed spectra are compared with the experimental data[12] in Fig.2. Good accord of the calculated and observed spectra at all three angles suggests that the hard photons are indeed emitted from moving quasideuterons. This is yet another proof of the similar observation made earlier.[12,9] The calculated spectra seem to underestimate systematically the data at the highest photon energies. This may likely be improved by using the geometry dependent hybrid model, much in analogy with the preequilibrium particle emission spectra.[1]

We also analyse the photon spectra measured at still higher proton incident energy by Edgington and Rose.[13] Their data are often referred to as being measured at 140 MeV though the effective beam energy was generally somewhat lower. Shownm in Fig.3 are the spectra for the reactions p + Pb at 139 MeV and p + Al at 135 MeV. We transform the experimental cross sections at θ_γ^{lab} = 54°, 90° and 126° into

the quasideuteron center of mass system and compare them with the calculated values. It is seen that we reproduce the shape of the spectra quite well, and our magnitude is approximately twice as high as the experimental values. This latter observation means that we predict the hard photon cross sections quite close to the expected values deduced from the systematics being developed in heavy-ions collisions.[3] Our finding is furthermore in line with possible difficulties in the magnitude of the Edgington and Rose data as discussed recently in Ref.12.

References

1. M. Blann and H.K. Vonach, Phys. Rev. C28, 1475 (1983).
2. K. Snover, Ann. Rev, Nucl. Part. Sci. 36, 599 (1986).
3. V. Metag, Nucl. Phys. A488, 483c (1988).
4. G. Reffo, M. Blann and B.A. Remington, Phys. Rev. C38, 1190 (1988); erratum Phys. Rev. C39, 1188 (1989).
5. P. Obložinský, Phys. Lett. B215, 597 (1988).
6. B.A. Remington, M. Blann and G. Bertsch, Phys. Rev. C35, 1720 (1987).
7. J.S. Levinger, Phys. Rev. 84, 42 1961); J.S. Levinger, Phys. Lett. B82, 181(1979).
8. N. Hermann et al., Phys. Rev. Lett. 60, 1630 (1988).
9 M. Prakash et al., Phys. Rev. C37, 1959 (1988).
10. P. Obložinský, in Proc. NEANDC Specialists' Meeting on Preequilibrium Nuclear Reactions, Semmering, Austria, 1988, ed. B. Strohmaier (OECD, Paris 1988) p.157.
11. J.R. Wu and C.C. Chang, Phys. Rev. C16, 1812 (1977).
12. M. Kwato Njock et al., Phys. Lett. B207, 269 (1988).
13. J.A. Edgington and B. Rose, Nucl. Phys. 89, 523 (1966).
14. P. Obložinský, Nucl. Phys. A453, 127 (1986).
15. K. Kikuchi and M. Kawai, Nuclear Matter and Nuclear Interactions (Norths Holland, Amsterdam 1968) p.33.
16. E. Byckling and K. Kajantie, Particle Kinematics (John Wiley, London 1973) chapters II, VII.
17. P. Obložinský, Phys. Rev. C40, 1591 (1989).

NEUTRON-GAMMA COMPETITION IN NUCLEON-INDUCED REACTIONS

E. Běták
Institute of Physics, Slovak Academy of Sciences, Dúbravská cesta 9, CS-84228 Bratislava
F. Cvelbar
Institute J. Stefan, E. Kardelj University, Jamova 39, POB 100,YU-61111 Ljubljana

ABSTRACT
The pre-equilibrium model of the γ emission is used to study the competition of γ and nucleon emission. Mainly, we investigated the ratio of γ-to-total emission widths $\Gamma\gamma/\Gamma_{tot}$, the exclusive nucleon spectra, the γ multiplicities (also the differential ones), and the relation of the activation to the integrated cross section for the nucleon radiative capture. All the calculations were performed within an unique master-equation approach to the exciton model, which has been formally extended to cover also the equilibrium (i.e. the compound-nucleus) emission. The results are in strong support to the pre-equilibrium model used for the γ emission.

The incorporation of the γ emission into the pre-equilibrium model of nuclear reactions some ten years ago [1,2] enlarged the variety of physical quantities which can be calculated and compared to the data. Even the complicated quantities based on cascade processeswere touched.

Obviously, to do this, one must have to his disposal not only the γ emission rates themselves, but also a sufficiently powerful algorithms as to treat the successive emission of γ's, interspersed by nucleons as needed. This can be easily done within the master-equation approach to the exciton model, where the corresponding set of master equations reads [3,4,5]

$$\begin{aligned}\frac{dP(n,t,E,i)}{dt} &= P(n-2,t,E,i)\,\lambda^{+}(n-2,E,i) \\ &+ P(n+2,t,E,i)\,\lambda^{-}(n+2,E,i) \\ &- P(n,t,E,i)\,[\lambda^{+}(n,E,i) + \lambda^{-}(n,E,i) + L(n,E,i)] \\ &+ \sum_{j,m,x} \int_{\varepsilon} P(m,t,E',j)\,\lambda_{x}^{c}(m,E',j,\varepsilon)\,d\varepsilon \qquad (1)\end{aligned}$$

In eqs. (1), $P(n,t,E,i)$ is the occupational probability of an

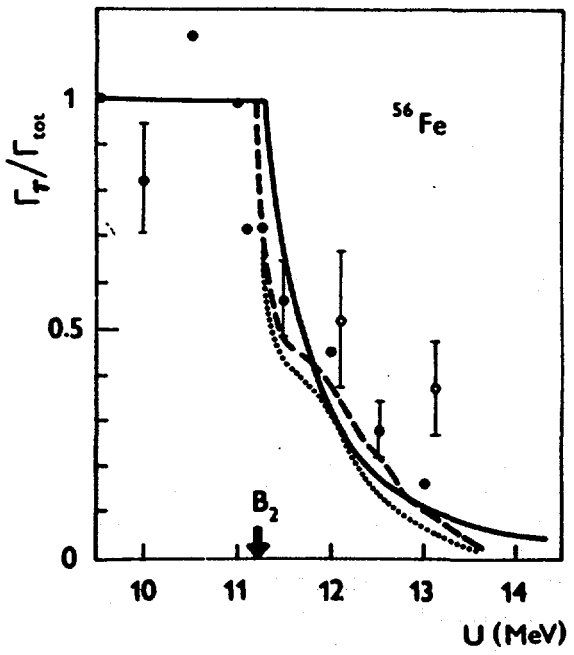

Fig. 1. Calculated $\Gamma\gamma/\Gamma_{tot}$ for 56Fe(n,n'γ) at 14 MeV. Closed points are the data of ref. [7], open ones are of ref. [4]. Heavy curve is the pre-eq. calculation [4], dotted and dashed curves are the CN calculations of [7].

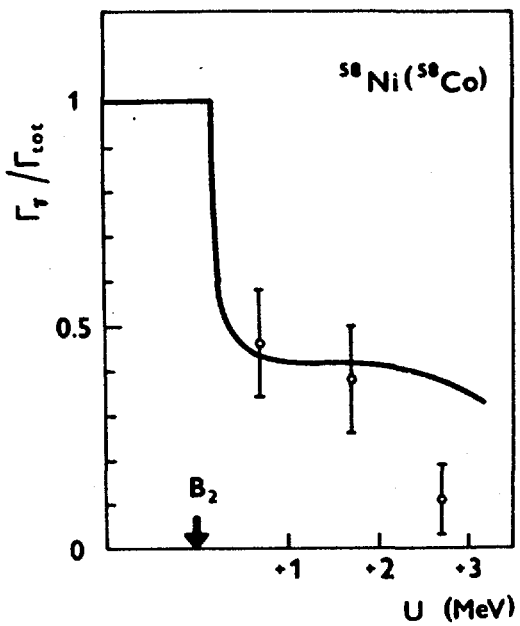

Fig. 2. The same as in Fig. 1, but for 58Ni(n,np). Data points of ref. [4], calculations of refs. [4] and [8].

n-exciton state of a nucleus i at the excitation energy E and time t, λ's are the transition rates (per unit time) to the neighbour states, and L is the total emission rate (including particles and gammas, integrated over the outgoing energy and summed over all possible emission channels) of the specified exciton state,

$$L(n,E,i) = \sum_x \int_\varepsilon P(n,t,E,i)\, \lambda_x^c(n,E,i,\varepsilon)\, d\varepsilon \qquad (2)$$

The last term in eq. (2) ensures the coupling of different nuclei

and various excitation energies. For the details of the pre-equilibrium γ emission, see ref. [6].

In practice, all the calculations reported here were performed using codes written at Bratislava [3,5] (here, ref. [5] is a PC version of code [3]).

The most simple and the most straightforward is the calculation of $\Gamma_\gamma/\Gamma_{tot}$. If we denote

$$\tau(n,E,i) = \int_0^\infty P(n,E,i)\,dt, \tag{3}$$

then

$$\Gamma_\gamma(E,i) = \frac{\sum_n \tau(n,E,i) \int \lambda_\gamma^c(n,E,i,\varepsilon_\gamma)\,d\varepsilon_\gamma}{\sum_n \tau(n,E,i)} \tag{4a}$$

and similarly

$$\Gamma_{tot}(E,i) = \frac{\sum_{n,x} \tau(n,E,i) \int \lambda_x^c(n,E,i,\varepsilon_\gamma)\,d\varepsilon_\gamma}{\sum_n \tau(n,E,i)}. \tag{4b}$$

The results of these calculations compared to the data are in Figs. 1 and 2 [4,8].

A very interesting case is the calculation of the exclusive nucleon spectra, i.e. the spectra from a reaction finishing at given nucleus. The experimental data of the $(\alpha,2n\gamma)$ reaction at 35 MeV [9] manifest a double-peaked (camel-like) shape for some nuclei, whereas normal shapes are observed for the others. Here, we explained the differences by the pre-equilibrium γ-to-neutron competition, as seen in Fig. 3 [10]. Some other nucleon exclusive

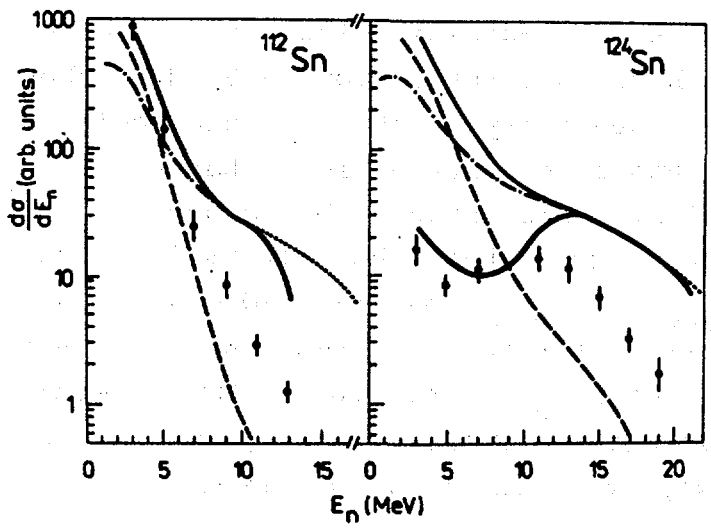

Fig. 3. Exclusive neutron spectra from the reaction $(\alpha,2n\gamma)$ at 35 MeV. Data of ref. [9], calculations of ref. [10]. Heavy curves are the resulting pre-eq. exclusive spectra, which are to be compared to the data. Dashed, dotted, etc. lines are their components (for details, see the original paper [10]).

spectra are also of interest. Fig. 4 brings an illustration of $^{52}Cr(n,n'\gamma)$ at 14 MeV; and some still more bizarre shapes can be found in ref. [8].

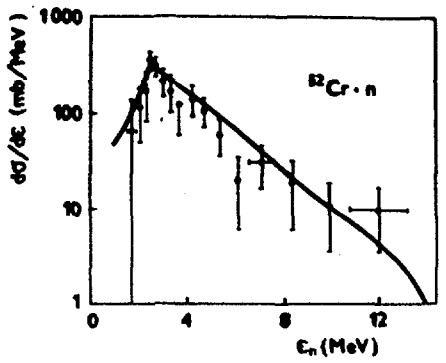

Fig. 4. Exclusive neutron spectra from 52Cr(n,n'γ). The data are of ref. [11], calculations of ref. [4].

Relatively complicated is the calculation of differential γ multiplicities in 14 MeV neutron induced reactions, i.e. the multiplicities of γ's in coincidence with neutrons of given energy. An example can be seen in Fig. 5 [12].

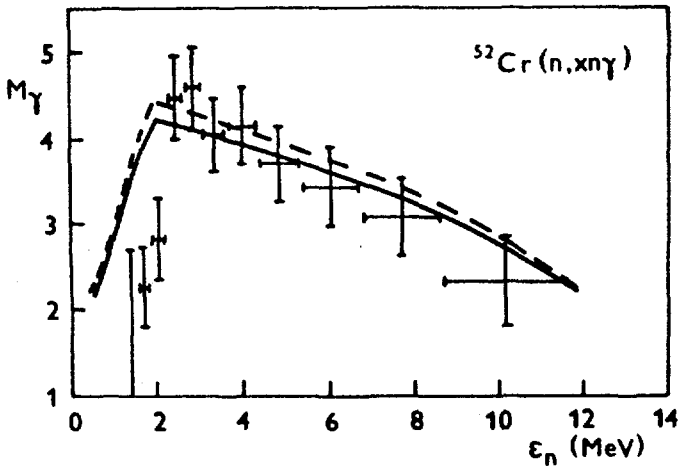

Fig. 5. Differential γ multiplicities from reaction 52Cr(n,xnγ) at 14 MeV. Full line is the result of calculations, the dashed one is based on slightly different model for the γ emission. (Ref. [12]).

Probably the latest of the coincidence-type calculations are he integrated ($\sigma_{\gamma int}$) and the activation ($\sigma_{\gamma act}$) reaction cross sections and the corresponding excitation functions. In $\sigma_{\gamma int}$ we integrate the part of the γ energy spectrum corresponding to the prompt direct capture transitions to bound final states. As is well known, if we arrive by such γ-deexcitation to a loosely unbound state instead of the bound one (say, about 0.5 MeV above the particle threshold), the probability of the particle emission is still weak, and a nucleus has a relatively high chance for a successive (cascade) γ emission. This should be added to the integrated cross section, and we get thus the activation cross section $\sigma_{\gamma act}$. Obviously, $\sigma_{\gamma act} > \sigma_{\gamma int}$, if we take the same incident energy. However, this difference is often small (see also below). A comparison of $\sigma_{\gamma int}$ and $\sigma_{\gamma act}$ for several 14 MeV neutron radiative capture data(to our knowledge all 14 those, where both the $\sigma_{\gamma act}$ and $\sigma_{\gamma int}$ are known) for slightly different initial

and various excitation energies. For the details of the pre-equilibrium γ emission, see ref. [6].

In practice, all the calculations reported here were performed using codes written at Bratislava [3,5] (here, ref. [5] is a PC version of code [3]).

The most simple and the most straightforward is the calculation of $\Gamma_\gamma/\Gamma_{tot}$. If we denote

$$\tau(n,E,i) = \int_0^\infty P(n,E,i)\,dt, \tag{3}$$

then

$$\Gamma_\gamma(E,i) = \frac{\sum_n \tau(n,E,i) \int \lambda_\gamma^c(n,E,i,\varepsilon_\gamma)\,d\varepsilon_\gamma}{\sum_n \tau(n,E,i)} \tag{4a}$$

and similarly

$$\Gamma_{tot}(E,i) = \frac{\sum_{n,x} \tau(n,E,i) \int \lambda_x^c(n,E,i,\varepsilon_\gamma)\,d\varepsilon_\gamma}{\sum_n \tau(n,E,i)}. \tag{4b}$$

The results of these calculations compared to the data are in Figs. 1 and 2 [4,8].

A very interesting case is the calculation of the exclusive nucleon spectra, i.e. the spectra from a reaction finishing at given nucleus. The experimental data of the $(\alpha,2n\gamma)$ reaction at 35 MeV [9] manifest a double-peaked (camel-like) shape for some nuclei, whereas normal shapes are observed for the others. Here, we explained the differences by the pre-equilibrium γ-to-neutron competition, as seen in Fig. 3 [10]. Some other nucleon exclusive

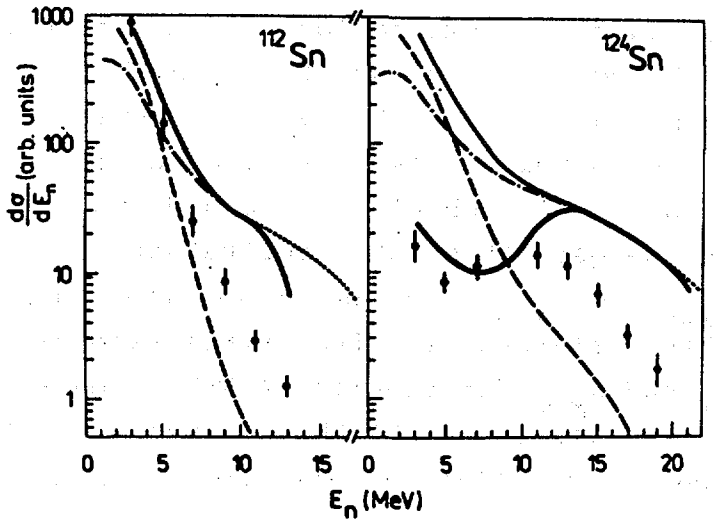

Fig. 3. Exclusive neutron spectra from the reaction $(\alpha,2n\gamma)$ at 35 MeV. Data of ref. [9], calculations of ref. [10]. Heavy curves are the resulting pre-eq. exclusive spectra, which are to be compared to the data. Dashed, dotted, etc. lines are their components (for details, see the original paper [10]).

spectra are also of interest. Fig. 4 brings an illustration of $^{52}Cr(n,n'\gamma)$ at 14 MeV; and some still more bizarre shapes can be found in ref. [8].

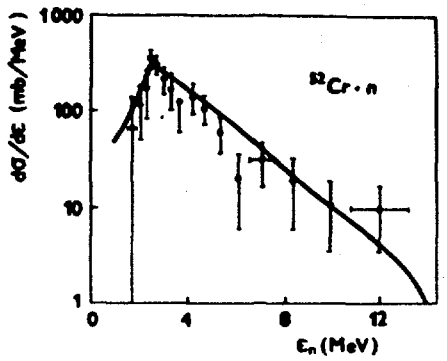

Fig. 4. Exclusive neutron spectra from 52Cr(n,n'γ). The data are of ref. [11], calculations of ref. [4].

Relatively complicated is the calculation of differential γ multiplicities in 14 MeV neutron induced reactions, i.e. the multiplicities of γ's in coincidence with neutrons of given energy. An example can be seen in Fig. 5 [12].

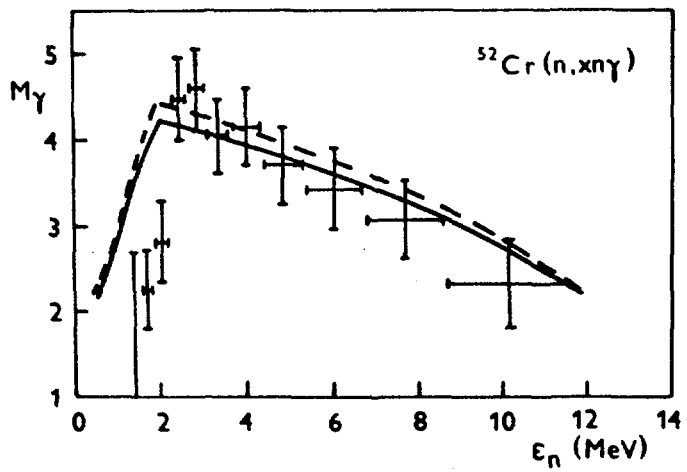

Fig. 5. Differential γ multiplicities from reaction 52Cr(n,xnγ) at 14 MeV. Full line is the result of calculations, the dashed one is based on slightly different model for the γ emission. (Ref. [12]).

Probably the latest of the coincidence-type calculations are he integrated ($\sigma_{\gamma int}$) and the activation ($\sigma_{\gamma act}$) reaction cross sections and the corresponding excitation functions. In $\sigma_{\gamma int}$ we integrate the part of the γ energy spectrum corresponding to the prompt direct capture transitions to bound final states. As is well known, if we arrive by such γ-deexcitation to a loosely unbound state instead of the bound one (say, about 0.5 MeV above the particle threshold), the probability of the particle emission is still weak, and a nucleus has a relatively high chance for a successive (cascade) γ emission. This should be added to the integrated cross section, and we get thus the activation cross section $\sigma_{\gamma act}$. Obviously, $\sigma_{\gamma act} > \sigma_{\gamma int}$, if we take the same incident energy. However, this difference is often small (see also below). A comparison of $\sigma_{\gamma int}$ and $\sigma_{\gamma act}$ for several 14 MeV neutron radiative capture data(to our knowledge all 14 those, where both the $\sigma_{\gamma act}$ and $\sigma_{\gamma int}$ are known) for slightly different initial

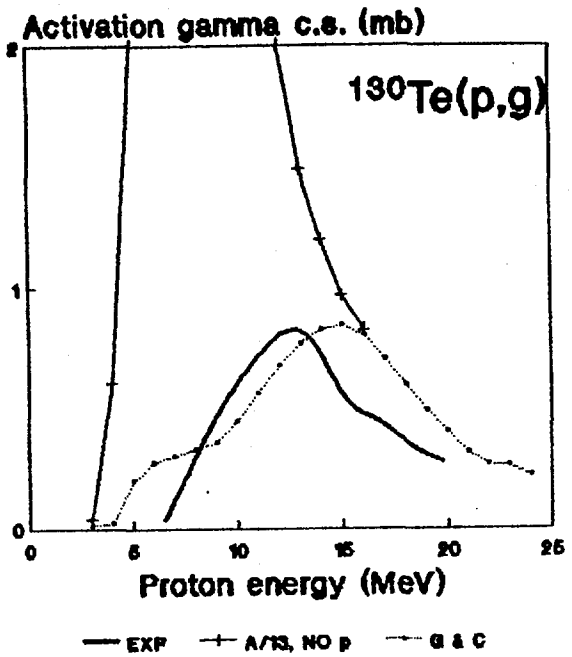

Fig. 6. Activation excitation function of 130Te(p,γ). Heavy line is the experiment [14], full line with crosses is the result of calculation without pairing and with overall values of g, weak line with dots is from the calculations with Gilbert and Cameron values for the level density parameters. From ref. [15].

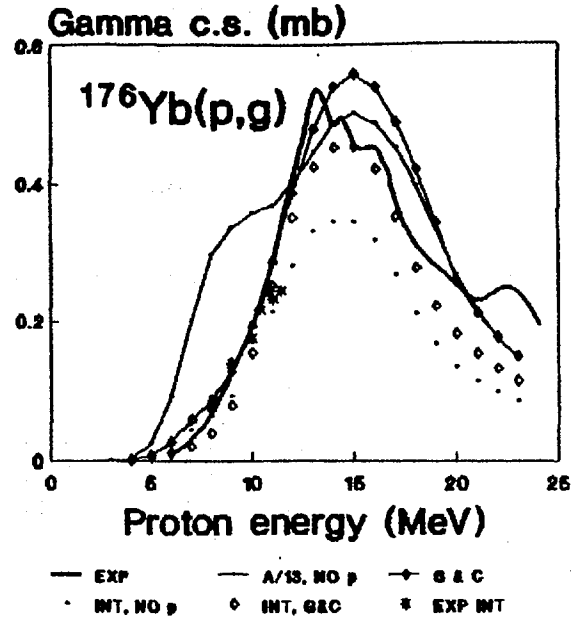

Fig. 7. Excitation function of 176Yb(p,γ). Both the activation and the integrated values are plotted. Activation experiment is drawn as a heavy line, integrated one as stars. Calculated activation cross sections are depicted as points connected by lines, the integrated values by the same points without lines: simple points stand for no pairing, diamonds for Gilbert and Cameron values. From ref. [15].

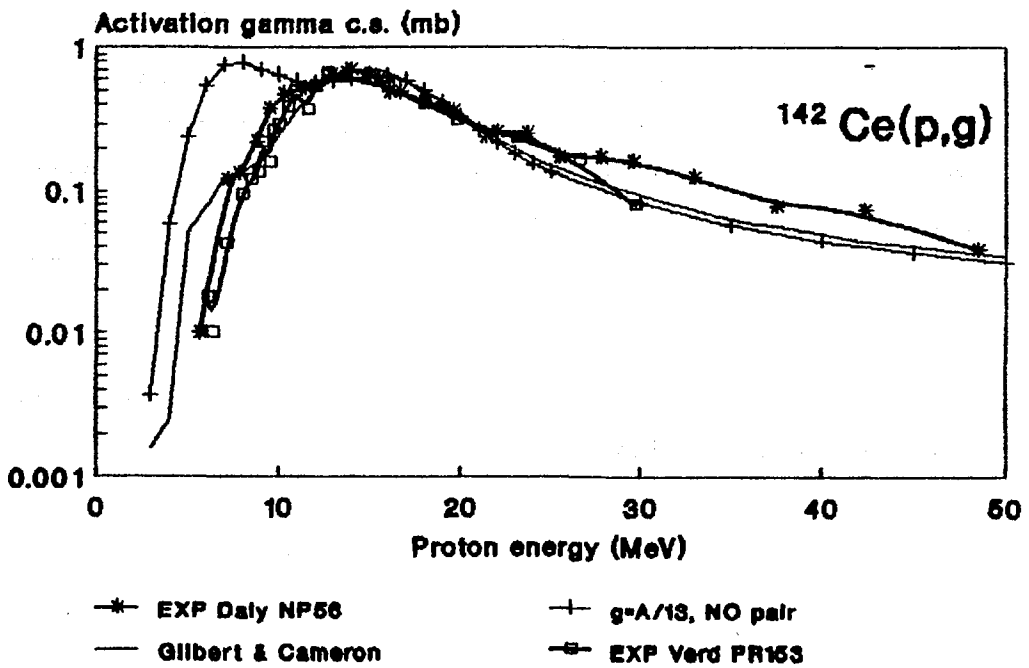

Fig. 8. As in Fig. 6, but for 142Ce. From ref. [15].

energies (i.e. 14.1 MeV for the integrated, and 14.6 MeV for the activation ones) is given in Table I [13].

Table I

Comparison of 14 MeV neutron activation and integrated cross sects

Target	Experiment $\sigma_{\gamma act}(14.6)$	Experiment $\sigma_{\gamma int}(14.1)$	Preequil.calc. $\sigma_{\gamma int}$	Preequil.calc. $\sigma_{\gamma act}$	CN calc $\sigma_{\gamma act}$
Al-27	480+- 60	415+- 60	342	368	51
Sc-45	530+- 60	800+-120	502	507	90
V-51	720+- 70	575+- 95	420	442	20
Mn-55	675+- 70	655+- 95	682	685	49
I-127	1120+-250	770+-160	716	713	13
Pr-141	1190+-180	980+-165	834	819	4
Pb-208	1000+-200	930+-200	715	620	1
Bi-209	1200+-200	880+-165	710	636	1

(Cross sections are in μb)
Table from ref. [13].

Figs. 6 to 8 bring the radiative capture excitation functions of three nuclei [14,15]. Here, a significant difference can be found between the neutron- and the proton-induced reactions. It origins from the tendency of the pre-equilibrium decay to enhance the emission of a particle of the same type, as the incident one was. Taking into account that the proton emission is much weaker than the neutron one at the excitation energies close to (20-23) MeV (typical excitation energy of 14 MeV neutron induced reactions), we get stronger γ emission resulting in enhanced difference between $\sigma_{\gamma act}$ and $\sigma_{\gamma int}$ in the proton- compared to the neutron-induced reactions.

At low energies, the presence of the pairing and more appropriate single-particle level density g is significant in order to get more-or-less reasonable description of the data. At higher energies, those details of the level densities are practically smeared out, and the usual description of g=A/13 with no pairing serves well. Surprisingly, our model for the γ emission keeps valid up to pretty high energies (see Fig. 8).

The work has been supported in part by International Atomic Energy Agency contract No. 5148/RB.

REFERENCES

[1] E. Běták, J. Dobeš, Phys. Lett. *84B* (1979), 368.

[2] J.M. Akkermans, H. Gruppelaar, Phys. Lett. *157B* (1985), 95.

[3] E. Běták, J. Dobeš, Report IP EPRC SAS No. 43/1983 (Bratislava 1983).

[4] E. Běták et al., Izv. AN SSSR, ser. fiz., *49* (1985), 1023.

[5] E. Běták, Report INDC(CSR)-016/LJ (IAEA Vienna 1989); Report FUSAV 89/5 (Bratislava 1989).

[6] E. Běták, *in* Proc. 5 Int. Conf. Nucl. React. Mech., Varenna 1988 (Univ. Milano 1988), p. 92;
E. Běták, P. Obložinský, *This Meeting.*

[7] G. Stengl, M. Uhl, H. Vonach, Nucl. Phys. *A290* (1977), 109.

[8] E. Běták, *contribution to* EPS Conference Nucl. Reactions, Crete 1984 *(unpublished, available on request).*

[9] C.A. Fields et al., Nucl. Phys. *A366* (1981), 38; *ibid. A377* (1982), 217; Phys. Lett. *106B* (1981), 453.

[10] E. Běták, J. Dobeš, Phys. Lett. *130B* (1983), 350.

[11] S. Hlaváč, P. Obložinský, J. Pivarč, *in* Proc. 4 Int. Symp. Neutron Ind. Reacts., Smolenice 1985 (D. Reidel 1986), p. 298

[12] E. Běták, J. Dobeš, *in* Proc. 4 Int. Symp. Neutron Induced Reacts., Smolenice 1985 (D. Reidel 1986), p. 294.

[13] F. Cvelbar, E. Běták, Z. Phys. *A332* (1989), 163

[14] B. Daly, S. Shaw, Nucl. Phys. *56* (1964), 322;
E.V. Verdieck, J.M. Miller, Phys. Rev. *153* (1967), 1253;
B. Palsson et al., Nucl. Phys. *A345* (1980), 221.

[15] F. Cvelbar, E. Běták, J. Merhar, *to be published.*

Calculation of photon production cross sections and spectra from $^{52}Cr(n,x\gamma)$ reactions at 14.6 MeV*

G. Maino[1], A. Mengoni[1] and P. Obložinský[2]

[1]ENEA, Via Ercolani 8, 40138 Bologna, Italy
[2]Institute of Physics, Slovak Academy of Sciences
Dúbravská cesta 9 842 28 Bratislava, Czechoslovakia

Abstract:

Advanced statistical model of nuclear reactions is used to analyze $^{52}Cr(n,x\gamma)$ reactions at 14.6 MeV neutron incident energy. Calculated are discrete γ ray production cross sections, total γ ray spectrum and average γ ray multiplicities. It is found that integral quantities and data that involve sufficient averaging, such as γ multiplicities, can be predicted with good precision. This is valid also for strong discrete γ lines. Generally, however, discrete γ ray production cross sections cannot be safely predicted better than within a factor of two. Things may be even worse for particular portions of the total γ ray spectrum.

1. Introduction

Fairly detailed and complete measurement of photon production cross sections from $^{52}Cr(n,x\gamma)$ reactions at 14.6 MeV neutron incident energy has been reported in Ref.1. The purpose of the present work is to perform theoretical analysis of these data. We calculate discrete γ ray production cross sections, total γ ray spectrum as well as average γ ray multiplicities. Our approach is based on the advanced statistical model of nuclear reactions.

2. Nuclear models

Calculations were performed within the statistical model of nuclear reactions. Included were complete Hauser-Feshbach formalism, somewhat simplified treatment of the

*) Contribution presented by P. Obložinský

preequilibrium particle and γ ray decay, and detailed description of γ ray cascades with spins, parities and discrete γ ray transitions. Considered in calculations were reaction channels with up to two emitted particles and up to seven successive γ rays in each channel.

Compound nucleus formation cross sections and transmission coefficients were evaluated within the spherical optical model. Parameters for the neutron-channel were those of Prince[2], for the proton-channel those of Becchetti and Greenless[3] and for α particles those of Igo and Huizenga.[4]

Low-energy level schemes and γ ray branching ratios were taken from the current literature, see Ref.5. Level densities were evaluated by means of Ignatyuk's formalism[6] with inclusion of parity effects calculated within the framework of the microscopic Nilsson BCS model.[7] The relations were

$$\rho(E,J,\Pi) = \frac{(2J+1)e^{-J(J+1)/2\sigma^2}}{\sigma^3} \frac{e^{2\sqrt{aU}}}{24\sqrt{2}\, a^{1/4}\, U^{5/4}} F_{par}(E,\Pi), \qquad (1)$$

where E, J, and Π are the excitation energy, spin, and parity, respectively. The energy U is given as

$$U = E + \Delta_f \ , \qquad (2)$$

where Δ_f is the pairing correction. The single-particle level density parameter reads

$$a(U) = a(*) \left[1 + \frac{\delta E_{sh}}{U} (1 - e^{-\gamma U}) \right] \qquad (3)$$

and the parity term is

$$F_{par}(E,\Pi) = \begin{cases} \frac{1}{2} \tanh\frac{\alpha E}{2} \ , & \text{if } \Pi \text{ is the same as the ground-state parity} \\ 1 - \frac{1}{2} \tanh\frac{\alpha E}{2} & \text{otherwise.} \end{cases} \qquad (4)$$

The relevant parameters are summarized in Tab.1.

Use is made of the Brink-Axel hypothesis in order to deduce the transmission coefficients for neutron radiative

Table 1. Level density parameters used in Eqs.(1)-(4). Spin cutoff parameters σ^2(lev) were determined from spin distribution of low-lying discrete levels; c(σ^2) is the coefficient of the usual spin cutoff factor versus excitation energy.

Nucleus	a(*) (MeV^{-1})	γ (MeV^{-1})	α (MeV^{-1})	Δ_f (MeV)	c(σ^2)	σ^2(lev)
^{49}Ti	6.148	0.054	0.20	-0.0944	0.0139	7.2692
^{51}V	6.455	0.054	0.40	-0.5750	0.0139	8.2105
^{52}V	5.862	0.054	0.40	1.2657	0.0139	6.5536
^{51}Cr	5.582	0.054	0.22	0.7209	0.0139	8.9375
^{52}Cr	6.250	0.054	0.40	-1.2161	0.0139	9.0662
^{53}Cr	6.387	0.054	0.19	-0.1564	0.0139	8.9800

Table.2. Parameters for the giant dipole resonance used in ^{52}Cr(n,xγ) calculations.

E_1(MeV)	Γ_1(MeV)	σ_1(mb)	E_2(MeV)	Γ_2(MeV)	σ_2(mb)
17.5	3.5	80	20.5	4.0	60

capture from E1, E2 and M1 giant resonances. Adopted GDR has two-hump Lorentzian shape[8]

$$\sigma_{abs}(E_\gamma) = \sigma_1 \frac{E_\gamma^2 \Gamma_1^2}{(E_\gamma^2 - E_1)^2 + E_\gamma^2 \Gamma_1^2} + \sigma_2 \frac{E_\gamma^2 \Gamma_2^2}{(E_\gamma^2 - E_2)^2 + E_\gamma^2 \Gamma_2^2}, \quad (5)$$

where the parameters are given in Tab.2. Isoscalar and isovector GQR parameters have been obtained from semiclassical sum-rule estimates; M1 resonance is largely fragmented and partly suppressed.

Preequilibrium emission was limited to primary nucleons and primary γ rays and it was treated within the non-spin closed-form formulation of the exciton model. Particle-hole level densities took into account differences between neutron and proton degrees of freedom. The essential simplification consists in the assumption that the spin effects, in the energy-angular momentum range available for the present

reactions, are small. This simplification is justified by more detailed studies.[9,10] Once a neutron or proton has been emitted or nucleus has achieved statistical equilibrium, the system can further decay from its excited configuration by emitting another particle or by statistical γ ray deexcitation cascade. In this case, it was assumed that the preequilibrium configurations have the same spin and parity distributions as the corresponding statistical configurations at the same excitation energy.

The code was the modified version of the PENELOPE developed at the ENEA laboratory in Bologna.

3. Results and discussion

The total nonelastic reaction cross section for ^{52}Cr + n (14.6 MeV) was calculated to be 1315.2 mb. This cross section is divided among seven reaction channels as summarized in Tab.3. We note that the (n,2n) cross section is relatively small in view of extremely high Q-value of 12.04 MeV.

Table.3. Calculated ^{52}Cr neutron cross sections at E = 14.6 MeV.

Reaction	Cross section (mb)
(n,nonelastic)	1315.2
(n,n')	816.2
(n,2n)	369.1
(n,np)	47.6
(n,p)	57.6
(n,α)	24.3
(n,d)	0.2
(n,γ)	0.2

3.1. Discrete γ ray production cross sections

Discrete γ ray production cross sections in the (n,n'γ) channel are summarized in Tab.4. Comparison is made with the experimental data available at 14 MeV range,[1,11-13] which were normalized to 14.6 MeV whenever necessary. It is seen

Table 4. Discrete γ ray production cross section in the (n,n'γ) channel. Given are relative as well as absolute values. References quote experimental works.

Transition		$\sigma_{n,n'\gamma_i}$ (%)		$\sigma_{n,n'\gamma_i}$ (mb)		Ref.
$J_i^\pi \rightarrow J_f^\pi$	E_γ(MeV)	Exper.	Theor.	Exper.	Theor.	
$2_3^+ \rightarrow 2_1^+$	1.728	3.1±0.5	2.4	26± 4	20	1
$2_2^+ \rightarrow 2_1^+$	1.531	4.7±0.4	3.5	40± 3	29	1
		9.3±2.8		78±24		11
$2_1^+ \rightarrow 0_1^+$	1.434	92.1[+]	92.1	783±30	752	1
				773±54		11
				692±51		12
				588±47		13
$4_2^+ \rightarrow 2_1^+$	1.334	24.2±1.0	22.7	205± 8	185	1
		21.7±3.6		182±30		11
		29.1±4.4		218±33		12
		22.2±2.1		141±13		13
$5_1^+ \rightarrow 4_1^+$	1.246	4.6±0.5	3.1	39± 4	25	1
$0_2^+ \rightarrow 2_1^+$	1.214	2.9±1.3	0.6	25±11[*]	5	1
		19.8±3.6		166±30		11
		4.2±1.2		27± 8		13
$4_1^+ \rightarrow 2_1^+$	0.936	28.0±1.1	38.9	237± 9	318	1
		26.4±3.3		221±28		11
		27.0±3.8		202±28		12
		27.3±2.8		174±18		13
$5_1^+ \rightarrow 4_2^+$	0.848	4.5±0.4	2.2	38± 3	18	1
$6_1^+ \rightarrow 4_1^+$	0.744	8.4±0.5	15.9	71± 4	129	1
		16.1±5.4		134±45		11
$3_1^+ \rightarrow 4_2^+$	0.704	5.0±0.4	4.0	42± 3	33	1
$4_3^+ \rightarrow 4_2^+$	0.647	8.3±0.5	5.4	70± 4	44	1

[+] Adopted was the calculated value.

[*] This value was obtained from single measurement at 90°.

that the cross section for two strong γ lines, 1.434 and 1.334 MeV, are in good accord with our prediction. Less satisfactorial situation is with the 0.936 MeV line and quite poor agreement is with several weaker lines, 0.848, 0.744 and 0.647 MeV ones. We note that the cross section of Yamamoto for the 1.214 MeV line is clearly too high, their value being far above of both our prediction and all other data.

Discrete γ ray production cross sections for the (n,2nγ) channel are given in Tab.5. The accord with the data is roughly within 50% . We note, however, that the recent calculation by Hetrick et al.[14] gives in the case of the 0.749 MeV line quite different result, 39 mb, compared to our value of 69 mb.

Table 5. Discrete γ ray production cross sections in the (n,2nγ) channel. The experimental values are those of Ref.1.

Transition		$\sigma_{n,2n\gamma}^{i}$ (mb)	
$J_i^\pi \rightarrow J_f^\pi$	E_γ (MeV)	Exper.	Theor.
$\frac{3}{2}^-_1 \rightarrow \frac{7}{2}^-_1$	0.749	42± 2	69
$\frac{9}{2}^-_1 \rightarrow \frac{7}{2}^-_1$	1.164	36± 4	61

3.2. Total γ ray spectrum

Calculated total γ ray spectrum is compared with the experimental spectrum in Fig.1. The calculated spectrum has several distinct regions. The highest spectral energies avaliable, E_γ > 14.6 MeV, refer to the (n,γ) channel. This part of the spectrum is dominated by preequilibrium processes as shown by the full curve. At spectral energies below about 14 MeV, there are γ rays mostly due to (n,n'γ) and the key process is already purely statistical. At still lower energies cascading γ rays and other reaction channels contribute. They eventually give rise to several distinct discrete γ rays seen at the lowest spectral energy range.

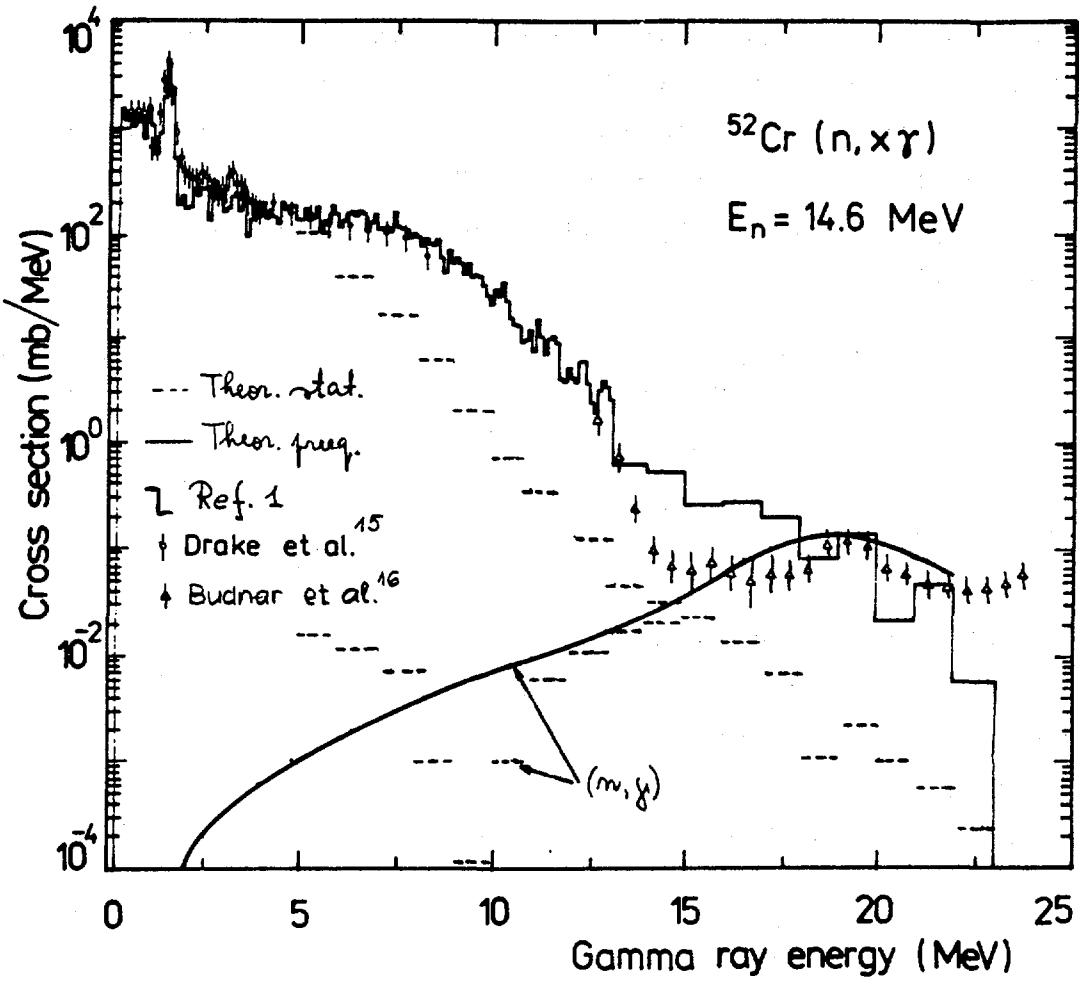

Fig.1. Calculated total γ ray spectrum for γ ray energies above 5 MeV is compared with the experimental spectrum of Ref.1. Also shown are experimental data of Drake et al.[15] and of Budnar et al.[16] Given by full smooth curve is the spectrum of primary preequilibrium γ rays in the (n,γ) channel. Shown by dashed histograms are statistical calculations that refer to (n,xγtotal) and (n,γ) spectra.

(The calculated spectrum below E_γ < 5 MeV is not shown in Fig.1. because of considerable overlap with the experimental data.)

The agreement between the calculated and the experimental spectrum seems satisfactory except of the region dominated by primary γ rays from the (n,n'γ) channel. A possible reason for the difference might be in level densities. We note, however, that the calculation by Hetrick et al.[14] seems to do better in this energy range.

From the above results on can obtain overall integral γ ray production cross section. The calculated overall γ ray production cross section is 3312 mb which compares well with

the experimental value of 3540±230 mb. The calculated integrated values for particular reaction channels are summarized in Tab.6. Of interest is also the overall average γ ray energy per one γ ray emitted. The calculated value of 2.45 MeV compares extremely well with the observed value of 2.49 ±0.15 MeV.

Table 6. Integral γ ray production cross sections and average γ ray energies for various reaction channels.

Reaction	$\sigma_{n,x\gamma}$ (mb)		$\langle E_\gamma \rangle$ (MeV)	
	Exper.	Theor.	Exper.	Theor.
(n,xγtotal)	3540±230	3312	2.49±0.15	2.45
(n,n'γ)	3155±170*)	2918	2.6 ±0.2*)	2.62
(n,2nγ)	78± 6*)	201	-	0.88
(n,npγ)	335± 70*)	19	-	0.53
(n,pγ)		140	-	1.67
(n,αγ)		34	-	2.47

*) Estimates only.

3.3 Average γ ray multiplicities

Average γ ray multiplicities defined by a specific low-lying discrete γ ray transition are compared with the experimental data in Tab.7. It is seen that the agreement is excellent except perhaps of the case of the 0.704 MeV line where the theoretical value seems to be too low.

Average γ ray multiplicities of cascades following neutrons with a specific energy are compared with the experimental values in Table 8. We give only those values that refer to (n,n'γ) channel (for small neutron energies there should be contribution from short (n,2nγ) cascades and the resulting multiplicities should be quite small). It is seen that the agreement is, as above, very good.

The average γ ray multiplicities referring to individual reaction channels are summarized in Table 9.

Table 7. Average γ ray multiplicities of cascades including specific discrete γ ray transition in the (n,n'γ) channel.

Transition		Multiplicity	
$J_i^\pi \rightarrow J_f^\pi$	E_γ(MeV)	Exper.	Theor.
$2_3^+ \rightarrow 2_1^+$	1.728	-	3.31
$2_2^+ \rightarrow 2_1^+$	1.531	-	3.31
$2_1^+ \rightarrow 0_1^+$	1.434	3.7±0.2	3.56
$4_2^+ \rightarrow 2_1^+$	1.334	3.7±0.4	3.85
$5_1^+ \rightarrow 4_1^+$	1.246	4.4±1.4	4.49
$0_2^+ \rightarrow 2_1^+$	1.214	-	4.22
$4_1^+ \rightarrow 2_1^+$	0.936	3.7±0.3	4.01
$5_1^+ \rightarrow 4_1^+$	0.848	4.8±1.5	4.55
$6_1^+ \rightarrow 4_1^+$	0.744	5.8±0.6	5.94
$3_1^+ \rightarrow 4_2^+$	0.704	6.8±0.7	5.48
$4_3^+ \rightarrow 4_2^+$	0.647	5.6±0.6	5.49

Table 8. Average γ ray multiplicity in the (n,n'γ) channel as a function of the observed energy of scattered neutron.

$E_{n'}$(MeV)	Multiplicity	
	Exper.	Theor.
2.3 - 2.6	4.48±0.48	4.63
2.7 - 3.0	4.59±0.47	4.51
3.1 - 3.6	4.05±0.43	4.44
3.7 - 4.3	4.15±0.45	4.35
4.4 - 5.3	3.70±0.45	4.31
5.4 - 6.7	3.42±0.46	4.10
6.8 - 8.6	3.08±0.45	3.60
8.7-11.6	2.32±0.43	2.66

Table 9. Average γ ray multiplicities in various reaction channels.

Reaction	Multiplicity	
	Exper.	Theor.
(n,xγtotal)	3.34±0.24	3.10
(n,n'γ)	3.7± 0.2*)	3.56
(n,2nγ)	1.0 *)	1.31
(n,npγ)	1.0 *)	1.03
(n,pγ)	3.0 ±0.5*)	2.82
(n,$\alpha\gamma$)	2.5 ±0.5*)	2.48

*) Estimates only.

4. Conclusions

We conclude that integral quantities and data that involve sufficient averaging, such as γ ray multiplicities, can be predicted with good precision. This is valid also for strong discrete γ lines. Generally, however, discrete γ ray production cross sections cannot be safely predicted better than within a factor of two. Things may be even worse for particular portions of the total γ ray spectrum. The preequilibrium exciton model is particularly useful in describing high-energy part of the γ ray spectrum due to (n,γ) processes.

References

1. S. Hlaváč and P. Obložinský :"Measurement of γ ray production from ^{52}Cr(n,xγ) reactions at 14.6 MeV", contributed paper to this meeting (see also preceding IAEA Reports quoted in this paper).
2. A. Prince, Proc. Inter. Conf. on Nuclear Data for Science and Technology, Antwerp (1983), p. 574.
3. F.D. Becchetti and G.W. Greenless, Phys. Rev. 182 (1969) 1190.
4. G. Igo and J.R. Huinzenga, Nucl. Phys. 29 (1962) 462.

5. A. Mengoni , F. Fabbri and G. Maino, Report RT/TIB/85/38 (ENEA, Rome 1985).
6. A. V. Ignatyuk et al., Sov. J. Nucl. Phys. 21 (1975) 21.
7. A. Mengoni, F. Fabbri and G. Maino, Nuovo Cim. A94 (1986) 297.
8. S.S. Dietrich and B.L. Berman, At. Nucl. Data Tab. 37 (1988) 199.
9. Shi Xiangjun, H. Gruppelaar, and J.M. Akkermans, Nucl. Phys. A466 (1987) 333.
10. P. Obložinský, Phys. Rev. C35 (1987) 407.
11. T. Yamamoto, Y. Hino, S. Itagaki, and K. Sugiyama, J. Nucl. Tech. 15 (1978) 797.
12. U. Abbondano, R. Giacomich, M. Lagonegro, and G. Pauli, J. Nucl. Energy 27 (1973) 227.
13. G. Grenier, in Proc. Int. Conf. on Neutron Physics, Kiev 1973, vol.3, p.217.
14. D.M. Hetrick, C.Y. Fu, and D.C. Larson, Report ORNL/TM 10417, ENDF-345 (Oak Ridge, September 1987).
15. D.M. Drake, E.D. Arthur, and M.G. Silbert, Report LS-5893-MS (LASL, Los Alamos 1975).
16. M. Budnar, F. Cvelbar, E. Hodgson et al., Report INDC(YUG)-6/L (IAEA, Vienna 1979).

PRESENT STATUS OF GAMMA-RAY STRENGTH FUNCTIONS AND THEIR IMPACT ON STATISTICAL MODEL CALCULATIONS

J. KOPECKY
Netherlands Energy Research Foundation, Petten, The Netherlands

M. UHL
Institut für Radioforschung und Kernphysik, Vienna, Austria

ABSTRACT

Photon strength functions derived from discrete resonance data in earlier surveys have been reviewed. Corrections for major non-statistical contributions have been applied and derived systematics for f(E1) and f(M1) values can be used for statistical model calculations.

1. INTRODUCTION

The compound nucleus mechanism is dominant for the capture process above the resolved resonance region upto several MeV incident neutron energy. Therefore a statistical model is often used to calculate capture cross-sections. The gamma-ray transmission coefficient T_{XL}, used in these calculations, is related to the gamma-ray strength functions as

$$T_{XL}(E_\gamma) = 2\pi\, E_\gamma^{2L+1}\, f_{XL}(E_\gamma). \qquad (1)$$

Therefore both theoretical and experimental knowledge of the gamma-ray strength functions is highly relevant to these model calculations.

The energy dependence of the E1, M1 and E2 gamma-ray strength functions and the impact of different formulations on the statistical model calculations have been discussed recently in [1,2] and in another contribution to this meeting [3].

In this paper we concentrate on the experimental data. In the past only one global survey [4] of the radiative E1 and M1 strength behaviour has been made as a function of mass. Most of the data have been derived from discrete neutron resonance experiments using the method of slow neutron time-of-flight spectroscopy. The aim of this paper is a careful revision of this data set because of the recommendation [1-3] to use absolute values of gamma-ray strength functions in reaction model calculations. We prefer this approach to the widely used normalization procedure by reproducing the experimental ratio $\langle\Gamma_\gamma\rangle/\langle D_0\rangle$.

2. SURVEY OF PREVIOUS WORK

The original survey of McCullagh et al. [4] was made for about 50 nuclides with absolute partial widths originating from (n,γ), (γ,n) and (γ,γ$_0$) reactions and resulted in derivation of model

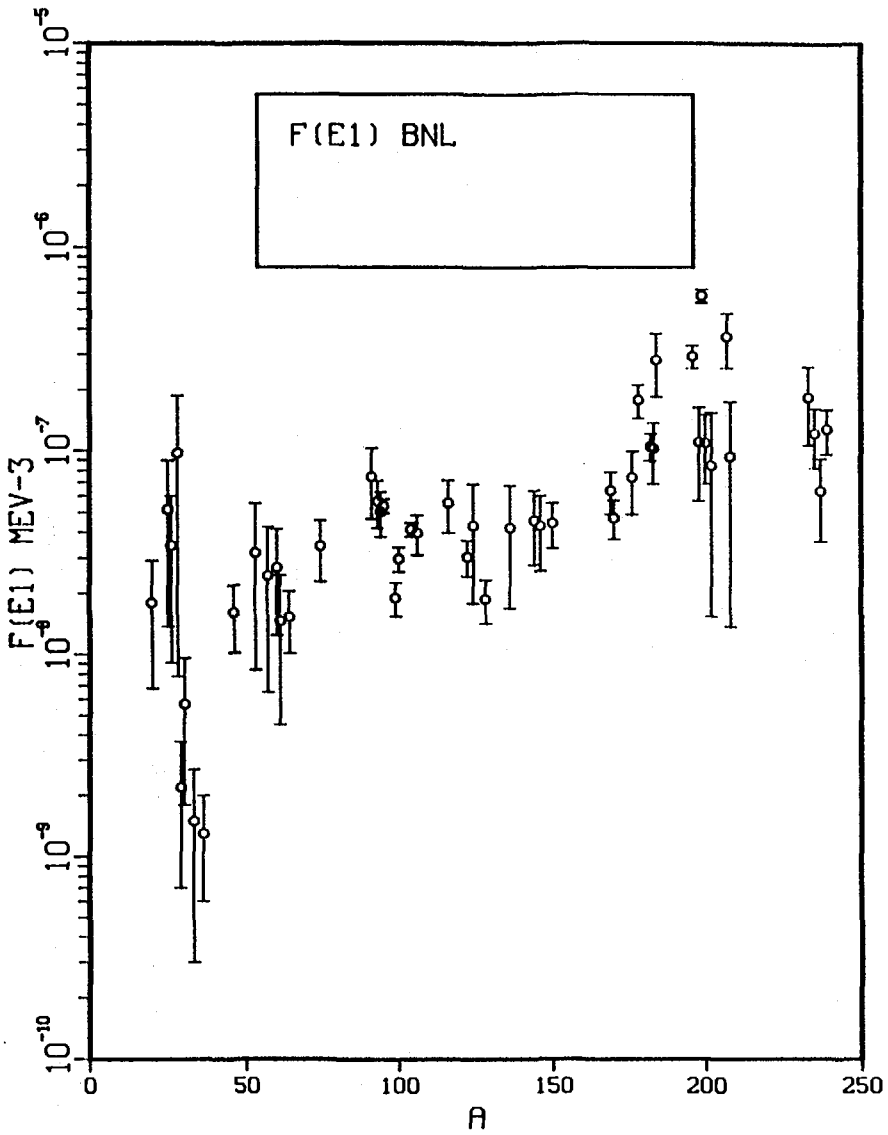

Fig.1 A plot of the E1 strength functions (Eq. 2) against mass number. The original data from ref. [4] are used.

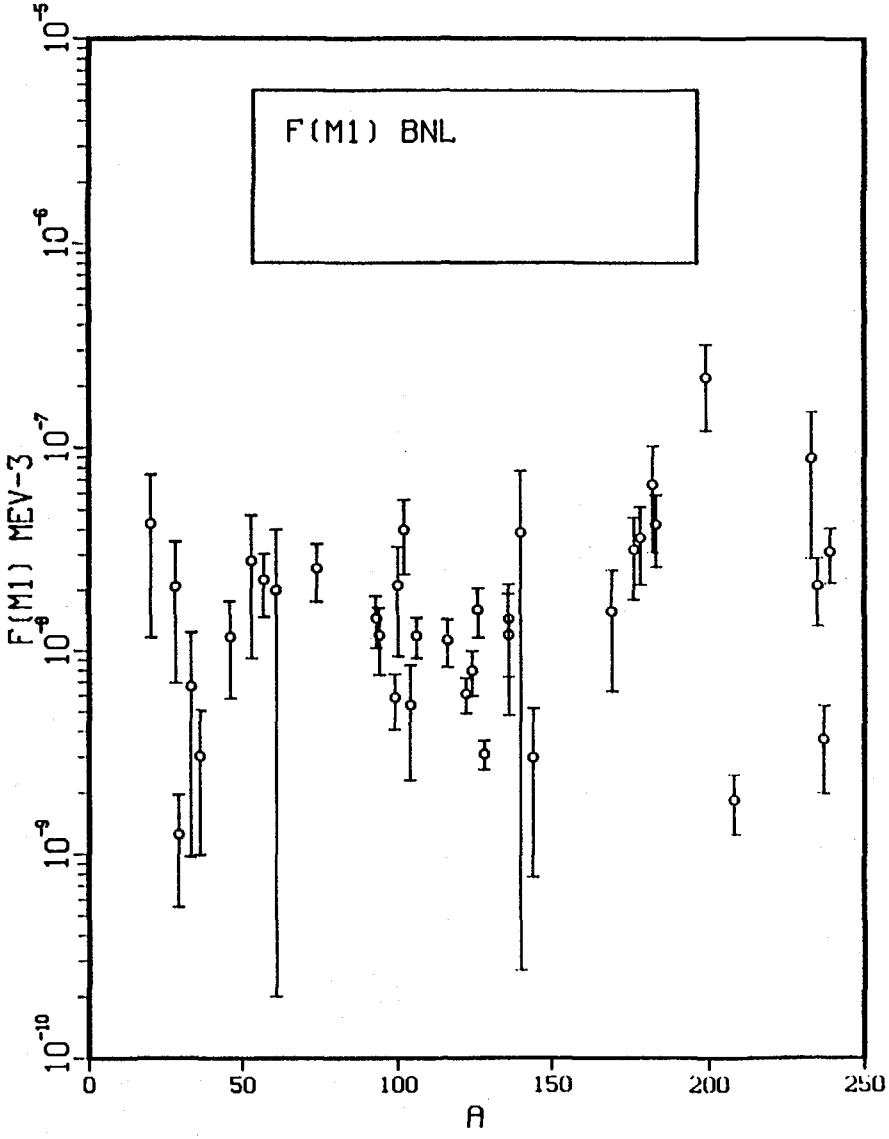

Fig.2 A plot of the M1 strength functions (Eq. 2) against mass number. The orirginal data from ref. [4] are used.

dependent (single particle and Brink-Axel models) strength functions for E1 and M1 radiation. The mean gamma-ray energy for this data set was about 7 MeV. From this data Kopecky [5] derived global formulae for the additional dependence of E1(M1) strength on A, compared with the above-mentioned models.

We prefer the model independent definition of strength functions, written as

$$f_L(E_\gamma) = \langle \Gamma_\gamma \rangle / E_\gamma^{2L+1} \, D_0 \, . \qquad (2)$$

The corresponding values, based on the original data from ref. [4], have been plotted for E1(M1) radiation as a function of mass (see figs. 1 and 2). For all necessary details the reader is refered to ref. [4].

For a meaningful application of the experimental $f_L(E_\gamma)$ values in the statistical model calculations it is necessary to check the data for the presence of a non-statistical component in the total or partial radiative widths. Such corrections have not been applied in the original work of McCullagh et al. [4]. The use of this data in statistical model calculations can therefore lead, if a non-statistical mechanism is strongly present in the resonance region, to a significant overestimation in the normalization. Another important quantity influencing the experimental values of $f_L(E_\gamma)$ is the s-wave resonance spacing D_0, which may have a large uncertainty.

Study of these two effects are the main objective of this paper. The aim was to develop γ-ray the strength function systematics, which can be used to test the predicted values, as discussed in refs. [1-3], if no experimental data are available.

3. APPLIED REVISIONS

3.1 E1 radiation

The standard method to display the surveyed data is to divide them by calculated values from the model that is usually adopted for determining strength functions. We have chosen, as in all earlier studies, the "classical" Lorentzian with the energy independent spreading width, although there is strong evidence [1-3] that this formulation overestimates the large body of experimental data both from discrete-resonance [4] and averaged-resonance capture experiments [6,7]. This is nicely demonstrated in fig. 3, where the ratio of experimental f(E1) values against the Lorentzian prediction is displayed. Applied giant-resonance parameters were taken from ref. [8]. Three regions deviate from the expected smooth trend, namely $40<A<70$, $90<A<110$ and $170<A<190$ and these were in particular the subject of a check of the evaluation in ref. [4].

First of all we scanned the D_0 values used in ref. [4], against those given in the recent compilation of Mughabghab [10]. These values are given in columns 2 and 3 of tables 1 and 2. In many cases differences

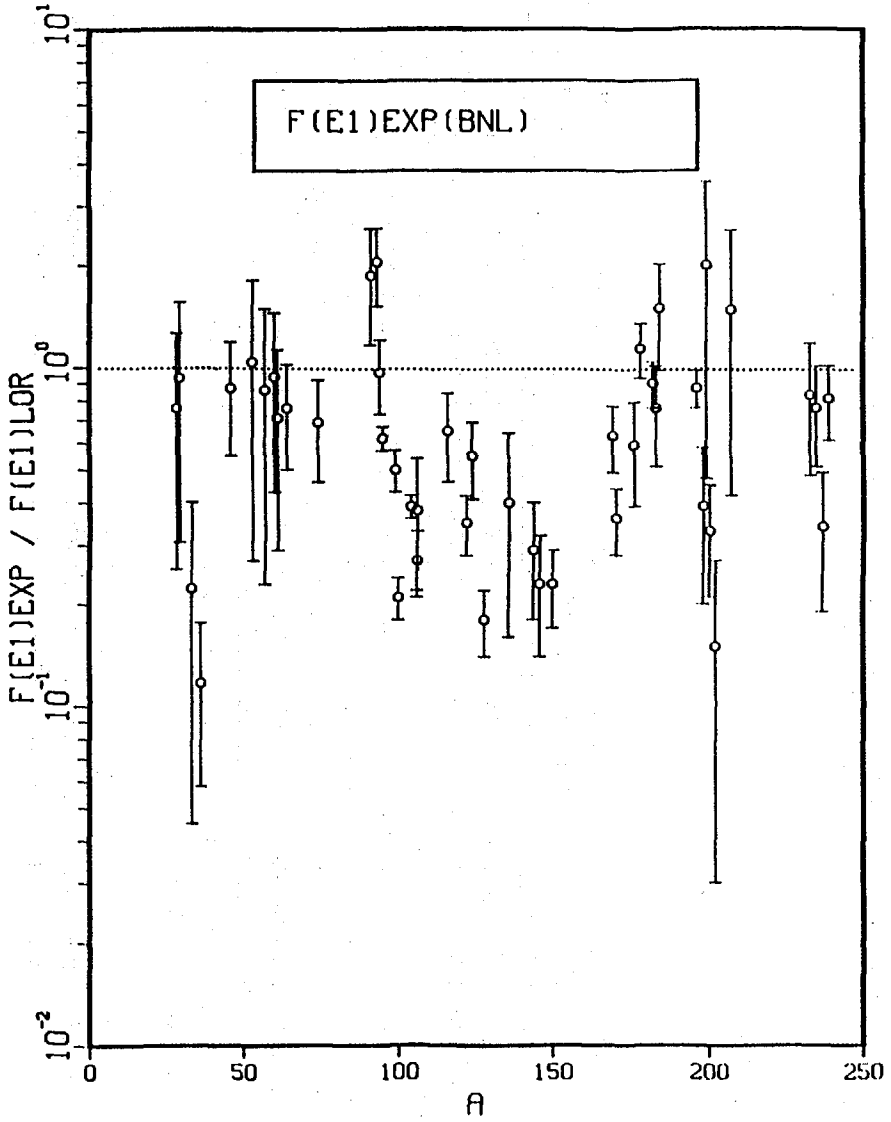

Fig.3 Ratio of experimental f(E1) values and the classical Lorentzian prediction plotted against mass number.

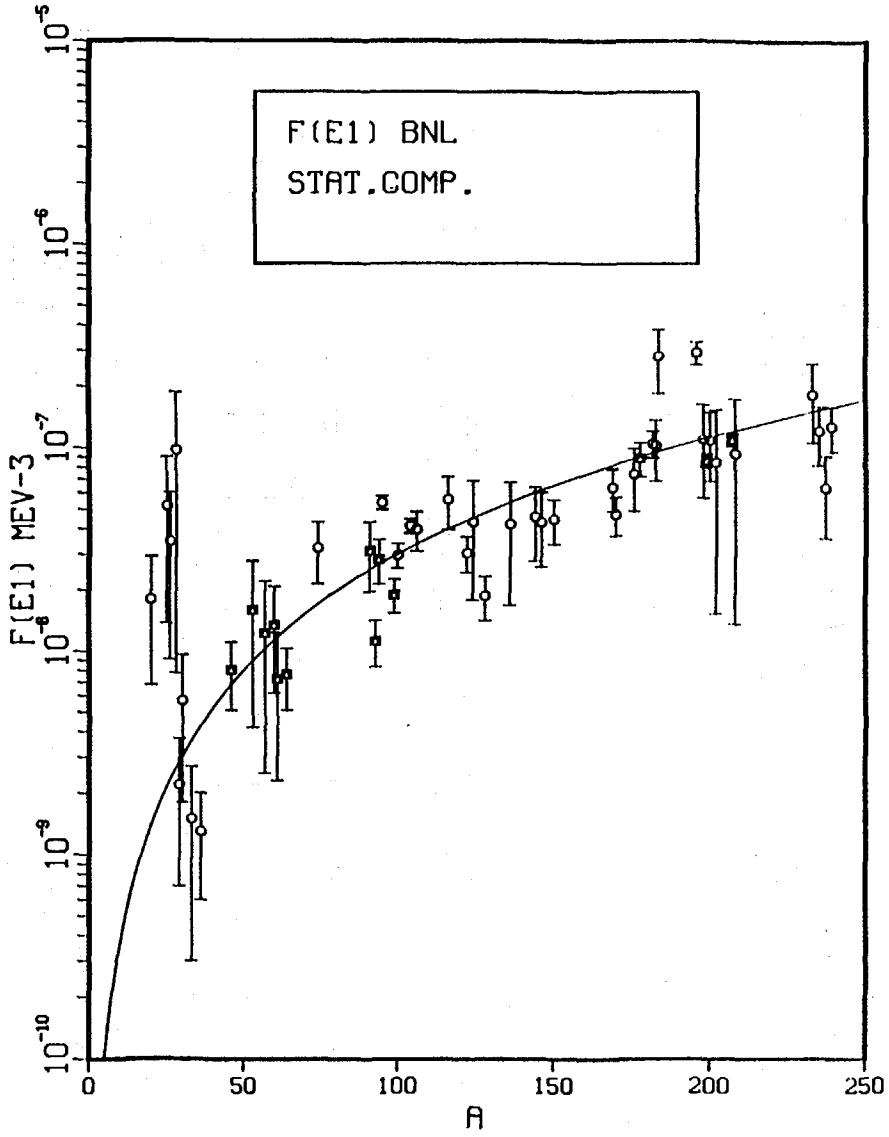

Fig.4 A plot of revised f(E1) values against mass number together with the fitted smooth dependence.

Table 1. Revision of experimental values for f(E1) based on s-wave, p-wave capture and photonuclear data denoted by s,p(J) and gn, respectively.

Product nucleus	D_0(eV) [4]	D_0(eV) [10]	Cor. factor	f(E1) [10^{-8} MeV^{-3}] [4][a]	f(E1) [10^{-8} MeV^{-3}] Present work
F -20 p	33200	-		1.80(112)	
Mg-25 p(1.5)	143500	-		5.17(380)	
Mg-26 gn	-	-		3.46(255)	
Al-28 s	19970	-		9.74(896)	
Si-29 s	40000	-		0.22(15)	
Si-30 p(2)	100000	-		0.57(39)	
S -33 s	203000	17000		0.15(12)	
Cl-36 s	24500	21000		0.13(7)	
Sc-46 s	1300	1300	f=0.5[b]	1.61(59)	0.81(30)
Cr-53 gn	-	7000	f=0.5[b]	3.19(235)	1.60(118)
Fe-57 gn	-	6000	f=0.5[b]	2.46(181)	1.23(99)
Co-60 s	1060	1100	f=0.5[b]	2.70(146)	1.35(73)
Ni-61 gn	-	1800	f=0.5[b]	1.46(101)	0.73(50)
Cu-64 s	629	320	f=0.5[b]	1.53(52)	0.77(26)
Ge-74 s	76	82		3.44(115)	
Zr-91 s	gn	570	f=0.42[b]	7.48(281)	3.14(118)
Mo-93 p(1.5)	1000	2100	f=0.20[b]	5.67(147)	1.13(29)
Mo-95 gn	-	975		5.38(41)	
Nb-94 sp	37.8	44	f=0.56[c]	5.04(124)	2.84(70)
MO-99 p(0.5)	429	970		4.32(81)	1.90(36)
Ru-100 s	31.4	25		2.97(41)	
Rh-104 s	23.2	16		4.13(33)	
Pd-106 s	11.9	10		3.79(87)	
In-116 s	9.5	9.4		5.56(159)	
Sb-122 s	13.5	18		3.05(61)	
Sb-124 s	20.7	38		3.48(203)	
I -128 s	13.3	9.7		1.88(46)	
Ba-136 s	47.6	40		4.23(254)	
Nd-144 s	44.6	45		4.59(181)	
Nd-146 s	18.7	22		4.31(171)	
Sm-150 s	2.3	2.2		4.46(110)	
Er-168 s	3.8	4.0		1.18(15)	
Er-169 s	94	94		6.39(147)	
Tm-170 s	7.3	7.3		4.72(101)	
Lu-176 s	3.47	3.45		7.41(251)	
Hf-178 s	2.5	2.4	f=0.5[d]	17.77(335)	8.89(168)
Ta-182 s	4.5	4.17		10.47(157)	
W -183 s	66	66		10.25(338)	
W -184 s	12	12		28.14(970)	
Pt-196 s	16.3	18		20.31(257)	
Au-198 s	16.2	16.5		11.00(530)	
Hg-199 s	83	105	f=0.15[e]	58.08(445)	8.71(67)
Hg-200 s	88.1	100		10.91(404)	
Hg-202 s	100.5	98		8.47(693)	
Pb-207 gn	-	35700	f=0.3[b]	36.61(261)	10.98(78)
Pb-208 gn	-	37500		9.37(800)	
Th-233 s	18.2	16.8		18.30(766)	
U -235 s	12.3	10.6		12.14(392)	
U -237 s	15.4	14.7		8.16(352)	
U- 239 s	16.4	20.9		12.74(314)	

[a] Given errors are in quadrature added statistical, normalizations (20%) and Porter-Thomas uncertainties.
[b] Corrected for the valence component.
[c] The value of D_0 = 67 eV [12] has been applied.
[d] Absolute calibration uncertainty.
[e] Only last two transitions taken.

Table 2. Revision of experimental values for f(M1) based on s-wave, p-wave capture and photonuclear data denoted by s,p(J) and gn, respectively.

Product nucleus		D_0(eV) [4]	D_0(eV) [10]	Cor. factor	f(M1) [10^{-8} MeV^{-3}] [4][a]	f(M1) [10^{-8} MeV^{-3}] Present work
F -20	p	33200	-		4.26(310)	
Al-28	s	19970	-		2.08(139)	
Si-29	s	40000	-		0.125(70)	
S -33	s	203000	17000		0.66(57)	
Cl-36	s	24500	21000		0.30(20)	
Sc-46	s	1300	1300		1.17(59)	
Cr-53	gn	-	7000		2.80(188)	
Fe-57	gn	-	6000		2.25(78)	
Ni-61	gn	-	1800		2.00(108)	
Ge-74	s	76.7	82		2.57(82)	
Mo-93	s	2350	2100		1.46(42)	
Nb-94	s	37.8	44	f=0.56[b]	1.20(44)	0.68(25)
M0-99	s	918	970		0.59(18)	
Ru-100	s	31.4	25		2.12(118)	
Ru-102	s	24.6	16	f=0.62[c]	4.00(160)	2.46(98)
Rh-104	s	23.2	16		0.54(31)	
Pd-106	s	11.9	10		1.19(27)	
In-116	s	9.5	9.4		1.13(30)	
Sb-122	s	13.5	18		0.61(12)	
Sb-124	s	20.7	38		0.79(20)	
Te-126	s	38	38		1.60(44)	
I -128	s	13.3	9.7		0.31(5)	
Ba-136	s	47.6	40		1.45(70)	
Nd-144	s	44.6	45		0.30(22)	
Er-169	s	94	94		1.57(95)	
Lu-176	s	3.47	3.45		3.19(139)	
Hf-178	s	2.5	2.4		3.65(152)	
Ta-182	s	4.5	4.17		6.64(356)	
W -183	s	66	66		4.25(183)	
Hg-199	s	83	105		22.1(1155)	
Pb-208	p(1)	25000	37500		0.185(60)	
Th-233	s	18.2	16.8		8.88(602)	
U -235	s	12.3	10.6		2.11(78)	
U -237	s	15.4	14.7		0.37(17)	
U- 239	s	16.4	20.9		3.22(96)	

a) Given errors are in quadrature added statistical, normalizations (20%) and Porter-Thomas uncertainties.
b) D_0 = 67 ev from ref.[12] have been applied.
c) Last three transitions taken (one enhanced).

are found, usually ref. [4] is underestimating the spacing. Except for ^{94}Nb no corrections based on new D_0 values have been applied because they caused changes in f(E1) within the experimental errors. A general word of caution, however, has to be given here. The recent study [11] and extended experience of many evaluators (e.g. work of Delfini et al. [16]) shows that the D_0 values in ref. [10] have not always been properly corrected for missed or wrongly assigned reso-

nances. This can sometimes result in a significant difference as nicely demonstrated in the above mentioned case of ^{94}Nb [3,12] and therefore it is strongly recommended for detailed evaluations to review the D_0 value and apply the above-mentioned corrections.

Another inspection has been applied to nuclides which can be influenced by a strong non-statistical component present in the resonance region. In several original data sets, used in the previous survey [4], these valence components have been estimated. In such a case the corresponding strength function has been corrected for. For the mass region of the s-wave giant resonance, $40<A<60$, an estimate of approximately 50% valence component has been applied, which seems to be a reasonable guess based on calculations of Allen and Musgrove [13] and also from the behaviour of total radiative widths of s-, p- and d-wave neutron capture. In some cases the selection of transitions used for datermination of f(E1) was inspected, especially where only a limited number of primary transitions were used. The arguments for the corrections applied are listed in table 1.

A plot of corrected f(E1) values, which represent the statistical component, is given in fig. 4. Values with $A<30$ have been disregarded from fitting from obvious reasons. The remaining data reasonably follow a smooth dependence on A, which can parameterized as

$$f(E1)_{stat.}\langle 7\ MeV\rangle = 4.62\times10^{-12}\ A^{1.91}\ . \qquad (3)$$

3.2 M1 radiation

Similar inspection of input data, as for E1 radiation, has been applied here. For M1 radiation, however, the situation is more complicated for two reasons. First of all there is no well-established general theoretical prescription for f(M1). The frequently used single-particle estimate is at variance with a finite-energy weighted sum rule and the recently proposed giant resonance model [7] lacks a global prescription for the sum rule. Furthermore there is no general theoretical explanation of non-statistical mechanisms in M1 radiation, despite the fact that these effects have been experimentaly observed [14,15]. The input data are scarce and often based on averaging over few transitions.

In fact, corrections have been applied only for two nuclides, as given in table 2, one for ^{94}Nb based again on inspection of the D_0 value and the other for ^{102}Ru due to limited selection of transitions. An interesting observation is that in the mass range $40<A<60$ the f(M1) values exhibit a comparable increase as for E1 radiation (for those enhanced by the valence capture). This may indicate a presence of a similar non-statistical mechanism or an effect of insufficient averaging. However, no correction has been applied here. The smooth dependence on A has been again fitted to the data above A=30 (see fig. 5) and reads as

$$f(M1)_{stat.}\langle 7\ MeV\rangle = 1.88\times10^{-11}\ A^{1.41}\ . \qquad (4)$$

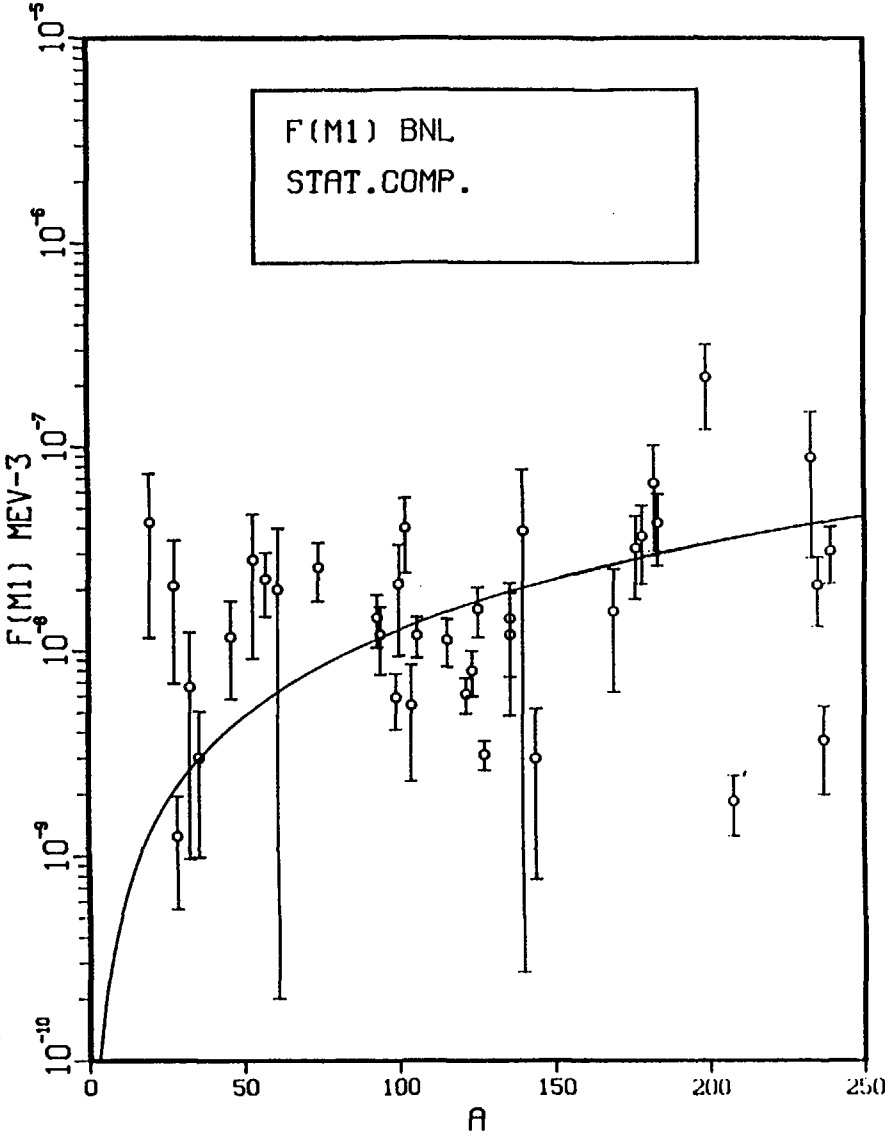

Fig.5 The same as fig. 4 for f(M1).

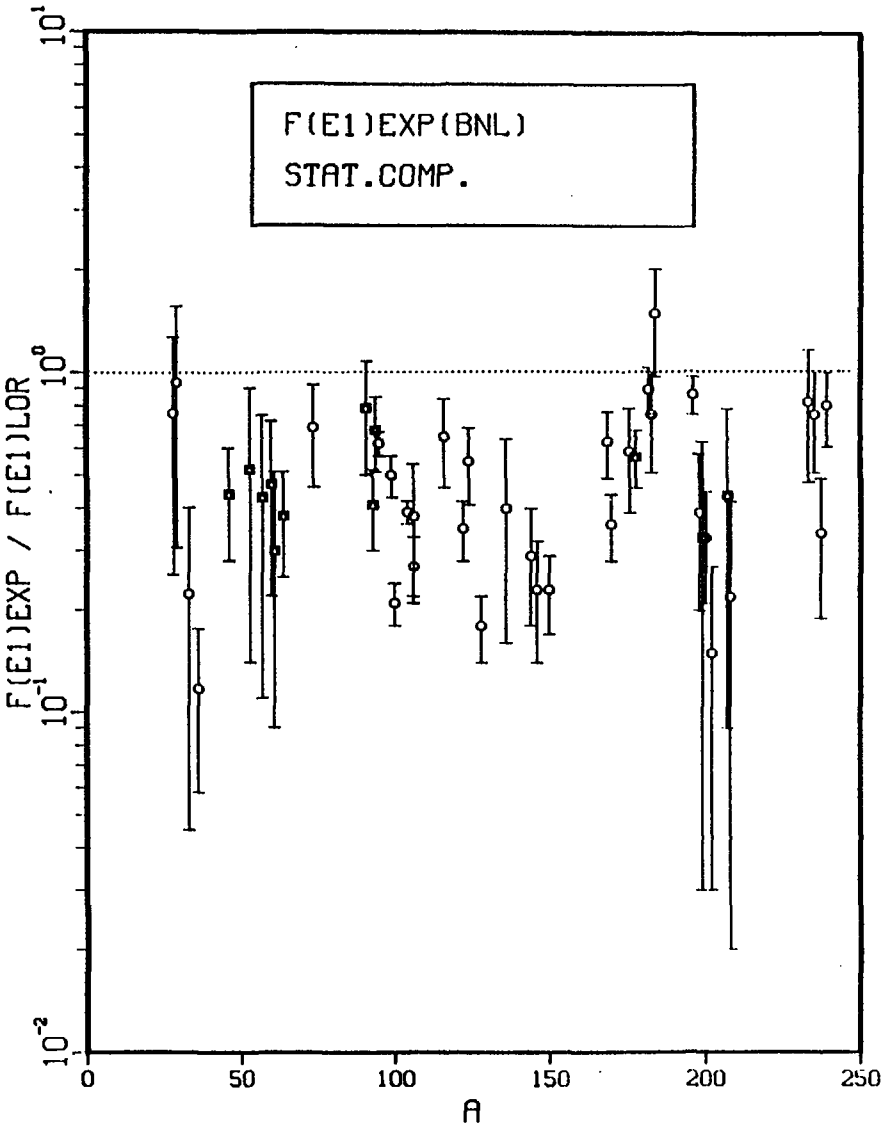

Fig.6 The same as fig. 3 using the revised f(E1) values.

4. CONCLUSION

The original data set for E1 gamma-ray strength functions [4] has been reviewed and corrected for non-statistical components in order to derive systematics which can be used for pure statistical model calculations. For some nuclides also the limited amount of selected transitions, used to derive the averaged radiative strength, seemed to be a source of enhancement in the gamma strength. The resulting set of f(E1) values shows a smooth dependence on A and is generaly overestimated by a classical Lorentzian extrapolation (see fig. 6). This behaviour forms a global argument for the use of the modified Lorentzian with the energy dependent spreading width as proposed in ref. [7] and discussed in ref. [1-3]. It is noted that no uncertainty estimate has been made of the correction for non-statistical effects.

The trend in the f(M1) values indicates also a region of enhancement ($40<A<60$) in the M1 strength and furthermore the data fluctuate far more compared to E1 data. The interpretation of this all is complicated by experimental uncertainties. However, the derived systematic dependence on A can be certainly used as a reasonable approximation of the f(M1) value, if necessary combined with the general trend in E1/M1 strength ratios.

REFERENCES

[1] J. Kopecky, M.G. Delfini, H. Gruppelaar and M. Uhl, Proc. Meet. on Neutron Activation Cross-Sections for Fission and Fusion Energy Applicartions, Argonne 13-15th September 1989, NEANDC-279 'U', p.201.

[2] J. Kopecky and M. Uhl, Phys. Rev., accepted for publ.

[3] M. Uhl and J. Kopecky, contribution to this meeting.

[4] C.M. McCullagh, M. Stelts and R.E. Chrien, Phys. Rev. C23(1981) 1394.

[5] J. Kopecky, Inst. Phys. Conf. Ser. No.62, Neutron-Capture Gamma Ray Spectroscopy and Related Topics, Grenoble 1981, (The Insitute of Physics, Bristol and London 1982) p. 423.

[6] S. Raman, idem, p. 357.

[7] J. Kopecky and R.E. Chrien, Nucl. Phys. A468(1987) 285.

[8] S.S. Dietrich and B.L. Berman, At. Nucl.Data Tables 38(1989) 199.

[9] S.F. Mughabghab and D.I. Garber, BNL 325, Third Edition, 1973.

[10] S.F. Mughabghab, M. Divadeenam and N.E. Holden, Neutron Cross Sections, (Academic Press, New York 1981) Vol.1 Part A and B.

[11] H. Vonach et al., Phys. Rev. C38(1988) 2541.

[12] P. Vertes and Y.V. Grigoryew, Proc. Int. Conf. on Nuclear Data for Science and Technology, Mito, Japan, May 30-June 3 1988, (Saikon Publ. Co., Tokyo 1988) p.623.

[13] B.J. Allen and A.R. Musgrove, Adv. Nucl. Phys., Vol.10 (Plenum, New York 1978) p.129.

[14] C.F. Clement, A.M. Lane and J. Kopecky, Phys. Lett. 71B(1977) 10.

[15] R.E. Chrien and J. Kopecky, Phys. Rev. Lett. 39(1977) 911.

[16] M.G. Delfini and H. Gruppelaar, ECN Report, ECN-82 (1980).

CALCULATIONS OF CAPTURE CROSS SECTIONS AND GAMMA-RAY SPECTRA AS A TOOL FOR TESTING STRENGTH FUNCTION MODELS

M. UHL
Institut für Radiumforschung und Kernphysik, Universität Wien, A1090 Wien, Boltzmanngasse 3, Austria

J. KOPECKY
Netherlands Energy Research Foundation ECN, P.O.Box 1, 1755 ZG Petten,The Netherlands

Abstract

The impact of the low energy behaviour of the E1 and the M1 gamma-ray strength functions on statistical model calculations of radiative neutron capture was studied for targets with mass numbers between 55 and 197. We found strong support for models of the E1 strength function with a non-zero limit if the transition energy tends to zero. Such a low energy behaviour is predicted in theoretical work by Kadmenskij et al. and by Sirotkin.

The employed strength functions are derived from a generalized Lorentzian in case of E1 and a standard Lorentzian in case of M1 and E2 radiation. The parameters of these strength functions are based on independent experimental data. No normalizations were applied to the strength functions. We therefore recommend to use these strength functions in reaction model calculations for applied purposes.

1. Introduction

For incident energies from overlapping resonances up to a few MeV the compound nucleus mechanism accounts for the majority of capture events. Therefore the statistical model alone is often used to calculate (average) capture cross-sections and gamma-ray spectra for applied purposes, though there are mass regions where also non-statistical processes should be considered. The ingredients of statistical model calculations are particle transmission coefficients, level densities and finally gamma-ray strength functions - the main object of this presentation. As supplement to our previous contribution / 1/ we concentrate here on their impact on model calculations. The most important strength functions in this context are those for E1, M1 and E2 radiation.

Popular models for strength functions $f_{XL}(\varepsilon_\gamma)$ (XL = multipole type, ε_γ = transition energy) are the single particle model / 2/ resulting in energy independent strength functions and models, which by means of Brink's hypothesis / 3/ relate $f_{XL}(\varepsilon_\gamma)$ to the absorption cross-section of photons of type XL. According to this celebrated hypothesis the photoabsorption cross-section for excited states is the same as for the ground state. Combined with the assumption that the photoabsorption cross-section is dominated by a giant resonance Brink's hypothesis provides simple expressions for the strength functions. Widely used is Axel's / 4/ global prescription for the E1 strength function in terms of a Lorentzian for the giant dipole resonance (GDR). Later it became clear that a Lorentzian for the E1 absorption cross-section, when extrapolated to energies near or below the neutron binding energy, often overpredicts $f_{E1}(\varepsilon_\gamma)$ data. For model calculations, however, the low energy behaviour of the strength function is essential. Therefore various empirical prescriptions have been proposed to correct for insufficiencies of the shape of the E1 absorption cross-section as e.g. a "depressed Lorentzian" / 5/ or an "energy dependent Breit-Wigner shape" / 6/. A comprehensive compilation of functional forms for the GDR can be found in Gardner's / 7/ review. Recent examples of calculations of capture cross-sections and gamma-ray spectra based on these ideas can be found in Refs. / 8/, / 9/, /10/ and /11/.

A quite different low energy behaviour of the E1 strength results from microscopic models as those proposed by Kadmenskij et al. /12/ and by Sirotkin /13/. While strength functions derived from a Lorentzian or from the above mentioned empirical formulas vanish as the energy tends to zero, these microscopic models predict a non-zero limit of $f_{E1}(\varepsilon_\gamma)$ for $\varepsilon_\gamma \rightarrow 0$ which moreover depends on the excitation energy of the final state. Thus these microscopic models are at variance with Brink's hypothesis. A "generalized Lorentzian" resulting in a finite, energy dependent $\varepsilon_\gamma \rightarrow 0$ limit was recently proposed /14/ and compared with average resonance capture (ARC) data by Kopecky and Chrien /15/. The non-zero $\varepsilon_\gamma \rightarrow 0$ limit could not be verified by the ARC results; there is, however, other experimental evidence for its existence /16/, /17/.

All these different prescriptions for the strength function of the dominant electric dipole radiation reflect uncertainties in this quantity which immediately affect the calculated capture cross-sections and gamma-ray spectra. As a consequence such calculations often use strength functions of a given shape and apply some normalization. A popular approach is to normalize the E1 strength by reproducing the ratio $<\Gamma_{\gamma 0}> / <D_0>$ of the average radiation width and the average spacing of s-wave resonances. Problems arise if experimental data for these quantities are lacking. M. and D. Gardner /18/, /19/ suggest in such cases to employ suitable parameterizations of the strength functions instead of resorting to separate systematics of $<\Gamma_{\gamma 0}>$ and $<D_0>$.

We report here on model calculations carried out for incident neutrons on spherical nuclei with mass numbers between 55 and 197. They comprise average total s- and p-wave radiation widths, capture cross-sections and gamma-ray spectra.

We prefer for M1 and E2 radiation strength functions derived from a standard Lorentzian. By comparing the results to experimental data we aim at first to verify for E1 radiation the aforementioned generalized Lorentzian or more specifically the non-zero $\varepsilon_\gamma \rightarrow 0$ limit of $f_{E1}(\varepsilon_\gamma)$ in an energy region not accessible to ARC experiments. Our second goal is to improve the capability to predict capture and gamma-ray production cross-sections by recommending strength function models which are i) supported by theory, ii) determined by parameters relying on experimental data independent of the calculated quantities (see previous contribution / 1/) and finally are iii) free from arbitrary normalizations.

2. Models and parameters

At present we only consider the statistical model contribution and restrict the upper limit of the incident energy so that this contribution dominates. The calculations were performed with the code MAURINA /20/. The code employs for the width fluctuation correction Moldauer's /21/ prescription. A detailed treatment of gamma-ray cascades as e.g. described in Ref. /22/ allows the calculation of gamma-ray spectra. The calculations require the knowledge of the following quantities and parameters.

2.1 Gamma-ray transmission coefficients

The gamma-ray transmission coefficients $T_{XL}(\varepsilon_\gamma)$ are related to the corresponding strength functions by

$$T_{XL}(\varepsilon_\gamma) = 2\pi\, \varepsilon_\gamma^{2L+1}\, f_{XL}(\varepsilon_\gamma)\,. \qquad (1)$$

For the (very small) contributions of M2, E3 and M3 radiation we employed the single particle model with $f_{XL}(\varepsilon_\gamma) = 1$ WU (Weisskopf unit). An energy independent strength function is occasionally used for M1 radiation. In this case, however, we adjusted the absolute value so as to reproduce experimental data or systematics ("adjusted single particle model").

Assuming that the absorption cross-section for XL radiation is dominated by a giant resonance of standard Lorentzian shape (resonance energy E in MeV, damping width Γ in MeV and peak

cross-section σ_0 in mb) one obtains for the strength function $f_{XL}(\varepsilon_\gamma)$ by means of Brink's hypothesis / 3/

$$f_{XL}(\varepsilon_\gamma) = 26 \times 10^{-8} [\mathrm{mb}^{-1}\mathrm{MeV}^{-2}] \frac{1}{2L+1} \frac{\sigma_0 \varepsilon_\gamma^{3-2L} \Gamma^2}{(\varepsilon_\gamma^2 - E^2)^2 + \varepsilon_\gamma^2 \Gamma^2} . \quad (2)$$

Theoretical considerations /23/ suggest a giant dipole resonance with an energy dependent spreading width leading to the the following expression for the E1 strength function

$$f_{E1}(\varepsilon_\gamma) = 8.68 \times 10^{-8} [\mathrm{mb}^{-1}\mathrm{MeV}^{-2}] \frac{\sigma_0 \varepsilon_\gamma \Gamma\Gamma(\varepsilon_\gamma)}{(\varepsilon_\gamma^2 - E^2)^2 + \varepsilon_\gamma^2 \Gamma(\varepsilon_\gamma)^2} , \quad (3)$$

For $\Gamma(\varepsilon_\gamma)$ we used an expression based on the theory of Fermi liquids /12/

$$\Gamma(\varepsilon_\gamma) = \Gamma \frac{\varepsilon_\gamma^2 + 4\pi^2 T^2}{E^2} , \quad (4)$$

where $T = \sqrt{U/a}$ is the nuclear temperature corresponding to the excitation energy U of the final state; a stands for the Fermi gas level density parameter. As representative for strength function models with a non-zero limit for $f_{E1}(\varepsilon_\gamma)$ we chose the "generalized Lorentzian" /14/, /15/

$$f_{E1}(\varepsilon_\gamma, T) = 8.68 \times 10^{-8} [\mathrm{mb}^{-1}\mathrm{MeV}^{-2}] \left[\frac{\varepsilon_\gamma \Gamma(\varepsilon_\gamma)}{(\varepsilon_\gamma^2 - E^2)^2 + \varepsilon_\gamma^2 \Gamma(\varepsilon_\gamma)^2} + \frac{0.7\Gamma 4\pi^2 T^2}{E^5} \right] \sigma_0 \Gamma , \quad (5)$$

where $\Gamma(\varepsilon_\gamma)$ is given by Eq.(4) and $T = \sqrt{U/a}$. Finally, we used in some calculations also the result of Kadmenskij et. al. /12/ for the E1 strength function

$$f_{E1}(\varepsilon_\gamma, T) = 8.68 \times 10^{-8} [\mathrm{mb}^{-1}\mathrm{MeV}^{-2}] \frac{\sigma_0 \Gamma^2}{(\varepsilon_\gamma^2 - E^2)^2 + \varepsilon_\gamma^2 \Gamma^2} \times 0.7 \frac{\varepsilon_\gamma^2 + 4\pi^2 T^2}{E} ; \quad (6)$$

here T is defined under consideration of a pairing correction Δ : $T = \sqrt{(U - \Delta)/a}$. Strictly speaking, this equation is derived only for energies ε_γ smaller than the neutron binding energy.

The photoabsorption cross-section of some of the considered nuclei (^{55}Mn, ^{56}Fe, ^{60}Ni) can only be fitted by the sum of two Lorentzians /24/. In those cases we used in Eqs. (2), (3), (5) and (6) for f_{E1} the sum of two analogue terms calculated with parameters $(E_1, \Gamma_1, \sigma_{01})$ and $(E_2, \Gamma_2, \sigma_{02})$, respectively. In order to improve the reproduction of the experimental data for ^{197}Au + n and ^{93}Nb + n we incoherently added to $f_{E1}(\varepsilon_\gamma)$, if given by Eqs.(3), (5) or (6), the contribution a pigmy resonance of Lorentzian shape with parameters $(E_p, \Gamma_p, \sigma_{0p})$. As the E1 strength functions derived from a standard Lorentzian (Eq.(2)) already overpredicts the experimental data / 1/ we refrained from including a pigmy resonance to this model. The strength function parameters employed in the model calculations are listed in table 1.

2.2 Particle transmission coefficients

The neutron transmission coefficients were derived from optical potentials taken from the literature. We used potentials given by Joly /10/ for ^{197}Au , Wilmore and Hodgson /25/ for ^{143}Nd, Van der Kamp and Gruppelaar /26/ for ^{105}Pd , Delaroche et al. /27/ for ^{93}Nb and by Rapaport et al. /28/ for the targets with $A \leq 60$; the potential of Ref. /28/ was slightly modified for lower incident energies. For ^{60}Ni, ^{56}Fe and ^{55}Mn as target nuclei we considered also competition by emission of protons and alpha-particles with transmission coefficients obtained from global potentials /29/ and /30/. Test calculations showed that our results are not very sensitive to the choice of the particle transmission coefficients.

TABLE 1 : The strength function parameters employed in the calculations

		^{198}Au	^{144}Nd	^{106}Pd	^{94}Nb	^{61}Ni	^{57}Fe	^{56}Mn
E1	σ_{01}(mb)	541	317	199	200	34.1	40.4	51.4
	E_1(MeV)	13.72	15.05	15.92	16.59	16.30	16.63	16.82
	Γ_1(MeV)	4.61	5.28	7.18	5.05	2.44	3.53	4.33
	σ_{02}(mb)					55.2	51.8	45.2
	E_2(MeV)					18.58	19.38	20.09
	Γ_2(MeV)					6.37	5.74	4.09
	σ_p(mb)[a]	6.00			1.50			
	E_p(MeV)[a]	5.80			6.80			
	Γ_p(MeV)[a]	1.50			1.90			
M1	σ_0(mb)	1.12	0.37	1.06	1.39	5.90	3.80	4.50
	E(MeV)	7.05	7.82	8.80	9.02	10.42	10.65	10.72
	Γ(MeV)	4.00	4.00	4.00	4.00	4.00	4.00	4.00
	SP_{adj}(WU)[b]	0.48	0.14	0.38	0.26	0.95	0.48	0.38
E2	σ_0(mb)	5.03	3.40	2.46	2.14	1.42	1.30	1.22
	E(MeV)	10.81	12.02	13.31	13.86	16.00	16.37	16.47
	Γ(MeV)	3.73	4.38	4.84	4.98	5.38	5.43	5.44

[a]pigmy resonance

[b]adjusted single particle model

2.3 Level density

Besides the gamma-ray strength functions the most critical of the auxiliary quantities is the level density. This can easily be seen from the expression for the average total radiation width $<\Gamma_\gamma(U,I,\Pi)>$ of compound states with excitation energy U, spin I and parity Π

$$<\Gamma_\gamma(U,I,\Pi)> = \frac{1}{2\pi\rho(U,I,\Pi)} \sum_{XL} \sum_{I_f,\Pi_f} \int_0^U d\varepsilon_\gamma T_{XL}(\varepsilon_\gamma)\rho(U-\varepsilon_\gamma, I_f, \Pi_f)\,, \qquad (7)$$

where $\rho(U,I,\Pi)$ designates the density of levels with excitation energy around U, with spin I and parity Π. The total s- and p-wave radiation width are weighted averages of appropriate contributions $<\Gamma_\gamma(U,I,\Pi)>$. The integrand in Eq. (7), which also enters into radiative capture cross-sections and the gamma-ray spectra, critically depends on the low energy behaviour of $T_{XL}(\varepsilon_\gamma)$. For low excitation energy we used in Eq. (7) and other similar expressions instead of the level density the actually known levels listed in recent issues of the journal "Nuclear Data Sheets" /31/.

We employed level density formulas with parameters based on the following experimental data: i) average s-wave resonance spacings taken from Refs. /32/, /33/, /34/ and /35/ and ii) the spectrum of low lying levels taken from Ref. /31/. To check the influence of different formulas we performed most calculations with two different level density models: the backshifted Fermi gas model /36/

(BSFG model) and the model by Kataria et al. /37/ (KRK model) which accounts for shell effects in terms of the ground state shell correction to the nuclear binding energy. The KRK model was supplemented by the prescription of Gilbert and Cameron /38/: application of a conventional pairing shift and a constant temperature form at low excitation energy. More details on the chosen level density models can be found in Ref. /39/.

3. Results and discussion

For some target nuclei (^{197}Au, ^{143}Nd, ^{105}Pd) the compound nucleus contribution should dominate. Others are situated in regions with a maximum of the neutron strength function (^{93}Nb in the 3p region and ^{60}Ni, ^{56}Fe, ^{55}Mn in the 3s region) where one expects important valence contributions. We emphasize at this point that, because of strong non-statistical contributions and also because of less accurate experimental strength function data, our results for the structural materials are still very preliminary.

3.1 Average total s- and p-wave radiation widths

Tables 2 and 3 show the total s- and p-wave radiation widths $<\Gamma_{\gamma 0}>$ and $<\Gamma_{\gamma 1}>$, respectively, as well as available experimental results, mostly taken from Refs. /32/ and /33/. Further displayed are the three largest components $<\Gamma_{\gamma \ell}>_{M1}$, $<\Gamma_{\gamma \ell}>_{E1}$ and $<\Gamma_{\gamma \ell}>_{E2}$. To convey an idea of the importance of valence transitions, we show in the last column below the total experimental radiation width the result obtained by subtracting the corresponding valence contribution as given by Allen et al. /40/.

The calculations were carried out for both level density models and under the following assumptions on the strength of dipole radiation: A giant resonance of standard Lorentzian shape and the adjusted single particle model for M1 while for E1 we considered in addition to a standard Lorentzian also one with an energy dependent spreading width (Eq. (3) combined with Eq. (4)) and further the generalized Lorentzian (Eq. (5)) leading to a non-zero $\varepsilon_\gamma \rightarrow 0$ limit of $f_{E1}(\varepsilon_\gamma)$.

Though both level density models reproduce the same number of low lying levels and the same average spacings of s-wave resonances they often result in rather different radiation widths. This difference indicates the uncertainties introduced by such semi-empirical level density models; they affect the capture cross-sections and the gamma-ray spectra, too.

Both tables clearly illustrate the sensitivity on the low energy behaviour of the strength functions for dipole radiation. For ^{197}Au, ^{144}Nd, ^{105}Pd and ^{93}Nb the total s-wave radiation width, obtained with $f_{E1}(\varepsilon_\gamma)$ derived from a Lorentzian based on photoabsorption data, by far overpredicts the experimental results; this agrees with conclusions from ARC data. Assuming a Lorentzian for M1 radiation the s-wave width for the first three nuclei is best described by a generalized Lorentzian (Eq.5) for $f_{E1}(\varepsilon_\gamma)$; in this case also photoabsorption and ARC data are reproduced. In principle also a Lorentzian with an energy dependent spreading width for E1 (Eq.3) and the adjusted single particle model for M1 is compatible with all these experimental data. However, as explained in more detail in our previous contribution / 1/ an energy independent M1 strength is at variance with experimental information on gamma-ray transitions between low lying levels and violates the energy weighted sum rule of M1 strength. In case of ^{93}Nb the recommended strength function models - Eq.(5) for E1 and Eq.(2) for M1 - underpredict the experimental total s- and p-wave radiation width. This may be related to uncertainties in the average spacing $<D_0>$ of s-wave resonances. Values of 44 $\pm$4 eV, 65 eV, and 90$\pm$20 eV are reported in Refs. /32/, /34/ and /41/, respectively; our results are based on Ref. /34/.

The total average s-wave radiation widths of ^{61}Ni and ^{56}Mn contain a substantial valence contribution. The preliminary calculations with our preferred models for dipole radiation strength are somewhat below the experimental values, even after correction for valence capture. In view of all underlying uncertainties we don't regard this as a serious discrepancy.

TABLE 2 : Calculated and experimental total s-wave radiation widths in meV

	Level density : KRK Model				Level density : BSFG Model				
	$\langle\Gamma_{s0}\rangle_{M1}$	$\langle\Gamma_{s0}\rangle_{E1}$	$\langle\Gamma_{s0}\rangle_{E2}$	$\langle\Gamma_{s0}\rangle$	$\langle\Gamma_{s0}\rangle_{M1}$	$\langle\Gamma_{s0}\rangle_{E1}$	$\langle\Gamma_{s0}\rangle_{E2}$	$\langle\Gamma_{s0}\rangle$	$\langle\Gamma_{s0}\rangle_{EXP}$
^{198}Au	10.1[a]	344.9[a]	5.0[a]	360.0	10.1[a]	366.1[a]	5.6[a]	381.8	128±6 /33/
		84.0[b,e]		99.1		76.6[b,e]		92.3	
		127.2[c,e]		142.3		132.5[c,e]		148.2	128[f]
	36.7[d]	84.0[b,e]		125.7	43.4[d]	76.6[b,e]		125.6	
^{144}Nd	1.7[a]	149.1[a]	2.5[a]	153.3	2.5[a]	223.1[a]	3.9[a]	229.5	80±9 /32/
		15.9[b]		20.1		24.2[b]		30.7	
		44.5[c]		48.6		73.0[c]		79.5	79[f]
	9.7[d]	15.9[b]		28.2	14.9[d]	24.2[b]		43.0	
^{106}Pd	6.8[a]	249.9[a]	3.0[a]	259.8	10.8[a]	416.7[a]	5.0[a]	432.5	145±8 /32/
		30.1[b]		40.0		53.8[b]		69.6	
		84.7[c]		94.6		156.2[c]		172.0	
	45.2[d]	30.1[b]		78.3	72.4[d]	53.8[b]		131.3	
^{94}Nb	11.8[a]	148.8[a]	3.5[a]	164.1	16.5[a]	220.9[a]	5.0[a]	242.5	145±10 /61/
		28.3[b,e]		43.7		42.2[b,e]		63.8	
		53.3[c,e]		68.6		80.5[c,e]		102.1	
	43.3[d]	28.3[b,e]		75.2	61.6[d]	42.2[b,e]		108.9	
^{61}Ni	234.0[a]	1087.9[a]	9.9[a]	1332.7	159.7[a]	953.0[a]	8.8[a]	1122.3	1700 /32/
		171.1[b]		415.9		156.9[b]		326.1	
		256.1[c]		500.8		240.5[c]		409.8	1050[f]
	1050.9[d]	171.1[b]		1232.7	814.9[d]	156.9[b]		981.4	
^{56}Mn	184.0[a]	612.3[a]	10.2[a]	807.1	178.0[a]	603.2[a]	10.5[a]	792.3	750±150 /32/
		86.2[b]		280.9		88.5[b]		277.6	
		139.8[c]		334.5		156.6[c]		345.7	510[f]
	449.8[d]	86.2[b]		546.7	454.1[d]	88.5[b]		553.7	

[a] Lorentzian Eq. (2)
[b] Lorentzian with energy dependent damping width Eq. (3)
[c] generalized Lorentzian Eq. (5)
[d] adjusted single particle model
[f] corrected for valence contribution /40/

TABLE 3 : Calculated and experimental total p-wave radiation widths in meV

	Level density : KRK Model				Level density : BSFG Model				
	$\langle\Gamma_{s1}\rangle_{M1}$	$\langle\Gamma_{s1}\rangle_{E1}$	$\langle\Gamma_{s1}\rangle_{E2}$	$\langle\Gamma_{s1}\rangle$	$\langle\Gamma_{s1}\rangle_{M1}$	$\langle\Gamma_{s1}\rangle_{E1}$	$\langle\Gamma_{s1}\rangle_{E2}$	$\langle\Gamma_{s1}\rangle$	$\langle\Gamma_{s1}\rangle_{EXP}$
^{198}Au	10.7[a]	305.2[a]	5.1[a]	321.1	11.1[a]	336.9[a]	5.9[a]	353.9	
		67.7[b,e]		83.6		63.8[b,e]		80.8	
		110.0[c,e]		125.9		119.5[c,e]		136.5	
	36.6[d]	67.7[b,e]		109.4	44.0[d]	63.8[b,e]		113.7	
^{144}Nd	1.9[a]	136.3[a]	2.7[a]	140.9	2.7[a]	211.2[a]	4.1[a]	218.1	
		13.6[b]		18.2		22.0[b]		28.9	
		41.6[c]		46.2		70.3[c]		77.2	
	9.9[d]	13.6[b]		26.2	15.0[d]	22.0[b]		41.1	
^{106}Pd	5.9[a]	260.1[a]	2.7[a]	268.8	9.9[a]	428.9[a]	4.7[a]	443.5	
		34.2[b]		42.8		58.2[b]		72.8	
		88.3[c]		97.0		160.3[c]		174.9	
	43.8[d]	34.2[b]		80.8	71.3[d]	58.2[b]		134.2	
^{94}Nb	10.0[a]	162.8[a]	3.2[a]	176.0	14.7[a]	233.8[a]	4.7[a]	253.2	190 /32/
		35.1[b,e]		48.3		48.6[b,e]		68.0	
		60.0[c,e]		73.3		86.8[c,e]		106.3	185[f]
	41.9[d]	35.1[b,e]		80.2	60.1[d]	48.6[b,e]		113.4	
^{61}Ni	712.8[a]	434.3[a]	23.4[a]	1170.8	636.7[a]	326.7[a]	22.1[a]	985.7	900 /32/
		53.3[b]		789.8		42.1[b]		701.1	
		126.6[c]		863.0		115.8[c]		774.8	
	1592.7[d]	53.3[b]		1669.7	1395.1[d]	42.1[b]		1459.4	
^{56}Mn	287.5[a]	398.2[a]	14.9[a]	701.0	278.9[a]	391.7[a]	15.1[a]	686.0	400±100 /32/
		50.2[b]		353.0		52.6[b]		347.0	
		101.7[c]		404.5		118.6[c]		412.9	
	539.7[d]	50.2[b]		605.2	543.7[d]	52.6[b]		611.7	

[a] Lorentzian Eq. (2)
[b] Lorentzian with energy dependent damping width Eq. (3)
[c] generalized Lorentzian Eq. (5)
[d] adjusted single particle model
[f] corrected for valence contribution /40/

The total p-wave radiation width of ^{61}Ni and ^{56}Mn is not affected by strong valence contributions. Calculations with the recommended strength function models reasonably well agree with the experimental data. Here the M1 contribution, mostly due to transitions to low lying levels, exceeds that for E1 radiation. Because of the large and rather uncertain M1 contributions the total p-wave radiation width seems not to be very sensitive to the choice of the E1 strength function model.

3.1 Capture cross-sections

We employed for the strength of M1 and E2 radiation a standard Lorentzian. As examples of capture cross-sections with dominating statistical contribution we show in Figs. 1 and 2 the results for ^{197}Au and ^{105}Pd (results with the KRK model on the left and with the BSFG model on the right hand side). The full curves represent the results with the E1 strength derived from the generalized Lorentzian (Eq.(5)); the dashed and dotted curves correspond to a standard Lorentzian (Eq.(2)) and to a Lorentzian with energy dependent spreading width (Eq.(3)), respectively.

The different models for $f_{E1}(\varepsilon_\gamma)$ mainly influence the magnitude but hardly the shape of the capture cross-section, which is reasonably well reproduced by all all calculations. As far as the magnitude is concerned one observes a similar dependence as for the total radiation widths. A standard Lorentzian for E1 radiation overpredicts the experimental capture cross-section. The best reproduction of the data is obtained with the E1 strength derived from a generalized Lorentzian (Eq.(5)). In case of ^{197}Au also a Lorentzian with energy depending spreading width (Eq.(3)) cannot be excluded; however, the analysis of the spectrum of gamma-rays favours the generalized Lorentzian.

The weak dependence of the shape of the capture cross-sections on the low energy behaviour of the gamma-ray strength functions provides the basis for the normalization procedures mentioned before. As a drastic illustration we show in Fig. 3a again the capture cross section of ^{105}Pd, calculated with the BSFG model for the level density; the curves have the same meaning as in Figs. 1 and 2. This time, however, we normalized the peak cross-section σ_0 in such a way that the experimental value of the average total s-wave radiation width of 145 meV is reproduced; the required normalization constants for Eqs. (2), (3) and (5) are 0.31, 2.40 and 0.83, respectively. Fig. 3b shows that the corresponding E1 strength functions, though leading to the same value $<\Gamma_{\gamma 0}>/<D_0>$, differ in shape and two of them are at variance with the photoabsorption data. The resulting capture cross-sections hardly differ from each other and moreover reproduce the experimental data. This example shows that normalizations to $<\Gamma_{\gamma 0}>/<D_0>$ can be useful if reliable experimental data are available. On the other hand, a good reproduction of experimental capture cross- sections does not guarantee that the underlying strength functions are correct in the sense that they reproduce independent experimental data.

Fig. 4 shows preliminary results for the neutron capture cross-section of ^{60}Ni and ^{55}Mn, calculated with the same prescriptions for the strength functions and the BSFG model for the level density. The curves have the same meaning as in Fig.1. For ^{55}Mn our preferred strength function models (full curves) underpredict the experimental data at the low energy end. This is to be expected as we did not consider valence capture contributions. The relatively good reproduction of the ^{60}Ni-data around 0.5 MeV is surprising and perhaps accidental.

3.3 Gamma-ray spectra

In the energy range considered here the total radiation widths and the capture cross-sections provide similar integral information on the gamma-ray strength. Further details can be learned from the analysis of gamma-ray spectra as their magnitude and shape depend on the strength functions.

Figs. 5 and 6 compare angle-integrated gamma-ray spectra resulting from the reactions ^{197}Au(n, γ) and ^{93}Nb(n, γ) to experimental data at incident neutron energies around 0.5 MeV. The

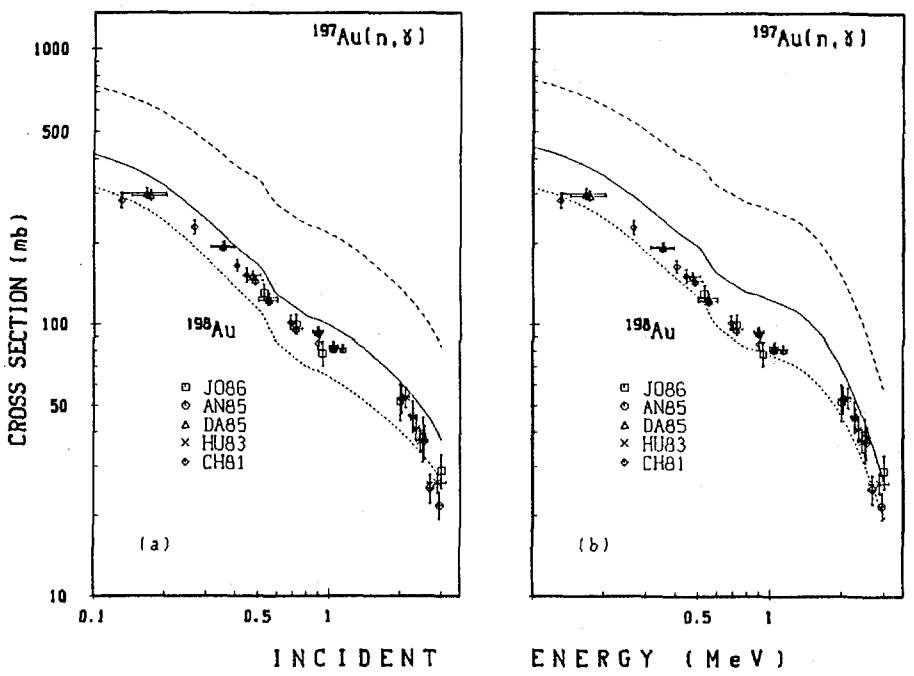

Figure 1. : The neutron capture cross-section of ^{197}Au calculated with the KRK model (a) and the BSFG model (b) for the level densities. The three curves represent calculations with different models for $f_{E1}(\varepsilon_\gamma)$ (see text). The experimental data were measured by Joly /10/ (symbol JO86), Andersson et al. /42/ (symbol AN85), Dalvetshin et al. /43/ (symbol DA85), Husain and Hunt /44/ and Chen Jing et al. /45/ (symbol CH81).

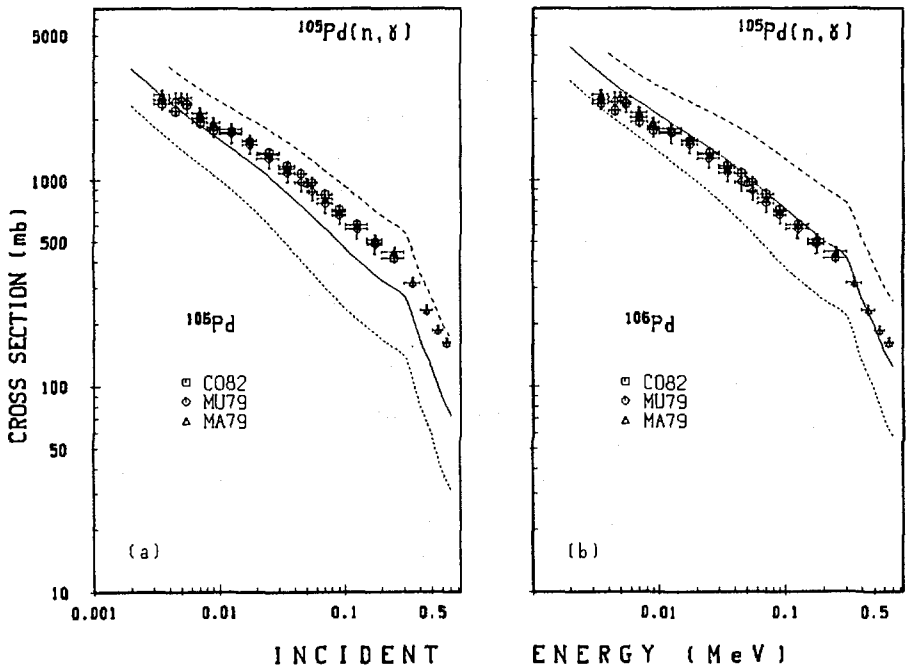

Figure 2. : The same as Fig.1, but for the neutron capture cross-section of ^{105}Pd . The experimental data were measured by Cornelis et al. /46/ (symbol CO82), Musgrove et al. /47/ (symbol MU79) and Macklin et al. /48/ (symbol Ma79).

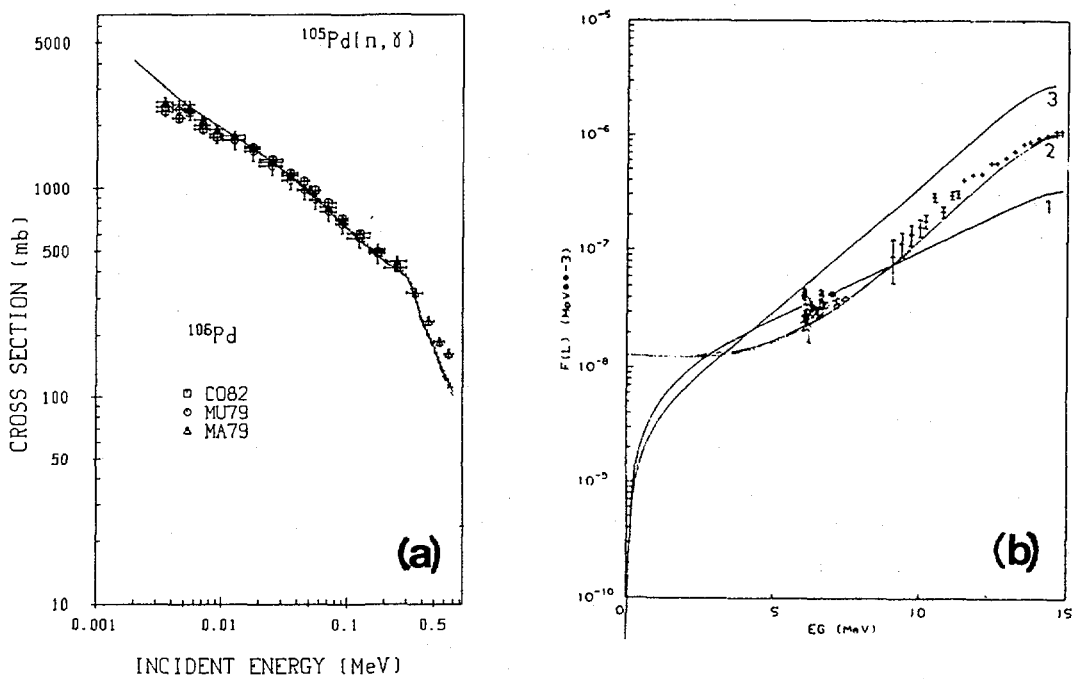

Figure 3. : (a) The neutron capture cross-section of ^{105}Pd calculated with the three models for the E1 strength, each normalized in such a way that an average total s-wave radiation width of 145 meV results (see text); the BSFG model was used for the level density.

(b) The underlying (normalized) E1 strength functions corresponding to a standard Lorentzian (curve 1), a generalized Lorentzian (curve 2) and a Lorentzian with energy dependent spreading width (curve 3) as well as experimental data derived from ARC and photoabsorption experiments.

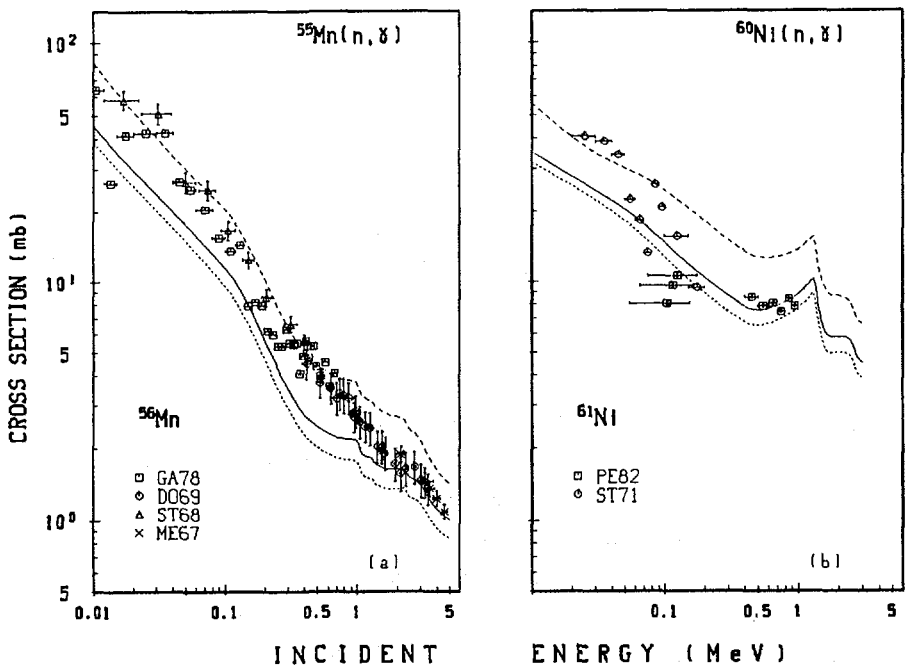

Figure 4. : The neutron capture cross-section for ^{55}Mn (a) and ^{60}Ni (b). The calculations employ the BSFG model for the level densities. The experimental data were taken from papers by Garg et al. /49/ (symbol GA78), Dovbenko et al. /50/ (symbol DO69), Stupegia et al. /51/ (symbol ST68), Menlove et al. /52/ (symbol ME67, Perey et al. /53/ (symbol PE82) and Stieglitz et al. /54/ (symbol ST71).

calculations were carried out for both level density models and the three models for the E1 strength function, represented by Eqs.(5) (full histgram), Eq.(3) (dashed histogram) and Eq.(2) (dotted histogram). The strength of M1 radiation was derived from a standard Lorentzian. Both figures clearly illustrate that for emission energies between 1 and 4 MeV also the shape of the spectra depends on the model for $f_{E1}(\varepsilon_\gamma)$. Of particular interest for ^{197}Au is the difference between the full and the dotted histogram which represent strengh function models, both compatible with ARC and photoabsorption data and with capture cross-sections. The experimental gamma-ray spectrum clearly favours the generalized Lorentzian or more generally the non-zero $\varepsilon_\gamma \rightarrow 0$ limit which is responsible for the different slopes in this energy region. The same also holds for ^{93}Nb (Fig.6). Of course, one could also here suspect that a Lorentzian with energy dependent spreading width (Eq. 3) combined with the adjusted single particle model for M1 radiation could produce similar spectra. This is indeed the case. However, we again refer to the aforementioned arguments against an energy independent M1 strength.

The generalized Lorentzian (Eq.(5)) and the formula by Kadmenskij et al. (Eq.(6)) exhibit the same $\varepsilon_\gamma \rightarrow 0$ limit. For gamma-rays starting from the neutron binding energy both expressions reasonably well agree but they give rather different results for transitions starting from much lower excitation energy. Therefore it is of interest to compare the gamma-ray spectra resulting from both expressions. Fig. 7 shows that for the gamma-ray spectra of ^{197}Au + n the difference between the two models is not very serious. As the same holds also for the average total radiation width and the capture cross-sections our conclusions apply to the formula of Kadmenskij et al. (Eq.(6)) and the generalized Lorentzian (Eq.(5)).

As an example for the structural materials Fig. 8 displays the gamma-ray spectrum resulting from ^{56}Fe + n at E_n = 0.925 MeV. The preliminary calculations employed the BSFG model for the level densities and the same strength function models as in Fig. 5. The level density of ^{57}Fe increases much slower with energy than that of ^{198}Au. Consequently the difference between the spectra resulting from the three models for the E1 strength function is smaller than in Figs. 5 and 6. Actually, in this example the rather large experimental errors prevent a decision between the different strength function models.

4. Conclusion

By comparing model calculations to appropriate experiments we found strong support for a representation /14/, /15/ of the E1 strength function in terms of a generalized Lorentzian with an energy dependent spreading width and a non-zero limit as the energy tends to zero. Such features are founded in theoretical work by Kadmenskij et al. /12/ and by Sirotkin /13/. Of particular interest is the non-zero $\varepsilon_\gamma \rightarrow 0$ limit; it depends on the excitation energy and thus implies a partial breakdown of Brink's / 3/ hypothesis.

The strength function models recommended in this paper i. e. a generalized Lorentzian for E1 and a standard Lorentzian for M1 and E2, all of them with parameters based on experimental data, are hopefully also relevant for applications. In view of the fact, that we did not adjust level density parameters and applied no normalization to the strength functions, the agreement between calculations and experiment is quite reasonable. As the low energy behaviour of the E1 strength which critically enters into the calculated quantities is supported by theory we expect an acceptable predictive power of calculations based on the recommended strength functions.

The last optimistic statements mainly apply to targets in mass regions where the statistical contribution dominates. Our preliminary results indicate problems for targets in the 3s region. It is harder to establish the recommended strength function models and moreover, the statistical model contributions should be supplemented by calculations of the valence components as described e.g. in Refs. /40/, /58/, /59/ and /60/.

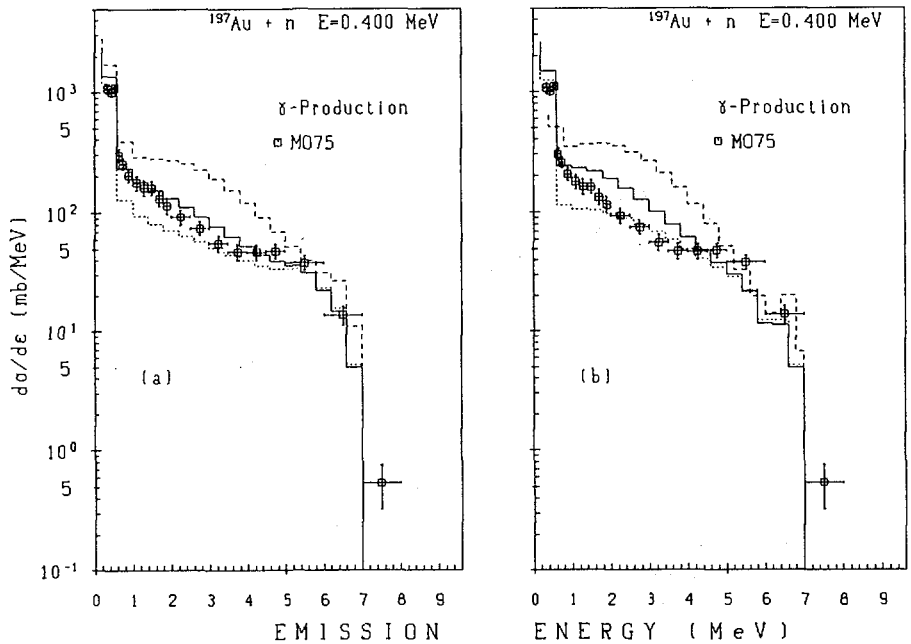

Figure 5. : The gamma-ray spectrum resulting from the reaction $^{197}Au(n, x\gamma)$ at an incident energy of 0.4 MeV. The calculations were performed with level densities according to the KRK model (a) and the BSFG model (b). The three histograms correspond to calculations with different E1 strength function models (see text). The experimental data by Morgan et Newman /55/ are given for the incident energy interval 0.2-0.6 MeV and correspond to an emission angle of 125^0. For the comparison with the calculations we assumed isotropic emission.

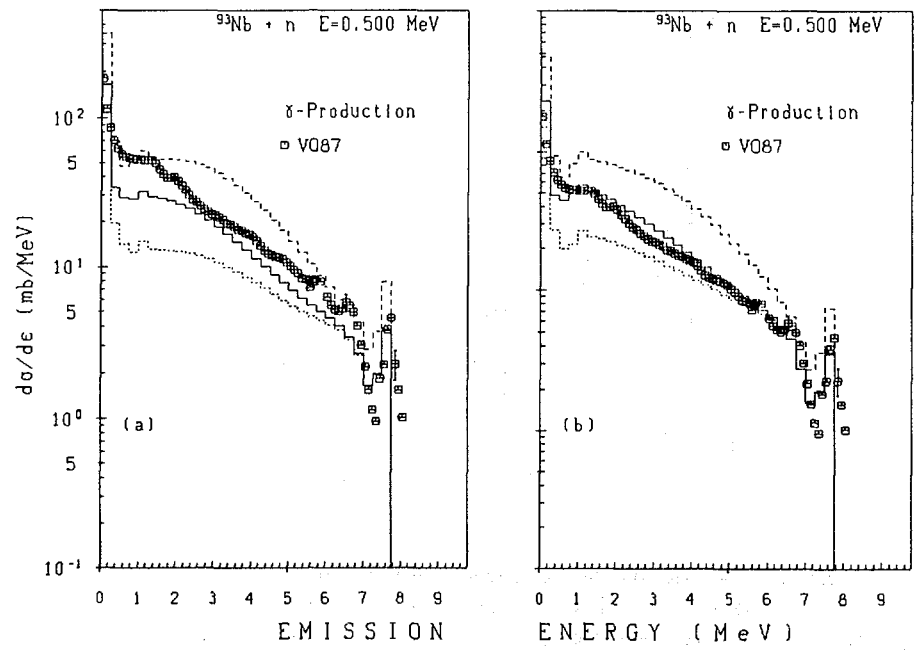

Figure 6. : The gamma-ray spectrum resulting from the reaction $^{93}Nb(n, x\gamma)$ at an incident energy of 0.5 MeV. Parts (a) and (b) and the different histograms have the same meaning as in Fig.5. The experimental data were taken from Voignier et al. /56/; below an emission energy of 1.5 MeV the authors extrapolated the measurements by means of model calculations. For the comparison with the calculations isotropic emission was assumed.

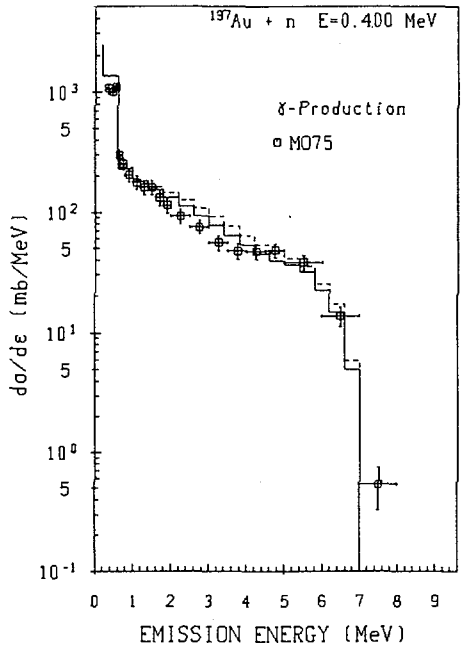

Figure 7. : The gamma-ray spectrum from $^{197}Au(n,x\gamma)$ calculated with the KRK model for the level density. The full and the dashed histogram correspond to the generalized Lorentzian (Eq.(5)) and the formula given by Kadmenskij et al. (Eq. 6)), respectively.

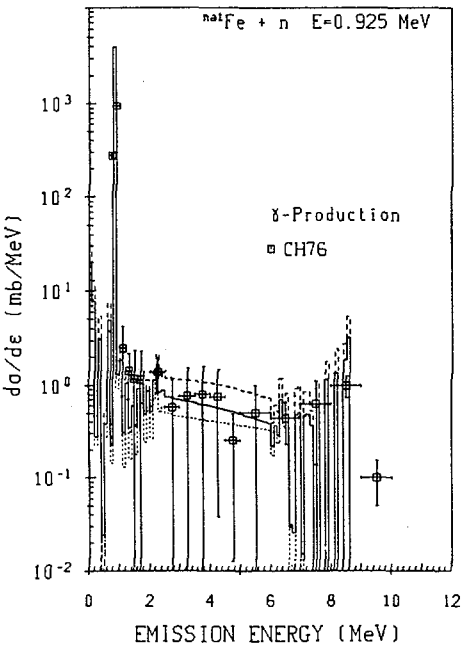

Figure 8. : The gamma-ray spectrum resulting from the reaction $^{56}Fe(n,x\gamma)$. The BSFG model was used for the level density. The meaning of the histograms is the same as in Fig. 6. The experimental data were measured for natural iron by Chapman et al. /57/. We used the spectra recorded at 125^0 and assumed isotropic emission.

Acknowledgment

All calculations were performed on a IBM 3090-400E VF computer installed at the University of Vienna in the frame of the European Academic Supercomputing Initiative (EASI) of IBM Corporation. We acknowledge the help by the staff of the Vienna University Computer Center.

References

/ 1/ J. Kopecky and M. Uhl, this meeting.
/ 2/ M. Blatt and V. F. Weisskopf, Theoretical Nuclear Physics (Wiley, New York, 1952).
/ 3/ D. M. Brink, Oxford Univ., thesis (1955).
/ 4/ P. Axel, Phys. Rev. 126, 671(1962).
/ 5/ S. Joly, D. M. Drake, and L. Nilsson, Phys. Rev. C20, 2072(1979).
/ 6/ D. G. Gardner and F. S. Dietrich, Proc. Int. Conf. on Nucl. Cross Sections for Technology, Knoxville, Tennessee, 22-26 Oct. 1979, publ. as NBS Spec. Publ. 594 (1980), p. 770.
/ 7/ B. J. Allen, I. Bergqvist, R. E. Chrien, D. Gardner, and W. Poenitz, Neutron Radiative Capture, Pergamon Press 1982, p. 62.
/ 8/ G. Reffo, F. Fabbri, K. Wisshak ,and F. Käppler, Nucl. Sci. Eng., 80, 630(1982).
/ 9/ M. Igashira et al., Nucl. Phys. A457, 301(1986).
/10/ S. Joly, Nucl. Sci. Eng., 94, 94(1986).
/11/ R. L. Macklin, and P. G. Young, Nucl. Sci. Eng. 95, 189(1987).
/12/ S. G. Kadmenskij, V. P. Markushev, and V. I. Furmann, Sov. J. Nucl. Phys. 37,165(1983).
/13/ V. K. Sirotkin, Sov. J. Nucl. Phys. 43, 362(1986).
/14/ R. E. Chrien, Proc. V. International School on Neutron Physics, Alushta (USSR), Oct.20-31,1986, p.29.
/15/ J. Kopecky and R. E. Chrien, Nucl. Phys. A468, 285(1987).
/16/ L. Aldea et al. Z. Phys. A283, 391(1977).
/17/ G. A. Leander, Phys. Rev. C38, 728(1988).
/18/ D. Gardner, NEANDC(US)-214/L (1983) p. 63
/19/ M. A. Gardner, Proc. Int. Conf. Nucl. Data for Basic and Applied Science, Santa Fe, N.M., U.S.A., May 13-17 1985, edited by P.G. Young et al. (Gordon and Breach, New York 1986), p. 1481.
/20/ M. Uhl, unpublished
/21/ P. A. Moldauer, Nucl. Phys. A344, 185(1980).
/22/ B. Strohmaier, and M. Uhl, "STAPRE-A Statistical Model Code with Consideration of Preequilibrium Decay", Proc. Course Nuclear Theory for Applications, Trieste, Italy, January 17 - February 10, 1978, IAEA-SMR-43, International Atomic Energy Agency(1980), p.313.
/23/ C. B. Dover, R. H. Lemmer, and F. J. W. Hahne, Ann. of Phys. 70, 458(1972).
/24/ S. S. Dietrich and B. L. Berman, At. Nucl. Data Tables 38, 199(1989).
/25/ D. Wilmore, and P. E. Hodgson, Nucl. Phys. 55, 673(1964).
/26/ H. A. J. Van der Kamp and H. Gruppelaar, "Evaluation of Neutron Cross Sections for the Pd Isotopes (RCN-3 Data Library)", ECN-108, Netherlands Energy Research Foundation ECN(1981).
/27/ J. P. Delaroche, Ch. Lagrange, and J. Salvy, Proc. IAEA Consultants' Meeting on the Use of Nuclear Theory in Neutron Nuclear Data Evaluation, Trieste, Dec. 8-11 1975, IAEA-190, International Atomic Energy, Vienna 1976, Vol.I, p. 251.
/28/ J. Rapaport, V. Kulkani, and R. W. Finlay, Nucl. Phys A330, 15(1979).
/29/ G. S. Mani, M. A. Melkanoff, and I. Iori, Report CEA-2379, 1963 (unpublished).
/30/ L. McFadden and G. R. Satchler, Nucl. Phys. 84, 177(1966).
/31/ Nuclear Data Sheets, (Academic Press, New York).

/32/ S. F. Mughabgab, M. Divadeenam, and N. E. Holden, Neutron Cross Sections, (Academic Press, New York 1981), Vol.1, Part A.
/33/ S. F. Mughabgab, Neutron Cross Sections, (Academic Press, New York 1984), Vol.1, Part B.
/34/ P. Vertes and Y. V. Grigoryew, Proc. Int. Conf. on Nuclear Data for Science and Technology, Mito, Japan, May 30-June 3, 1988, publ. by Saikon Publishing Co., LTD., p. 623.
/35/ H. Vonach, M. Uhl, B. Strohmaier, B. W. Smith, E. G. Bilpuch, and G. E. Mitchel, Phys. Rev. C38, 2451(1988).
/36/ W. Dilg, W. Schantl, H. Vonach, and M. Uhl, Nucl. Phys. A217, 269(1973).
/37/ S. K. Kataria, V. S. Rhamaurthy, and S. S. Kapoor, Phys. Rev. C18, 549(1978).
/38/ A. Gilbert and A. G. W. Cameron, Can. J. Phys. 43, 1446(1965).
/39/ J. Kopecky and M. Uhl, accepted for publication in Phys. Rev.C
/40/ B. J. Allen and A. R. Musgrove, Adv. Nucl. Phys., Vol. 10 (Plenum, New York, 1978) p. 129.
/41/ G. Delfini and H. Gruppelaar, "Maximum-Likelyhood Analysis of Resolved Resonance Parameters for 18 Fission-Product Nuclei", ECN-82, Netherlands Energy Research Foundation ECN (1980).
/42/ P. Andersson et al., Nucl. Phys. A443, 404(1985).
/43/ A. N. Davletshin et al., Atomnaja Energia 58, 731(1983).
/44/ H. A. Husain and S. E. Hunt, Int. J. Appl. Radiat. And Isotop., 34 , 731(1983).
/45/ Chen Jing, Zhu Sheng-Yun, Luo De-Xing, and Jiang Song-Chen, Chinese J. of Nucl. Phys. 3, 52(1981).
/46/ E. Cornelis et al., Proc. Int. Conf. on Nuclear Data for Science and Technology, Antwerp, 6-10 September 1982, publ. by Dr. Reidel Publ. Company, p. 222.
/47/ A. R. del Musgrove, B. J. Allen, J. W. Boldemann, and R. L. Macklin, Proc. Int. Conf. on Neutr. Phys. and Nucl. Data for Reactors and Other Applied Purposes, AERE Harwell, U. K., 25-29 Sept. 1978, publ. by OECD/NEA, p. 449.
/48/ R. L. Macklin, J. Halperin, and R. R. Winters, Nucl. Sci. Eng. 71, 182(1979) and Nucl. Sci. Eng. 78, 110(1981).
/49/ J. B. Garg, R. L. Macklin, and J. Halpern, Phys. Rev. C18, 2079(1978).
/50/ A. G. Dovbenko, V. E. Kolesov, V. P. Koroleva, and V. A. Tolstikov, Atomnaja Energia 26, 67(1969).
/51/ D. C. Stupegia, Marcia Schmidt, C. R. Keedy, and A. A. Madson, J. Nucl. Energy 22, 267(1968).
/52/ M. O. Menlove, K. L. Coop, H. A. Grench, and R. Sher, Phys. Rev. 163, 1299(1967).
/53/ C. M. Perey, J. A. Harvey, R. L. Macklin, R. R. Winters, and F. G. Perey "Neutron Transmission and Capture Measurements and Analysis of ^{60}Ni from 1 to 450 KeV", ORNL-5893, 8211, Oak Ridge National Laboratory (1982).
/54/ R. G. Stieglitz, R. W. Hockenbury, and R. C. Block, Nucl. Phys. A163, 592(1971).
/55/ G. L. Morgan and E. Newman, "The Au(n,xγ) Reaction Cross Section for Incident Neutron Energies between 0.2 and 20.0 MeV", ORNL-TM-4973, Oak Ridge National Laboratory (1975).
/56/ J. Voignier, S. Joly, and G. Grenier, Nucl. Sci. Eng. 93 , 43(1986) and 97, 343(1987).
/57/ G.T. Chapman, G.L. Morgan, and F.G. Perey, " A re-measurement of the neutron-induced gamma-ray production cross-sections for iron in the energy range 850 keV $\leq E_n \leq$20.0 MeV", ORNL/TM-5416, Oak Ridge National Laboratory (1976).
/58/ A. M. Lane and S. F. Mughabghab, Phys. Rev. C19, 412(1974).
/59/ Y. K. Ho and M. A. Lone, Nucl. Phys. A406, 1(1983).
/60/ Yu-Kun Ho, Jing-Feng Liu, and Zhu-Shu Yuan, Phys. Rev. C40, 2541(1989).
/61/ J. Winter et al., Proc. Int. Conf. on Neutr. Phys. and Nucl. Data for Reactors and Other Applied Purposes, AERE Harwell, U. K., 25-29 Sept. 1978, publ. by OECD/NEA, p. 696.

TWO-STEP CASCADE TRANSITIONS FOLLOWING NEUTRON CAPTURE: A NEW SOURCE OF INFORMATION ON PHOTON STRENGTH FUNCTIONS

F. Bečvář

Charles University, Faculty of Mathematics and Physics
180 00 Prague 8, Czechoslovakia

R. E. Chrien

Brookhaven National Laboratory
Upton, New York 11973, USA

J. Kopecký

Netherlands Energy Research Foundation ECN
1755 ZG Petten, The Netherlands

ABSTRACT: The applicability of the sum-coincidence measurements of two-step cascade γ-ray spectra to determination of photon strength functions at intermediate γ-ray energies (3 ÷ 4 MeV) is discussed. An experiment based on thermal neutron capture in Nd was undertaken at the BNL High Flux Beam Reactor to test this method. To understand the role of various uncertainties in similar experiments a series of model calculations was performed. We present an analysis of our experimental data which demonstrates the high sensitivity of the method to E1 and M1 photon strength functions.

1. INTRODUCTION

In past three decades large amount of information has been accumulated about the strength of radiative transitions proceeding from highly excited nuclear states, especially those states populated in slow neutron capture. This information concerns mainly the hard primary γ-rays that correspond to the transitions from the capturing states to the low-lying levels. On the other hand, very little has been learned on soft primary and secondary γ-rays with energies E_γ < 4 MeV, although such information seems crucial for better understanding of the photoproduction mechanism.

The radiative strength is usually treated in terms of the conventionally defined photon strength functions $S_\gamma(E_\gamma)$ for various multipolarities of γ-radiation.

The richest information is available for the E1 photon strength function. Axel [1] used the principle of detailed balance and made the first attempt to understand this strength function quantitatively in terms of the electric Giant Dipole Resonance (GDR). Brink [2] assumed that the same GDR is built on the ground state and on each excited state. Nevertheless, in typical cases the calculations made according to the Axel-Brink model [1,2] produce values of $S_\gamma^{E1}(E_\gamma)$ about a factor of 3 too large as compared to the experimantal values.

Later, Kadmenskij, Markushev and Furman [3] pointed out that for the cases of spherical and transitional nuclei the limit for $S_\gamma^{E1}(E_\gamma)$ as $E_\gamma \to 0$ should be *non-zero*. Using the Fermi liquid model these authors also predicted a specific dependence of width Γ_G of the electric GDR on the γ-ray energy, as well as a dependence of the shape of the GDR on the nuclear temperature of the final level on which the GDR in built. These consequencies are in contradiction with the Brink's hypothesis and with a widespread assumption about purely Lorentzian shape of the electric GDR.

As shown in a separate contribution to this Meeting by Uhl and Kopecký [4], a detailed analysis of the experimental data on slow and fast neutron capture in ^{94}Nb, ^{106}Pd, ^{144}Nd and ^{198}Au supports all the above-outlined predictions of Kadmenskij et al. [3]. In particular, by combining the data from photonuclear and neutron capture reactions a strong support has been found for the electric GDR with an energy-dependent damping width Γ_G. On the other hand, conclusions made in Ref. [4], concerning the existence of the non-zero limit of $S_\gamma^{E1}(E_\gamma)$, need an verification that would lean on more direct information on radiative strength at low energies.

In this contribution we describe an experimental method that makes such information available. We present preliminary results based on an experimental study of the $^{143}Nd(n,\gamma)^{144}Nd$ reaction and compare them with analogous results, following from model calculations. In discussion the main emphasis is put on sensitivity of the proposed method to various models

used for photon strength functions, rather than on final conclusions concerning the energy dependence of S_γ^{E1} in the reaction studied.

2. THE METHOD

The method is based on a two-detector coincident measurement of two-step cascades that follow the thermal neutron capture and end at a final level of a known spin and parity. By fixing an energy sum a final level can be selected and an energy spectrum of all the transitions involved in two-step cascade de-excitation can be obtained. This spectrum, called hereafter *a two-step cascade γ-ray spectrum*, consists of two components: a discrete set of lines and a broad, bell-shaped quasi-continuum. The discrete lines contain spectroscopic information and involve transitions between well-separated, low-energy nuclear excitations. The quasi-continuum involves primary and secondary transitions spanning the excitation region which extends from several hundreds of keV almost up to the adjusted energy sum. The size of the quasi-continuum carries information about the photon strength functions that govern the emission of γ-rays in a de-excitation process. As the maximum of the quasi-continuum is expected to be approximately at 3 or 4 MeV, behavior of the photon strength functions at these energies can be studied. A set of the two-step cascade spectra can be obtained, one for each final level.

3. THE EXPERIMENT

We have undertaken the above-described measurement for the thermal $^{143}Nd(n,\gamma)^{144}Nd$ reaction. A sample of natural Nd was irradiated in a beam of thermal neutrons at the Brookhaven High Flux Beam Reactor. Two back-to-back HPGe detectors were used, having a measured overall photopeak efficiency of 3.3 % at an energy of 696 keV, including the effect of solid angle. A total number of 2×10^8 coincident pairs of γ-rays were detected. Each event, represented by energies of the γ-rays and the associated detection time difference, was recorded on

a magnetic tape. This information was later scanned off-line to yield the needed γ-ray spectra.

Fig. 1 represents a spectrum of γ-ray energy sums. The labeled lines belong to the energy sums for two-step cascades, terminating at the first five final levels of ^{144}Nd. Energies, spins and parities of these levels are shown.

In order to isolate a two-step cascade γ-ray spectrum the continuous background visible in Fig. 1 has to be carefully eliminated. As the detector energy response function is very far from being confined to a single peak, these corrections are very large. Analogous corrections have to be done in case of a random background in the time spectra. The procedure we used for these corrections guarantees that the quasi-continuum component in the resulting spectra represents a real effect, free from background.

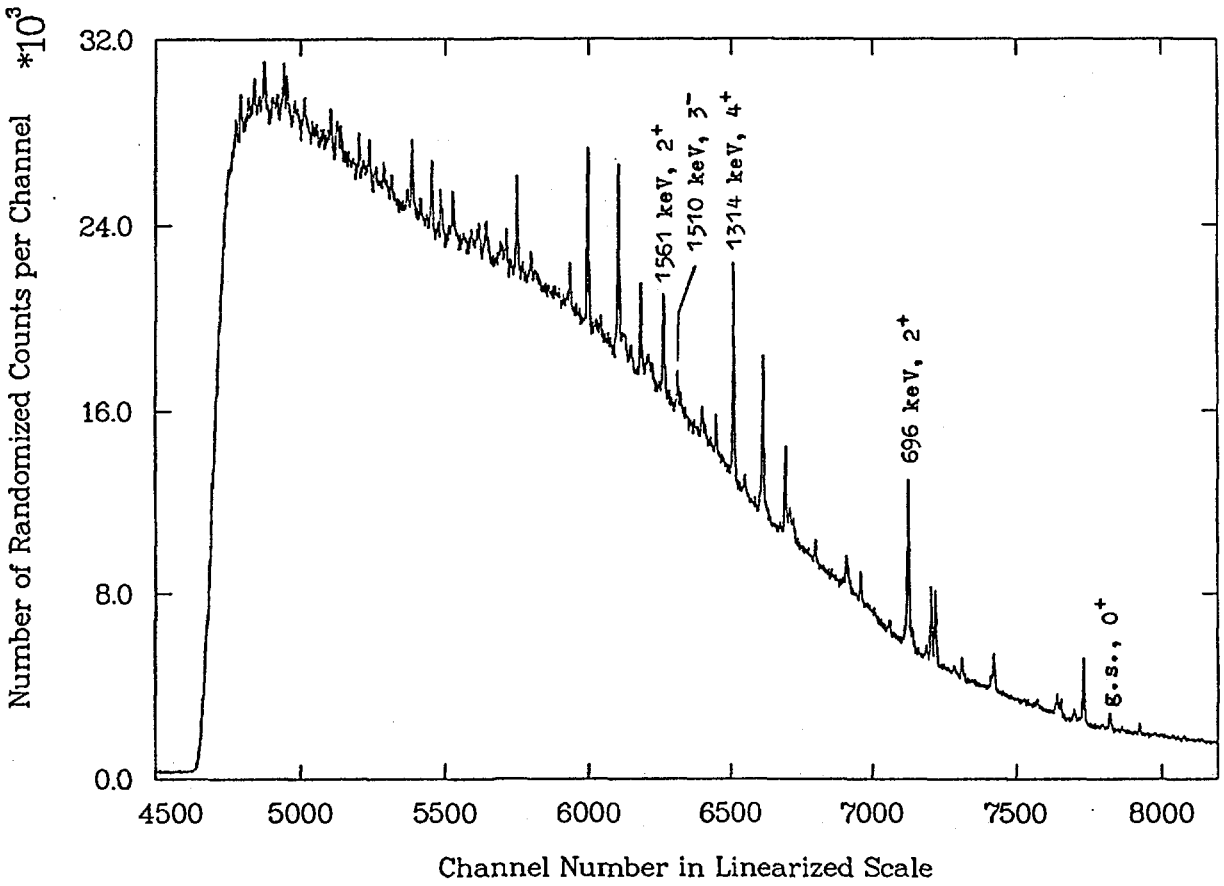

Fig. 1. A spectrum of γ-ray energy sums for the ^{143}Nd(n,γ)^{143} reaction.

An example of a two-step cascade γ-ray spectrum is given in Fig. 2. It corresponds to all cascades, terminating at the first $J^{\pi} = 2^{+}$ level in ^{144}Nd at 696 keV. The spectrum shown is corrected for energy variation of the detector efficiency. As a result, the spectrum is reasonably symmetric. The symmetric appeareance of this kind of spectra follows from impossibility to distinguish between the primary and the secondary γ-rays. A large number of discrete lines can be seen in Fig. 2. For some of them, energies of the corresponging intermediate levels in ^{144}Nd are given. Intensity fluctuations of these lines are very broad: the strongest line in the spectrum, corresponding to the $J^{\pi} = 4^{+}$ intermediate state at 1314 keV, reaches a peak value of $\simeq$ 1900 efficiency-corrected counts, while a large number of still well separated lines are weaker by a factor of 10^{2}.

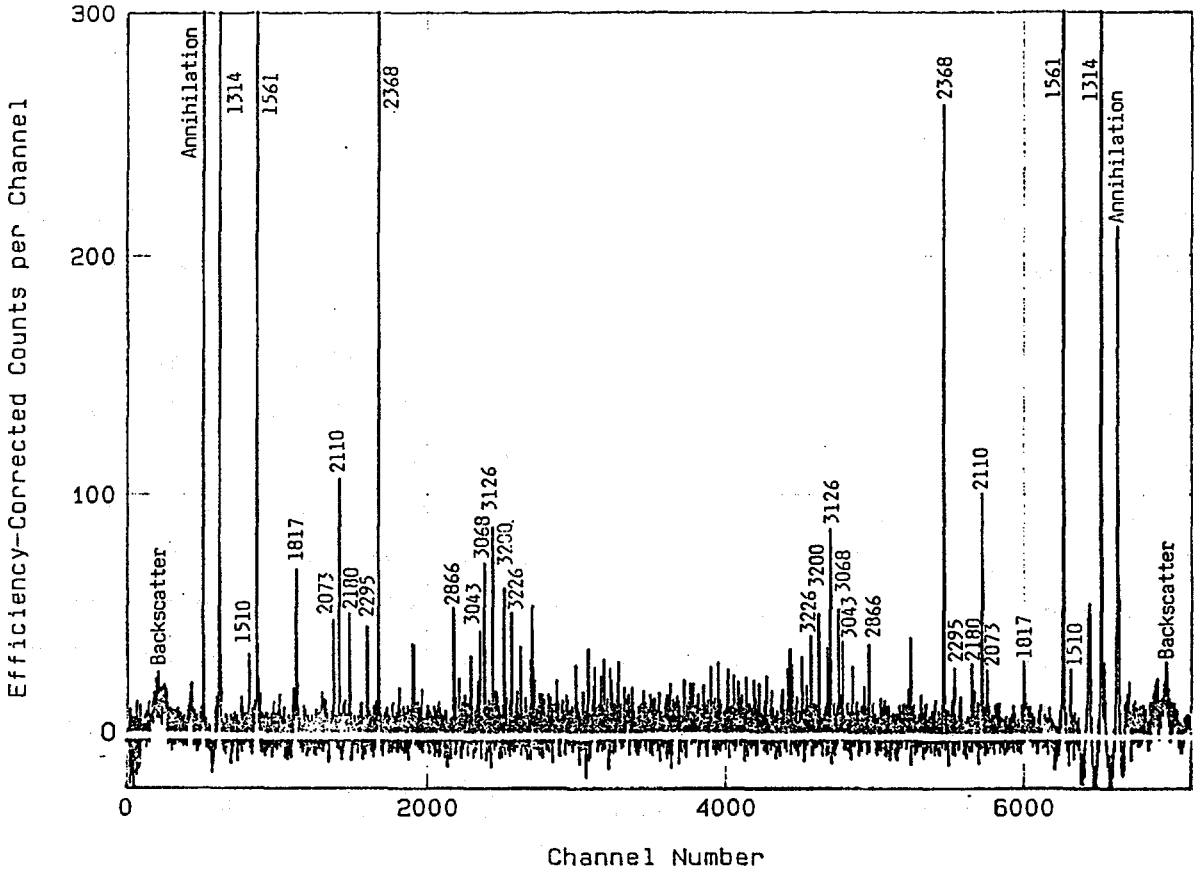

Fig. 2. The two-step cascade γ-ray spectrum for the $J^{\pi} = 2^{+}$ final level in ^{144}Nd at 696 keV. Only a small fraction of the range of efficiency-corrected number of counts is shown.

The most important constituent of the spectrum is the quasi-continuum that shows up as a smear in a vicinity of the base line. In order to minimize the uncertainty due to the noted fluctuations of strong discrete lines, integral over a restricted energy interval, situated in the middle of the spectrum, can be chosen as a measure of the size of the continuum component. We selected an energy interval of 3.2 MeV. In this case, the integral could be determined with a statistical accurracy of 2.4 %. The smear in the spectrum thus represents a positive, statistically significant effect.

In a similar manner, two-step cascade γ-ray spectra were obtained also for the $J^{\pi} = 0^{+}$ ground state and for the levels at 1314, 1510 and 1561 keV with J^{π} equal to 4^{+}, 3^{-} and 2^{+}, espectively. The quasi-continuum in these spectra could be determined with a statistical accurracy of 10, 6, 7 and 11 %, respectively.

4. MODELING

In order to test various hypotheses about photon strength functions we modeled the two-step cascade process and compared the resulting spectra with those observed experimentally.

For clarity, some basic expressions must be given. Let us assume a cascade $EJ\pi \rightarrow E'J'\pi' \rightarrow E''J''\pi''$. Here, $EJ\pi$ stands for an excitation energy, spin and parity of the initial state. Similarly, $E'J'\pi'$ and $E''J''\pi''$ belong to the intermediate level and the fixed final level, respectively. Following the definition of the photon strength function an expectation value of a partial radiation width for the first step $EJ\pi \rightarrow E'J'\pi'$ can be expressed as

$$\langle \Gamma_{\gamma}(EJ\pi \rightarrow E'J'\pi') \rangle = E_{\gamma 1}^{2L+1} \, S_{\gamma}^{XL}(E_{\gamma 1}) \; / \; \varrho(E,J), \qquad (1)$$

where XL stands for multipolarity of the transition $EJ\pi \rightarrow E'J'\pi'$, i.e. XL = E1, M1, E2, etc., $E_{\gamma 1}$ is a γ-ray energy of this transition and $\varrho(E,J)$ - density of levels with spin J at an excitation energy E.

An expectation value of the total radiation width for the state EJπ is

$$\langle \Gamma_{\gamma EJ\pi} \rangle = \sum_{J'\pi'} \int_{E_0}^{E} \varrho(E',J') \langle \Gamma_\gamma (EJ\pi \to E'J'\pi') \rangle \, dE' + \sum_k \langle \Gamma_\gamma (EJ\pi \to E_k J_k \pi_k) \rangle . \quad (2)$$

The first term of this expression includes levels with $E' > E_0$ that are described by level density ϱ. The second term belongs to transitions to the remaining levels, labelled by subscript k. It is assumed that below the energy E_0 a full set of levels is known from experiments. Analogous expressions can be written for $\langle \Gamma_\gamma (E'J'\pi' \to E''J''\pi'') \rangle$ and $\langle \Gamma_{\gamma E'J'\pi'} \rangle$.

An expectation value of a *two-step* cascade intensity can be expressed via expectation values of ordinary *one-step* intensities:

$$\langle I_{\gamma\gamma}(E_{\gamma 1}) \rangle = \sum_{J'\pi'} \langle I_\gamma (EJ\pi \to E'J'\pi') \rangle \langle I_\gamma (E'J'\pi' \to E''J''\pi'') \rangle \varrho(E',J') . \quad (3)$$

Here $E' = E - E_{\gamma 1}$ and

$$\langle I_\gamma (EJ\pi \to E'J'\pi') \rangle = \langle \Gamma_\gamma (EJ\pi \to E'J'\pi') \rangle / \langle \Gamma_{\gamma EJ\pi} \rangle . \quad (4)$$

A similar expression can be written for $\langle I_\gamma (E'J'\pi' \to E''J''\pi'') \rangle$. Eq. (3) is valid for primary γ-ray energies $E_{\gamma 1} < E - E_0$. The introduced quantity $\langle I_{\gamma\gamma}(E_{\gamma 1}) \rangle$ is *differential*, i.e. it represents an intensity per unit of energy.

An example of calculated two-step cascade γ-ray spectrum is given in Fig. 3. Besides the values of $\langle I_{\gamma\gamma}(E_{\gamma 1}) \rangle$, the values of individual terms of the right-hand side of Eq. (3) for various J'π' are also plotted. The spectrum in Fig. 3 has been calculated using the level density formula, based on the

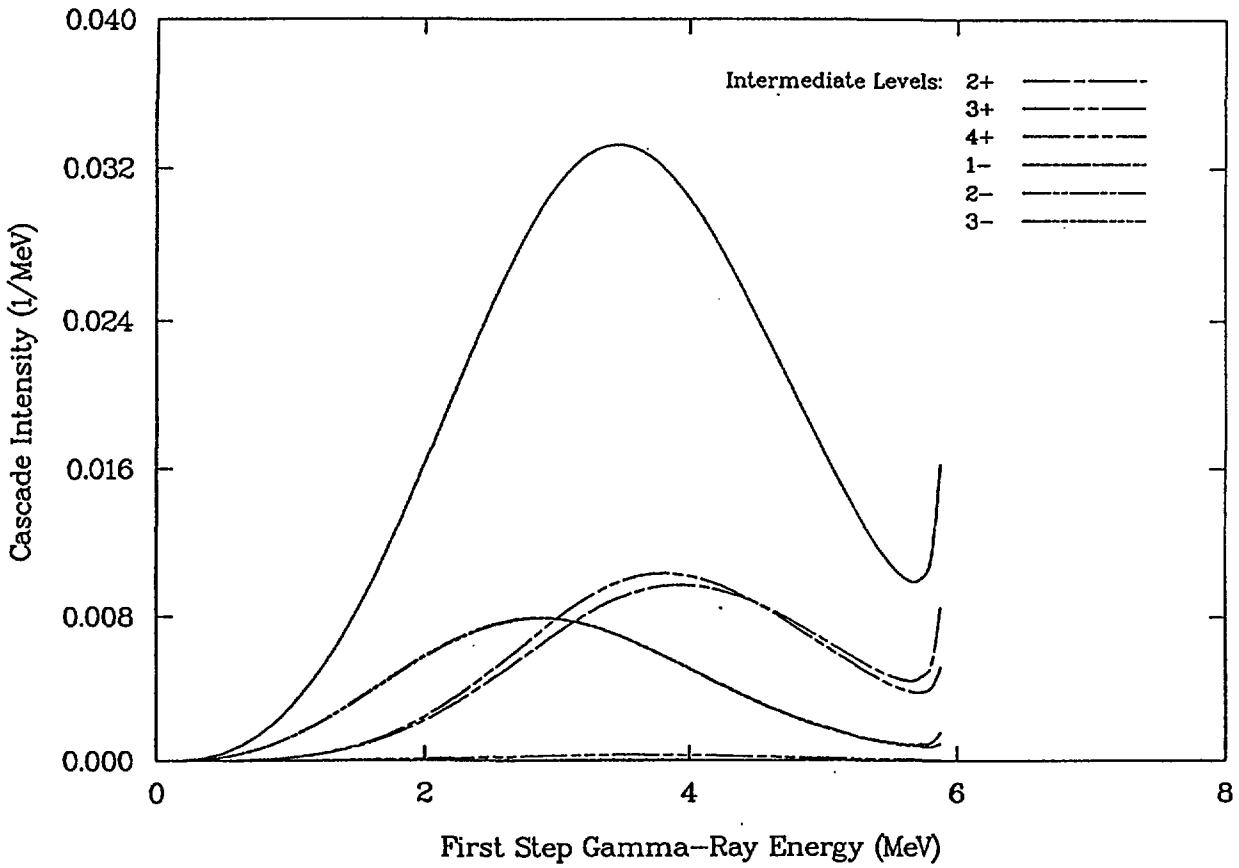

Fig. 3. Calculated expectation values of the two-step cascade intensity v.s. γ-ray energy for the $J^{\pi} = 2^{+}$ final level in Nd^{144} at 696 keV. The contributions belonging to individual values of J^{π} of intermediate levels are also shown.

standard Fermi gas model with the shell-model level-density parameter as the only free parameter. The photon strength function S_{γ}^{E1} used in calculations was deduced from the traditional Lorentzian GDR with a constant spreading width Γ_G. For S_{γ}^{M1} and S_{γ}^{E2} single-particle approximations were assumed. The role of M2, E3 and higher multipolarities was neglected.

In order to study the influence of Porter-Thomas fluctuations of partial radiation widths we modified Eq. (3) to yield fluctuating values of two-step cascade intensity. Specifically, in Eq. (3) we used summation instead of integration and included additional factors $\Theta^{(1)}_{E',J'\pi'}$ and $\Theta^{(2)}_{E',J'\pi'}$ that are responsible for fluctuations of one-step intensities. The fluctuating two-step cascade intensity can be expressed as

$$I_{\gamma\gamma}^{(fluct)}(E_{\gamma 1}) = \sum_{E'J'\pi'} \langle I_\gamma(EJ\pi \to E'J'\pi') \rangle \langle I_\gamma(E'J'\pi' \to E''J''\pi'') \rangle$$

$$\times \theta_{E'J'\pi'}^{(1)} \; \theta_{E'J'\pi'}^{(2)} \; \delta(E_{\gamma 1} - E + E'). \qquad (5)$$

Summation in Eq. (5) is assumed over a full set of all the intermediate levels, whose values of excitation energy E' are distributed in accordance with the adopted level-density formula.

Assuming Porter-Thomas fluctuation for partial radiation widths it can be shown that products of factors $\theta_{E'J'\pi'}^{(1)}$ and $\theta_{E'J'\pi'}^{(2)}$ behave as completely independent statistical variables, obeying a distribution, whose first moments can be easily calculated. This makes it possible to model the values of $I_{\gamma\gamma}^{(fluct)}$ by the method of Monte Carlo.

Fig. 4 shows an example of such a modeling for the case of two-step cascades, populating the $J^\pi = 2^+$ level at 696 keV. The level-density formula and explicit expressions for photon strength functions used were the same as those mentioned in connection with Fig. 3. The spectrum in Fig. 4 is presented as a histogram with a bin width of 3 keV so that it is roughly similar to what is viewed by a typical HPGe-detector. We note that this spectrum, as well as the previous one in Fig. 3, should be additionally symmetrized to resemble the corresponding experimental spectrum (Fig. 2.) in its overall shape.

The spectrum in Fig. 4 exhibits violent fluctuations. It seems therefore that it is difficult to separate the quasi-continuum component. Nevertheless, if one integrates the values of $I_\gamma^{(fluct)}$ over a carefully adjusted energy interval, fluctuations of the resulting integral can be kept reasonably low. Specifically, for the case of energy interval of 3.2 MeV the residual fluctuations are represented by a r.m.s. value of 8.3 %. It seems therefore that the said integral can be taken as a reasonable measure of the quasi-continuum. Calculations

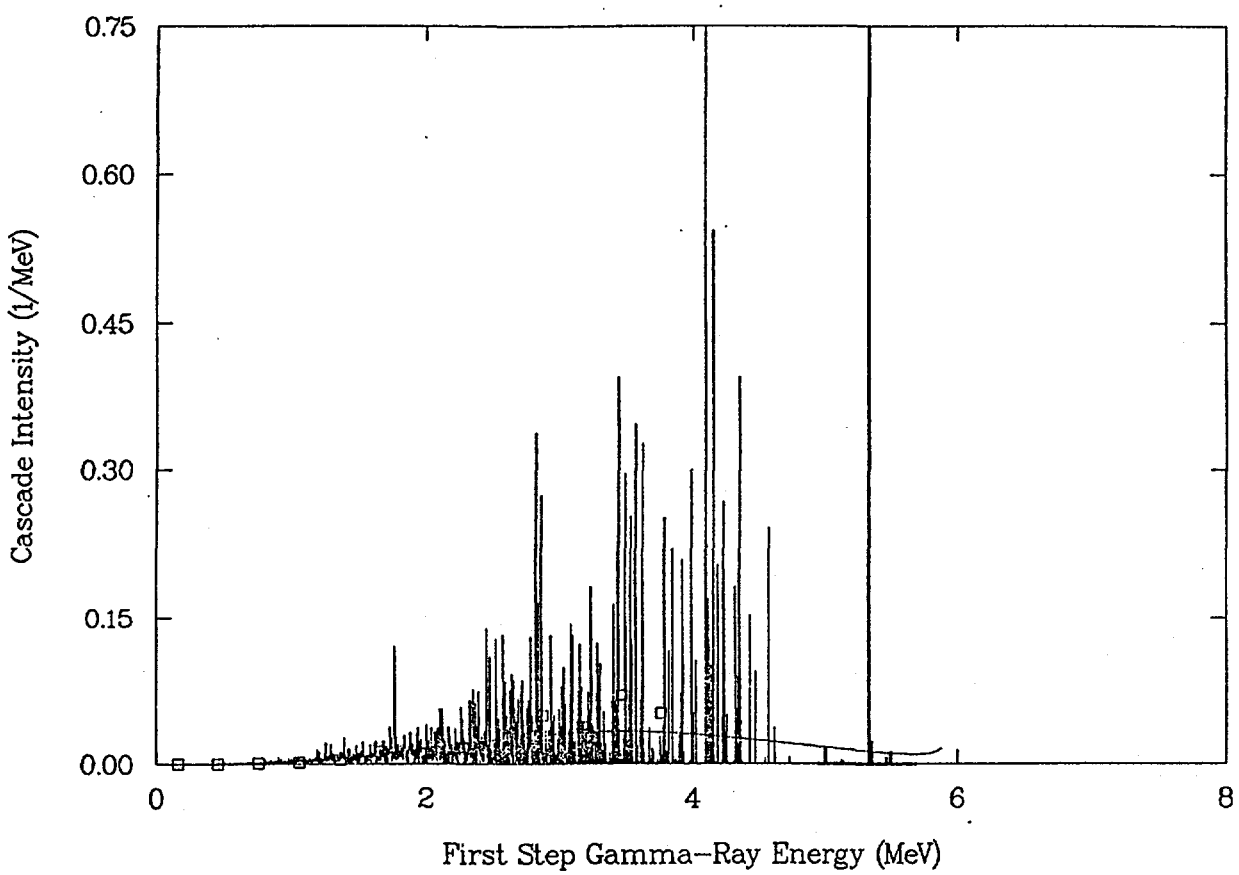

Fig. 4. Values of $I_{\gamma\gamma}^{(fluct)}$ v.s. γ-ray energy for the $J^{\pi} = 2^{+}$ level in ^{144}Nd at 696 keV.

performed for the cascades, populating the 1314, 1510 and 1561 keV levels, yielded the the r.m.s. values for residual fluctuations of 8.4, 8.0 and 9.7 %, respectively.

The quoted experimental uncertainties in determination of quasi-continuum are comparable to, or even lower than those, following from the Porter-Thomas fluctuations, see Sec. 3.

5. DISCUSSION AND SUMMARY

Quantities $\langle I_{\gamma\gamma} \rangle$ and $I_{\gamma\gamma}^{(fluct)}$ were calculated for ^{144}Nd levels at 696, 1314, 1510 and 1561 keV with J^{π} values of 2^{+}, 4^{+}, 3^{-} and 2^{+}, respectively. In these calculations various explicit expressions for photon strength functions were used.

The results deduced from these calculations are illustrated in Figs. 5-7, where the integrated two-step

cascade intensities $\langle I_{\gamma\gamma}(E_\gamma)\rangle$ are plotted for individual final levels (broken lines) and compared with analogous quantities, deduced from the measured spectra (open circles). In view of the fact that experimental conditions did not allow us to determine *absolute* intensities, the values of experimental integrated intensities were additionally normalized to yield the "best fit" to the modeled values.

In our calculations we used the following three approximations for the electric dipole photon strength function:

(*i*) The expression, based on a traditional electric GDR of Lorentzian shape with an energy-independent damping width Γ_G.

(*ii*) The expression (*i*) modified by inclusion of an energy- and temperature-dependent damping width, specifically

$$\Gamma_G = \Gamma_G^{\,o} \, (E_\gamma^{\,2} + 4\,\pi^2\,T^2) \,/\, E_G^{\,2}\,, \qquad (6)$$

where T is the nuclear temperature of the level on which a given electric GDR is built, $\Gamma_G^{\,o}$ - a constant factor and E_G - the energy of GDR.

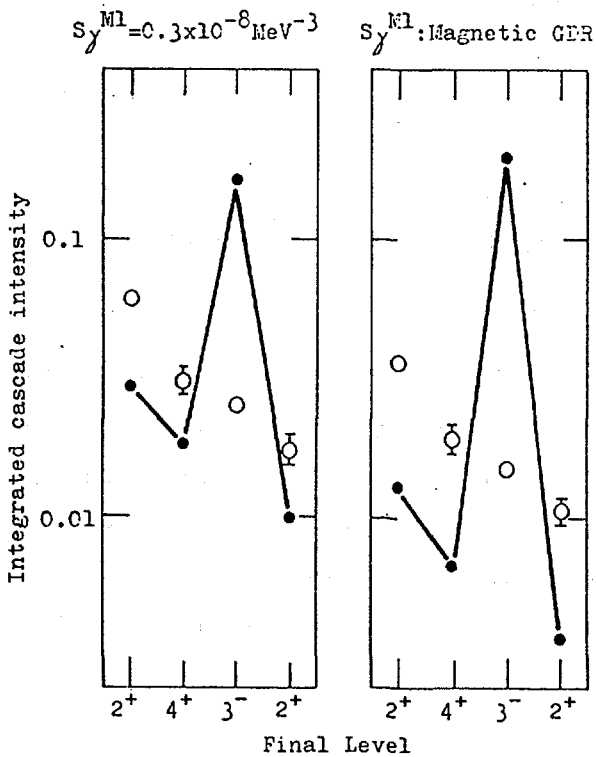

Fig. 5. Comparisons between calculated and measured cascade intensities for the first four excited levels in ^{144}Nd. The calculated values (broken lines) were obtained using the E1 photon strength function (*i*), see the text.

(*iii*) The expression (*ii*) modified by inclusion of an additional energy- and temperature-dependent term that ensures the non-zero limit of S_γ^{E1} for $E_\gamma \to 0$, as suggested by Kadmenskij *et al.* [3]. The explicit expression for the term we used is given in Ref. [5].

In conformity with the single-particle model, we assumed that the magnetic photon strength function is energy-independent. As an alternative choice we represented this strength function by a magnetic GDR with parameters taken from Ref. [4].

The results presented in Figs. 5-7 are based on the use of the expression for $\varrho(E,J)$ mentioned in Sec. 4.

As can be seen in Fig. 5, the choice (*i*) is not adequate. Much better agreement between the data and the calculations is observed in Figs. 6 and 7 for the remaining two choices. It is evident that the degree of agreement depends also on the choice of S_γ^{M1}. A particularly good agreement is achieved for S_γ^{E1} that is represented by the electric GDR with the energy-dependent Γ_G and whose limit for $E_\gamma \to 0$ is zero, while S_γ^{M1} is assumed to be represented by the magnetic GDR, see Fig. 6. Nevertheless, in order to draw firm final conclusions concerning the validity of these choices of S_γ^{E1} and S_γ^{M1} one should also analyze the integrated intensities $\langle I_{\gamma\gamma}(E_\gamma)\rangle$ for other level-density formulas than that we used in our calculations. In addition, for reliable conclusions *absolute* experimental two-step cascade intensities are needed. All this remains to be done.

In majority of cases, illustrated in Figs. 5-7, the deviations between the modeled and measured values of the integrated intensities are much larger than experimental uncertainties. It can be shown that even the uncertainties, associated with Porter-Thomas fluctuations (see Sec. 4), are very low. The observed deviations are thus statistically significant.

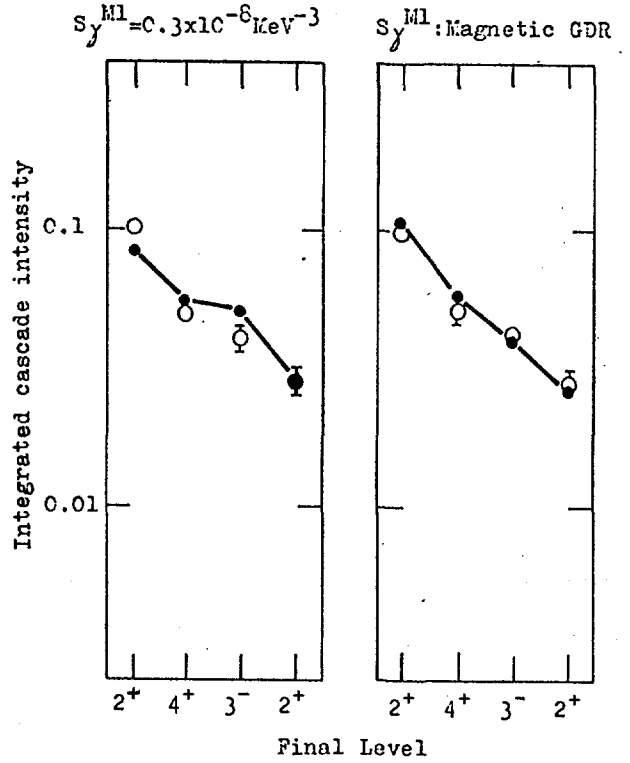

Fig. 6. Comparisons between calculated and measured cascade intensities for the first four excited levels in ^{144}Nd. The calculated values (broken lines) were obtained using the E1 photon strength function (*ii*), see the text.

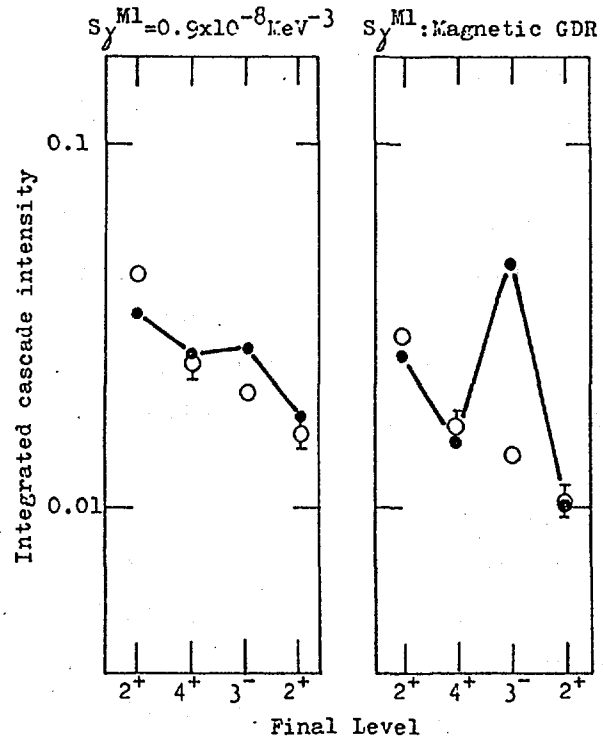

Fig. 7. Comparisons between calculated and measured cascade intensities for the first four excited levels in ^{144}Nd. The calculated values (broken lines) were obtained using the E1 photon strength function (*iii*), see the text.

The data shown if Figs. 5-7 clearly demonstrate that the two-step cascade intensities are highly sensitive to the choices of various explicit expressions for S_γ^{E1} and S_γ^{M1}. A closer inspection of these data reveals that a crucial role is played by the integrated intensity for the cascades ending at the negative-parity 1510 keV level.

Under certain simplifying conditions a rough estimate of the integrated cascade intensity can be expressed by the following two proportionalities:

$$\int I_{\gamma\gamma}(E_{\gamma 1})\, dE_{\gamma 1} \sim 2\, S_{\gamma}^{E1}(\bar{E}_{\gamma 1})\, S_{\gamma}^{M1}(\bar{E}_{\gamma 1}) \qquad (7)$$

for $\pi'' = -\pi$ and

$$\int I_{\gamma\gamma}(E_{\gamma 1})\, d\, E_{\gamma 1} \sim [S_{\gamma}^{E1}(\bar{E}_{\gamma 1})]^2 + [S_{\gamma}^{M1}(\bar{E}_{\gamma 1})]^2 \qquad (8)$$

for $\pi'' = \pi$. Here, $\bar{E}_{\gamma 1}$ is an average γ-ray energy of the two-step cascade spectrum. A systematic dependence of the left-hand sides of (7) and (8) on an excitation energy E" is neglected.

Looking at these proportionalities it is evident that for $S_{\gamma}^{E1} \simeq S_{\gamma}^{M1}$ at energies $E_{\gamma} \simeq 3 \div 4$ MeV the integrated intensity will not depend on the parity π'' of the final level. However, for S_{γ}^{E1} significantly different from S_{γ}^{M1} the integrated intensity for the cascades ending at levels with $\pi'' = \pi$ will be enhanced. By this specific feature our proposed method differs substantially from previous methods that are sensitive mostly to the sum of S_{γ}^{E1} and S_{γ}^{M1}. The reason why the role of the level at 1510 keV is so important is now evident.

In summary it can be stated that our model calculations demonstrate high sensitivity of the proposed method to the shapes and sizes of photon strength functions at intermediate energies $E_{\gamma} \simeq 3 \div 4$ MeV where direct information from traditional experiments is missing. It is important that the residual Porter-Thomas fluctuations are low enough to draw meaningful conclusions concerning photon strength functions in the considered γ-ray energy region. In addition, the presented experimental data for the thermal $^{143}Nd(n,\gamma)^{144}Nd$ reaction clearly show that the integrated two-step cascade intensities can be measured with *experimental accuracy* high enough not to cause appreciable limitations of the method.

REFERENCES:

[1] P. Axel, Phys Rev. **126**, 671 (1962).

[2] D. M. Brink, Oxford University Thesis (1955).

[3] S. G. Kadmenskij, V. P. Markushev and V. I. Furman, Sov. J. Nucl. Phys. **37**, 165 (1982).

[4] M. Uhl and J. Kopecký, cntribution to this meeting. See also: J. Kopecký and M. Uhl, Report ECN-89-165 (ECN, Petten, 1989).

[5] J. Kopecký and R.E. Chrien, Nucl. Phys. **A468**, 285 (1987).

SESSION III: EVALUATION

Chairman: S. Wender

HIGH ENERGY GAMMAS IN NUCLEAR COLLISIONS : NECESSARY DATA

A.A.Nosov, A.A.Rimski-Korsakov, R.M.Yakovlev, M.N.Zubkov
V.G.Khlopin Radium Institute, Leningrad, USSR

Yields and spectra of high-energy gammas, produced in nuclear collisions, present interest for several reasons, from purely scientific and from practical point of view. We shall demonstrate the insufficiency of relevant data in this field by two examples, where such data is most important :

- the study of superdense state of nuclear matter in heavy ion collisions at energies about 100 MeV/nucleon by means of preequilibrium gammas [1].
- the high energy (above 20 MeV) component of gamma-radiation, produced by proton-nucleus reactions at energies above 150 MeV [2] , necessary for space applications, development of accelerator-breeder targets and shielding benchmark experiments [3] and of their computer models.

The first example is related to purely scientific experiments of heavy-ion collisions at energies from 10 to about 200 MeV/nucleon. Such experiments are becoming numerous, involving nuclei from 14-N to 238-U at energies from 10 to more than 100 MeV/nucleon in various combinations. In such collisions very important information on properties of superdense state of nuclear matter can be derived from spectra and angular distributions of gammas above 10-20 MeV [1]. These spectra consist of three (or more) general features - first, a continuous exponentional decrease (5-15 MeV) due to equilibrium radiation of reaction products, plus irregular "bumps" of giant dipole resonance (GDR) decays (10-20 MeV). Above 30 MeV the prompt gammas, emitted from nuclear fireball before the equillibrium is reached, form another exponential decrease. The most interesting (at present) part is above 140 MeV, previously concidered solely due to neutral pion decay. In recent experiments [4,5,6] it has been repeatedly shown, that yield of such gammas exceeds greatly the expected one, that can be derived from simultaneous measurement of charged pions. Experimental data in this field are controvercial even for spectral shape, and

totally insufficient for angular distributions (compare [8,9] and [7]).

Of course, this matter can be clarified only after adequate theoretical nuclear models will be developed, but even then their verification will depend on systematic data concerning all lower energy gamma-production and more extensive work on high-energy heavy-ion accelerators at GANIL , GSI [10] and JINR (Dubna,USSR). We think this effort should be encouraged both in our national program and in international cooperation projects.

The second example also relates to high-energy gamma-production, but has more practical aspect. It concerns gammas above 20 MeV, emitted in proton-nucleus collisions at proton energies above 150 MeV . A new mechanism of nuclear bremsstahlung has been proposed lately [2] to explain prompt component of such gammas and their unexpectedly high yields (cross-sections up to 0.9 millibarn were measured in 200 MeV proton-gold collisions for gammas above 40 MeV). In paper [2] C,Al,Cu,Ag,Tb and Au targets were investigated at 168 - 200 MeV proton incident energies. This indicates that usual nuclear cascade gamma-emission calculations should be corrected adequately - or at least some new empirical fitting should be done for practical application of such cross-sections, which are numerous.

Data on gammas above 20 MeV are very important in calculation and development of space shielding against proton radiation, and in similar accelerator shielding problems. We met with this necessity in a benchmark experiment for an accelerator-breeder target [3]. In our case 1 GeV proton beam was stopped in a lead cylinder 20 cm dia. and 60 cm long. and produced about 30 neutrons per incident proton. The cylinder was surrounded by threshold activation detectors to measure neutron spectra and yields. In all our detectors spuriouus (gamma,n) reactions increased the cumulative yield of products of (n,2n) reactions by several percent, but could not be taken into account adequately, since no reliable data on gamma spectra and yields inside the target were avaliable. The same problem was met when effective fission cross-section had to be measured in depleted uranium samples around the target. The cumulative

fission product yield was found to be 12% higher, than the calculated one for the same neutron spectrum and flux. But we could not be sure, whether this was due to photofission or due to some inadequacy of our calculation, since gamma-spectrum and flux at the same points were unknown.

Of course, even if we had systematic and reliable data for gamma-production inside the target, the calculation would be difficult. But this part must be included in every model calculation, being verified by benchmark experiment. THe new evidence [2] of doubt, concerning existing data of high-energy gamma yields, suggests both experimental and theoretical effort in this field. Such work in energy region from 150 to 2000 MeV should be encouraged both by national programs and international projects in the nearest future.

REFERENCES :

1. Каманин В.В., Куглер А., Пенионжкевич Ю.Э. "Физика элементарных частиц и атомного ядра", т.20, вып.4, стр.741 (1989)
2. J.A.Pinston et al. Phys.Lett. v.218, No.2, p. (1989)
3. Бахмуткин С.В. и др. Атомная Энергия, т.62, вып.1, стр.59 (1989)
4. K.Hanold, D.Morissey Phys. Rev. C 38, No.5, p.2465, (1988)
5. J.Stevenson et al., Phys.Rev. C38, No.4 (1988)
6. K.Beard, W.Bennenson et al., Phys.Rev. C32, 1111 (1985)
7. N.Alamanos et al., Phys. Lett. B, v.173, p.392, (1986)
8. J.Stevenson et al., Phys.Rev.Lett.v.59, p.555 (1986)
9. R.Bertholet et.al, Nucl.Phys.A., v.474, p.541 (1987)
10. P.Kienle, "Present status of the GSI-SIS/ESR Project" in "Релятивистская ядерная физика и квантовая хромодинамика", Дубна, 1988, v.2, p.327

Evaluation of discrete γ ray production cross sections in (n,xγ) reactions on Al for nuclear geophysics

P. Obložinský and S. Hlaváč

1. Introduction

Applications of nuclear techniques in earth sciences, minerals exploration, extraction and processing are becoming increasingly more and more important. These applications require variety of fairly accurate nuclear data.

Direct geological applications have already been established which are based on elemental analysis obtained through neutron-induced γ ray spectroscopy. Determination of elemental concentrations using prompt γ ray analysis with fast neutrons requires detailed knowledge of microscopic cross sections of (n,xγ) reactions from threshold up to about 20 MeV and a knowledge of the uncertainty in these data to allow calculation of final elemental concentration uncertainties.

It is widely acknowledged (confer the Krakow 1983 and Vienna 1986 meetings)[1-3] that the knowledge of (n,xγ) data, both experimental and evaluated, is inadequate. Thus, one of the most pressing requirements is to identify gaps and discrepancies in existing experimental data files and evaluated nuclear data libraries and to produce recommended microscopic (n,xγ) cross sections for use in nuclear geology. This holds for a number of elements and among them aluminum is of primary importance for geological applications.

In the present work we are concerned with aluminum and the task is performed under the Research Contract No.4997/RB of the International Atomic Energy Agency.A basic objective is to develop a set of recommended γ production cross sections on Al for use in applied nuclear geophysics. This is achieved by analysis of existing experimental, theoretical and evaluated[4-9] production cross sections of discrete γ rays in (n,xγ) reactions on Al in the incident neutron energy range from threshold up to 20 MeV.

Of most interest in applied nuclear geophysics are several strongest γ lines. These are analyzed in the entire neutron

energy range. In view of the importance of 14 MeV neutrons,[10] a special interest is paid to this energy. Here, a rather comprehensive set of discrete γ lines is considered.Finally, identified are gaps and discrepancies in experimental data, gaps in evaluated data as well as discrepancies between experimental and evaluated data.

2. Reaction channels and observed γ lines

Natural aluminum represents a monoisotope of ^{27}Al. For incident neutron energies up to 20 MeV, several nonelastic reaction channels are opened. Excitation functions for these reactions, taken from the JENDL-2 evaluation [8], are reproduced in fig.1 and fig.2. In the energy range up to 17 MeV the most important channel is the inelastic neutron scattering, see fig.1. The total inelastic cross section reaches its maximum of 870 mb at the neutron incident energy of 6 MeV and is steadily decreasing with increasing neutron energy. Also shown are excitation functions for the first 5 excited levels. It is interesting to note that the total (n,n') cross section represents an upper limit for discrete γ ray production, whereas cross section for discrete level excitation represents a lover limit for the corresponding deexciting γ rays. To this direct part of the γ ray production cross section an additional contribution from the statistical level population should be added.

Excitation functions for the charged particle reactions (n,p) and (n,α) as well as for the secondary reactions (n,np) and (n,2n) are given in fig.2. Thresholds for these reactions are 1.8, 3.1, 8.1 and 13.3 MeV respectively. All excitation functions show a typical statistical behavior with broad bump and decreasing cross sections as additional reaction channels are subsequently opened with increasing neutron energy.

Excitation functions of energetically possible reactions (n,γ) and (n,nα) are not shown in fig.2. The former reaction is important at very low neutron energies only. The later has a rather low cross section and consequently none of them is interesting for the present application.

From the excitation functions given in figs.1,2 it is readily seen that the most important reaction for the analytical

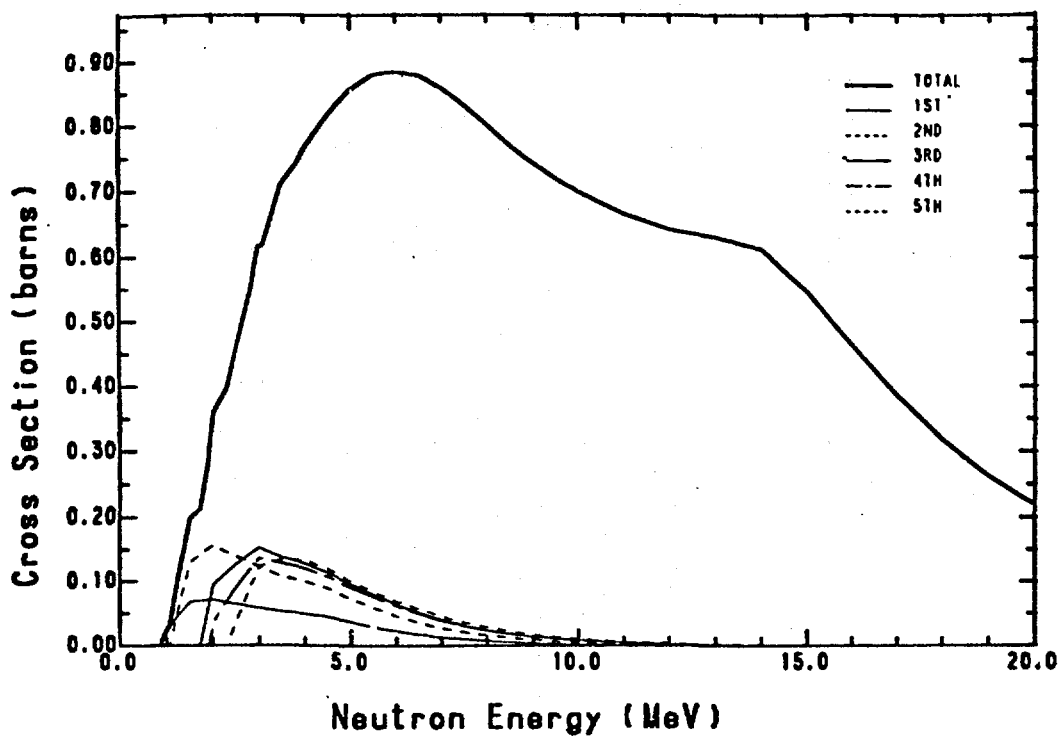

Fig.1. Excitation functions for inelastic neutron scattering on ^{27}Al. Solid line represents total inelastic scattering. Other lines are excitation functions for the first 5 excited levels. Figure is taken from ref.8.

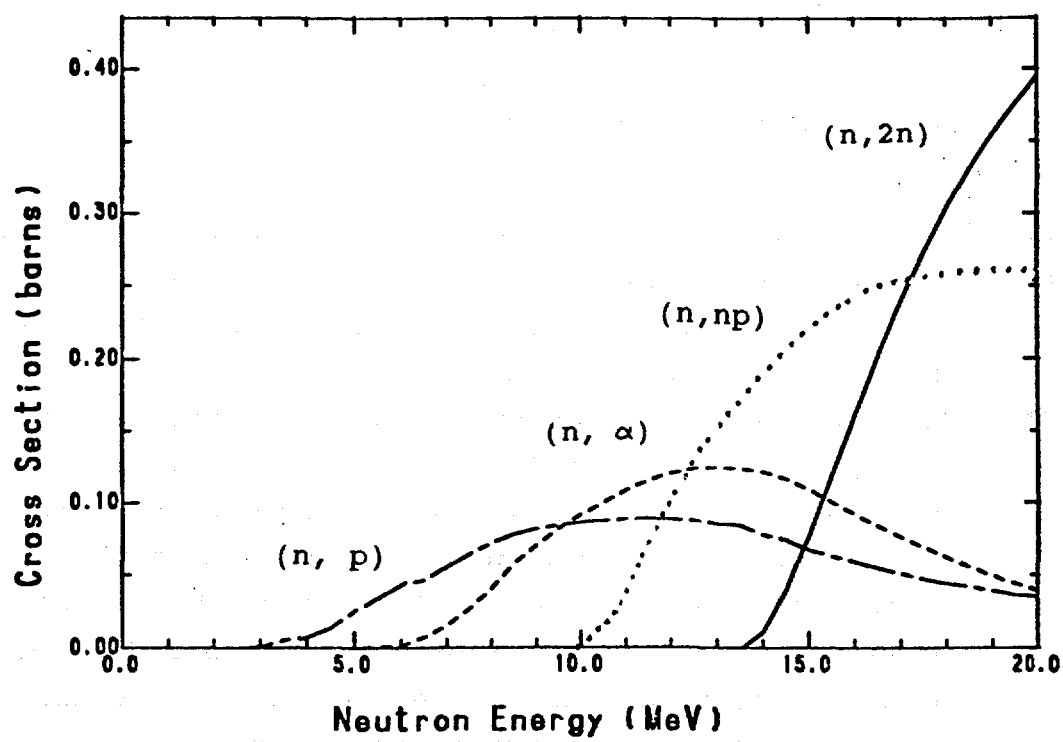

Fig.2. Excitation functions for different neutron induced reactions with ^{27}Al. Figure is taken from ref.8., except for (n,np) channel which is from the ENDF/B-4.

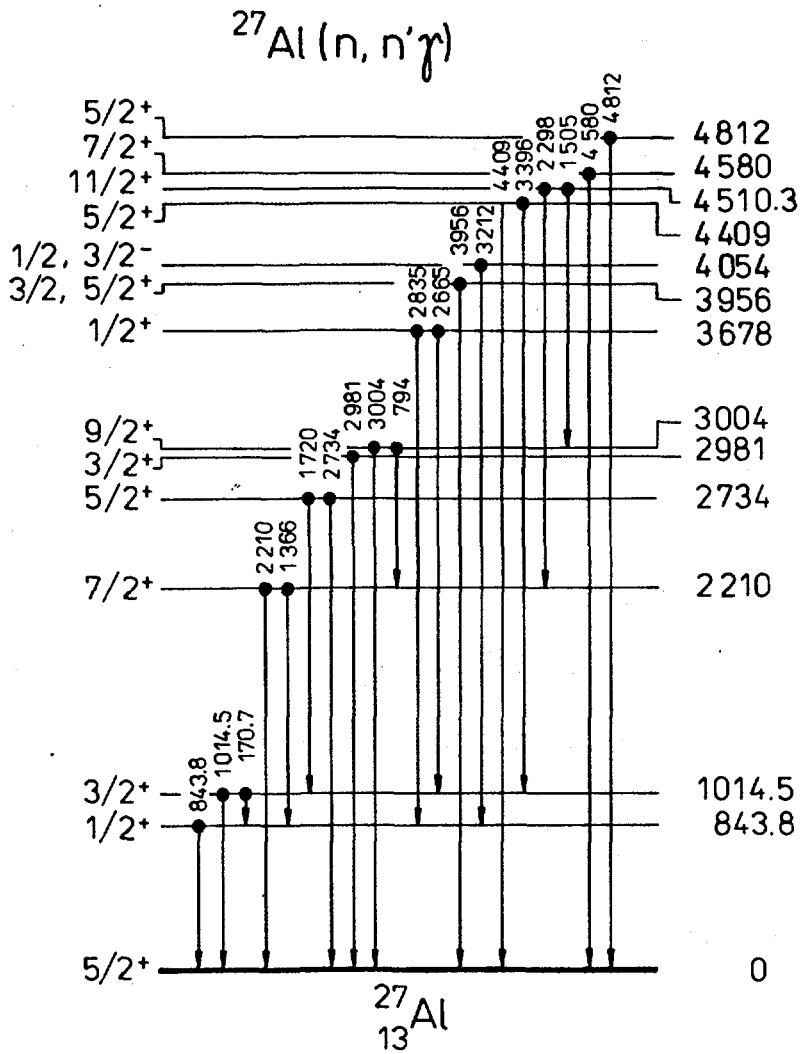

Fig.3. Simplified level scheme of ^{27}Al with γ transitions observed in inelastic neutron scattering. Based on the Table of Isotopes[11].

purposes in the whole energy range is the inelastic neutron scattering. Above the 14 MeV incident neutron energy the (n,np) reaction may be also suitable. For still higher neutron energies the (n,2n) reaction may be utilized.

The discrete γ ray production cross section is not determined only by the reaction cross section. Specific properties of product nucleus play also an important role. The level scheme of ^{27}Al with discrete γ rays observed in the inelastic neutron scattering is given in fig.3. The scheme is based on the widely distributed Table of Isotopes[11]. In the present report we follow strictly the nuclear structure data given in this reference. This seems to be necessary because in older sources slightly different energies were assigned to several discrete γ transitions. For instance the energy of the $1/2^+ \rightarrow$ g.s. transition was often referred to as 842 keV instead of

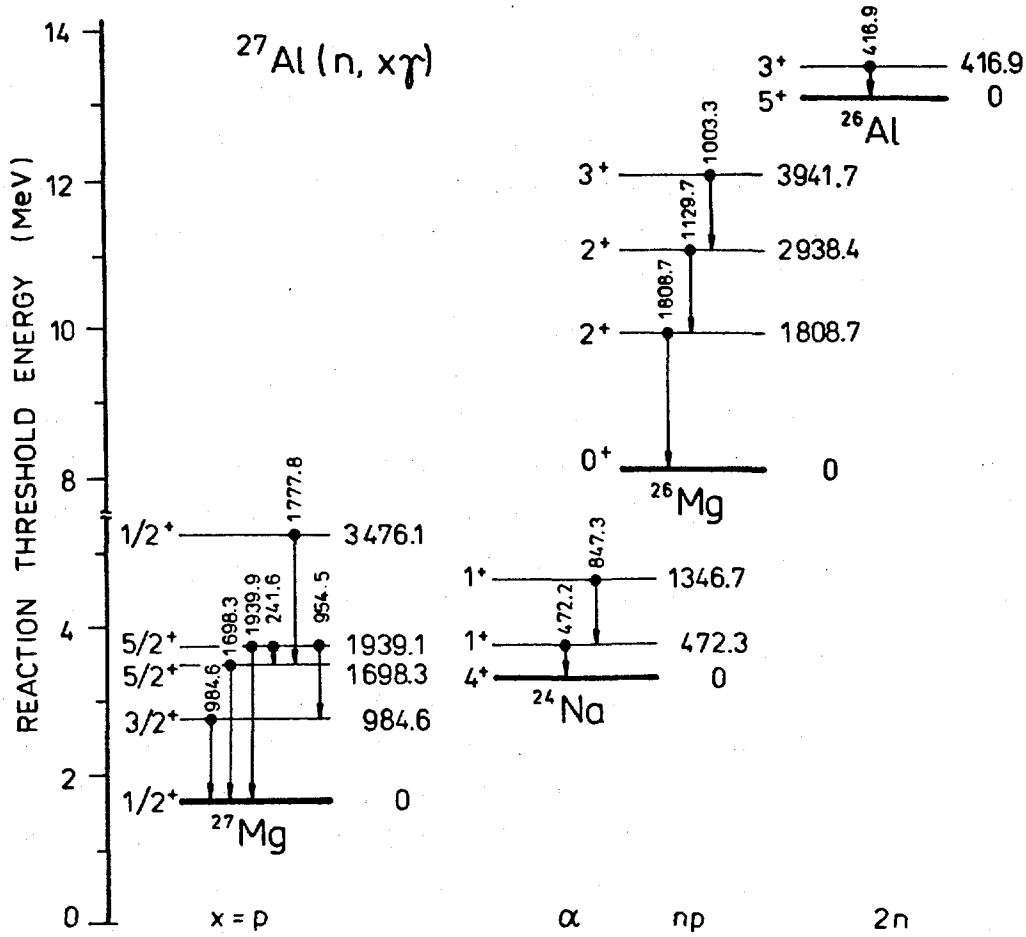

Fig. 4. Level schemes and γ transitions in nuclei produced in several neutron induced reactions with ^{27}Al. The scale on the left hand side gives threshold energies, x designates the particle(s) emitted in nuclear reaction leading to the indicated product nucleus.

843.8 keV. Other older γ transition energies are 1013 keV and 3001 keV which we replaced by the energies 1014.5 keV and 3004 keV, respectively.

^{27}Al is an odd-even nucleus and its excited states decay predominantly via γ transitions directly to the ground state (g.s.). A single cumulative γ transition, commonly found in the medium heavy even-even nuclei, is not present in ^{27}Al and the whole inelastic cross-section is distributed among several g.s. γ transitions. From these the most prominent are 843.8 keV , 1014.5 keV, 2210 keV and 3004 keV. Weaker decay branches between excited levels include 1720 keV γ ray. These discrete γ lines should represent transitions interesting for analytical purposes in nuclear geophysics.

Level schemes and γ transitions in other nuclei produced in the neutron induced reactions with ^{27}Al are given in fig.4.

Threshold energies for the reaction as well as for the excitation of a specific level are given on the left hand side of fig.4.

The lowest threshold has the (n,p) reaction. The product nucleus ^{27}Mg is an even-odd nucleus with decay pattern similar to the ^{27}Al. Prominent γ lines are g.s. transitions with energies of 984.6 keV and 1698.3 keV.

The (n,α) reaction leads to ^{24}Na. The first excited state of ^{24}Na, which is probably the most strongly populated, is an isomer with half-life of 20.2 ms. The deexciting γ transition to the g.s. with the energy 472.3 keV is therefore difficult to observe in the prompt γ ray spectra, where suitable time resolution is of the order of several ns. Analytical usefulness of this reaction is therefore questionable and we will exclude this reaction from our further considerations.

The product of ^{27}Al(n,np) reaction is ^{26}Mg, an even-even nucleus. Its excited states decay via cascading transitions through the first 2+ level at the energy of 1808.7 keV. The g.s. γ transition from this level collects therefore the whole reaction cross section except for the direct particle population of the g.s. Therefore, the 1808.7 keV γ ray should also be considered for analytical purposes, especially at neutron energies above 10 MeV.

The (n,2n) reaction has a rather high threshold and becomes interesting only in the upper region of neutron energies. The γ ray with the energy of 476 keV is the most prominent transition in this channel.

3. Analysis of existing data

There are numerous measurements of the discrete γ ray production cross sections reported in the literature [12-20]. They can be divided in two groups, according to the γ ray detection method used. Most of the data are rather old NaI(Tl) measurements with only few discrete γ ray cross sections at a single neutron energy. The most recent data of this type are those of Islam et al.[21], who report production cross sections of 843.8, 1014.5, 2210, 1720 and 3004 keV γ transitions from threshold up to 10 MeV incident neutron energy.

The Ge(Li) measurements represent the second type of data. Dickens [22] gives cross sections of 18 γ ray transitions in the

(n,n'γ) channel for several neutron energies between 5.3 and 9 MeV. This is the most complete measurement what concerns the number of γ rays. The most complete set of cross sections from threshold up to 13 MeV incident neutron energy is reported by Voss[23] for γ ray transitions 843.8, 1013, 1720, 2210 and the sum of 2980 + 3000.3 keV. Orphan[28] on the other hand measured cross sections of all these strong γ rays up to 15.8 MeV but with rather coarse energy step.

In addition, two groups have measured just around 14 MeV incident neutron energy. Nyberg et al.[24] report 20 cross sections at 15 MeV for γ rays from (n,n'γ), (n,pγ), (n,npγ) and (n,$\alpha\gamma$) reactions. The most recent measurements in this energy range are those of Zhou Hongyu et al.[25,26] at 14.9 MeV, who give 34 cross sections of discrete γ transitions in the above mentioned channels as well as in the (n,2nγ) channel.

Several compilations and/or evaluations of discrete γ ray cross sections were performed for various purposes. The best known ENDF/B-IV evaluation accomplished by Young et al.[29] contains in a file MF=13 the discrete γ ray smooth cross sections for (n,n'γ), (n,npγ) and (n,pγ) under MT=4,28 and 103, respectively. The evaluation is based mainly on the older NaI(Tl) measurements and did not take into account the more recent Ge(Li) experimental data. The experimental data are supplemented at higher neutron energies by rather simple statistical theory calculations.

A JAERI group performed a compilation of neutron cross sections for fusion reactor development[30]. In this compilation several discrete γ ray cross sections for (n,n'γ) channel are included.

Finally, an IAEA group compiled several discrete γ ray cross sections from the EXFOR file for geophysical applications[31]. This compilation contains in a graphical form excitation functions of 5 strongest γ rays in the (n,n'γ) channel.

3.1. Discrete γ ray production in inelastic scattering

In this chapter we consider in detail production of discrete γ rays in the inelastic neutron scattering. As mentioned above, there is rather voluminous set of experimental data available. To illustrate the present situation more explicitly we show in fig.5 cross section for production of the 1014.5 keV γ line, as taken from evaluations/compilations mentioned above.

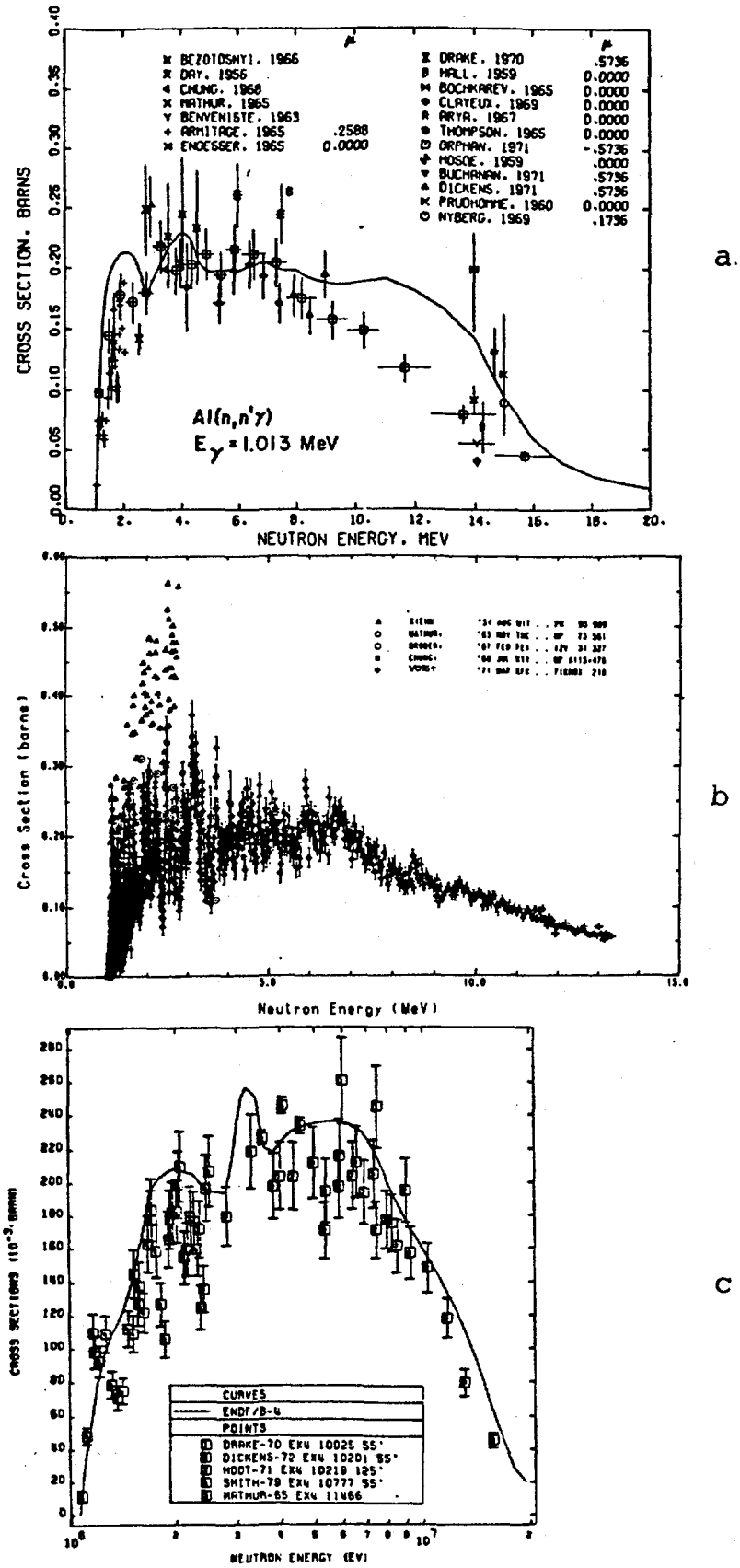

Fig.5. Experimental and evaluated cross sections for the 1014.5 keV γ ray emitted in $^{27}Al(n,n'\gamma)$. a) Data used in the ENDF/B-4 evaluation and the result of this evaluation[29], b) data compiled by the JAERI group[30] and c) data compiled by the IAEA group[31]. Both the Ge(Li) and NaI(Tl) measurements are displayed.

In fig.5a, there are experimental data collected by Young and Foster[29] for the ENDF/B-4 evaluation. Evaluated cross sections are given by the full curve. However, some of the data already shown here were not available at the time of the evaluation and were not taken into account. The set of the experimental data compiled by JAERI the group[30] is reproduced in fig.5b. The essential part of this set are the Karlsruhe data by Voss[23]. They cover the whole energy interval from the threshold up to 13 MeV incident neutron energy. Finally, the IAEA compilation[31] is given in fig.5c. Majority of experimental data shown in fig.5 were obtained using NaI(Tl) spectrometers. Only data of Chung[20],Dickens[22], Voss[23], Nyberg[24],Orphan[28] and Clayeux[28] were obtained with high resolution Ge(Li) spectrometers. Two recent HPGe measurements by Zhou Hongyu et al.[25,26] at 14.9 MeV neutron energy are not included.

Several conclusions can be drawn from fig.5. Experimental data are available in the energy region from the threshold up to 15.8 MeV incident neutron energy. Above this energy there are no experimental data. At neutron energies below 7 MeV and around 14 MeV there are rather large discrepancies between experimental data. The Voss's measurement shows much more pronounced structure in the excitation function than the ENDF/B-4 evaluation. This structure has solid physical background and may be partly responsible for discrepancies at lower neutron energies mentioned above. Finally, the ENDF/B-4 evaluation systematically overestimates the experimental cross sections at neutron energies above 8 MeV with the exception of several data points around 14 MeV.

As will be shown later, the above situation is rather typical for cross sections of all strong g.s. γ ray transitions observed in the $^{27}Al(n,n'\gamma)$ reaction.

In the following analysis we will lay the greatest emphasis on the Ge(Li) measurements. The most obvious reason is the superior energy resolution of Ge(Li) spectrometer. Furthermore, these data are the most recent ones available.

In order to help to resolve difficulties in recommended cross sections we used theoretical values as well. At present there are few state-of-art computer codes, which utilize in full the present knowledge of statistical nuclear reactions. Features normally included are preequilibrium emission, spin and parity conservation as well as the realistic treatment of γ decay

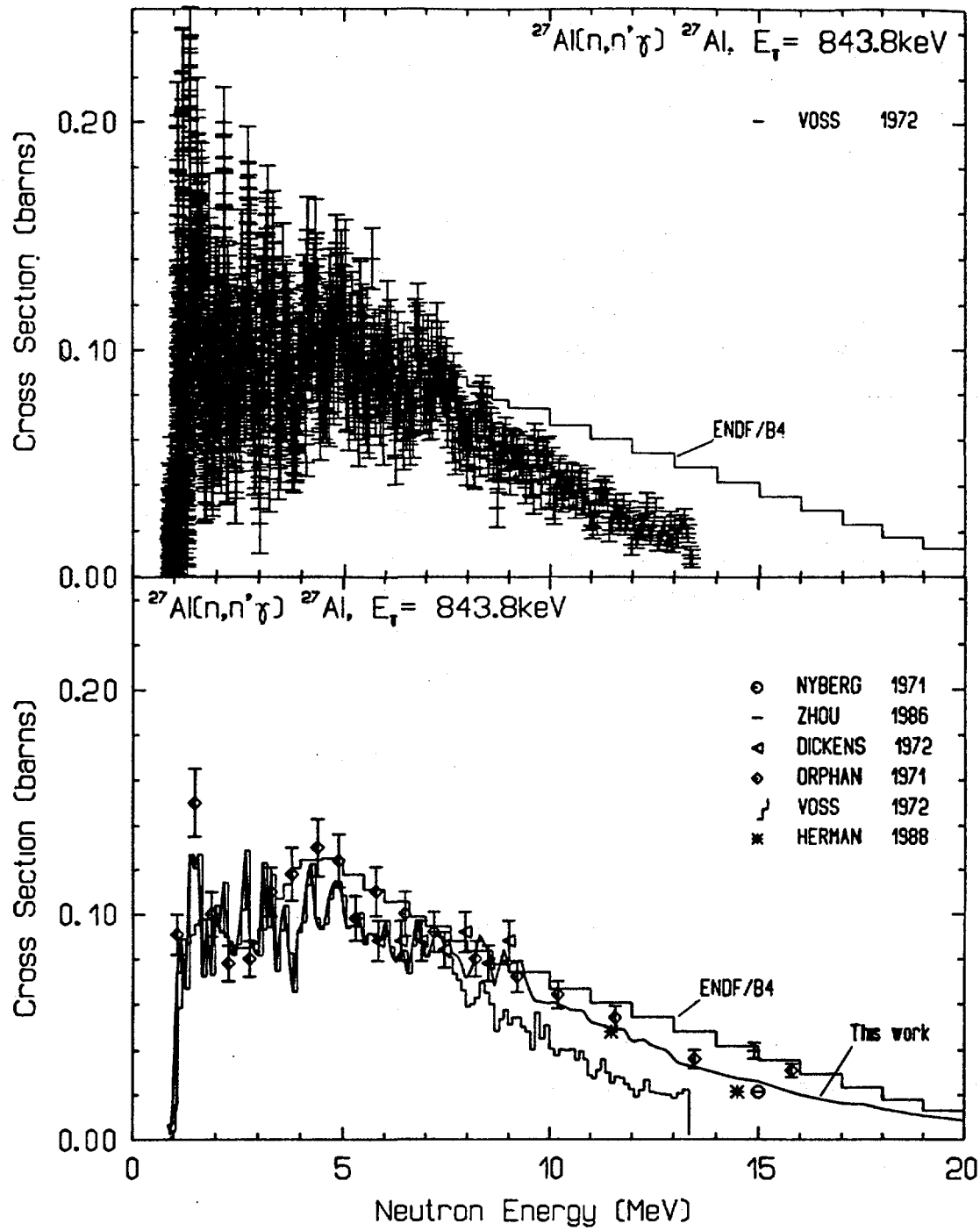

Fig.6. Cross sections for the production of the 843.8 keV γ ray in the ^{27}Al(n,n'γ), as measured with Ge(Li) detectors. The results of Voss[28] and the results of other authors are displayed in the upper and lower part, respectively.. The origin of each point is decsribed on the right hand side of each picture. Herman results are theoretical calculations.The coarse step histogram in both parts is the evaluation from the ENDF/B-4. The fine step histogram in the lower part represents averaged Voss data. The curve represents our recommended cross sections.

between experimentally known discrete levels. However, such calculations are generally not available. In the present case the available theoretical data of this type were only thoseprovided by Herman[32], calculated with the computer code PENELOPE at incident neutron energies of 11.5 and 14.5 MeV.

3.1.1. The 843.8 keV transition

This transition corresponds to the γ decay of the first $1/2^+$ excited state to the ground state of ^{27}Al.The available Ge(Li) data for the production cross section of 843.8 keV transition are displayed in fig.6. For the sake of lucidity we divided the data into two parts. The most complete and probably most careful measurements of Voss et al.[29] are given in fig.6a. There are 1663 experimental points in this figure. The histogram represents the ENDF/B-4 evaluation. All other experimental data are presented in fig.6b. Again the coarse histogram is the ENDF/B-4 evaluation. To facilitate the comparison with the Voss's data we show their values averaged over 0.1 MeV intervals.

The experimental data in fig.6b are supplemented by two theoretical values provided by Herman[32] at 11.5 and 14.5 MeV incident neutron energy.

The excitation function measured by Voss et al.[29] shows in the energy interval from the threshold up to 8 MeV rather strong fluctuations. They are not seen in other measurements because of poor resolution of incident neutron energies. Bearing in mind the physics of these fluctuations, the experimental values in fig.6 are in reasonable accord up to neutron energy about 7 MeV. Discrepancies arise above this energy, where all experimental values are higher than the Voss data, the differences reaching eventually up to a factor of 2. At 14.9 MeV the value of Zhou at al.is still higher than the Orphan data. On the other hand, the Nyberg value is in agreement with the trend indicated by Voss data. However, the Nyberg experimental value means only an upper limit to the cross section.

The ENDF/B-4 evaluation is rather smooth in the displayed interval and is consistent with Orphan experimental values up to 10 MeV neutron energy, the only exception being the 2.4 MeV point. Up to 3.5 MeV it is also in accord with the gross trend of the Voss data. Above 3.5 MeV the evaluated values are systematically greater than the same experimental data. Above 10

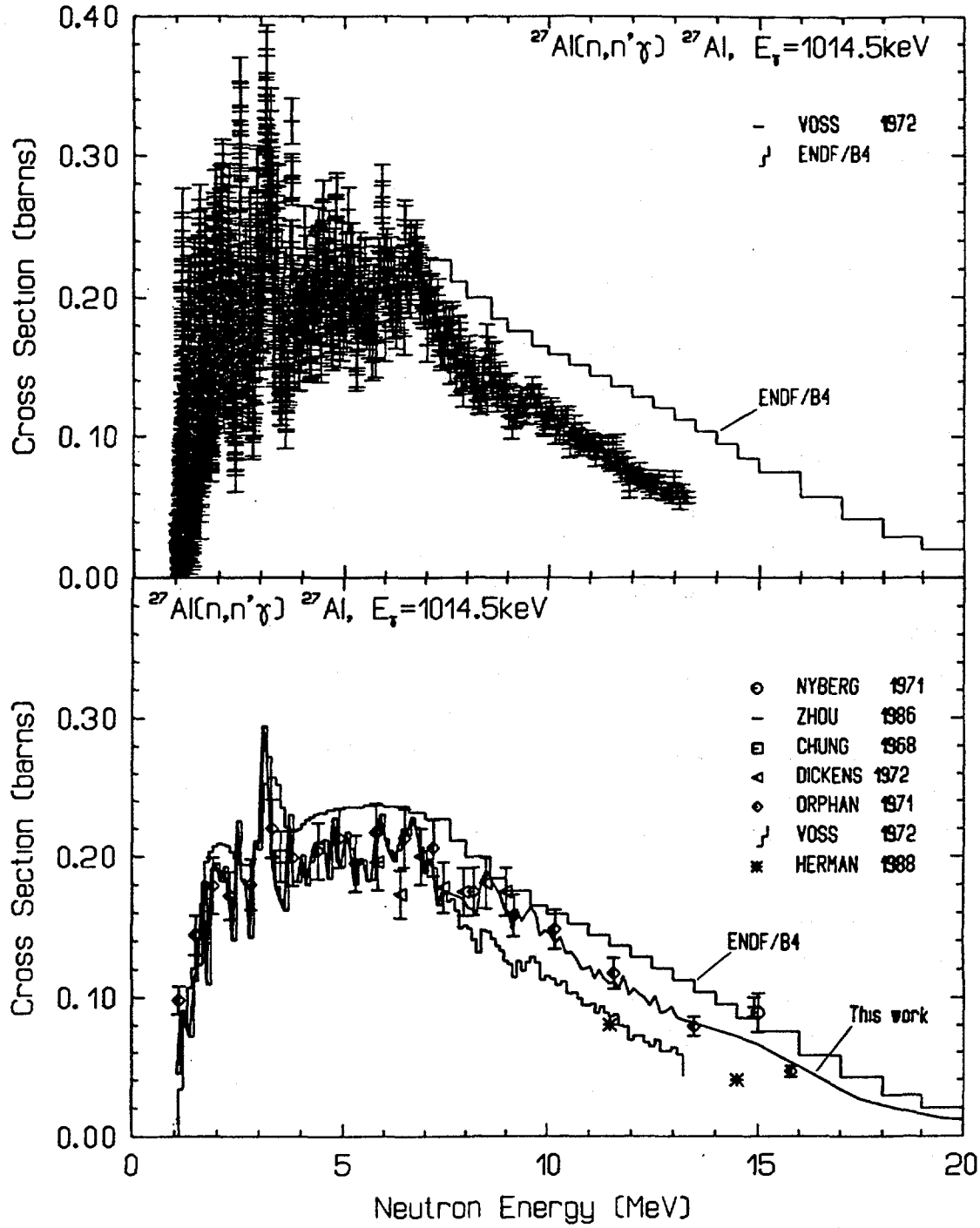

Fig.7. Cross sections for production of the 1014.5 keV γ ray in the inelastic neutron scattering on ^{27}Al. For more details see caption of fig.6.

MeV the evaluation overestimates all experimental data with the exception of the Zhou value at 14.9 MeV and the Orphan value at 15.8 MeV.

After the analysis of available information about collected experimental data, we arrived to following conclusions. Up to incident neutron energy 7 MeV, where strong fluctuations takes

place, the Voss data should form the basis for evaluated cross sections. Above this energy there are two sets of data, the difference between them reaching eventually a factor of 2. The ENDF/B-4 evaluation is rather smooth in comparison with available experimental data and systematically overestimates the experiment in the high energy range. At higher energies the cross section should be obtained by careful analysis of cross sections of all open channels at least at one neutron energy, probably around 14 MeV.

3.1.2. The 1014.5 keV γ ray transition

This transition corresponds to the γ decay of the second excited level with spin $5/2^+$. Available Ge(Li) data are displayed in fig.7. Again, in the upper part of fig.7 we show Voss experimental data together with the ENDF/B-4 evaluation. All other experimental cross sections are displayed in the lower part of fig.7. There, the coarse histogram is the ENDF/B-4 evaluation and the fine histogram represents averaged Voss data. The whole situation resembles that of the 843.8 keV transition. The excitation curve measured by Voss shows strong fluctuations absent in other data. Apart from this fluctuations, the experimental data are in good agreement up 7 MeV incident neutron energy. Above this energy Orphan and Dickens values are higher than Voss data, although the differences are smaller than for the 843.8 keV, reaching roughly a factor of 1.3. Zhou and Nyberg values around 15 MeV are in mutual agreement, both being too high in comparison with other data. Theoretical values of Herman are in this case in excellent agreement with Voss data.

The ENDF/B-4 seems to overestimate the experimental cross sections in the whole energy range with the exception of the threshold region and the sharp maximum around 3 MeV incident neutron energy. At 15 MeV neutron energy it is in accord with values given by Nyberg and Zhou, both being too high in comparison with other experiments.

The overall agreement of experimental values is better than in the case of 843.8 keV transition, except at 15 MeV. Again the Voss measurement gives the most complete set of data.

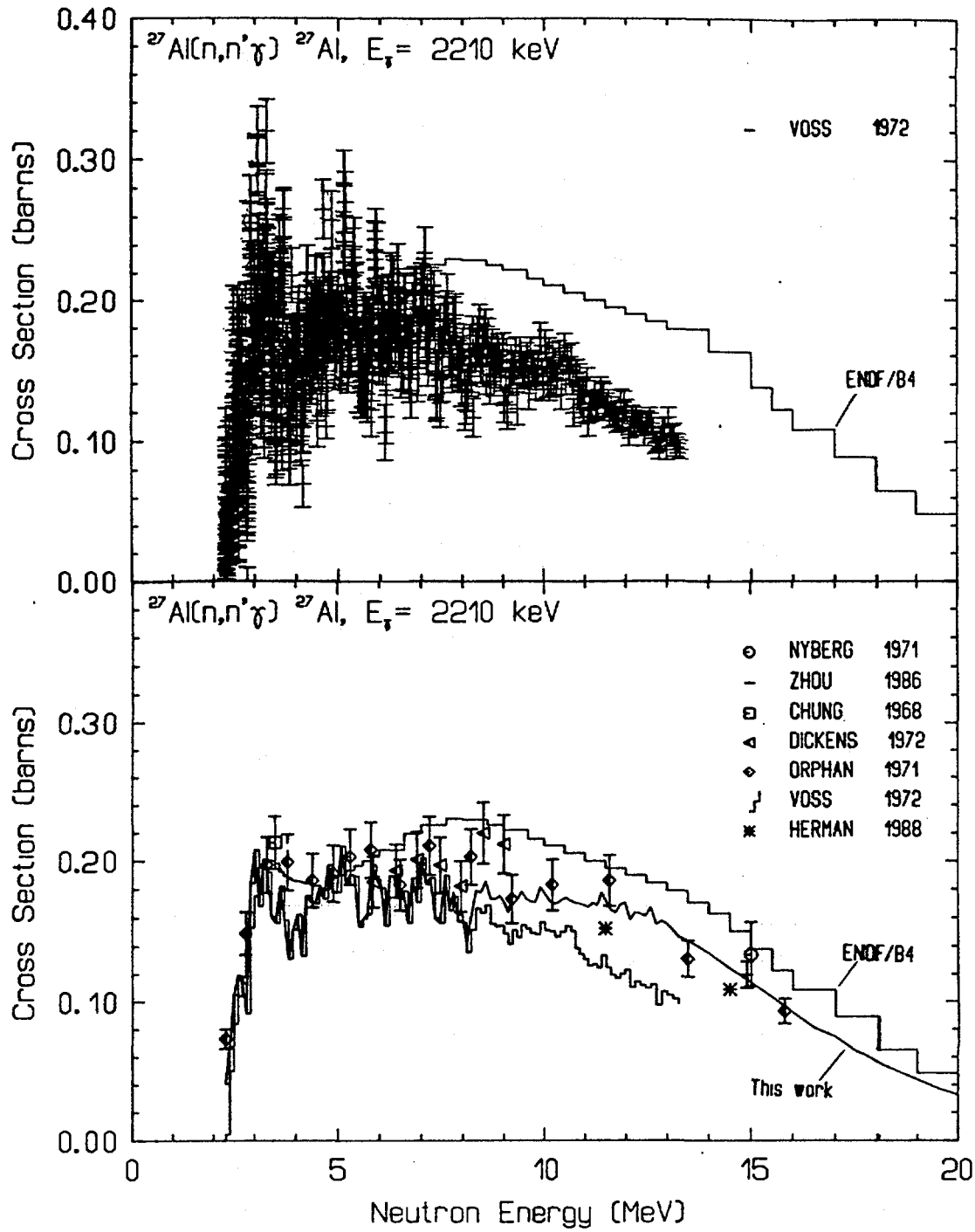

Fig.8. Cross sections for production of the 2210 keV γ ray in the inelastic neutron scattering on ^{27}Al. For more details see caption of fig.6.

3.1.3. The 2210 keV γ ray transition

This discrete γ ray originates in the γ decay of the third excited $7/2^+$ level in ^{27}Al, which goes to the ground state with a weak branch to the 843.8 keV level. Experimental cross sections of the 2210 keV γ ray are displayed in fig.8. The Voss data show

again more pronounced fluctuations than any other experimental values. The various experimental values are in reasonable accord up to neutron energy of 8 MeV. Above this energy the cross sections measured by Voss are lower than cross sections of Orphan and Dickens. Zhou and Nyberg values at 14.9 and 15 MeV,respectively are in agreement. However, they are slightly above experimental values given by Orphan. The Herman's theoretical value at 14.5 MeV is also in accord with the Orphan experiment. However, the theoretical cross section at 11.5 MeV is in favor of lower cross section than the value of Orphan.

The ENDF/B-4 evaluation is above the Voss excitation function in the whole energy range except at the threshold and around 5 MeV. Above 5 MeV incident neutron energy it seems to overestimate all experimental data, although it is within error bars of some Dickens and Orphan values up to 11.5 MeV as well as the Nyberg point at 15 MeV.

3.1.4. The 3004 keV γ ray transition

The 3004 keV transition originates in the γ decay of $9/2^+$ level at this energy. The experimental cross sections measured with Ge(Li) detectors are displayed in fig.9. The Voss data are shown in the upper part of fig.9. Even with the Ge(Li) spectrometer used in his experiment it was not possible to resolve 3004 keV transition from the next lower γ ray of 2981 keV and the cross section displayed is actually a sum of cross sections of these two unresolved transitions. According to Dickens, who resolved the two γ rays in his experiment, the cross section of 2981 keV transitions is about 30% of that of the 3004 keV transition in the neutron energy interval 5 - 9.5 MeV.

Other experimental data together with Voss averaged data as well as the ENDF/B-4 evaluation are shown in the lower part of fig.9. However, the averaged Voss values were reduced in the whole energy range by a factor extracted from the Dickens experiment. Assuming that this factor is correct also outside of the 5 - 9.5 MeV energy interval, the histogram representing Voss data corresponds now to the net cross section of the 3004 keV γ ray.

The excitation curve measured by Voss shows two pronounced maxima at 4.5 and 6.5 MeV with superimposed fluctuations.Rather strong fluctuations are visible in Voss data also above 7 MeV.

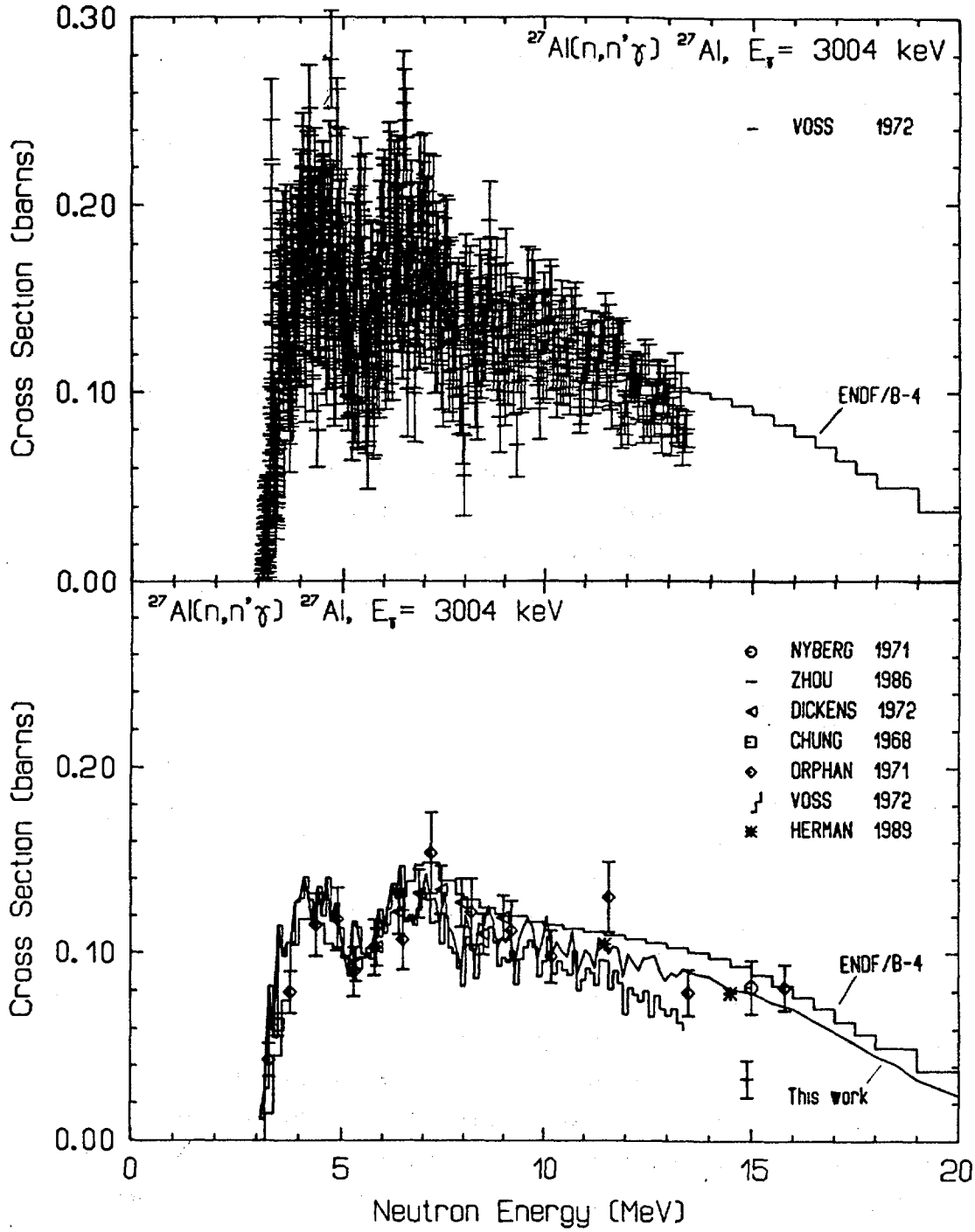

Fig.9. Production cross sections of the 3004 keV transition. Voss data in the upper part are the sum of 3004 keV and 2980 keV cross sections. The fine histogramm in the lower part is the net 3004 keV cross section obtained from averaged Voss data. For more details see the caption of fig.6.

However, the averaged values are in this region consistent with experimental results of other authors. Cross sections measured by Chung, Dickens and Orphan are in good agreement up to 10 MeV, with the exception of the Orphan value at 11.6 MeV. The Nyberg value measured at 15 MeV is in accord with Orphan data. The Zhou

cross section at 14.9 MeV is too low and inconsistent with other experimental values. The last two Orphan values as well as that of Nyberg suggest increasing cross section with increasing neutron energy, contrary to the general behavior observed in all (n,n'γ) excitation curves. Theoretical values of Herman are higher than experimental values of Voss and at 14.5 MeV they are in accord with experimental cross sections of Orphan and Nyberg.

The ENDF/B-4 evaluation shows also two broad maxima in the low energy region and is in good accord with experimental values of Chung, Dickens and Orphan up to 9 MeV. Between 10 and 15 MeV the evaluated cross sections are above experimental points of Orphan, with the exception of the point at 11.6 MeV, which seems to be rather high.

3.1.5. The 1720 keV γ ray transition

The excited level at the energy of 2734 keV with spin $5/2^+$ decays by emission of the 1720 keV γ ray with branching ratio 0.77. Experimental cross sections measured with Ge(Li) spectrometers are displayed in fig.10. The Voss data alone with the ENDF/B-4 evaluation are shown in the upper part, all other experimental data as well as the histogram representing averaged Voss data are shown in the lower part of fig.10. Voss experimental values show again strong fluctuations, which are not seen in other experiments. All displayed experimental data are in good mutual agreement. The only exception is the 15 MeV point, where both Nyberg and Zhou values are much higher then the cross section of Orphan as well as the trend indicated by Voss data.

The ENDF/B-4 evaluation is in accord with with available experimental values up to 13 MeV incident neutron energy. Above 13 MeV the evaluation again overestimates the experimental values with the exception of two above mentioned cross sections of Zhou and Nyberg.

3.2. Discrete γ rays from other reactions

Experimental information concerning production cross sections of discrete γ rays in other neutron induced reactions on ^{27}Alis rather poor in comparison with the inelastic neutron scattering. We will concentrate here only on two γ lines produced in (n,pγ) and (n,npγ) reactions, 984.6 keV and 1808.7 keV,

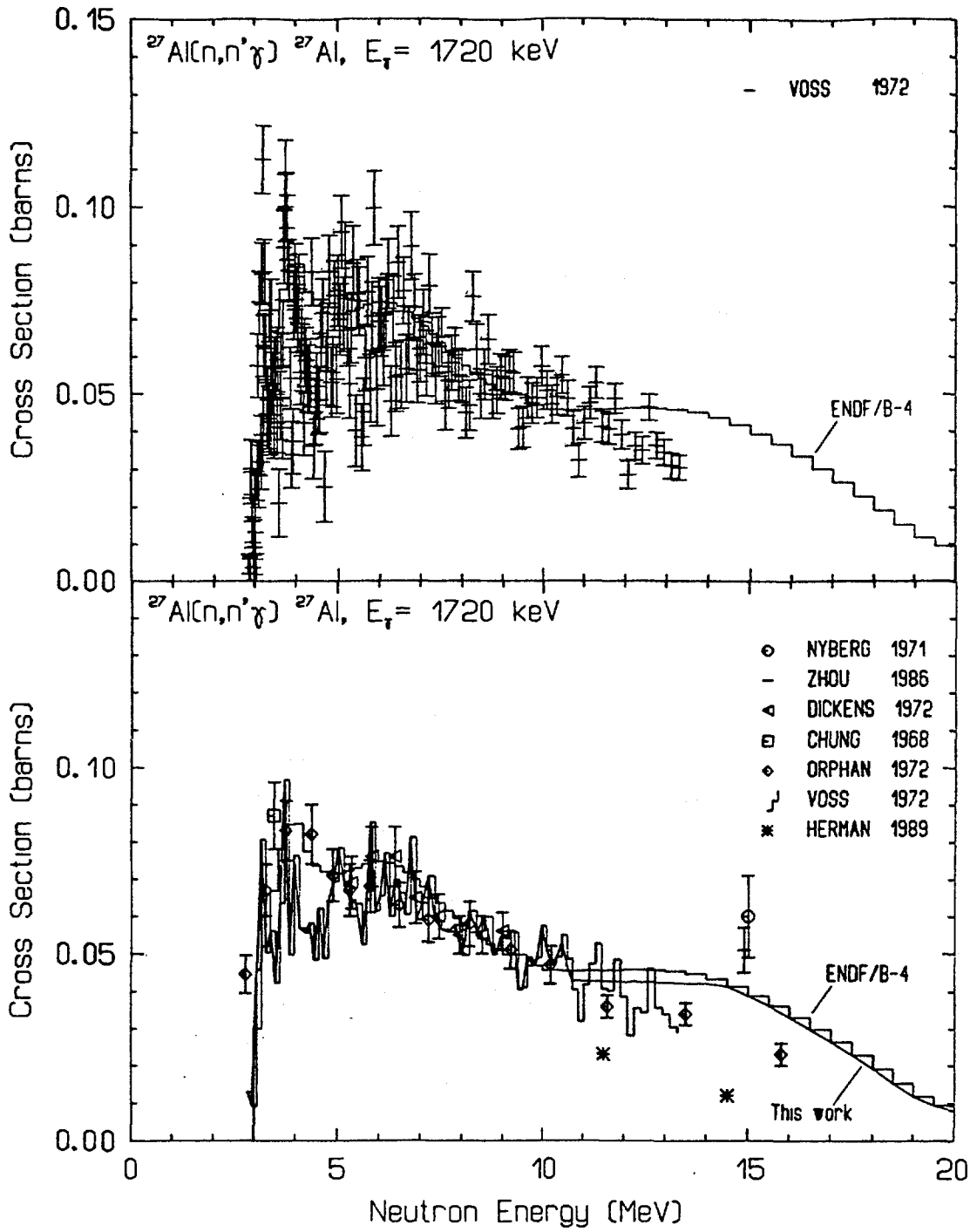

Fig.10. Cross sections for production of 1720 keV γ ray in inelastic neutron scattering on ^{27}Al. For more details see caption of fig.6.

respectively. To complete the discussion, we will mention also the (n,2nγ) reaction, where only single experimental point at 15 MeV is available.

3.2.1. The 984.6 keV γ ray produced in $^{27}Al(n,p\gamma)^{27}Mg$

This γ transition is the strongest one in the (n,p) channel, produced in the decay of the first $3/2^+$ excited level of ^{27}Mg. Available experimental cross sections are summarized in fig.11. where also the ENDF/B-4 evaluation is displayed. There are only three independent measurements of this cross section. Dickens[22] gives several values at neutron energies between 5.5 and 9 MeV. Other values displayed in fig.11 are measurements of Nyberg and Zhou at 15 and 14.9 MeV, respectively. There is large discrepancy between the last mentioned values. Furthermore, both values and especially the value of Nyberg seem to be very high.

The ENDF/B-4 evaluation is based mainly on Dickens data, therefore good agreement with these data is not a surprise.

3.2.2. The 1808.7 keV γ ray produced in $^{27}Al(n,pn\gamma)^{26}Mg$

This reaction is important at higher incident neutron energies. The experimental information is rather poor, concentrated only around 14 MeV neutron energy. Experimental cross sections are shown in fig.12. All experimental values are in good accord. Also the ENDF/b-4 evaluation seems to be a good representation of the physical reality.

3.2.3. Discrete γ ray production in (n,2n) reaction

This reaction has a rather high threshold and becomes important only well above 15 MeV neutron energy. Experimental information is limited to 15 MeV point. The strongest γ ray is the 416.9 keV transition from the first excited level in ^{26}Al. The cross section for this transition, as measured by Zhou at 14.9 MeV is 4.5(1.0) mb.

3.3. Discrete γ rays produced at 15 MeV incident neutron energy

The γ ray production cross sections around 14 - 15 MeV are of great importance from practical point of view. This is probably the neutron energy at which first geophysical applications will take place. The reason is that 14 MeV neutron

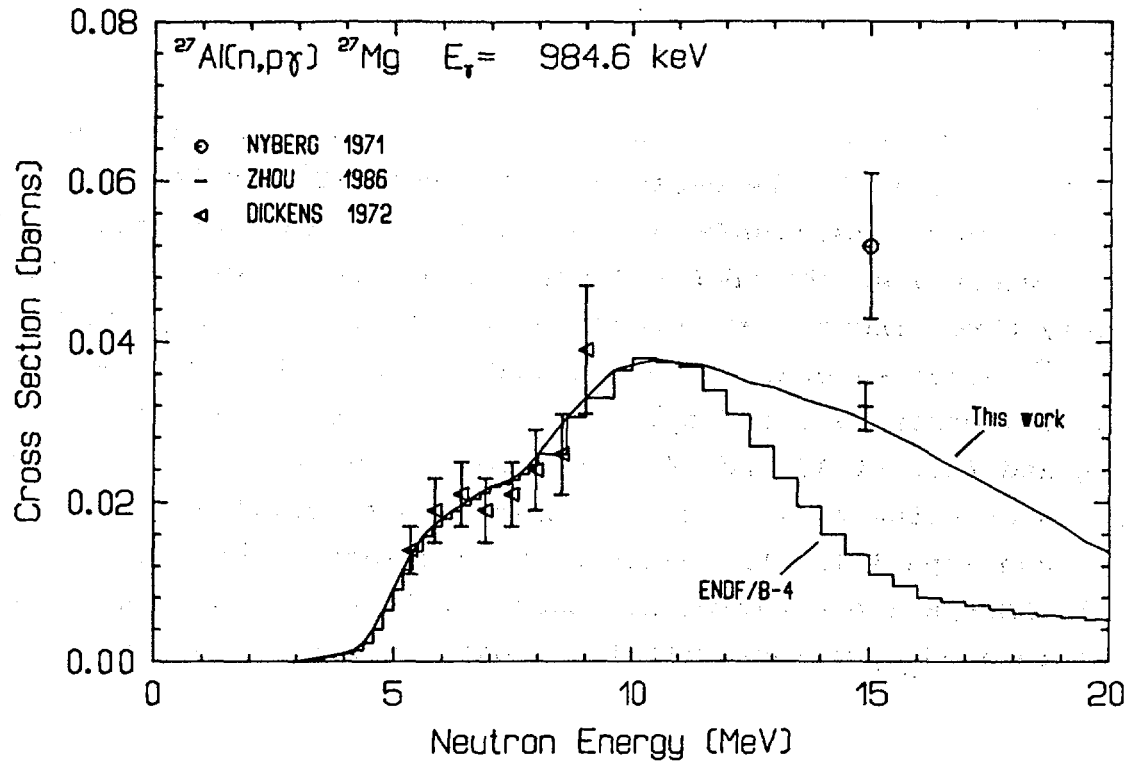

Fig.11. Cross sections of the 984.6 keV γ ray in the ^{27}Al(n,pγ)^{27}Mg reaction. The histogram represents the ENDF/B-4 evaluation. The origin of data is indicated on the left hand side of the figure.

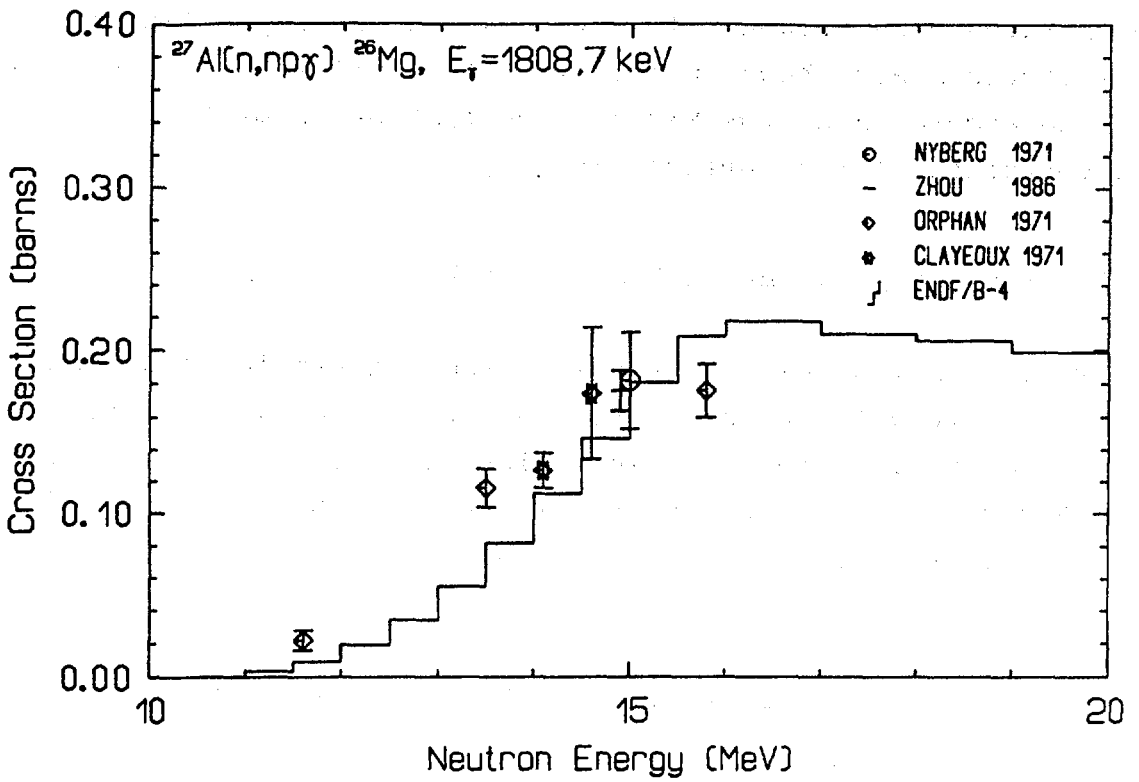

Fig.12. Cross sections of the 1808.7 keV γ ray in the ^{27}Al(n,npγ)^{26}Mg reaction. The histogram represents evaluated cross sections from the ENDF/B-4. The origin of experimental data is shown on the right hand side of figure.

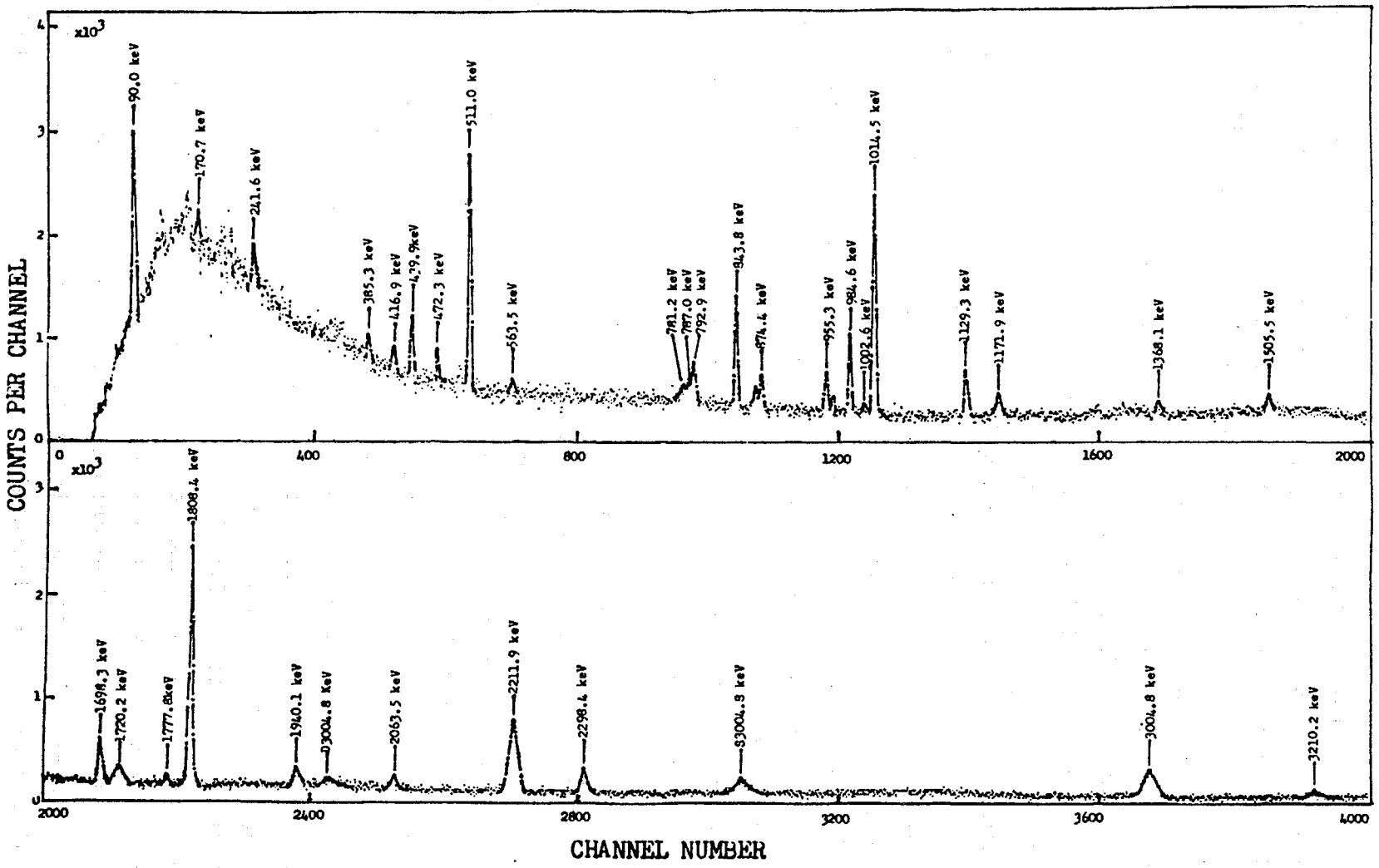

Fig.13. γ ray spectrum from $^{27}Al(n,x\gamma)$ reactions at 14.9 MeV. Spectrum was taken by Zhou Hongyu et al[26] with the HPGe detector with the resolution of 1.85 keV FWHM (at 1332 keV) and efficiency of 24.5 %.

sealed tubes are technically feasible and they are the most advanced neutron sources used in applied nuclear geophysics.

At 14 MeV quite great number of discrete γ rays are produced in $^{27}Al(n,x\gamma)$ reactions. In experimental work it is often useful to have a look at the whole γ ray spectrum to see which γ rays are of primary importance for present application. We reproduce therefore in fig.13. the prompt γ ray spectrum from $^{27}Al(n,x\gamma)$ reactions measured by Zhou Hongyu et al.[26]. The spectrum was taken using the HPGe spectrometer with energy resolution of 1.85 keV at 1332 keV and efficiency of 23.5 %. The dominant γ lines in this spectrum are 1014.5 keV and 1808.7 keV transitions from $(n,n'\gamma)$ and $(n,np\gamma)$ reactions, respectively. Both of them will be the most important γ rays for analytical applications in nuclear geophysics around 14 MeV incident neutron energy. fig.13 shows that none of this γ lines will be free of interferences , if one uses γ spectrometer with poorer energy resolution, for instance a NaI(Tl) detector. With this later type of spectrometer more suitable γ rays would be 2210 keV or 3004 keV. However, using even very good NaI(Tl) spectrometer with the energy resolution of 8 % at 1332 keV both lines will be contaminated with contribution from neighboring transitions of 2298 keV and 2980 keV, respectively.

There are only 3 measurements of discrete γ ray cross sections, where Ge(Li) spectrometers were utilized. Cross sections obtained in these measurements are summarized in tab.1. There are two independent measurements of Zhou Hongyu et al.[25,26] at 14.9 MeV and single measurement of Nyberg at 15 MeV. Zhou measured at $\Theta = 90^{\circ}$ and 125°, Nyberg values were measured at $\Theta = 80^{\circ}$. All experimental cross sections given in tab.1 were obtained from differential cross sections multiplied by 4π. Zhou gives more complete set of cross sections for γ rays with energies up to 3 MeV. Nyberg measured cross sections also for high energy γ rays up to 6.5 MeV.

As was shown in the previous section for several γ transitions, experimental values of both Nyberg and Zhou have tendency to overestimate the data of other authors. The general agreement between this three sets of cross sections is good only in several instances, predominantly in cases where the cross section is high, e.g. for 1014.5 keV, 1808 keV and 2210 keV transitions. In several cases even the values given by the same author differs drastically, e.g. 794 keV and 3004 keV measured by

Tab.1. Cross sections of discrete γ rays from $^{27}Al(n,x\gamma)$ reactions at neutron energy around 15 MeV. All cross sections are in mb, given in parenthesis are uncertainties.

E_γ(keV)	Reaction	Nyberg[24]	Zhou[25]	Zhou[26]	ENDF	Theory[32]
170.7	(n,n')	-	6(2)	2.3(0.7)	-	-
241.6	(n,p)	-	-	4.8(1.1)	-	-
416.9	(n,2n)	-	4.5(1.0)	3.7(0.8)	-	-
472.3	(n,α)	88(14)	5.8(1.1)	8.2(1.4)	-	-
563.5	(n,α)	-	-	4.0(1.2)	-	-
781.2	(n,α)	-	-	4.6(1.2)	-	-
794	(n,n')	11(2)	7.9(1.5)	23.2(2.5)	-	-
843.8	(n,n')	<21	40(3)	38.6(2.0)	35.5	21.3
874.4	(n,α)	-	5.9(1.1)	14.8(2.5)	-	-
954.5	(n,p)	20(6)	19.7(2.8)	17.7(1.9)	-	-
984.6	(n,p)	51(9)	31.9(2.9)	32.5(1.8)	11	-
1003.3	(n,np)	-	4.3(1.1)	3.2(1.3)	12.3	-
1014.5	(n,n')	89(14)	93(7)	83.6(4.3)	75.4	39.7
1129.7	(n,np)	-	26.6(2.3)	23.1(1.4)	27.2	-
1366	(n,n')	-	8.2(1.6)	8.7(2.6)	-	-
1505	(n,n')	-	6.3(2.0)	20.3(5.1)	5.1	5.1
1698.3	(n,p)	-	29.8(2.9)	34.4(7.5)	23.9	-
1720	(n,n')	60(11)	51.3(5.8)	34.8(5.1)	38.8	11.7
1777.8	(n,p)	-	-	6.7(3.3)	-	-
1808.7	(n,np)	182(29)	176(12)	198(9)	181	-
2063	(n,p)	-	4.1(1.5)	12(3.4)	-	-
2210	(n,n')	134(23)	119(10)	156(10)	138	109
2298	(n,n')	25(6)	20.5(3.6)	40.9(4.5)	19.1	40.9
3004	(n,n')	82(14)	33(10)	116(10)	88.4	79
3212	(n,n')	14(7)	-	30.6(8.0)	-	3.6
3956	(n,n')	6(1)	-	-	7.3	0.7
4409	(n,n')	19(5)	-	-	-	2.6
4580	(n,n')	19(4)	-	-	9.1	6.9
5448	(n,n')	12(4)	-	-	-	-
5535	(n,n')	8(3)	-	-	-	-
6271	(n,n')	11(3)	-	-	-	-

Tab. 2. Results of cross section balance calculation at 14.8 MeV. Cross sections are in mb, uncertainties are given in parenthesis. σ_γ is sum of cross sections of 843.8, 1014.5, 2210 and 3004 keV g.s. γ transitions, $\sigma_{(n,n')}$ is cross section of (n,n') reaction and σ_r stands for unobserved cross section.

	Nyberg[24]	Zhou[25]	Zhou[26]	Voss[23]	Orphan[28]	ENDF	Theory[32]
σ_γ	326(31)	285(16)	394(15)	283(13)	172(20)	336	249
$\sigma_{(n,n')}$	504(48)	440(25)	609(23)	437(21)	266(31)	519	385
σ_r	89(72)	159(54)	-32(52)	153(52)	324(57)	76	205

Zhou. In the case of 472.2 keV transition observed in the (n,α) reaction the difference is caused by different measuring technique. Nyberg have not utilized fast timing in his experiment, contrary to Zhou and his cross section for the γ ray deexciting the level with half life of 20.2 ms is much higher than the Zhou value.

3. Discussion

As was shown above, there are rather significant differences between experimental discrete γ ray production cross sections in neutron induced reactions with ^{27}Al. The differences show up predominantly at higher neutron energies.

The origin of the differences between experimental values of various authors in the high energy region is not known. A possible origin is in systematic errors, from which errors in the absolute efficiency of γ spectrometers, neutron flux determination and errors in different corrections applied to the raw experimental data are of most importance. However, none of them alone can explain the observed differences. Some of them could be often even excluded , as for instance error in the absolute detector efficiency in two sets of data[23,28]. These data cover broad energy interval from the threshold up to 13 and 15.8 MeV, respectively. They are in good accord in the lower neutron energy range, but differ at higher neutron energies. Consequently, the difference depends on neutron energy and is independent from the γ ray energy or absolute detection efficiency.

Tab.3. Recommended cross sections for the 843.8 keV γ ray transition in $^{27}Al(n,n')$

E_n (MeV)	σ (mb)	E_n (MeV)	σ (mb)
.9	6.5	7.5	88.4
1.0	12.7	7.6	82.4
1.1	74.1	7.7	81.3
1.2	88.9	7.9	77.9
1.3	66.7	8.0	71.3
1.4	126.8	8.1	74.3
1.5	120.7	8.2	79.7
1.6	126.9	8.3	90.5
1.7	72.2	8.4	86.8
1.8	97.7	8.5	82.1
1.9	72.9	8.7	67.9
2.0	103.9	8.8	76.8
2.1	91.9	8.9	84.0
2.2	114.3	9.0	76.3
2.3	87.8	9.1	78.3
2.4	81.8	9.2	78.2
2.5	86.7	9.3	79.3
2.6	101.9	9.4	70.6
2.7	128.8	9.5	65.2
2.8	88.3	9.6	61.3
2.9	83.8	9.8	61.0
3.0	81.6	9.9	60.4
3.1	123.1	10.0	60.2
3.2	94.3	10.1	60.6
3.3	117.9	10.2	59.5
3.4	74.6	10.4	58.8
3.5	92.8	10.5	57.4
3.6	103.7	10.6	57.2
3.7	82.6	10.7	57.1
3.8	65.3	10.8	56.7
3.9	92.0	10.9	53.5
4.0	96.4	11.0	51.8
4.1	113.1	11.1	51.4
4.2	122.6	11.3	50.8
4.3	98.3	11.4	50.0
4.5	93.5	11.5	49.6
4.6	95.7	11.6	49.3
4.7	106.8	11.7	49.1
4.8	113.5	11.8	48.7
4.9	114.5	11.9	45.0
5.0	108.4	12.1	43.7
5.1	93.9	12.2	44.2
5.2	94.8	12.3	44.3
5.3	94.5	12.4	42.5
5.4	100.5	12.6	41.4
5.5	86.6	12.7	40.6
5.6	91.1	12.8	39.8
5.7	91.1	13.0	37.3
5.8	88.0	13.1	34.6
5.9	88.7	13.2	33.7
6.0	97.0	13.4	33.0
6.1	85.4	13.5	32.6
6.2	79.5	14.0	29.9
6.3	81.8	14.5	26.4
6.4	83.5	15.0	25.1
6.6	73.4	15.5	22.0
6.7	85.8	16.0	20.0
6.8	97.1	16.5	18.0
6.9	87.9	17.0	16.2
7.0	80.9	17.5	15.6
7.1	83.3	18.0	13.6
7.2	90.2	18.5	12.0
7.3	92.5	19.0	10.5
7.4	86.8	19.5	9.6
7.5	88.4	20.0	8.5

Tab. 4. Recommended cross sections for the 1014.5 keV γ ray transition in $^{27}Al(n,n')$

E_n (MeV)	σ (mb)	E_n (MeV)	σ (mb)
1.1	44.6	7.6	173.8
1.2	90.3	7.7	172.5
1.3	80.3	7.8	171.6
1.4	71.4	7.9	169.4
1.5	112.1	8.0	163.8
1.6	123.0	8.2	162.6
1.7	182.0	8.3	159.7
1.8	109.3	8.4	182.7
1.9	190.4	8.5	190.0
2.0	194.8	8.6	183.3
2.1	182.4	8.8	177.3
2.2	192.6	8.9	172.6
2.3	170.9	9.0	163.0
2.4	140.6	9.1	160.3
2.5	225.2	9.2	148.4
2.6	183.7	9.3	162.5
2.7	179.3	9.4	154.0
2.8	142.4	9.5	159.0
2.9	210.7	9.6	163.7
3.0	204.8	9.7	158.8
3.1	294.3	9.8	143.6
3.2	272.5	10.0	147.1
3.3	203.0	10.1	144.8
3.4	178.5	10.2	138.3
3.5	168.9	10.3	142.2
3.6	161.8	10.5	131.1
3.7	229.8	10.6	132.2
3.8	182.0	10.7	126.7
3.9	181.9	10.8	120.4
4.0	200.8	10.9	120.6
4.1	179.7	11.0	122.0
4.2	196.4	11.1	113.6
4.3	209.9	11.3	119.4
4.4	209.7	11.4	113.6
4.5	211.6	11.5	110.0
4.6	184.6	11.6	111.3
4.7	227.2	11.7	106.7
4.8	196.8	11.8	115.1
4.9	192.7	11.9	101.9
5.1	217.2	12.1	106.1
5.2	205.6	12.2	102.5
5.3	180.4	12.3	99.7
5.4	198.2	12.4	94.3
5.5	197.5	12.6	100.6
5.6	182.8	12.7	89.2
5.7	183.6	12.8	89.8
5.8	214.5	13.0	93.3
5.9	230.0	13.1	85.7
6.0	212.4	13.2	83.7
6.1	204.0	13.5	81.5
6.2	196.9	14.0	76.6
6.3	204.7	14.5	71.3
6.4	219.4	15.0	64.3
6.5	215.5	15.5	55.6
6.7	227.6	16.0	48.7
6.8	221.0	16.5	41.5
6.9	206.6	17.0	32.5
7.0	188.5	17.5	25.7
7.1	198.2	18.0	21.5
7.2	192.1	18.5	16.3
7.3	165.7	19.0	15.4
7.4	174.9	19.5	12.4
7.5	175.5	20.0	11.3

Tab.5. Recommended cross sections for the 2210 keV γ ray transition in the $^{27}Al(n,n')$

E_n (MeV)	σ (mb)	E_n (MeV)	σ (mb)
2.3	40.7	8.3	178.7
2.4	67.2	8.4	177.6
2.5	104.9	8.6	185.4
2.6	118.8	8.7	173.2
2.7	113.8	8.8	173.2
2.8	91.5	8.9	175.3
2.9	183.9	9.0	170.6
3.0	207.7	9.1	163.7
3.1	168.1	9.2	176.6
3.2	200.9	9.3	172.5
3.3	192.0	9.4	178.3
3.4	160.6	9.5	173.1
3.5	156.5	9.7	171.3
3.6	181.8	9.8	170.8
3.7	158.5	9.9	181.3
3.8	131.2	10.0	176.3
3.9	151.8	10.1	171.2
4.0	162.0	10.3	169.5
4.1	133.3	10.4	171.6
4.3	175.2	10.5	173.8
4.4	170.9	10.7	171.5
4.5	169.8	10.8	170.9
4.6	180.4	10.9	169.8
4.7	173.2	11.0	168.6
4.8	196.9	11.1	167.3
4.9	177.5	11.2	170.2
5.0	178.0	11.3	168.4
5.1	210.6	11.4	177.2
5.2	184.2	11.5	171.6
5.3	190.0	11.6	165.3
5.4	189.0	11.7	163.4
5.5	154.0	11.9	169.0
5.6	159.4	12.0	170.9
5.7	162.5	12.1	158.7
5.8	197.1	12.2	163.4
5.9	186.5	12.3	162.9
6.0	180.8	12.5	161.6
6.1	154.6	12.6	167.1
6.2	189.4	12.7	155.6
6.4	188.4	12.9	157.8
6.5	173.3	13.0	155.5
6.6	178.7	13.1	151.2
6.7	156.6	13.3	146.4
6.8	187.8	13.5	144.0
6.9	170.9	14.0	135.0
7.0	202.2	14.5	124.0
7.1	183.6	15.0	114.0
7.2	188.0	15.5	103.0
7.3	159.7	16.0	91.8
7.4	156.5	16.5	80.9
7.6	189.7	17.0	74.4
7.7	166.3	17.5	63.8
7.8	178.0	18.0	56.0
7.9	162.0	18.5	49.8
8.0	162.8	19.0	43.6
8.1	142.8	19.5	37.4
8.2	160.9	20.0	32.7

Tab.6. Recommended cross sections for the 3004 keV γ ray transition in $^{27}Al(n,n')$

E_n (MeV)	σ (mb)	E_n (MeV)	σ (mb)
3.1	11.2	8.8	116.9
3.2	27.4	8.9	103.0
3.3	82.1	9.0	107.7
3.4	55.2	9.1	105.5
3.5	114.5	9.2	111.5
3.6	98.1	9.3	92.3
3.7	105.1	9.4	106.9
3.8	105.3	9.5	113.8
3.9	127.3	9.6	118.5
4.0	129.2	9.7	114.0
4.1	140.6	9.8	96.8
4.2	128.5	10.0	105.5
4.3	114.5	10.1	119.7
4.4	135.3	10.2	98.3
4.5	119.8	10.3	105.8
4.6	140.2	10.5	100.6
4.7	116.9	10.6	97.9
4.8	126.3	10.7	111.6
4.9	113.0	10.8	88.8
5.1	98.3	10.9	94.8
5.2	87.8	11.0	101.4
5.3	116.8	11.1	98.8
5.4	113.8	11.3	91.9
5.5	99.2	11.4	106.4
5.6	99.3	11.5	105.9
5.7	96.7	11.6	99.4
5.8	109.1	11.7	103.3
5.9	123.3	11.8	102.3
6.0	110.4	11.9	87.0
6.1	123.8	12.1	99.2
6.2	136.9	12.2	94.8
6.3	129.4	12.3	90.7
6.4	146.6	12.4	97.0
6.5	116.7	12.6	97.3
6.7	120.3	12.7	98.5
6.8	115.0	12.8	89.8
6.9	123.3	13.0	85.5
7.0	132.1	13.1	89.3
7.1	142.5	13.2	87.7
7.2	128.6	13.4	91.6
7.3	129.4	13.5	89.7
7.4	116.2	14.0	87.5
7.5	132.8	14.5	80.9
7.6	113.7	15.0	79.1
7.7	110.4	15.5	74.1
7.8	100.8	16.0	71.0
7.9	91.2	16.5	64.6
8.0	120.0	17.0	58.6
8.2	112.0	17.5	52.6
8.3	95.5	18.0	45.4
8.4	115.6	18.5	40.9
8.5	114.2	19.0	32.9
8.6	125.2	19.5	28.4
8.8	116.9	20.0	24.0

Tab.7. Recommended cross sections for the 1720 keV γ ray transition in $^{27}Al(n,n')$.

E_n(MeV)	σ(mb)	E_n(MeV)	σ(mb)
2.8	12.8	8.9	50.9
3.0	9.1	9.0	54.7
3.1	45.7	9.1	54.1
3.2	80.5	9.2	56.1
3.3	50.3	9.3	55.6
3.4	56.0	9.4	40.5
3.5	42.3	9.5	41.0
3.6	63.5	9.6	48.9
3.7	96.7	9.7	47.4
3.9	49.8	9.9	48.8
4.0	76.3	10.0	57.3
4.1	56.8	10.1	50.8
4.2	55.6	10.2	47.0
4.3	58.1	10.3	49.1
4.4	48.4	10.5	54.9
4.6	62.1	10.6	48.5
4.7	48.9	10.7	42.8
4.8	63.9	10.9	42.8
4.9	69.3	11.0	42.7
5.0	78.2	11.2	42.6
5.2	68.5	11.3	42.6
5.3	64.3	11.5	42.7
5.5	63.4	11.6	42.7
5.6	52.5	11.8	42.5
5.7	64.4	11.9	42.7
5.8	85.2	12.1	42.4
5.9	61.5	12.2	42.8
6.0	65.5	12.4	42.4
6.2	76.9	12.6	42.6
6.3	60.0	12.8	42.4
6.4	69.8	12.9	42.3
6.5	66.3	13.1	42.3
6.6	60.5	13.3	42.2
6.8	81.2	13.5	42.1
6.9	59.1	14.0	42.1
7.1	63.5	14.5	41.3
7.2	70.9	15.0	38.8
7.4	59.0	15.5	36.2
7.5	56.5	16.0	33.1
7.7	55.9	16.5	29.8
7.8	57.7	17.0	26.4
8.0	49.7	17.5	22.8
8.2	61.5	18.0	19.1
8.4	55.9	18.5	15.2
8.6	59.8	19.0	11.7
8.8	49.8	19.5	9.4
8.9	50.9	20.0	7.9

In all above mentioned experiments a rather massive samples were used and various corrections for γ ray and neutron self absorption as well as for multiple scattering were applied. Absolute values of specific corrections depend on a type of correction as well as on the experiment. Typical values vary between 5 % and 30 %, although a value over 100 % was also reported.

Tab.8. Recommended cross sections for the 986.4 keV γ ray transition in ^{27}Al(n,p).

E_n (MeV)	σ (mb)	E_n (MeV)	σ (mb)
2.9	.0	7.8	24.6
3.0	.0	8.0	26.0
3.2	.2	8.6	30.6
3.4	.4	9.0	33.0
3.6	.6	9.6	36.5
3.8	.8	10.0	37.2
4.0	1.0	10.5	37.8
4.2	1.4	11.0	37.4
4.4	2.3	11.5	37.2
4.6	4.0	12.0	36.2
4.8	6.4	12.5	35.0
5.0	9.0	13.0	34.4
5.2	11.5	13.5	33.2
5.4	13.9	14.0	32.2
5.6	15.8	14.5	31.3
5.8	17.0	15.0	29.9
6.0	18.0	15.5	28.4
6.2	18.9	16.0	26.9
6.4	19.6	16.5	25.1
6.6	20.4	17.0	23.6
6.8	21.2	17.5	22.0
7.0	22.0	18.0	20.5
7.2	22.3	18.5	18.8
7.4	22.8	19.0	17.2
7.6	23.5	19.5	15.1
7.8	24.6	20.0	13.5

Tab. 9. Recommended cross sections of discrete γ rays observed in ^{27}Al(n,xγ) reactions at 14.8 MeV.

E_γ (keV)	Reaction	Transition	Cross section (mb)
170.7	(n,n')	$3/2^+ \rightarrow 1/2^+$	2.1
416.9	(n,2n)	$3^+ \rightarrow 5^+$	4.5
794	(n,n')	$9/2^+ \rightarrow 7/2^+$	8.1
843.8	(n,n')	$1/2^+ \rightarrow 5/2^+$	26.5
954.5	(n,p)	$5/2^+ \rightarrow 3/2^+$	18.9
984.6	(n,p)	$3/2^+ \rightarrow 1/2^+$	30.5
1003.3	(n,np)	$3^+ \rightarrow 2^+$	3.6
1014.5	(n,n')	$3/2^+ \rightarrow 5/2^+$	67.2
1129.7	(n,np)	$2^+ \rightarrow 2^+$	23.7
1366	(n,n')	$7/2^+ \rightarrow 3/2^+$	7.5
1698.3	(n,p)	$5/2^+ \rightarrow 1/2^+$	28.7
1720	(n,n')	$5/2^+ \rightarrow 3/2^+$	37
1808	(n,np)	$2^+ \rightarrow 0^+$	185
2210	(n,n')	$7/2^+ \rightarrow 5/2^+$	118
2298	(n,n')	$11/2^+ \rightarrow 7/2^+$	16
3004	(n,n')	$9/2^+ \rightarrow 5/2^+$	80
3212	(n,n')	$1/2^+ \rightarrow 1/2^+$	10.7
3956	(n,n')	$3/2^+ \rightarrow 5/2^+$	4.6

Among these, the correction for multiple scattering seems to play a rather important role, because it depends on neutron energy. Multiple scattering apparently increases the cross section at higher neutron energies, when the excitation function has the form shown in fig.6. The multiple scattering is a complicated function of the incident energy, geometry and of cross sections of all open channels. Consequently, there is no simple way to calculate this correction reliably. Analyzing the way in which these corrections were calculated by various authors, we came to the conclusion that the most correct way was chosen by Voss et al[29], who simulated the whole experiment by the Monte Carlo technique.

In a consistent set of the experimental cross sections, the following relation for the total cross section holds

$$\sigma_{tot} = \sigma_{el} + \sigma_{n,n'} + \sigma_{n,p} + \sigma_{n,\alpha} + \sigma_{n,2n} + \sigma_{n,np} + \sigma_{r} ,$$

where σ_r accounts for the sum of cross sections of all neglected weak open channels like (n,γ), (n,d), (n,nα) and (n,t) as well as for unobserved cross section in all other channels. In a consistent set of cross sections σ_r should be rather small positive number.

As the check of consistency of experimental cross sections, we performed this test at 14.8 MeV neutron energy. We have chosen this energy because of its practical importance as well as because the cross sections of charged particle reactions are known at this point to a high degree of accuracy. We used the following known cross sections

σ_{tot}	= 1750	mb	(ENDF/B-4)
σ_{el}	= 758(45)	mb	(ref. 33)
$\sigma_{n,p}$	= 72.5(2.9)	mb	(ref. 34)
$\sigma_{n,\alpha}$	= 111.9(1.3)	mb	(ref. 34)
$\sigma_{n,2n}$	= 32.8(4.3)	mb	(ref. 35).

The point is that the (n,n') cross section may be extracted from the measured (n,n'γ) cross sections. In general, the (n,n') cross section is the sum of (n,n'γ) cross sections of all ground state γ ray transitions. If only limited number of these transitions is observed a correction for unobserved transitions must be applied. We calculated the (n,n') cross section from production cross sections of the ground state γ transitions with energies of 843.8, 1014.5, 2210 and 3004 keV. The correction for

unobserved γ transitions was extracted from the theoretical calculation Herman[32] as 1.546. This gives

$$\sigma_{n,n'} = (\sigma_{843.8} + \sigma_{1014.5} + \sigma_{2210} + \sigma_{3004}) \times 1.546 = \sigma_{\gamma} \times 1.546$$

The product of important (n,np) reaction is stable nucleus ^{26}Mg and activation cross section could not be measured. Therefore, we have taken the cross section of the 1808.7 keV γ ray, which collects the cross section off all discrete excited states in ^{26}Mg as cross section of the whole reaction. This is surely the lower limit for the reaction cross section, because we neglect direct particle population of the ground state as well as that part of the cross section which goes via unobserved statistical and high energy γ rays directly to the ground state. In those data sets of tab.1, where the σ_{1808} is not given, we used averaged experimental value of 185(11) mb.

The results of this balance check are displayed in tab.2. In the first row the sum of 4 above mentioned γ ray cross sections is shown. The Orphan value was obtained by interpolation of his experimental data measured at 13.5 and 15.8 MeV. The Voss value is smooth extrapolation of his experimental data. In the second row the (n,n') cross sections are given as obtained from the data in the first row corrected for unobserved γ rays. Finally, in the last row σ_r is shown.The values of σ_r shown in the third row vary from 324(57) mb to -32(52) mb.The mean experimental value of σ_r is 139 mb. We adopted this value of unobserved cross section, from which probably the most important part corresponds to (n,np) cross section.

Taking this mean value of σ_r and working back the above procedure we arrived at the following cross sections of 4 strongest γ rays in (n,n') channel

σ_{843}= 26.5 mb, σ_{1014}=67.2 mb, σ_{2210}= 118 mb and σ_{3004}=80 mb.

At lower neutron energies we performed similar tests. However at 2.5 MeV neutron energy only the (n,n') channel is opened, at 3.5 MeV also the (n,p) channel is slightly above the threshold. At each of these two energies the total cross section is the sum of cross sections of discrete γ ray transitions in the (n,n') channel and the Voss data are in reasonable agreement with the ENDF/B-4 evaluation. Indeed, total cross sections derived from the Voss data are 396(44) mb and 621(75) mb at 2.5 MeV and

3.5 MeV, respectively. The correcpondingENDF/B-4 values are 364 mb and 656 mb , respectively.

In the (n,p) channel are the difference between cross sections of the 984.6 keV γ ray measured by Nyberg et al.[24] and Zhou et al[25] around 15 MeV is rather high. To distinguish between these two values of cross section we used experimental cross sections for γ rays of 954.5 keV, 984.6 keV and 1698.3 keV measured by Zhou[25] (see tab. 1.) which are 19.7(2.8) mb, 31.9(2.9) mb and 29.8(2.9) mb, respectively. From these cross sections and taking γ ray branching ratios as given by Endt et al.[26], we arrive at the following populations of discrete levels in ^{27}Mg : $3/2^+$ at 984.6 keV - 12.4(4.0) mb, $5/2^+$ at 1698.3 keV - 29.4(3.0) mb and $5/2^+$ at 1939.1 keV - 29.9(3.0) mb. The sum of these cross sections is 71.5(5.8) mb which exhausts the whole (n,p) cross section of 72.5(2.9) mb[24]. Consequently, there is no room for direct particle population of the $1/2^+$ ground state. This is understandable in view of rather high g.s. spin of the target nucleus. Therefore, the Zhou cross section represents an upper limit for the 984.6 keV γ ray production, while the Nyberg value is clearly too high.

5. Recommended production cross sections

In this chapter we present recommended cross sections for 5 discrete γ rays observed in the (n,n'γ) reaction and for single γ ray observed in both the (n,pγ) and the (n,npγ) reactions in the whole energy region from threshold up to 20 MeV. Furthermore, we present cross sections for 18 discrete γ rays at 14.8 MeV incident neutron energy

We start woth the (n,n'γ) cross sections. In the low energy region ($E_n \leq 8$ MeV) a reasonable agreement between various experimental values was found, apart from fluctuations visible only in the Voss experiment. The total cross sections calculated from his data are also in accord with the ENDF/B-4 evaluation. Therefore, we based our present evaluation on the Voss experimental data. However, in his experiment very fine energy step was used. In practical applications the width of the energy distribution of available neutron sources is much broader. This is also true for the D^+T and the D^+D^- "mono energetic" neutron sources, when bulk sample geometry is used. One should therefore use cross sections properly averaged over the neutron

energy distribution. It is therefore useful to recommend averaged cross sections for the present application. The averaging interval is surely a matter of question. It should not be very wide in order not to lose information. We feel that averaging over 0.1 MeV is suitable for applied geophysics and we give the evaluated cross sections averaged over this interval.

In the higher neutron energy interval (8 MeV $\leq E_n$ 15 $\leq$ MeV) we followed variations indicated by the Voss data but we changed the absolute values to reach the above mentioned cross sections of strongest γ lines at 14.8 MeV.

At still higher neutron energies ($E_n \geq$ 15 MeV) we followed the slopes of the respective excitation curves from the ENDF/B-4 evaluation.

The recommended cross sections for γ rays emitted in the inelastic neutron scattering on ^{27}Al, namely 843.8 keV, 1014.5 keV, 1720 keV, 2210 keV and 3004 keV are given in tabs. 3. - 7.

The experimental information about γ ray production in charged particle reactions (n,p) and (n,np) is rather poor. However experimental and evaluated cross sections of the 1808.7 keV transition produced in ^{27}Al(n,npγ)^{26}Mg reaction are in good mutual agreement, therefore we recommend to use the ENDF/B-4 evaluation for practical applications.

The recommended cross sections of the 984.6 keV γ ray in the (n,pγ) reaction are based in the low energy region on the Dickens data and on the ENDF/B-4 evaluation. In the high energy part the single value of Zhou at 14.9 MeV was utilized as well as the shape of the excitation curve of (n,p) reaction, taken from the ENDF/B-4 evaluation. Recommended ross sections are given in tab.8.

Aforementioned balance calculation is a firm basis also for recommended cross sections at 14.8 MeV. To the cross sections of 4 strongest γ rays in (n,n'γ) we adopted cross section of the 1808.7 keV γ ray observed in the (n,np) channel. We adopted the value of 185 mb, which is the average from measurements of Nyberg and Zhou. This value is also in excellent agreement with the ENDF/B-4 evaluation. From these 5 values we arrived at cross sections of 6 additional γ rays in the (n,n'γ) channel and 2 γ rays in the (n,npγ) channel using relative values of experimental cross sections of individual authors as well as γ ray branching ratios taken from the literature[86]. We adopted also cross sections of 3 γ rays observed in the (n,pγ) channel and cross

section of single γ ray observed in the (n,2nγ) channel, based on the measurement by Zhou Hongyu et al.[25] The recommended cross sections are given in the last column of tab.9.

5. Conclusions

We have collected and analyzed cross sections of discrete γ rays produced in fast neutron ractions on ^{27}Al. For the present evaluation we used only experimental cross sections measured with high resolution germanium detectors. In the whole energy range from the threshold up to 20 MeV we analyzed cross sections of 5 prominent γ rays in the (n,n'γ) channel, i.e. 843.8, 1014.5, 1720, 2210 and 3004 keV as well as strongest γ rays of 984.6 keV and 1808.7 keV observed in (n,pγ) and (n,npγ) channels, respectively. At 14.8 MeV incident neutron energy we give evaluated cross sections for additional 11 discrete γ rays.

For inelastic γ rays a quite good accord between various experimental data was found in the low energy neutron range up to 8 - 10 MeV, depending on the γ ray. However, rather strong fluctuations in cross sections found in the experiment performed by Voss[23] were not found in other experiments, where neutron energy step was rather big (0.5 - 2 MeV) or cross sections at single neutron energy were measured. In the upper part of the neutron energy range investigated here, rather large differences are present between values measured by different authors.

In the low energy range where good agreement between experimental values of different authors has been found, the evaluated cross sections are based on the Voss data. In his experiment the excitation curves were measured with very fine neutron energy step. Evaluated cross sections were obtained rather from values averaged over 0.1 MeV. Total cross section at 2.5 MeV and 3.5 MeV calculated from these averaged data are in good agreement with total cross sections recommended by the ENDF/B-4.

At 14.8 MeV, in the energy interval where the discrepancies between experimental cross section were found, we obtained the recommended cross sections with the aid of balance calculation. We used the total cross section, cross sections of all open channels and cross sections of 4 prominent ground state γ transitions in the (n,n'γ) channel. We used also the theoretical

correction for unobserved γ rays in this channel, taken from the calculation of Herman[38], as well as the relative γ ray cross sections of individual authors normalized to σ_{2210}.

It was shown that the excitation curve of the 1808.7 keV γ ray produced in (n,npγ) reaction as recommended by the ENDF/B-4 evaluation is in accord with the available experimental information.

At 14.8 MeV neutron energy we evaluated cross sections of 18 discrete transitions. We used cross sections of 4 above mentioned γ rays in the (n,n'γ) channel, the cross section of the 1808.7 keV γ ray in the (n,npγ) channel, normalized relative cross sections as well as the γ ray branching ratios[36]. In addition, we give cross sections of most prominent γ transitions in the (n,pγ) and (n,2nγ) channels based on experimental values given by Zhou Hongyu et al.[25]

Acknowledgement

The authors are indebted to Dr. P. Ďuriš, ing. P. Zima and the staff of the Computing Center of the Slovak Academy of Sciences for providing us with the graphical package used for preparation of graphical outputs presented in this report.

References

1. C.G. Clayton et al., in the Proceedings of the IAEA Consultants' Meeting on Nuclear Data for Bore-Hole and Bulk-Media Assay Using Nuclear Techniques, Krakow 1983 ,Report INDC(NDS)/-151/L, (IAEA, Vienna 1984) p.17.
2. P. Obložinský and S. Hlaváč, in the Proceedings of the IAEA Consultants' Meeting on Nuclear Data for Applied Nuclear Geophysics, Vienna 1986, Report INDC(NDS)-184/GM; (IAEA, Vienna 1987) p.79.
3. P. Obložinský and S. Hlaváč, Nucl. Geophys. 1(1987)263.
4. CINDA, Computer Index of Neutron Data (IAEA, Vienna).
5. EXFOR, Computerized Neutron Data File (IAEA, Vienna).
6. ENDF/B4, US Evaluated Nuclear Data Library: Summary Documentation, compiled by D. Garber, BNL 17541(Brookhaven National Laboratory, 1975).

7. ENDF/B5, US Evaluated Nuclear Data Library: Summary Documentation, compiled by R. Kinsey, BNL-NCS-17541 (Brookhaven National Laboratory, 1979).
8. JENDL-2, Japanese Evaluated Nuclear Data Library: Summary Documentation, edited by T. Nakagawa, Reports JAERI-M 84-052 and 84-103 (JAERI, Tokai-mura, Ibaraki-ken 1984).
9. BROND, USSR Recommended Evaluated Neutron Data Library, ed. V.N. Manokhin, Report INDC(CCP)-283 (IAEA, Vienna 1988).
10. S. Hlaváč and P. Obložinský, Nucl. Instr. Meth. B28 (1987) 93.
11. C. M. Lederer and V. S. Shirley eds., Table of Isotopes, (J. Wiley&Sons, New York 1978).
12. V. E. Sherrer, R. B. Theus and W. R. Faust, Phys. Rev. 51 (1953) 1476.
13. R. M. Kiehn and C. Goodman, Phys. Rev. 95 (1954) 989.
14. R. A. Rothman, H. S. Hans and C. E. Mandeville, Phys. Rev. 100 (1955) 83.
15. G. L. Griffith, Phys. Rev. 98 (1955) 579.
16. R. D. Day, Phys. Rev. 102 (1956) 767.
17. I. L. Morgan, Phys. Rev. 103 (1956) 1031.
18. J. L. Perkin, Nucl. Phys. 60 (1964) 561.
19. S. C. Mathur, W. E. Tucker, R. W. Benjamin and I. L. Morgan, Nucl. Phys. 73 (1965) 561.
20. K. C. Chung, D. E. Velkley, J. D. Brandenburger and M. T. McEllistrem, Nucl. Phys. A115 (1968) 476.
21. M. N. Islam, J. D. Kellie and G. I. Crawford, J. Phys G(GB) 7 (1981) 371.
22. J. K. Dickens, Phys. Rev. C5 (1972) 100.
23. F. Voss, Report KfK 1611, (KfK, Karlsruhe 1972).
24. K. Nyberg-Ponnert, E. Jonnson and I. Bergqvist, Phys. Scripta 4 (1971) 165.
25. Zhou Hongyu, Tang Liu, Yan Yimin, Wen Shelling, Lou Liquiao, Zhang Shengji, Wang Qi, Sun Shun, Can Changzhou, Diy Xiaoji, Wang Wanling, Report INDC(CAR)-010/L, (IAEA, Vienna 1986).
26. Zhou Hongyu, Institute of Low Energy Nuclear Physics, Being Normal University, Private communication, (April 1989).
27. G. Clayeux, G.Grenier, Centre d'Etudes de Limeil report CEA-R-3807, (Limeil 1969).
28. V. J. Orphan, C. G. Hoot, Gulf Radiation Technology Report GULF-RT-A10743, (Gulf 1971).
29. P. G. Young, D. G. Foster, Report LA-4726(ENDF-175), (Los Alamos National Laboratory, Los Alamos 1972).

30. T. Asami and S. Tanaka, eds., Report JAERI-M 8136, (JAERI, Tokai-mura, Ibaraki-ken 1979).
31. V. Piksaikin, V. Goulo and O. Schwerer in INDC(NDS)-184/GM, (IAEA, Vienna 1987) p. 175.
32. M. Herman, ENEA Bologna, Private communication (March 1989).
33. C. S. Whisnant, J. H. Dave and C. R. Gould, Phys. Rev. C30 (1984) 1435.
34. J. Csikai, Zs. Lantos, S. Sudar, T. Chimoye, T. Vilaithong and N. Chirapatpimol, Z. Phys. A325 (1986) 69.
35. M. Sasao, T. Hayashi, K. Taniguchi, A. Takahashi and T. Ida, Phys. Rev. C35 (1987) 2327.
36. P. M. Endt, C. Van Der Leun, Nucl. Phys. A310 (1978) 196.

CONCLUSIONS AND RECOMMENDATIONS

Session Chairman: S. Wender

The following conclusions were drawn by the participants regarding the topics of measurement, calculation and evaluation of photon production cross sections.

1. Measurements

The participants discussed several experimental techniques and experimental facilities where gamma-ray measurements may be performed.

1.1 The Los Alamos continuous energy "white" neutron source is capable of discrete gamma-ray measurements of cross sections and angular distributions from below 1 MeV to over 200 MeV incident neutron energy. The gamma-ray energies from below 1 MeV to 6 MeV are covered with high resolution Ge detectors. The gamma-ray energies from 2 MeV to over 30 MeV are covered using BGO detectors. Continuum measurements are possible with this source with somewhat greater errors due to uncertainties in background subtractions.

Hard photons (above 30 MeV) following high energy neutron induced reactions may be measured using a gamma-ray telescope which is not sensitive to neutrons.

1.2 The technique of in-beam gamma-ray measurements with a pulsed 14 MeV neutron source together with n-TOF spectorscopy has been demonstrated by S. Unholzer and can be used for:

- small sample differential cross section measurements
- benchmark experiments (leakage spectra)
- extended integral experiments (such as model of fusion reactor blanket). Neutron spectra are measured simultaneously with gamma-rays.

In cases of small samples good angular and time resolution is achievable, allowing (n,γ) and (γ,γ) correlation experiments as well as the investigation of time dependent deexcitation processes.

1.3 The method of in-beam gamma-ray measurements at 14 MeV using continuous beam with associated-particle technique is well developed. This method is able to provide data on continuum and discrete gamma-ray spectra as well as gamma multiplicities. This was demonstrated by the measurement of gamma-ray production from $^{52}Cr(n,x\gamma)$.

The opinion of participants is that the majority of gamma-ray data should be obtained by calculation. It is important to have complete and precise gamma-ray production data for several nuclei from the entire mass region to verify codes. When particular elements are important such as structural materials (Fe, Ni, Cr) complete measurements should be made.

2. Calculations

2.1 The participants stated that there are two approaches to calculating the continuum gamma ray spectra following fast neutron capture:

(i) in the exciton model the giant dipole resonance part of the spectrum is described by emission from exciton state with n=1. The physical foundation of this concept is still unclear but the model has proved very useful for evaluations;

(ii) in the statistical multistep approach the spectra are calculated as the sum of a multistep compound and direct processes. The latter mechanism would dominate the production of high energy photons. Therefore theoretical formulation of multistep direct process should be pursued.

Within the exciton model, also multiple γ-cascades and different correlational quantities can be obtained (Betak, Cvelbar).

The exciton model generally describes the observed photon spectra in the GDR region (Betak, Oblozinsky).

The multistep compound theory of Feshback-Kernan and Koonin has been developed (Oblozinsky and Chadwick) to include gamma-ray emission. The theory has been used to calculate the primary gamma-ray spectrum for 14 MeV neutron-induced reactions on ^{59}Co, ^{93}Nb and ^{181}Ta

and is able to account for between 20 and 50% of the data in the GDR region.

Within a statistical multistep model (Kalka) emissions of nucleons and gammas are calculated for A>27 and incident energies below 30 MeV. The high-energy part of γ-spectra are modelled by a direct two-step process. For the description of the low-energy part γ-multiplicities $\bar{M} > 1$ are needed.

2.2 The participants have discussed the experimental results on two-step gamma-ray cascades following the thermal neutron capture. They recommended to continue this effort to enlarge the information on photon strength for E_1 and M_1 radiations at gamma-ray energies below 3 MeV. It is of particular importance to extend the above measurements for a broader class of nuclei, especially including the nuclei from the deformed rare earth region. For these nuclei rich and reliable data on photon strength functions at energies $E \geq 6$ MeV already exist. The deformed region seems crucial for understanding the role of valence transitions and their contributions to the photon strength.

2.3 The importance of the absolute values and the energy dependence of gamma-ray strength functions for the statistical model calculations has been demonstrated by Uhl and Kopecky. It is recommended to re-evalute the experimental data on E_1 and M_1 gamma-ray strength functions (compilation of C. McCullagh, 1981) and to include recent data from Dubna (F. Becvar). This new data base could be used to derive the systematic behaviour of gamma-ray strength functions.

2.4 Statistical model calculations of capture cross sections and gamma-ray spectra depend on the low energy behaviour of the strength function for E_1 and M_1 radiation. Of particular interest are the microscopic theories for the E_1 strength which predicts a non-zero limit as the gamma ray energy approaches zero. By analysing total s- and p-wave radiation widths, capture cross sections and gamma-ray spectra for selected spherical nuclei strong evidence for this non-zero limit was found. These investigations should be extended to a broader mass range, in particular to deformed target nuclei. One can hope to find recommended strength functions which are supported

by theory and based on independent experimental data. Model calculations employing these recommended strength functions promise an improved predictive power.

2.5 In addition to strength functions the following ingredients are needed to perform reliable model calculations:

(i) Good knowledge of the level densities. Separate activities (also within the IAEA) are devoted to this problem.

(ii) Decay schemes and branching ratios should be known with good precision. This knowledge is important for the calculation of discrete gamma-ray production cross-sections.

2.6 There is substantial interest in hard photon production cross sections. Experimental possibilities for relevant measurements have opened up at Los Alamos (Talk by Wender). Hard photons cover spectral energy range from about 30 MeV up to several hundred MeV. It seems that the dominant radiative mechanism in this spectral energy range is related to neutron-proton interactions and can be viewed as a bremsstrahlung process or inverse quasideuteron photoabsorption (talks by Oblozinsky and Betak). We propose that experimental measurements and theoretical studies be performed. It was recommended to convene the next meeting on this topic in 1992.

3. Data needs and evaluations

3.1 The participants stated that until recently there has not been enough attention paid to evaluations of gamma-ray production cross sections based on theoretical models. There is a growing need for high quality gamma-ray production data in several application areas. Such data are needed for nuclear geophysical applications, especially nuclear well logging and mineral analysis. These data are vital for fusion reactor design because the major heat transfer mechanism is the interaction of 14 MeV neutrons with reactor structural materials.

3.2 The participants also stressed the fact that there is a need for gamma production data for incident particle energies up to about 1 GeV for space applications, accelerator shielding and

IAEA Specialists' Meeting on the
MEASUREMENT, CALCULATION AND EVALUATION OF
PHOTON PRODUCTION CROSS-SECTIONS

Co-sponsored by the Czechoslovak Atomic Energy Commission

Smolenice
The Czech and Slovak Federal Republic
5 - 7 February 1990

LIST OF PARTICIPANTS

AUSTRIA	M. Uhl Institut für Radiumforschung und Kernphysik Boltzmanngasse 3 A-1090 Vienna
CZECHOSLOVAKIA	P. Oblozinsky (Local Organizer) Electro-Physical Research Centre Department of Nuclear Physics Institute of Physics of the Slovak Academy of Sciences Fyzikalny Ustav Sav CS-842 28 Bratislava
	E. Betak (address as above)
	J. Kliman (address as above)
	S. Hlavac (address as above)
	D. Belizova (address as above)
	F. Becvar Charles University Prague
GERMAN Dem. Rep.	H. Kalka Sektion Physik Technische Universität Dresden Mommsenstr. 13 DDR-8027 Dresden
	S. Unholzer Sektion Physik Technische Universität Dresden Mommsenstr. 13 DDR-8027 Dresden

NETHERLANDS	J. Kopecky Department of Physics Netherlands Energy Research Foundation (ECN) P.O.B. 1 NL-1755 ZG Petten
U.S.S.R.	A.I. Blokhin Centr po Jadernym Dannym Fiziko-Energeticheskij Institut Ploschad Bondarenko 249 020 Obninsk, Kaluga Region
	A.A. Filatenkov V.G. Khlopin Radium Insitute Ul. Rentgena 1 Leningrad P-22
	A.A. Rimski-Korsakov V.G. Khlopin Radium Insitute Ul. Rentgena 1 Leningrad P-22
UNITED KINGDOM	M.B. Chadwick University of Oxford Department of Nuclear Physics Keble Road Oxford OX1 3RH
UNITED STATES	S. Wender Los Alamos National Laboratory P.O. Box 1663 Los Alamos, NM 87545
I.A.E.A.	N.P. Kocherov (Scientific Secretary) IAEA Nuclear Data Section Wagramerstr. 5, P.O. Box 100 A-1400 Vienna, Austria

accelerator-breeder target development (A.A. Rimsky-Korsakov's talk). Systematic production cross-sections and (if possible) angular distributions of gamma-rays above 70 MeV induced by GeV protons should be measured and developed.

3.3 The participants feel that a concentrated effort is needed to address the above problems. To speed up the necessary developments they suggest to set up a Co-ordinated Research Programme on Measurement, Calculation and Evaluation of Photon Production Cross Sections under the auspicies of the IAEA.